

**Allosteric Modulators of Metabotropic Glutamate
Receptors: From Virtual Screening to Experimental
Validation**

Dissertation
zur Erlangung des Doktorgrades
der Naturwissenschaften

vorgelegt beim Fachbereich
Biochemie, Chemie und Pharmazie
der Johann Wolfgang Goethe-Universität
in Frankfurt am Main

von
Tobias Noeske
aus Frankfurt am Main

Frankfurt 2007
(D30)

vom Fachbereich Biochemie, Chemie und Pharmazie der
Johann Wolfgang Goethe-Universität als Dissertation angenommen.

Dekan:	Prof. Dr. Harald Schwalbe
Erster Gutachter:	Prof. Dr. Gisbert Schneider
Zweiter Gutachter:	Prof. Dr. Theodor Dingermann
Datum der Disputation:	19. Juni 2007

Im Fachbereich Biochemie, Chemie und Pharmazie der Johann Wolfgang Goethe-Universität wurde diese Arbeit im Zeitraum von Juli 2003 bis Dezember 2006 am Institut für Organische Chemie und Chemische Biologie in der Arbeitsgruppe Chemie- und Bioinformatik (Prof. Dr. Gisbert Schneider) angefertigt.

„Felix, qui potuit rerum cognoscere causas.”

(Vergil, Georgica 2, 490)

Danksagung

In erster Linie bedanke ich mich an dieser Stelle bei meinem Doktorvater Professor Dr. Gisbert Schneider, unter dessen Leitung ich die Gelegenheit gehabt habe, diese Dissertation anzufertigen. Er hat mir in allen Situationen mit Rat und Tat zur Seite gestanden und oftmals für die nötige Aufmunterung gesorgt.

Besonders möchte ich mich aber auch bei meinen unmittelbaren Betreuern, Dr. Tanja Weil und Dr. Christopher Parsons von Merz Pharmaceuticals GmbH bedanken, wo ich die Doktorarbeit durchgeführt habe. Sie haben mich in der notwendigen Weise in die wissenschaftliche Arbeit eingeführt und mit ihrer Unterstützung für ein erfolgreiches Gelingen derselben gesorgt.

Bei meinen Arbeitskollegen in der *in-vitro* Pharmakologie und in der Medizinischen Chemie von Merz Pharmaceuticals GmbH bedanke ich mich für die schöne gemeinsame Zeit und Unterstützung. Vielen Dank an Andrea Baude, Swetlana Derksen, Dr. Kate Gilling, Dr. Mirko Hechenberger, Dr. Manuela Lopez de la Paz, Meik Sladek und Sylvia Willi. Im einzelnen danke ich Tanja Bauer, Sabine Denk und Christina Wollenburg dafür, dass sie so manche Testsubstanz im funktionalen mGluR1-Assay oder im mGluR5 Bindungs-Assay für mich gemessen haben. Dr. Claudia Jatzke hat mir besonders in den ersten Monaten vielerorts bei der Eingewöhnung in das neue Tätigkeitsfeld geholfen sowie wichtige Substanzmessungen bei den Rezeptorinteraktionsstudien von mGluR1/5 Antagonisten durchgeführt.

Ein nicht unwesentlicher Dank gilt auch Dr. Steffen Renner für die fruchtbare Zusammenarbeit beim mGluR1/5-Projekt. Nach seinem Wechsel zu Merz Pharmaceuticals GmbH hat er mir bei relevanten Software-Problemen geholfen und mich mit so manchem brauchbaren Skript versorgt.

Alireza Givehchi, einem Mitarbeiter aus dem Arbeitskreis von Professor Dr. Gisbert Schneider, danke ich für seine Hilfe bei der Suche nach neuen mGluR1/5-Antagonisten mittels der von ihm entwickelten Software *ChemSpaceShuttle*. Er hat mir bei mancher anregenden Diskussion zu interessanten Ideen verholfen. In diesem Zusammenhang bedanke ich mich auch bei den übrigen Arbeitskreis-Angehörigen für ihre freundliche Unterstützung:

Dr. Alexander Böcker, Dr. Evgeny Byvatov, Norbert Dichter, Uli Fechner, Lutz Franke, Tina Grabowski, Michael Meissner, Manuel Nietert, Brigitte Scheidemantel-Geiß, Michael Schmucker, Dr. Petra Schneider und Andreas Schüller.

Dr. Aigars Jirgensons vom Institut für Organische Synthese (IOS) in Riga, Lettland danke ich für die erfolgreiche Zusammenarbeit bei der Leitstruktur-Optimierung der Cumarin-Derivate als mGluR1 Antagonisten. Darüber hinaus danke ich Dr. Alexandrs Gutcaits, ebenfalls vom IOS, für interessante Diskussionen bezüglich unseres gemeinsamen Übersichtsartikels sowie für wertvolle Anregungen und große Hilfe bei software-spezifischen Fragen.

Professor Dr. Holger Stark und seiner wissenschaftlichen Mitarbeiterin Dr. Britta Sasse vom Lehrstuhl der Pharmazeutischen Chemie an der Goethe-Universität danke ich für die ebenfalls von Erfolg gekrönte Zusammenarbeit bei den Studien zur Rezeptorinteraktion von Gruppe I mGluR-Antagonisten.

Zuletzt möchte ich mich bei meinen Eltern bedanken, die mir durch ihre finanzielle Hilfe das Studium der Pharmazie ermöglicht haben und somit für den Grundstein der hier vorgelegten Doktorarbeit gesorgt haben.

Diese Doktorarbeit wurde über ein Forschungs-Stipendium der Firma Merz Pharmaceuticals GmbH finanziert.

Publications resulting from this thesis:

Contributions to scientific journals:

- (1) Renner, S., Noeske, T., Parsons, C.G., Schneider, P., Weil, T. and Schneider, G. (2005) New allosteric modulators of metabotropic glutamate receptor 5 (mGluR5) found by ligand-based virtual screening. *ChemBioChem*, 6, 620-625.
- (2) Noeske, T., Gutcaits, A., Parsons, C.G. and Weil, T. (2006) Allosteric modulation of family 3 GPCRs. *QSAR & Comb. Sci.*, 25, 134-146.
- (3) Noeske, T., Sasse, C.B., Stark, H., Parsons, C.G., Weil, T. and Schneider G. (2006) Predicting Compound Selectivity by Self-Organizing Maps: Cross-Activities of Metabotropic Glutamate Receptor Antagonists. *ChemMedChem*, 1, 1066-1068.
- (4) Noeske, T., Jirgensons, A., Starchenkovs, I., Renner, S., Jaunzeme, I., Trifanova, D., Bauer, T., Schneider, G., Parsons, C.G. and Weil, T. (2007) Virtual Screening for Selective Allosteric mGluR1 Antagonists and Structure-Activity Relationship Investigations for Coumarine Derivatives. *Submitted*
- (5) Renner, S., Hechenberger, M., Noeske, T., Böcker, A., Jatzke, C., Schmuker, M., Parsons, C.G., Weil, T. and Schneider, G. (2007) Scaffold-Hopping by 3D-Pharmacophores and Neural Network Ensembles. *In press*
- (6) Noeske, T., Trifanova, D., Renner, S., Parsons, C.G., Schneider, G. and Weil, T. (2007) Self-Organizing Maps to Cluster Compound-Libraries: Identification and Optimization of Allosteric Metabotropic Glutamate Receptor 1 Antagonists. *Submitted*

Abstracts on scientific meetings:

- (1) Noeske, T., Bauer, T., Givehchi, A., Schneider, G., Parsons, C.G., Weil, T., Non-competitive antagonists of mGluR1 – Assay development and molecular modeling investigations. #627.2, *Society for Neuroscience 34th Annual Meeting*, October 23-27, 2004, San Diego, CA, USA.
- (2) Jatzke, C., Wollenburg, C., Liepina, I., Noeske, T., Parsons, C.G., The influence of N-acetyl-aspartyl-Glutamate (NAAG) concentration on the potency of N-acetylated alpha-linked L-Amino dipeptidase (Naaladase) Inhibitors. #627.3, *Society for Neuroscience 34th Annual Meeting*, October 23-27, 2004, San Diego, CA, USA.
- (3) Parsons, C.G., Noeske, T., Bauer, T., Renner, S., Schneider, G., Weil, T., Non-competitive antagonists of mGluR5 – Assay development and molecular modeling investigations. #627.11, *Society for Neuroscience 34th Annual Meeting*, October 23-27, 2004, San Diego, CA, USA.
- (4) Renner, S., Noeske, T., Böcker, A., Weil, T., Schneider, G., Combining supervised and unsupervised neural networks for the identification of novel scaffolds of Metabotropic Glutamate Receptors 5 (mGluR5) modulators. #P008, *1st German Conference on Chemoinformatics*, November 13-15, 2005, Goslar, Germany.
- (5) Noeske, T., Derksen, S., Sasse, BC., Stark, H., Parsons, CG., Weil, T., Schneider, G., Selectivity Profiles for Ligands of Family C GPCRs. #CDD20, *2nd German Conference on Chemoinformatics*, November 12-14, 2006, Goslar, Germany.

- (6) Noeske, T., Renner, S., Parsons, CG., Schneider, G., Weil, T., Successful scaffold-hopping to novel selective allosteric mGluR1 antagonists using a topological atom-pair descriptor. #CDD21, 2nd German Conference on Chemoinformatics, November 12-14, 2006, Goslar, Germany.

Patents:

- (1) Parsons, C.G., Jirgensons, A., Trifanova, D., Kalvinsh, I., Starchenkova, I., Henrich, M., Noeske, T., Weil, T., Kaus, V., Danysz, W. Chromenones and their use as modulators of Metabotropic Glutamate Receptors. *PCT Int. Application* **2007**, WO2007045876.

Abbreviations

2D	Two-dimensional
3D	Three-dimensional
ACPD	<i>1S,3R</i> -1-Aminocyclopentane-1,3-dicarboxylic acid
AD	Alzheimer disease
ADME	Absorption, distribution, metabolism and excretion
AMMPP	1-Adamantan-1-yl-3-(4-methoxy-3-methyl-phenyl)-propenone
ANN	Artificial neural networks
AOS	All orientation search
APS	All placement search
AQP	1-Adamantan-1-yl-3-quinolin-3-yl-propenone
BAY36-7620	3-Ethyl-6-piperidin-1-yl-1,2,3,4-tetrahydro-thioxanthen-9-one
BEM	Basal Eagle's medium
BR	Bacteriorhodopsin
bRho	Bovine rhodopsin
cAMP	Cyclic adenosine monophosphate
CaSR	Calcium sensing receptor
CATS	Chemically advanced template search
CNS	Central nervous system
COBRA	Collection of bioactive reference analogues
CoMFA	Comparative molecular field analysis
CoMSIA	Comparative molecular similarity indices analysis
CPCCOEt	7-Hydroxyiminocyclopropan[b]chromen-1a-carboxylic acid ethyl ester
CPM	Counts per minute
CPPHA	<i>N</i> -[4-Chloro-2-[(1,3-dioxo-1,3-dihydro-2 <i>H</i> -isoindol-2-yl)methyl]phenyl]-2-hydroxybenzamide
CRC	Concentration response curve
CSS	<i>ChemSpaceShuttle</i>
DAG	Diacylglycerol
DCB	3,3'-Dichlorobenzaldazine
DCTT	9-Dimethylamino-3-cycloheptyl-3 <i>H</i> -5-thia-1,3,6-triazafuoren-4-one
DFB	3,3'-Difluorobenzaldazine
DHPG	(<i>R,S</i>)-3,5-Dihydroxy-phenylglycine
DMEM	Dulbeco's modified Eagle's medium
DMeOB	3,3'-Dimethoxybenzaldazine
DMSO	Dimethylsulfoxide
DPM	Disintegrations per minute
ECD	Extracellular domain
<i>ef</i>	Enrichment factor
EMQMCM	(3-Ethyl-2-methyl-quinolin-6-yl)-(cis-4-methoxy-cyclohexyl)-methanone methanesulfonate (synonym: R128494)
EM-TBPC	1-Ethyl-2-methyl-6-oxo-4-(1,2,4,5-tetrahydro-benzo[d]azepin-3-yl)-1,6-dihydro-pyrimidine-5-carbonitrile
FLIPR	Fluorometric imaging plate reader
GABA _B R	γ -Aminobutyric acid type B receptor
GPCR	G-Protein coupled receptor
HD	Heptahelical domain
HEPES	4-(2-Hydroxyethyl)-1-piperazineethanesulfonic acid
HTS	High throughput screening
<i>IC</i> ₅₀	Drug concentration exerting 50% of inhibition

ICD	Intracellular domain
iGluR	Ionotropic glutamate receptor
IP ₃	Inositol trisphosphate
K_d	Dissociation constant
K_i	Inhibition constant
LGO	Leave group out
LOO	Leave one out
LY367385	(+)-2-Methyl-4-carboxyphenylglycine
LY456066	1-Ethyl-2-methyl-6-oxo-4-(1,2,4,5-tetrahydro-benzo[d]azepin-3-yl)-1,6-dihydro-pyrimidine-5-carbonitrile
mGluR	Metabotropic glutamate receptor
MACCS	Molecular Access System
MCPG	(<i>S</i>)- α -Methyl-4-carboxyphenylglycine
Merck1	3'-Fluoro-5'-(5-pyridin-2-yl-tetrazol-2-yl)-biphenyl-2-carbonitrile
Merck2	3-Cyano- <i>N</i> -(1,3-diphenyl-1 <i>H</i> -pyrazol-5-yl)benzamide
(+)MK-801	(+)-5-Methyl-10,11-dihydro-5 <i>H</i> -dibenzocyclohepten-5,10-imine maleate
M-MPEP	2-methyl-6-(3-methoxy-phenyl)ethynyl-pyridine
MOE	Molecular operating environment
MPEP	2-Methyl-6-(phenylethynyl)-pyridine
MTEP	3-(2-Methyl-thiazol-4-ylethynyl)-pyridine
MW	Molecular weight
NIPALS	Non-linear iterative partial least squares
NMR	Nucleic magnetic resonance
NPS 2390	<i>N</i> -(Adamantan-1-yl)quinoxaline-2-carboxamide
PBR	Bacterial periplasmatic amino acid binding protein
PCA	Principal component analysis
PD	Parkinson disease
PHCCC	<i>N</i> -Phenyl-7-(hydroxyimino)cyclopropa[<i>b</i>]chromen-1 <i>a</i> -carboxamide
PKC	Protein bound kinase type C
PLC	Phospholipase C
PLS	Partial least squares <i>or</i> Projection to latent structures
PPI	Prepulse inhibition
PRESS	Predicted error of sum of squares
QSAR	Quantitative structure activity relationship
R193845	(3-Ethyl-2-methyl-quinolin-6-yl)-(rac-4-methoxy-cyclohexyl)-methanone methanesulfonate
R214127	1-[2-Cycloheptyloxy-2-(2,6-dichlorophenyl)-vinyl]-1 <i>H</i> -[1,2,4]triazole
Ro01-6128	Diphenylacetylcarbamic acid ethyl ester
Ro67-4853	2-(4-Fluoro-phenyl)-1-(toluene-4-sulfonyl)-pyrrolidine
Ro67-7476	<i>N,N'</i> -Bis-(3-fluoro-benzylidene)-hydrazine
SAR	Structure activity relationship
SEE	Standard error of estimate
SEM	Standard error of measurement
SEP	Standard error of prediction
SIB-1757	6-Methyl-2-(phenylazo)-pyridin-3-ol
SIB-1893	(<i>E</i>)-2-Methyl-6-styryl-pyridine
SNN	Supervised artificial neural networks
SOM	Self-organizing map
STRESS	Standardized residual sum of squares
TM	Transmembrane helix
UNN	Unsupervised artificial neural networks

Contents

<i>Title</i>	<i>Page</i>	
1	Introduction	1
1.1	The Drug Development Process	1
1.2	G-protein Coupled Receptors	2
1.3	Family 3 G-protein Coupled Receptors	3
1.3.1	The Transmembrane Region	4
1.4	Metabotropic Glutamate Receptors	6
1.4.1	Implications of Group I mGluRs in CNS Diseases	7
1.4.2	Allosteric Modulators of Group I Metabotropic Glutamate Receptors.....	9
1.5	Virtual Screening.....	14
1.5.1	The Pharmacophore Hypothesis.....	16
1.5.2	Similarity Searching	18
1.5.3	Feature Extraction Methods	20
1.5.4	Kohonen-Maps	22
1.5.5	Other Classification Methods.....	24
1.6	Quantitative Structure Activity Relationship.....	25
1.7	Scope of this Thesis	26
1.8	Initial Hypotheses.....	28
2	Assay Development	30
2.1	Membrane Quality - Preliminary Tests	31
2.1.1	Characterization of NMDA receptors within the membrane	31
2.1.2	Conclusions	34
2.2	Development of a Binding Assay for mGluR1.....	35
2.2.1	Experiments.....	35
2.2.2	Conclusions	39
2.3	Development of a Binding Assay for mGluR5.....	39
2.3.1	Experiments.....	39
2.3.2	Conclusions	42
2.4	The Influence of DMSO	43
2.4.1	Experiments.....	43
2.4.2	Conclusions	45
2.5	Scatchard Analysis	45
2.5.1	Saturation Experiments on Cerebellar Membranes.....	46
2.5.2	Saturation Experiments on Cortical Membranes	48
2.5.3	Conclusions	50
2.6	Kinetic Experiments.....	51
2.6.1	On-set and Off-set Studies on Cortical Membranes.....	52
2.6.2	Conclusions	54
3	Methods	55
3.1	Experimental Details.....	55

3.1.1	Preparation of Solutions	55
3.1.2	Membrane Preparation	55
3.1.3	[³ H]-EMQMCM Binding Assay	56
3.1.4	[³ H]-MPEP-Binding Assay	56
3.1.5	Preparation of Cerebellar Granule-cells*	57
3.1.6	IP ₃ -Assay with [³ H]-myo-Inositol*	57
3.1.7	Preparation of and Cultivation of Rat Cortical Astrocytes*	58
3.1.8	Calcium FLIPR Studies*	58
3.1.9	Association Kinetic Studies	59
3.1.10	Dissociation Kinetic Studies	59
3.1.11	Estimation of IC ₅₀ -values	60
3.1.12	Muscarinic Acetylcholine Receptor Assay*	61
3.1.13	Dopamine D ₂ short- and D ₃ -Receptor Binding Assay*	62
3.1.14	Histamine H ₁ -Receptor Binding Assay*	62
3.2	Computational Methods	63
3.2.1	CATS 2D Similarity Search	63
3.2.2	Self-Organizing Maps	64
3.2.3	Principal Component Analysis	65
3.2.4	Comparative Molecular Field Analysis	68
3.2.5	Homology Modeling	70
3.2.6	Datasets	73
4	Scaffold Identification	74
4.1	Data Consolidation	74
4.1.1	Assembling a Data collection	75
4.2	Pharmacophore Model	75
4.2.1	Molecules from the Reference Data collection	76
4.2.2	Creating the Pharmacophore Model	78
4.2.3	Validation	80
4.2.4	Conclusions	83
4.3	Virtual Screening by CATS Similarity Search	83
4.3.1	Reference Compounds and Test Compounds	83
4.3.2	Results of the CATS Similarity Searches and Discussion	84
4.3.3	Conclusions	91
4.4	Data mining by ChemSpaceShuttle	91
4.4.1	Compilation of a focused library	92
4.4.2	Processing the Data	93
4.4.3	Results of the Neighborhood Search and Discussion	96
4.4.4	Conclusions	99
4.5	Virtual Screening using Self-Organizing Maps	99
4.5.1	Training the Maps	100
4.5.2	Selection of Virtual Hits	103
4.5.3	Discussion	107
4.5.4	Conclusions	108
5	Scaffold Optimization	109
5.1	QSAR Studies on Quinoline Derivatives	109
5.1.1	Statistical Evaluation of a CoMFA Model	110
5.1.2	Contour Maps	114

5.1.3	Conclusions	117
5.2	Cross-Activities of Group I mGluR Antagonists.....	117
5.2.1	Target Prediction and Proof of Cross-Activity	118
5.2.2	Conclusions	121
5.3	Hit Optimization and SAR Analysis of Coumarines.....	122
5.3.1	Synthesis Strategy	122
5.3.2	Structure-Activity Relationship.....	124
5.3.3	Discussion and Summary	130
5.3.4	Conclusions	134
5.4	The Hypothesized Allosteric Binding Pocket of mGluR1.....	134
5.4.1	Binding of Coumarines	134
5.4.2	Binding of Quinolines	137
5.4.3	Conclusions	140
6	Summary	141
6.1	Conclusions and Outlook.....	141
6.2	Summary	142
6.3	Zusammenfassung.....	144
7	Appendix.....	149
7.1	Complete mGluR-Data Collection.....	149
7.2	Register of Pharmacophore Features.....	154
7.3	Similarity Lists obtained in Section 4.3.....	155
7.4	Collection of Virtual Hits obtained in Section 4.4.....	161
7.5	Collection of Virtual Hits obtained in Section 4.5.....	162
7.6	Statistical Indices and Compounds from Section 5.1.1.....	165
8	References.....	169
9	Curriculum Vitae.....	191

1 Introduction

1.1 The Drug Development Process

The development of an innovative drug is a long-lasting process with many stages being involved (Figure 1.1-a) [Ng, 2004]. It often starts with the identification of a target (receptor, enzyme, etc.) that has to be modulated to treat a particular disease. Under physiological conditions, the target itself is modulated by endogenous ligands mostly in a relatively unselective manner, that is, a particular ligand interacts with more than one receptor or enzyme. Exogenous ligands which subtype-specifically affect a given target can be detected by high throughput screening (HTS) or computational methods (Section 1.5). They are referred to as “hits” and have to be further refined to a “lead candidate” in a lead optimization process according to their potency, metabolic stability and ADME (absorption – distribution – metabolism – excretion) -properties. The development work has to follow Good Laboratory Practice (GLP) to ensure that proper quality systems are established. Animal models serve as inevitable tools to experimentally test whether or not a given lead candidate evokes the desired effects in a living individual. The drug designated for clinical trials and large-scale production has to be manufactured according to Good Manufacturing Practice (GMP). Here the leading compound is brought into an optimal drug delivery system (e.g., tablet, parenteral solution, etc.), which denotes the final stage of the preclinical phase.

Year	0	1	2	3	4	5	6	7	8	9	10	11	12	13	14	
Costs			€70 million								€240 million			€~360 million		
R&D	Basic R&D, Proof of Principle		Preclinical Research		Clinical Development						Manufacturing & Post Marketing Surveillance					
					Phase 1		Phase 2		Phase 3		Phase 4					
Paperwork	Patent Application		Certificate for Clinical Trial Application								Product License Application		Product License Approval			
Compounds	~ 10,000		10 - 20		5 - 10		2 - 3		1							

Figure 1.1-a. Schematic representation of the different stages involved in the development of a modern drug [Druquest, 2005].

The following clinical development encompasses three phases of clinical trials in which a drug is tested at humans according to three important parameters: harmlessness, effectiveness and quality. Clinical trials are conducted in accordance with Good Clinical Practice (GCP) and they follow regulations and guidelines from the FDA and other approval agencies. Once a drug has successfully passed these stages the manufacturer can apply for a product license followed by a product license approval provided by an approval agency. Phase 4 describes clinical trials that aim at evaluating new indications for the drug.

Today, roughly half of all drugs receiving product license approval are targeted against GPCRs and a considerable number of the best selling prescription drugs act at GPCRs [Klabunde & Hessler, 2002] making them to a promising class of targets for pharmaceutical industries.

1.2 G-protein Coupled Receptors

G-protein coupled receptors (GPCRs) are the largest family of cell-surface receptors involved in signal transmission. They have been successful during evolution in recognizing a wide range of stimuli from photons to large glycoproteins [Bockaert & Pin, 1999]. These receptors transduce extracellular signals in cellular responses *via* heterotrimeric G proteins. Several different signal transduction pathways as well as second messengers are involved in GPCRs function, which are even different among the subtypes of a given receptor. This is a reason for the broad therapeutic potential of GPCRs. Numerous diseases have been linked to specific mutations within the genes encoding GPCRs, marking these receptors as targets for specific therapeutic interventions [Schoneberg *et al.*, 2002; Rattner *et al.*, 1999]. Today 50% of all recently launched drugs are targeted against GPCRs with annual worldwide sales exceeding \$50 billion annually [Med. Ad News Staff, 2004].

All GPCRs share a common central domain composed of seven transmembrane helices, the heptahelical domain (HD), which is also referred to as the transmembrane region [Baldwin, 1993]. On the basis of sequence similarity, mammalian GPCRs have been classified into three major categories, namely the rhodopsin/ β -adrenergic receptors (family 1) which contain many receptors for classical neurotransmitters, the secretin receptor family (family 2) comprising receptors for distinct hormones and peptides and family 3 comprising metabotropic glutamate receptors [Wess, 1998].

1.3 Family 3 G-protein Coupled Receptors

Apart from metabotropic glutamate receptors (mGluRs), family 3 G-protein-coupled receptors (3-GPCRs) comprise the γ -aminobutyric acid type B receptors, (GABA_BR1 and -2) [Jones *et al.*, 1998; Kaupmann *et al.*, 1998], the parathyroid calcium sensing receptors (CaSR) [Brown *et al.*, 1993] and the vomeronasal receptors [Bargmann, 1997], e.g., some taste and putative pheromone receptors [Hoon *et al.*, 1999]. A detailed description about mGluRs will be given in Section 1.4. The calcium-sensing receptor (CaSR) is an ion-sensing GPCR that is allosterically regulated by extracellular calcium and different aromatic amino acids, e.g., L-phenylalanine and L-tyrosine [Conigrave *et al.*, 2000; Kobilka, 2000]. GABA_B is involved in the presynaptic inhibition of transmitter release and mediates the slow synaptic inhibition by increasing the potassium conductance responsible for long-lasting inhibitory postsynaptic potentials [Jones *et al.*, 1998; Kaupmann *et al.*, 1998].

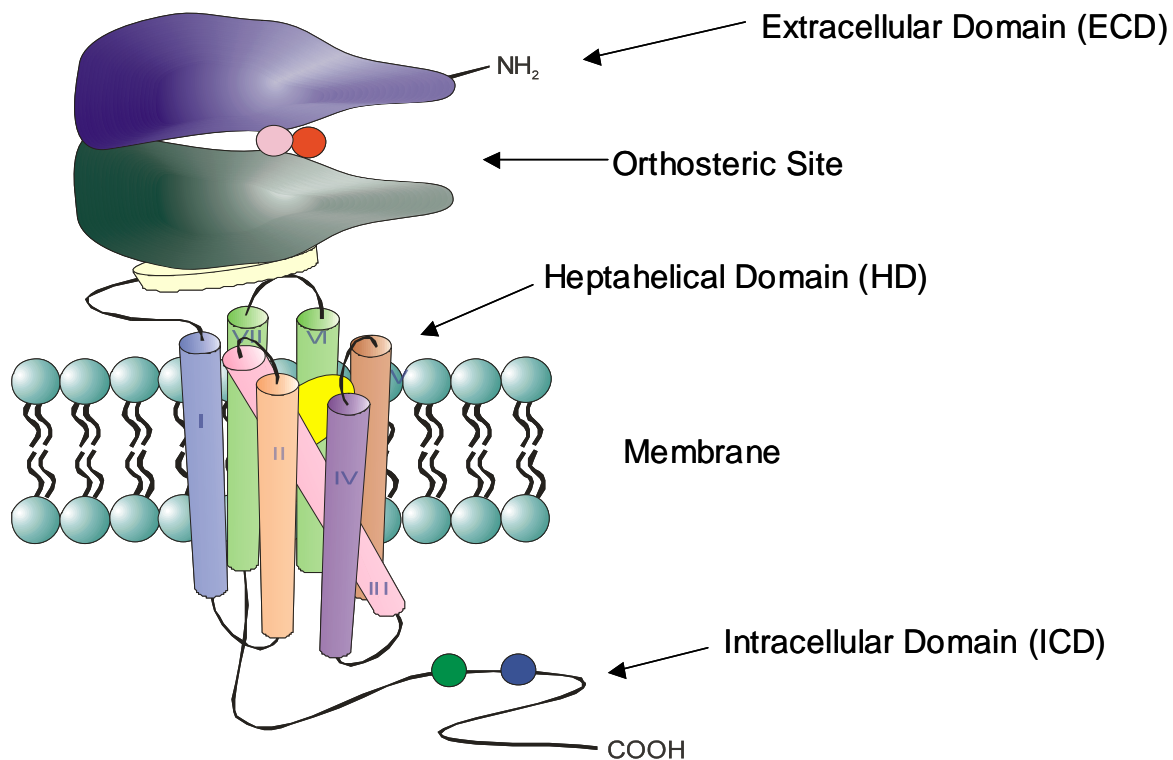


Figure 1.3-a. Schematic representation of a family 3 GPCR according to W. Spooren [Spooren *et al.*, 2001].

3-GPCRs are characterized by an extracellular domain (ECD), a HD consisting of seven transmembrane helices, which are linked by six alternating extracellular and intracellular loops and an intracellular domain (ICD), which contains the C-terminus and the G-protein

interaction sites (Figure 1.3-a). They possess a typical but unique feature: A large extracellular ligand-binding domain (ECD) that shares some sequence similarities with bacterial periplasmic amino acid-binding proteins (PBPs) [O'Hara *et al.*, 1993]. The ECD is characterized by a bilobate structure and adopts a closed conformation on agonist binding in the cleft that separates both lobes and is often called “Venus flytrap module” [Pin *et al.*, 2003; Acher & Bertrand, 2005]. This stands in contrast to most other GPCRs, where natural ligand binding occurs in the HD [Wess, 1993]. The orthosteric binding sites of 3-GPCRs are well understood today, which is mainly due to the success in crystallizing the ECD of mGluR1 with and without glutamate associated [Kunishima *et al.*, 2000] as well as due to detailed mutation studies of both mGluRs [Pin *et al.*, 1999], GABA_B [Galvez *et al.*, 2000] and CaSR [Petrel *et al.*, 2003]. In contrast, little is known about the 3D-structure and dynamics of the HD as well as the binding mode of allosteric modulators. However, in the past, there have been a lot of efforts in the identification of new allosteric modulators, especially in the mGluR area [Eastman *et al.*, 2004; Wang *et al.*, 2004; Poon *et al.*, 2004; Zheng *et al.*, 2005; Kohara *et al.*, 2005; Bonnefous *et al.*, 2005], just to name some. This is mainly due to the fact that ligands binding in the HD possess more drug-likeness than their analogues interacting with the orthosteric site. In particular the application of HTS technologies in pharmaceutical industry facilitated the discovery of agonists and antagonists binding exclusively in the HD of the receptor.

1.3.1 The Transmembrane Region

The precise knowledge of the 3D structure of a given target is a key concern in drug discovery since it facilitates a better understanding of ligand binding, which could be used for a rational design of novel ligands as prospective drug compounds [Cavasotto *et al.*, 2003]. To gain an insight into the 3D-structure and binding sites of proteins the application of X-ray crystallography, electron microscopy and NMR are state of the art. However, the expression, purification and crystallization of membrane proteins remains a challenging process which impedes their structure elucidation [Becker *et al.*, 2003; Stenkamp *et al.*, 2002; Burley & Bonanno, 2002]. Therefore, only a high-resolution X-ray structure of an inactive state of bovine rhodopsin (bRho) and bacteriorhodopsin (BR) is available so far [Okada *et al.*, 2000; Pebay-Peyroula *et al.*, 1997]. In the past, particularly the X-ray structure of bRho has been applied as a template for building homology models of a given GPCR.

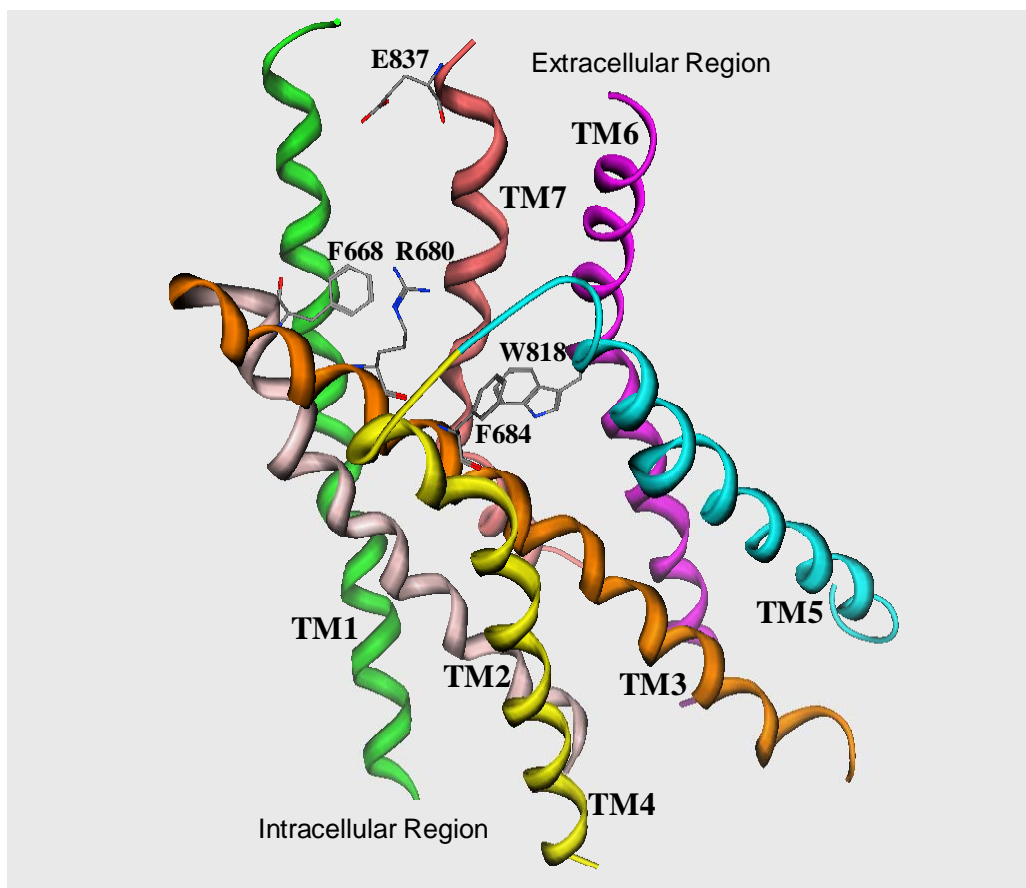


Figure 1.3.1-a. Homology model of the HD of CaSR according to A. Gutcaits [Noeske *et al.*, 2006]. Backbone residues potentially contributing to the ligand binding are depicted.

All GPCRs bear a similar membrane topology. Seven transmembrane segments (H1–H7), predominantly helical, are linked together sequentially by extracellular (EC1, EC2 and EC3) and cytoplasmic loops (C1, C2 and C3) [Baldwin, 1993]. The transmembrane helices are tilted to varying degrees with respect to the putative plane of the membrane bilayer. Despite the common heptahelical architecture of their transmembrane regions, GPCRs are characterized by a relatively low sequence identity (less than 20%), especially when amino acid sequences of two GPCRs from different families are compared such as family 1 and 3. However, it has been demonstrated recently that the backbone of the bRho (family 1) appears to be a reasonable template for building a model of the HD of group I mGluRs and the CaSR (family 3) [Pin *et al.*, 2003; Malherbe *et al.*, 2003a; Miedlich *et al.*, 2004; Hammerland *et al.*, 1999; Hawrot *et al.*, 1998]. In case of GABA_B-receptors their extracellular domain has been investigated in detail [Pin *et al.*, 2003; Hawrot *et al.*, 1998; Galvez *et al.*, 1999; Bernard *et al.*, 2001] as well as the roles of receptor dimers in G-protein signaling and coupling efficacy [Galvez *et al.*, 2001]. Still, no homology model of the transmembrane region of GABA_B-receptors has been published to date.

Using the bRho template despite low sequence similarities is supported by the fact that the HD of mGluRs behaves like any other family 1 GPCR in terms of G protein coupling and regulation by various types of ligands [Goudet *et al.*, 2004]. Like bRho, the HD of mGluRs constitutively couples to G-proteins and is negatively and positively regulated by ligands [Goudet *et al.*, 2004]. Site-directed mutagenesis and molecular modeling performed a detailed analysis of the antagonist binding sites of mGluRs and the binding pocket was found to be equivalent to that of retinal in bRho [Malherbe *et al.*, 2003a; Malherbe *et al.*, 2003b; Pagano *et al.*, 2000].

It has been shown recently that the application of homology models with the aim of performing a virtual screening for new allosteric binders requires special knowledge of the functional activity of the ligand which was used during the construction of the homology model [Bissantz 2003; Bissantz *et al.*, 2003]. Since the X-ray structure of bRho corresponds to the ground state in which retinal is covalently bound [Palczewski *et al.*, 2000] and since GPCRs are known to adopt different conformational states [Gether & Kobilka, 1998] the inactive state of the receptor resembles the “antagonist-bound” instead of the “agonist-bound” state [Bissantz *et al.*, 2003].

Table 1.3.1-a. Definitions of prominent ligand types according to the International Union of Pure and Applied Chemistry (IUPAC) [Wermuth *et al.*, 1998].

Type	Action
<i>Agonist</i>	Endogenous substance / drug that can interact with a receptor and initiate a physiological or a pharmacological response characteristic of that receptor.
<i>Antagonist</i>	Chemical entity that opposes the receptor-associated responses normally induced by another bioactive agent.
<i>Inverse Agonist</i>	Drug which acts at the same receptor as that of an agonist, yet produces an opposite effect. Also called negative antagonists.
<i>Partial Agonist</i>	Agonist, which is unable to induce full activation of a receptor population, regardless of the amount of drug applied.

1.4 Metabotropic Glutamate Receptors

The mGluR family comprises eight subtypes and several splice variants, which have been cloned and named mGluR1-8 according to the succession of the molecular cloning [Pin *et al.*, 2003; Conn & Pin, 1997]. These eight receptors can be further subdivided into three groups based on sequence homology, pharmacology and transduction mechanism: Group I (mGluR1

und mGluR5), Group II (mGluR2 and mGluR3) and Group III (mGluR4, mGluR6, mGluR7 and mGluR8).

Glutamate neurotransmission is primarily mediated by postsynaptic ligand-gated cation channels termed ionotropic glutamate receptors, which regulate membrane potential by opening sodium and calcium channels but it can also be mediated by metabotropic glutamate receptors. Glutamate receptors mediate excitatory transmission on the cellular surface through initial binding of glutamate [Nakanishi & Masu, 1994; Hollmann & Heinemann, 1994]. mGluRs are involved in the generation of excitatory and inhibitory synaptic potentials and synaptic and neuronal plasticity [Nakanishi *et al.*, 1998]. In addition to glutamate, mGluRs are activated by ibotenate and quisqualate.

Group I receptors (mGluR1 and mGluR5) for instance, are localized postsynaptically in the somatodendritic membrane and coupled to the activation of phospholipase C (PLC) [Nakamura *et al.*, 1994] and, thus, are considered to be stimulatory. In contrast, group II and group III receptors are often localized presynaptically. They are negatively coupled to cAMP (Gi/Go-coupled receptors) and inhibit forskolin-induced increases of cAMP in brain slices and neuronal cultures [Prezéau *et al.*, 1994; Bruno *et al.*, 1995].

Group I metabotropic glutamate receptors are positively coupled to PLC. PLC in turn enables the conversion of phosphatidylinositol 4,5-bisphosphate (PIP₂) to diacylglycerol (DAG) and inositol trisphosphate (IP₃). IP₃ has several intracellular effects, e.g., stimulation of Ca²⁺ release from intracellular stores. DAG remains in the membrane activating membrane-bound protein kinase (PKC), which phosphorylates ionotropic glutamate receptors. In contrast to mGlu5 receptors, which can be found in the cortex, mGlu1 receptors are localized in Purkinje cells in the cerebellum targeted to perisynaptic regions [Mateos *et al.*, 2000].

Group I mGluRs have been proven to play an important role in numerous neurodegenerative, cognitive and psychiatric disorders [Spooren *et al.*, 2003] (Section 1.4.1). This thesis is focused on the identification of non-competitive antagonists of this group especially of mGluR1.

1.4.1 Implications of Group I mGluRs in CNS Diseases

mGlu1 and -5 receptor activation influences NMDA responses and consequently cell excitability [Fitzjohn *et al.*, 1996; Awad *et al.*, 2001]. NMDA receptors (activated *via* the neurotransmitter glutamate) are associated with ischemic brain damage, thus mGluRs are assumed to affect the treatment of neurodegenerative disorders like stroke, Alzheimer and

Parkinson disease (AD/PD) and epilepsy. To evaluate the influence of mGluR1 to stroke, the mGluR1 antagonists BAY36-7620 and EMQMCM, an analogue of R214127 (Figure 1.4.2-a), were tested in animal mid cerebral artery occlusion (MCAO) models. Both displayed neuroprotection and the latter also reduced total infarct volume [De Vry *et al.*, 2001; Lesage *et al.*, 2002]. In this context, the mGluR5 antagonist MPEP showed neuroprotective effects in a NMDA-induced toxicity model [Bruno *et al.*, 2000].

Likewise, the pathogenesis of AD and PD is connected with excitotoxicity. It has been reported that stimulation of mGluR1 causes significant increase in β -amyloid formation [Nitsch *et al.*, 1998] and plays a pivotal role in regulating locomotor activity via dopaminergic neurotransmission [Rouse *et al.*, 2000], which in turn is disordered in PD. Moreover, excitation in neurons of the sub thalamic nucleus, induced by the stimulation of mGluR1 and mGluR5 can be completely inhibited by MPEP [Awad *et al.*, 2001].

Glutamate is involved in epileptogenesis [Meldrum & Chapman, 1999]. Orthosteric group I mGluR agonists like ACPD, DHPG and CHPG induce limbic seizures in rats and mice [Tizzano *et al.*, 1993; Camon *et al.*, 1998; Chapman *et al.*, 2000] due to increased glutamate release whereas allosteric antagonists like LY367385 showed anticonvulsant activity [Chapman *et al.*, 1999].

Hypofunction of the glutamatergic system was postulated to be involved in schizophrenia. Thus, receptors modulating the glutamate activity have, at least theoretically, antipsychotic potential. Prepulse inhibition (PPI) of acoustic startle response is an experimental model to assess symptoms connected to schizophrenia (e.g., sensorimotor gating deficits). mGlu1 agonists like DHPG and ACPD are known to disrupt PPI whereas the mGlu1 antagonist MCPG reversed these effects [Grauer & Marquis, 1999]. MTEP, but not EMQMCM, enhanced disruption of PPI induced by the NMDA antagonist (+)MK-801, demonstrating that blockade of mGluR1 and mGluR5 evokes different effects on behavior induced by NMDA receptor antagonists [Pietraszek *et al.*, 2005]. The mGlu5 receptor antagonist MPEP exhibited no effect on the acoustic startle response at anxiolytic doses or above [Spooren *et al.*, 2000].

mGlu1 receptor ligands modulate synaptic plasticity [Manahan-Vaughan *et al.*, 1999] in terms of disruption of long-term potentiation. Antagonists like BAY36-7620 and LY367385 have proven to disrupt learning and memory formation [Manahan-Vaughan & Schuetz, 2002] whereas agonists like ACPD enhanced memory formation in the passive avoidance test [Riedel *et al.*, 1996]. In mice, selective mGlu1 receptor blockade with a R214127 analogue impaired spatial acquisition processes, irrespective of spatial load, as well as spatial reacquisition performed in water maze [Steckler *et al.*, 2004].

Finally, mGlu1 receptor ligands have shown considerable impact on pain, which is reviewed by Lesage [Lesage, 2004]. Agonists like DHPG induced nociceptive behavior in rats [Fisher & Coderre, 1998]. In contrast, antagonists like BAY36-7620 reduced thermal hyperalgesia in a rat model of neuropathic pain [De Vry, 2002].

Summarized, ligands mediating the effects of group I mGlu receptors have considerable impact on the treatment of CNS disorders. Especially modulators binding to the allosteric site seem to be promising since they do not directly affect endogenous ligands binding to the orthosteric site.

1.4.2 Allosteric Modulators of Group I Metabotropic Glutamate Receptors

Within the past years, a substantial number of potent allosteric inhibitors and potentiators of mGluRs has been identified (Figure 1.4.2-a and 1.4.2-b). Their binding sites have been determined to reside exclusively within the HD, far away from the orthosteric site in the ECDs of the receptor [Litschig *et al.*, 1999; Carroll *et al.*, 2001; Knoflach *et al.*, 2001; Schaffhauser *et al.*, 2003; Lavreysen *et al.*, 2003]. In contrast to the orthosteric binding site of mGluRs which is well conserved during evolution, there was no selective pressure to maintain allosteric binding sites. Therefore, most allosteric modulators appear as structurally diverse ligands and several of them bear a high selectivity for a given receptor subtype. *Via* site-directed mutagenesis, specific residues responsible for the subtype selectivities of several ligands have been identified which also enables a characterization of their binding site in the HD [Litschig *et al.*, 1999; Knoflach *et al.*, 2001; Schaffhauser *et al.*, 2003].

Several structurally diverse and highly potent mGluR1 antagonists have been reported [Knoflach *et al.*, 2001; Lavreysen *et al.*, 2003]. Among those, CPCCOEt (Figure 1.4.2-a) was one of the first subtype selective non-competitive mGluR1 antagonists with low micro molar affinity (hmGluR1b) [Litschig *et al.*, 1999; Hermans *et al.*, 1998]. Further mGluR1 antagonists such as R214127, EM-TBPC, LY456066, DCTT and YM-298198 have detected novel scaffolds and shown highest affinities down to the sub-nano molar level (Figure 1.4.2-a) [Mabire *et al.*, 2005, Li *et al.*, 2002; Malherbe *et al.*, 2003a; Zheng *et al.*, 2005; Kohara *et al.*, 2005]. Binding of EM-TBPC to mGluR1 was reported to involve Val-757 and Thr-815. The latter residue is also involved in CPCCOEt binding whereas conversion of Ala-818 did not affect EM-TBPC binding [Malherbe *et al.*, 2003a; Litschig *et al.*, 1999; Knoflach *et al.*, 2001]. Based on a homology model, Malherbe *et al.* suggested that the aromatic ring of EM-TBPC interacts with the cluster of aromatic residues formed from Trp-798, Phe-801 and Tyr-805, thereby blocking the movement of the TM6 helix, which is crucial for receptor activation

[Malherbe *et al.*, 2003a]. Interestingly, they found that radio labeled EM-TBPC showed high affinity for rat mGluR1 (rmGluR1) but only low affinity for human mGluR1 (hmGluR1) and none for mGluR5. Val-757 was identified as the critical residue for the binding selectivity of EM-TBPC at the rat *versus* human mGlu1 receptor since all other mGlu receptors bear leucine at this position. It is worthy of note that the absence of one additional methyl group (valine *versus* leucine) already leads to a considerable decrease in affinity of EM-TBPC for hmGluR1 and the observed selectivity of this ligand for rmGluR1. Since CPCCOEt and BAY36-7620 were shown to displace binding of radio-labeled R214127 to mGluR1a it was suggested that most of the mGluR1 antagonists share the same binding pocket involving TM 5-7.

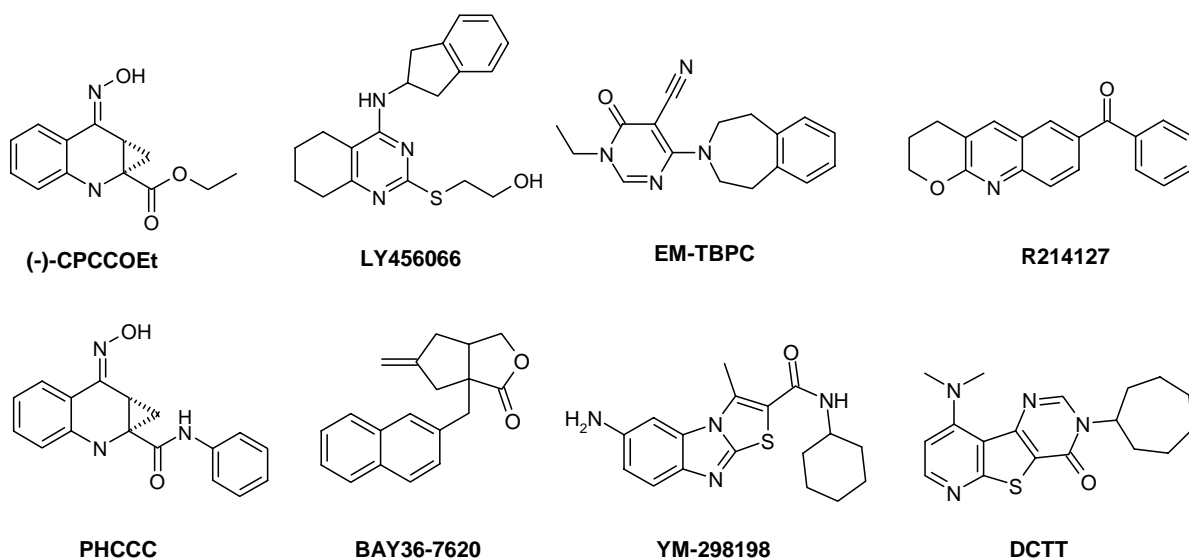
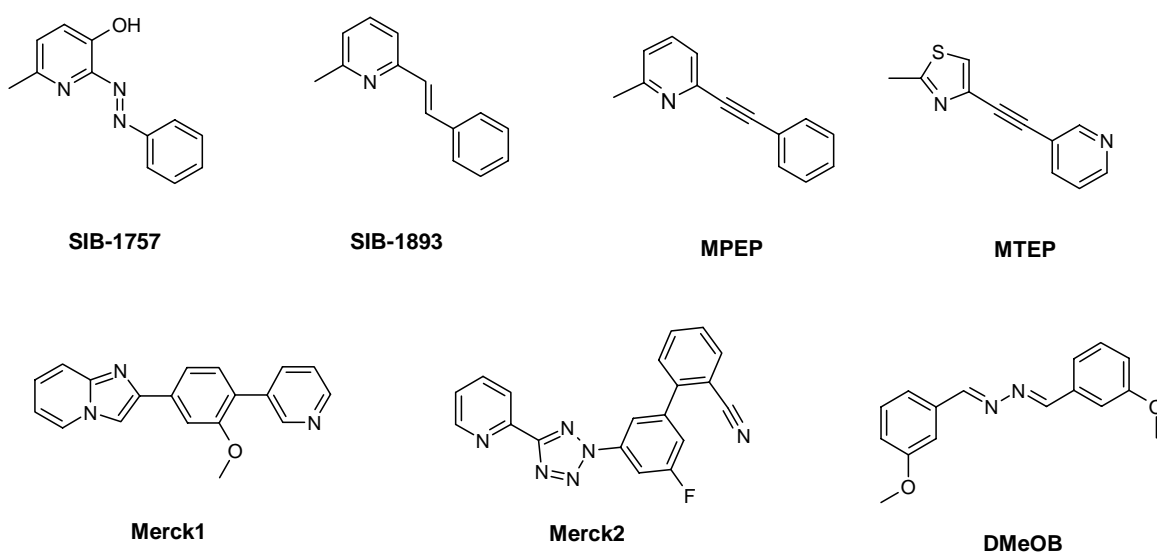
mGluR1:**mGluR5:**

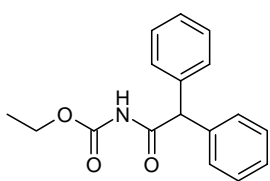
Figure 1.4.2-a. Chemical structures of known negative allosteric modulators of the mGlu1 and mGlu5 receptor.

The first compounds that selectively bind to the allosteric site of mGluR5 were SIB-1757 and SIB-1893 [Varney *et al.*, 1999]. However, both of which revealed only moderate potency. Briefly thereafter, a novel class of mGlu5 receptor antagonists emerged: The pyridine derivative MPEP was the first mGluR5 antagonist that was found to bind to mGluR5 with nano molar affinity [Gasparini *et al.*, 1999] followed by the structural analogue MTEP, a thiazole derivative [Cosford *et al.*, 2003a]. At the beginning, most of the allosteric mGluR5

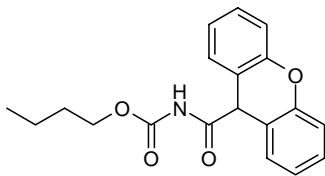
antagonists revealed an MPEP-like structure and only recently, new antagonists with different scaffolds (e.g., compounds Merck1 and Merck2) have been reported [Bonnefous *et al.*, 2005; Eastman *et al.*, 2004; Wang *et al.*, 2004; Poon *et al.*, 2004]. In the past, mainly MPEP was investigated for the characterization of mGluR5 and crucial determinants of the subtype selectivities of MPEP have been identified in TM3 and TM7 [Goudet *et al.*, 2004; Pagano *et al.*, 2000; Litschig *et al.*, 1999]. In two recent studies, several additional residues in TM5 and TM6 of mGluR5 have been demonstrated to contribute to the binding of MPEP. It has been shown that MPEP and the mGluR1 antagonist CPCCOEt bind to overlapping binding pockets in the TM region of mGluR1 and mGluR5, respectively, but interact with different non-conserved residues [Pagano *et al.*, 2000]. Their models suggest that the pyridine ring of MPEP occupies the same space between TM7 and TM3 as the benzene ring of CPCCOEt. However, other parts of these antagonists do not overlap and imply interactions with different TM helices. Recently, a similarity between the critical residues in the TM6 region involved in MPEP-binding site with those of EM-TBPC was described pointing to a common mechanism of inhibition shared by both antagonists [Malherbe *et al.*, 2003b].

A considerable number of positive modulators of group I mGluRs exists based on different structural motives (Figure 1.4.2-b). It was suggested that these enhancers bind to and stabilize the activated receptor states [Malherbe *et al.*, 2003a; Knoflach *et al.*, 2001; Gasparini *et al.*, 2002]. Knoflach *et al.* have described a novel class of ligands Ro 67-7476, Ro 01-6128, and Ro 67-4853 acting as positive allosteric modulators of the mGlu1 receptor. A detailed mutational analysis revealed that in particular Val-757 in the TM5 of the receptor is responsible for the enhancing effect of both Ro 01-6128 and Ro 67-7476 [Knoflach *et al.*, 2001]. Interestingly, Ro 01-6128 and the structurally different Ro 67-7476 bear only high affinity for rat mGluR1 whereas Ro 67-4853, structurally similar to Ro 01-6128, exhibits activity at both h/rmGluR1 and rmGluR5 suggesting a different binding mode for this compound. Moreover, Ro 01-6128 closely resembles a recently found selective, non-competitive agonist of the mGlu7 receptor [Mitsukawa *et al.*, 2005]. Further critical amino acids are located in TM3 and TM5 of mGluR1, at homologous residues where MPEP interacts with the mGluR5 receptor, e.g., close to the inverse agonist binding site [Knoflach *et al.*, 2001; Pagano *et al.*, 2000]. It has been shown that the position of valine (Val-757) is critical not only for the enhancing effect of positive allosteric modulation of rat mGlu1 [Knoflach *et al.*, 2001] but also for negative modulation (MPEP, EM-TBPC) [Malherbe *et al.*, 2003a; Malherbe *et al.*, 2003b]. Therefore, even though Ro 67-7476, EM-TBPC, and MPEP belong to different chemical series, this result indicated that this amino acid occupies a strategic

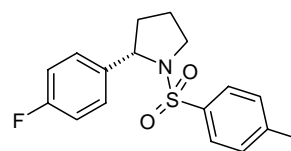
position to gate the effect of positive and negative allosteric modulation [Malherbe *et al.*, 2003b; Cosford *et al.*, 2003a].

mGluR1:

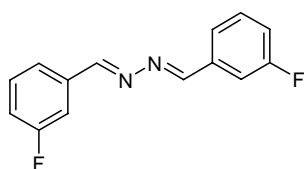
Ro 01-6128



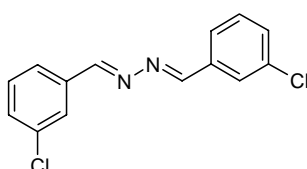
Ro 67-4853



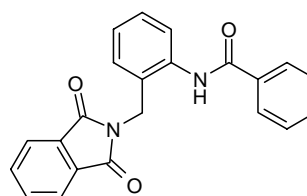
Ro 67-7476

mGluR5:

DFB



DCB



CPPHA

Figure 1.4.2-b. Chemical structures of known positive and neutral allosteric modulators of the mGlu1 and mGlu5 receptor.

Furthermore, allosteric inhibitors of mGluR1 or mGluR5 signaling, such as PHCCC, SIB-1893 and MPEP, have shown to be weak allosteric potentiators of mGluR4 signaling [Maj *et al.*, 2003; Marino *et al.*, 2003; Mathiesen *et al.*, 2003] and a series of benzaldazine analogues (Figure 1.4.1-b) has exhibited everything from allosteric potentiation to allosteric inhibition to neutral cooperativity on mGluR5 signaling [O'Brien *et al.*, 2003]. Recently, allosteric potentiators of the mGlu5 receptor have been described [Kinney *et al.*, 2005]. Most interesting examples include DFB [O'Brien *et al.*, 2003] and CPPHA. Although both potentiators increase the affinity for glutamate, only DFB partially displaces allosteric antagonists such as the radio labeled MPEP-derivative [3H]-3-methoxy-5-(pyridin-2-ylethynyl)pyridine [O'Brien *et al.*, 2003; Cosford *et al.*, 2003b]. Therefore, it was proposed that CPPHA binds to a different binding site within the HD. Since DFB shares a similar binding pocket with mGluR5 antagonists, a series of DFB analogues was designed where a transition from positive (DFB) *via* silent to negative modulation was achieved [O'Brien *et al.*, 2003]. The crucial substituent that determines the mechanism of action were found to be the 3-fluoro-phenyl-groups of DFB. Substitution of both groups by a chloro-substituents (DCB)

resulted in a “silent” or neutral agonist without functional activity whereas substitution with a dimethoxy-group (DMeOB) yielded the respective allosteric antagonist. All these ligands were found to compete with each other as well as with the radio labeled antagonist and MPEP-derivative [³H]methoxy-PEPy pointing to the same binding pocket [O’Brien *et al.*, 2003].

The identification of novel ligands selectively interacting with a group I mGlu receptor subtype via the allosteric site was one goal of this thesis. In general two major strategies exist which are commonly pursued by pharmaceutical companies: High throughput screening (HTS) and virtual screening (Section 1.5).

1.5 Virtual Screening

Pharmaceutical research in chemical industry aims at discovering novel ligands that potently and selectively affect a given target of interest. This initial investigation can be assumed as a first step on a long way from a hit to a drug (Section 1.1). Two major strategies addressing this phase emerged within the second half of the last century: HTS and virtual screening. HTS and its technical extension *ultra*-HTS provide a common way to detect a first hit *via* a “blind-screening” and they allow for scanning hundreds of thousands of compounds using an appropriate assay system with highly sensitive detection devices in order to limit the occurrence of false positives and false negatives [Bajorath, 2002]. Large amounts of compounds are tested quickly within a relatively short period of time. However, this screening technique is combined with several inherent disadvantages. Although handling with small volume fluids lots of wasted laboratory material result from HTS. Noteworthy are the low hit rates significantly ranging below 1% and the relatively high costs of establishing and maintaining HTS assays. The common single point determination of a compound, regularly employed to speed up the throughput is inherently associated with an increase of false positives and, even worse, false negatives. High throughput automatically leads to high volumes of data being recorded during the screening process. Methods to efficiently retrieve, manipulate and analyze biological and chemical data (“data mining”) to determine the best series to follow up have been reviewed elsewhere [Böcker *et al.*, 2004].

The HTS-approach based upon manifold pharmacological experiments can be rationalized by means of computational methods [Agrafiotis *et al.*, 2002; Bajorath, 2002]. Several techniques exist attempting to virtually retrieve potential hits from the synthetically feasible

chemical space and they are named virtual screening methods [Böhm & Schneider, 2000]. The idea of these “intelligent” approaches is to drastically reduce the amount of compounds prior to experiments, thus saving money, time and waste. This strategy is particularly pursued by small pharmaceutical companies in order to circumvent HTS campaigns, but also large companies trust on the advantages of virtual screening methods. Consequently, pharmaceutical companies rely on virtually screening commercial compound libraries, hence retrieving potential hits and assembling activity-enriched subsets to achieve higher hit rates than HTS approaches. It must be emphasized that virtual screening techniques require structural information about the receptor and/or its ligands. If no such knowledge is available HTS becomes essential.

Some virtual screening techniques like pharmacophore (Section 1.5.1) and topological searches (Section 1.5.2) will be introduced here as well as other related methods of data reduction and data visualization (Section 1.5.3 and 1.5.4). Finally, methods that are not within the scope of this thesis will be presented (Section 1.5.5). Combined with subsequent screening assays of limited (i.e., medium to low) throughput virtual screening techniques avoid many of the issues (*vide supra*) connected with HTS.

These techniques have in common that they describe approaches to prioritize molecules from (commercial) compound libraries, hence producing activity-enriched subsets of compounds that can then be tested for some desired properties [Xu & Agrafiotis, 2002]. Such databases may contain already synthesized compounds as well as synthetically accessible virtual molecules.

Often hierarchical approaches are applied starting with filters, which step wise reduce the number of molecules to be tested. Starting from simple filters that remove molecules not obeying common criteria of drug-likeness, e.g., the “Rule of Five” [Lipinski *et al.*, 1997] or molecules bearing reactive and/or toxic groups, the initial database becomes considerably reduced. Subsequent methods, e.g., based on several similarity searches (Section 1.5.2) [Willett *et al.*, 1998] or 3D pharmacophore searches, for instance, (Section 1.5.1) further minimize the molecular subset of interest. Docking experiments which sample conformations of small molecules into a protein-binding site describe one of the last possible step. Automated docking is time consuming and requires detailed information about the structure of the protein. Thus, they are often disfavored as primary virtual screening tools [Bissantz *et al.*, 2005, Evers *et al.*, 2005]. Nevertheless, docking is frequently applied as far as sufficient computing capacity is available.

Complexity and target specificity increase from filter to filter in this hierarchy whereas the number of molecules (not necessarily) drastically decreases. Eventually, the remaining few molecules can be characterized in pharmacological experiments. Apart from docking methods which are named structure-based approaches, methods like pharmacophore or similarity searches belong to the ligand-based approaches since they are solely based on information derived from ligands affecting a particular target. In general, the latter approaches are applicable to prescreen databases and in particular, e.g., for investigations lacking information about the architecture of the target.

Success or failure of ligand-based approaches depends on the availability of (ideally but not necessarily) potent and selective ligands serving as a starting point whereas structure-based approaches rely on precise receptor information as well as the choice of a docking method combined with an appropriate scoring function [Warren *et al.*, 2005]. Nevertheless, the suitability of docking experiments based on homology models has also been discussed [Bissantz *et al.*, 2003b, Hillisch *et al.*, 2004].

Even though HTS and virtual screening (here: mainly ligand-based virtual screening methods like clustering or similarity searches) pursue different approaches in finding novel ligands it should be stressed that the drug discovery process benefit from combining both [Stahura & Bajorath, 2004].

1.5.1 The Pharmacophore Hypothesis

Many investigations and applications of 3D-SAR analyses are based on pharmacophore hypotheses. The term “Pharmakophor” was introduced by Paul Ehrlich in 1909, nearly a century ago, to describe the molecular structure or pattern, which “carries” (*phoros*) the biological activity of a drug (*pharmakon*) [Ehrlich, 1909]. According to Lemont Kier “pharmacophore” is derived from “chromophore”, which denotes the associated conjugation length that impart a particular color to a chromophoric molecule [Kier, 1971]; likewise, combination of structural features impart a certain bioactivity to a molecule. The International Union of Pure and Applied Chemistry (IUPAC) recently stated that a pharmacophore is the ensemble of steric and electronic features that is necessary to ensure the optimal supramolecular interactions with a specific biological target structure and to trigger (or to block) its biological response [Wermuth *et al.*, 1998].

Pharmacophore hypotheses are generally applied to propose certain properties (features) of structurally diverse ligands that are required to affect a macromolecular target when the three-dimensional architecture of this binding site is not known. Often, they display common 3D-

patterns based upon distances (often also planes) and angles between particular features of the ligands and the complementary points of these features in the binding site of the macromolecule. Instead of this classical geometric definition a spherical coordinate system has been proposed recently where geometric parameters are put together and each pharmacophore point is, thus, described alone in spherical reference coordinates [Guérin *et al.*, 2006].

Ligands can interact with amino acids of a given target *via* hydrogen-bonding (H-bond donor/acceptor), hydrophobic (dispersive) interactions, aromatic π - π stacking, cation- π interactions or electrostatic properties (partial charges). As different atoms may have similar properties (e.g., O and S in carbonyl or thiocarbonyl groups) different atoms of potential ligands can affect a particular target in the same way. Consequently, structurally diverse molecules may bind to a receptor in the same manner as long as they provide a similar ensemble of features. An ideal pharmacophore model should specify not only information about these interactions; accurate descriptions of hydrogen-bond vectors pointing from the H-bond donor or acceptor centers towards the virtual receptor (spherical caps) complete a pharmacophore hypothesis [Guérin *et al.*, 2006].

A careful selection of appropriate ligands considered in a pharmacophore model and a reasonable alignment of these molecules form a crucial step in setting up a hypothesis. Potential difficulties for this approach might arise from scaffolds showing different binding modes. Even a single ligand may adopt different binding modes. Occasionally, molecules bind to the target in a way distinct to the pharmacophore hypothesis' prediction.

Molecules, virtually retrieved from databases, can be tested for their activity or affinity towards a given target. They, in turn, may give a hint about the reliability of a pharmacophore hypothesis, i.e., they allow for refining an existing model. However, a hypothesis remains as long a model as the crystal structure of the receptor is unknown. This representation of the receptor helps to confirm or disprove the correctness of the model. It has, however, been evidenced that side chains or even backbone movements can occur when different ligands bind to a given target structure ("induced fit"), which impairs automated rigid docking [Birch *et al.*, 2002]. Detailed informations about the advantages of automated docking in fast screening and molecular dynamics (MD) simulations suitable to explore the binding of a few selected hit candidates can be found elsewhere [Alonso *et al.*, 2006].

Pharmacophore hypotheses, based on the alignment of ligands, have been adressed to several aspects in drug discovery, namely to search queries for virtual screening of databases [Sheridan *et al.*, 1989; Kuntz, 1992], to target structures of *de novo* design [Tschinke &

Cohen, 1993; Waszkowycz *et al.*, 1994; Lloyd *et al.*, 2004] and molecular-graphics-aided molecular design [Glen *et al.*, 1995] and, eventually, to many 3D-QSAR analyses [Cha *et al.*, 2003; Zhu *et al.*, 2005] (Section 1.5.5).

1.5.2 Similarity Searching

Similarity searching denotes techniques to pair-wise compare a set of molecules. These methods enable scientists to virtually screen a database for compounds that resemble the query molecule. The underlying idea of this concept is the “similarity principle”, which was explicitly stated some years ago: Structurally similar molecules should exhibit similar physicochemical and biological properties [Johnson & Maggiora, 1990].

Similar to molecular docking which comprises (i) suitable docking methods and (ii) scoring functions, similarity searches in general consist of (i) descriptors appropriately encoding the molecules and (ii) similarity functions. Substructure similarity can be defined based upon exact chemical fragments - e.g., MACCS keys [MDL Information System] – or pairs and triplets [Carhart *et al.*, 1985; Good & Kuntz, 1995; Schneider *et al.*, 1999;]. Since similarity searching is not restricted to a common core it allows for detecting molecules with a topology distinct from the structure of the compound the search is based on (“scaffold hopping”) [Schneider *et al.*, 1999]. A general benefit of similarity searches in contrast, e.g., to 3D-pharmacophore searches or automated docking is the high computation rate as it only compares descriptors.

This approach has considerable influence on the drug discovery path medicinal chemists pursue. Once a substructure is known to be associated with certain desirable activities or affinities, other molecules bearing the same fragment can be detected and assayed for that profile [Barnard, 1993]. Manually searching for compounds with the same substructure was time-consuming and has become more and more ineffective due to the increasing number of experimentally determined hits.

The characteristics of substructure searching have led to the development of similarity searching [Downs & Willett, 1995]. Similarity searching needs representations of the molecules that are effective (i.e., representations that can differentiate between different molecules) and efficient (quick to calculate) [Willett *et al.*, 1998]. These representations or molecular descriptors in turn can be compared using suitable numerical measures or coefficients. Some coefficients are measures of the distance (e.g., Hamming distance, Euclidean distance), or dissimilarity between objects (0 value for identical objects), while

others directly measure similarity (most commonly 1 for identical objects) [Willett *et al.*, 1998].

One of the most prominent similarity indices is the Jaccard coefficient also known as the Tanimoto coefficient [Jaccard, 1901], which compares binary descriptors of molecules and can be formulated as follows:

$$s_{AB} = \frac{|\chi_A \cap \chi_B|}{|\chi_A \cup \chi_B|}, \quad (\text{Eq. 1.5.2-a})$$

where χ_A is the number of bits set to 1 in the bit string vector coding for compound A, and χ_B is the number of bits set to 1 in the bit string vector coding for compound B. Tanimoto coefficient values range from 0 to 1. In general, a similarity score larger than 0.85 is assumed to reveal molecules with similar biological activity [Matter, 1997]. Recent findings showed that biological similarity is not so strong: At ≥ 0.85 Tanimoto similarity in Daylight fingerprints [Daylight], only 30% of compounds similar to an active were themselves active [Martin *et al.*, 2002]. The enrichment factor *ef* provides a simple way to quantitatively express the ability of a method to retrieve an activity-enriched subset from a library [Xu & Agrafiotis, 2002]:

$$ef = \frac{\left(\frac{A_{sub}}{D_{sub}} \right)}{\left(\frac{A_{all}}{D_{all}} \right)}, \quad (\text{Eq. 1.5.2-b})$$

where D_{sub} is a virtually retrieved subset of molecules from the complete library D_{all} . This subset contains a certain amount A_{sub} of bioactive molecules, whereas A_{all} denotes the total amount of bioactive compounds within the library. An *ef* of 1 describes an activity-enriched subset with a random distribution of active compounds. Values above 1 correspond to successful searches.

Since similarity searching relies on the comparison of descriptor vectors rather than on the computationally more demanding alignment of two molecules, it allows for rapidly retrieving a set of candidates from a large library [Willett *et al.*, 1998]. Therefore, two pivotal aspects need to be considered when performing a similarity search [Schneider & So, 2003]:

1. The chosen molecular descriptors must appropriately cover the structural features that are connected to the corresponding SAR.
2. There must exist a strong correlation between varieties in molecular descriptions and varieties in biological function provided by the applied similarity measure.

Molecular similarity is employed for many objectives in virtual screening: Design of diverse libraries, discovery of novel scaffolds and as support for establishing SAR [Glen & Adams, 2006]. Several techniques have been proposed and evaluated like fingerprint searches [Whittle *et al.*, 2004], two-dimensional atom environment searches [Bender *et al.*, 2004] topological pharmacophore searches [Schneider & Nettekoven, 2003], feature tree searches [Rarey & Dixon, 1998], simple, yet effective substructure analyses [Gillet *et al.*, 1998] and, recently, 2D property descriptor value range-derived fingerprints (PDR-FP) [Eckert & Bajorath, 2006], just to name a few.

1.5.3 Feature Extraction Methods

Molecular compounds can be described by a large number of attributes or features like topological indices, molecular field parameters, etc. leading to multidimensional data representations. Feature extraction describes approaches to transform such a set of raw data into a new coordinate system, generally from a high-dimensional into a low-dimensional (most commonly 2D and 3D) space by removing irrelevant features. Several linear and non-linear data reduction techniques have been proposed that might help to describe the shape of the original data distribution. Some information-theoretic functions have been compared and combined with classifiers to assess the effectiveness of the selection methods [Liu, 2004]. The probably most prominent statistical feature extraction method with widespread applications is the principal component analysis (PCA) [Lugger *et al.*, 1998; Otto, 1999], which conducts a linear data projection from a multi-dimensional data matrix to a low-dimensional space by means of a projection matrix resulting in a score matrix. The score matrix in turn comprises rows (e.g., molecules) and columns (principal components). Figure 1.5.3-a gives an example how such a data distribution is visualized. Axes in the new coordinate system denote “factors” or “latent variables”.

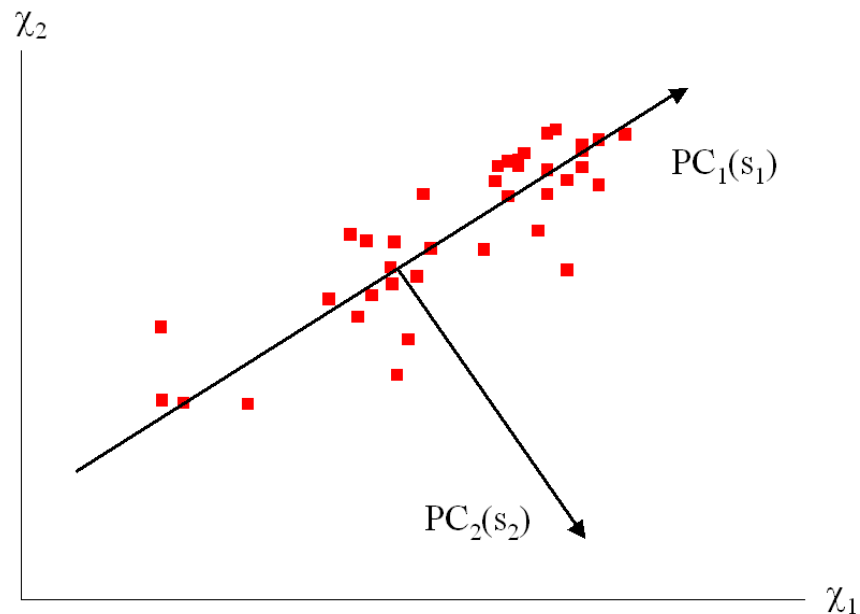


Figure 1.5.3-a. Linear mapping of a set of two-dimensional data by two principal components. Abscissa (χ_1) and ordinate (χ_2) span the coordinate system. The perpendicular score vectors s_1 and s_2 were calculated according to the maximal convergence criterion.

Since multidimensional data of SAR often do not follow a linear distribution [Agrafiotis & Lobanov, 2000], the linear reduction can produce misleading relationships between individual data points [Devillers, 1995]. Therefore, also non-linear data projection methods, namely SOMs [Zupan & Gasteiger, 1999] and non-linear PCA based upon NIPALS algorithms or encoder networks [Livingstone, 1996] found their way to applications like machine learning, artificial intelligence and parallel processing. These methods are unsupervised procedures (Section 1.5.4) and can be employed as a first step of data analysis. Encoder networks or ReNDeR (reversible non-linear dimension reduction) networks [Livingstone, 1996] reduce the input patterns to an arbitrary number of neurons, forming the parameter layer (i.e., the coordinates or “factors” of the low-dimensional map), followed by transferring the information to the output layer. Thus, the input layer is reproduced at the output layer *via* a simple internal representation. The number of input neurons and accordingly of output neurons depends on the amount of data vectors to be used. Assumed that there exist no hidden layers and hence the neurons have a linear transfer function the number of factors (output vectors) is identical to the amount of principal components. Here, non-linear mapping is facilitated by non-linear activities of the neurons forming the hidden layers.

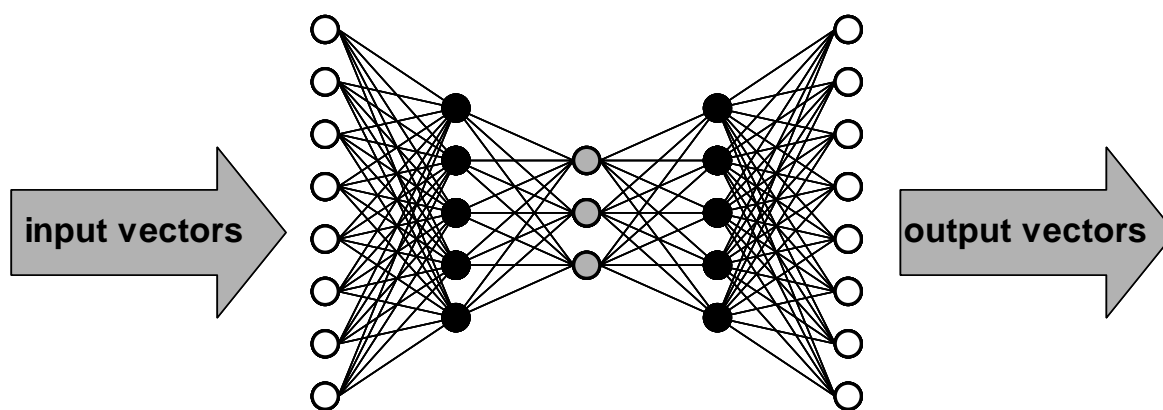


Figure 1.5.3-b. Architecture of a typical encoder network. Empty circles denote input neurons (“fan out units”) and output neurons, respectively. Lines represent weights. Filled circles are hidden layers with sigmoidal or linear activity. Grey circles display the parameter layer.

An integrating tool for data projection and 3D visualization termed *ChemSpaceShuttle* has been reported [Givehchi *et al.*, 2003]. It performs non-linear data reduction based upon encoder networks and the NIPALS algorithm and served within this thesis as a method to manually select potential virtual hits from a large subset (Section 4.4).

1.5.4 Kohonen-Maps

Artificial neural networks (ANN) are straightforward statistical methods to construct linear or nonlinear correlations of features (e.g., descriptors) that classify molecule patterns [Katz *et al.*, 1992; Schneider & Wrede, 1998]. They exhibit a relationship between features and observed data [Zupan & Gasteiger, 1999].

ANN can be divided into supervised neural networks (SNN) and unsupervised neural networks (UNN). In contrast to unsupervised neural networks supervised neural networks require not only a set of molecules but also the knowledge of target values or class-membership (active/inactive). Nonlinear modeling of QSAR, classification, pattern recognition, data compression, etc. are the main applications for SNN (e.g., multilayer feed forward networks, encoder networks) whereas UNN (e.g., Kohonen- or Hopfield-networks) can be used for clustering, visualization and methods similar to those employed for SNN without the prior knowledge of pharmacological molecular activities [Schneider & Wrede, 1998].

SOMs or Kohonen-networks constitute a special type of unsupervised neural networks and have been employed for a variety of tasks in chemistry and chemical biology ever since [Zupan & Gasteiger, 1999], predominantly for clustering, topology preserving projections and

feature extraction [Schneider & So, 2003]. Each neuron or “receptive field” denotes a cluster of molecules as a result of the nonlinear mapping procedure where the Kohonen algorithm is applied (Section 3.2.2) [Kohonen, 1982]. The molecules of a particular neuron have a similar distribution of features and they can be represented by the molecule, which is in closest vicinity to the centroid of the corresponding neuron.

Kohonen has introduced the concept of self-organizing topological feature maps which can be arranged as a map, most often either in a one-dimensional array or a two-dimensional plane of neurons [Kohonen, 1982]. The toroidal wrapping of an array (to a circle) and a map (to a torus) circumvents potential boundary problems associated with a planar topology. Kohonen-maps are single layer networks and their neurons are located in a defined topology, meaning that each of them has a defined number of neighboring neurons. Maps are visualized by circles or by columns and rows forming squares (Figure 1.5.4-a). Each neuron has either four (squares) or six (hexagons) neighbors.

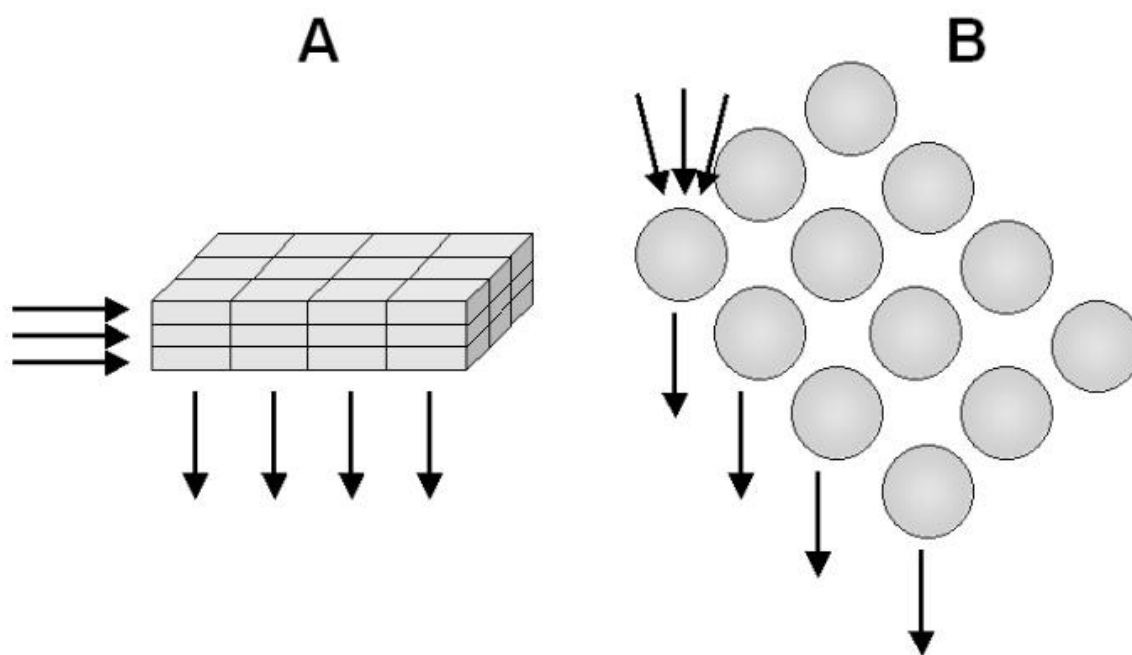


Figure 1.5.4-a. Visualization of neurons in the Kohonen network according to Zupan and Gasteiger [Zupan & Gasteiger, 1999]. Neurons can either be drawn as small boxes of several layers forming columns and rows (A) or as circles (B). Black arrows coming from the left (A) or above (B) represent the arbitrary number of input, the other arrows denote the output vectors.

1.5.5 Other Classification Methods

Until now only those virtual screening techniques applied within this thesis were presented. There exists a bunch of other methods that allow, e.g., for classifying molecule entries of large compound libraries into potentially active and inactive members. Some of the most prominent tools with widespread application in the field of computational chemistry and biology will be introduced here.

The naïve Bayesian method is a straightforward classification technique, which is mainly used for HTS data analysis to distinguish between “active” and “inactive” compounds. It is based on the Bayes rule for conditional probability and imparts the assumptions that descriptors in the reference set are equally important and independent from each other. Multiplying individual probabilities results in combined probability. This classifier can be used for virtual screening [Bender *et al.*, 2005] or to predict molecule properties like ADME [Klon *et al.*, 2006].

Support vector machines (SVM) belong to the supervised learning methods [Vapnik, 1998]. They provide a machine-learning algorithm that basically projects input vectors to a very high-dimensional feature space and constructs an optimal hyper plane, which best separates data points into two classes. The mapping is described by a kernel function, which performs either linear or non-linear classifications [Boser *et al.*, 1992]. In a retrospective study SVM have proven to yield comparable or better results than supervised ANN if employed for drug/nondrug classification [Byvatov *et al.*, 2003]. Prospective virtual screening for ligands affecting dopamine D_{2/3}-receptors benefits from the advantages of SVM [Byvatov *et al.*, 2005].

Decision tree learning describes a tree-shaped graph of decisions comprising nodes (or leaves) and branches where nodes represent decisions and branches denote conjunctions of these features [Breiman *et al.*, 1984]. Starting from a root node an object or situation has to undergo an arbitrary number of decisions of attributed tests resulting regularly in yes or no. Decision trees provide attractive classifiers due to their high execution rate. However, they cannot expand to unlimited complexity as they will lose accuracy. Random forest classifiers, in turn, grow multiple trees in random subspaces and avoid a loss of accuracy caused by overwhelming decision patterns [Ho, 1995]. Decision trees and random forests are commonly employed for classifying and prioritizing compounds for testing [Muegge *et al.*, 2001; Svetnik *et al.*, 2003].

In a recent study a set of seven classification methods was employed to divide databases into active and inactive compounds for five different targets [Plewczynski *et al.*, 2005]. The applicability of each method for each target was assessed by means of enrichment factor, precision and recall of all positives that have been retrieved. It turned out that random forests, artificial neural networks and support vector machines lead to high enrichments of actives, whereas random forests are successful in reducing the number of false positives (precision).

1.6 Quantitative Structure Activity Relationship

The concept of the quantitative structure activity relationship (QSAR) model is a classical example of ligand-based approaches where the physicochemical together with pharmacological and structural properties of ligands play an important role in terms of predicting bioactivity data. This field has been explored more than forty years ago [Hansch & Fujita, 1964]. QSAR methods try to exhibit correlations between structural informations of a set of molecules and their bioactivity data in order to give predictions for new molecules regarding these data. Compounds to be included in QSAR studies most often display related structures differing only in the type of substituents being attached to the common core. Free-Wilson analysis denotes an early 2D-QSAR method [Free & Wilson, 1964]. It is a regression technique using the presence or absence of substituents or groups as the only molecule descriptors in correlations with biological activity [Kubinyi, 1993]. This crude method has some pitfalls: (i) In contrast to Hansch analysis and more recent methods it lacks the influence of electrostatic properties and (ii) the properties of new substituents – even if they resemble already existing substituents (e.g., methyl vs. ethyl) – can not be predicted by this method.

Setting up a QSAR model is a multi-stage process. The first step is to select appropriate descriptors, i.e., descriptors, which best describes a set of molecules for a given task. The variety of descriptors is manifold. 1D descriptors (e.g., MW) are normally constitutive descriptors giving no hint about the chemical structure. 2D descriptors comprise structure key descriptors, e.g., the UNITY fingerprints [Tripos], Daylight fingerprints [Daylight] and other fragment fingerprints, which are, however, preferably used for similarity searching than for QSAR. They can be calculated from the connection table representation and, therefore, they are not dependent on the conformation of a molecule and are most suitable for large database studies. 3D descriptors are derived from the three-dimensional conformation of a molecule; they characterize molecules according to their molecular volume, several surface areas and molecular interaction fields [Van Aalten *et al.*, 1996; Lin *et al.*, 2000]. More recent 3D-QSAR

descriptors used for CoMFA (alignment dependent) [Cramer *et al.*, 1988] and CoMSIA studies [Klebe *et al.*, 1994] account for encoded combinations of steric, electrostatic and hydrophobic properties (Section 3.2.4).

The next step comprises feature selection, which describes the step where certain attributes are chosen that are assumed to be relevant to generate reasonable correlations between descriptors and biological data. The final step in constructing a QSAR model is to formulate a mathematical relationship and to determine the model parameters. Linear methods like multiple linear regression (MLR) and partial least squares (PLS) are commonly used methods [Fernandez *et al.*, 2006; Sirois *et al.*, 2005]. PLS, like PCA, uses latent variables for the molecule descriptors and the biological responses, from which a linear model is derived. Cross-validation is necessary to avoid overfitting of the data and to evaluate the quality of prediction. In contrast, self-organizing maps and encoder networks provide ways of non-linear correlation methods. Once a model is built it has to be validated, meaning the prediction accuracy has to be estimated. Leave-one-out (LOO), leave-group-out (LGO) and bootstrapping are the most common techniques [Topliss & Edwards, 1979; Diaconis & Efron, 1983, Cramer *et al.*, 1988b].

QSAR studies aim at investigating the binding modes of certain structural classes of molecules affecting a given target as this way was pursued within this thesis. They do not belong to the virtual screening techniques as neither databases will be searched nor will novel scaffolds be found. Predictions can be done only upon existing molecule patterns. In general, they are suitable for activity or affinity optimization projects for molecules representing the same scaffold.

1.7 Scope of this Thesis

One aim of this thesis was to identify new scaffolds for compounds that allosterically inhibit group I metabotropic glutamate receptors (mGluRs), in particular mGluR1. Computer assisted virtual screening can be applied either based on knowledge about the receptor's architecture (structure-based) or a set of bioactive reference ligands (ligand-based) [Böhm & Schneider, 2000]. We planned to pursue the latter approach since the precise structure of the heptahelical domain of group I mGluRs is still unknown. The idea within the scope of this thesis was to employ various virtual screening methods for the given task and to evaluate their effectiveness. However, before initiating such ligand based searches, as much information as feasible about already existing agents has to be gathered and exploited to increase the

probability of success, which was another goal of this thesis. In this context we planned to compile a reference data collection comprising mGluR1 and mGluR5 allosteric inhibitors. The chemical structures including bioactivity data of the reference compounds should be obtained from literature and patents. Based upon a small selection of highly potent and selective mGluR1 antagonists a pharmacophore hypothesis for mGluR1 should be established thereafter providing an initial insight into common features and structural requirements for receptor inactivation by these ligands.

The computer-assisted methods to be used within this thesis include similarity searching with the CATS atom-pair descriptor, 3D pharmacophore query searches as well as molecule clustering and mapping onto a plane by self-organizing maps (SOM) or into a 3D space by non-linear principal component analysis. These approaches denote ways to detect structurally new ligands, which is termed “scaffold hopping” [Schneider *et al.*, 1999]. Virtual hits should be ordered from commercial vendors and screened in-house for the desired affinity and activity at the receptor.

To realize this pharmacological screening, binding assays addressing allosteric sites of mGluR1 and mGluR5 must be developed, which was also a goal of this thesis. Comparable binding assays for non-competitive modulators of group I mGluRs have not been reported to the best of our knowledge. Compounds ordered from vendors have to be tested on these assays afterwards. Since it was our strategy to avoid HTS, binding assays to be developed herein should facilitate limited throughputs. Compounds to be found by virtual screening campaigns providing novel core structures with significant potency should help to continuously refine the existing pharmacophore hypothesis and, thus, to propose binding orientations for potentially new compounds as well as for representatives of an earlier published chemical series of quinolines [Mabire *et al.*, 2005]. Another aim was to obtain information about structural features important for the inhibitory potential of these quinolines, which should be realized by 3D QSAR studies.

If any virtual screening campaign turned out to detect a set of molecules with inhibitory activity at mGluR1, promising representatives shall be chemically modified to optimize their pharmacological properties (that is increase of affinity and inhibitory activity at mGluR1). Furthermore, we also planned to establish selectivity profiles for representative mGluR1 and mGluR5 antagonists. A virtual screening concept should allow to predict cross activities for these types of ligands.

1.8 Initial Hypotheses

Initially, we hypothesized that binding assays for allosteric mGluR1 and mGluR5 antagonists on a 96-well plate format could be established starting from an already running NMDAR binding assay on 24-well plates (Section 2.2, Section 2.3).

Following, hypotheses for the identification of new scaffolds of negative allosteric mGluR1 modulators were formulated. We postulated that a pharmacophore model based upon a selection of potent and selective non-competitive mGluR1 antagonists should be capable of retrieving an activity-enriched subset of a vendor compound library (Section 4.2).

We further hypothesized that reference molecules employed for the pharmacophore model could also serve as reference compounds for similarity searching and that the CATS descriptor [Schneider *et al.*, 1999] would best describe topological similarities (Section 4.3).

The application of a tool performing non-linear principal component analyses (*ChemSpaceShuttle*) should narrow down a large set of compounds characterized by a multidimensional space so that a small subset of the initial database could be retrieved for further experimental testing (Section 4.4).

According to our hypothesis the CATS descriptor should be applicable to adequately encode molecules for clustering by means of self-organizing maps (SOM). SOM should enable a discrimination between all available non-competitive mGluR1 and mGluR5 antagonists. Moreover, the SOMs employed in this project should be capable of detecting hidden relationships between a large set of structural diverse reference (mGluR1) and test molecules (Section 4.5).

Some hypotheses were proposed after first results of the scaffold identification were obtained. Since clustering of reference and test compounds according to the SOM algorithm led to promising results regarding molecule distribution and visualization (Section 4.5.1), we were tempted to speculate that this method should also facilitate the prediction of cross-activities for reference compounds (Section 5.2).

We also hypothesized that a meaningful CoMFA model could be derived from a recently published set of quinoline derivatives acting as non-competitive mGluR1 antagonists [Mabire *et al.*, 2005] (Section 5.1). The conclusions drawn from this QSAR model in turn should improve our understanding about the orientation of quinolines in the mGluR1 binding site.

A hit optimization project was launched for coumarines (Section 5.3). All side chains of this chemotype should systematically be modified. The idea was to generate a set of structural analogues large enough to derive comprehensive SAR data. We postulated that these data

might simplify considerations about the hypothetical ligand orientation at the recognition site of mGluR1 (Section 5.4).

2 Assay Development

We wished to identify ligands binding to group I mGluRs. To this means, it was necessary to characterize not only whether they bind to the allosteric binding site of the given receptor but also what functional consequences this binding evokes. The question arises: Does ligand interaction with the receptor cause an activation or blockade of the intracellular signal cascade (here: Ca^{2+} -mobilization from intracellular Ca^{2+} -stores). Binding assays address the first issue whereas functional assays address the latter one. Summarized, together they are indispensable tools to pharmacologically characterize new ligands. We wished to avoid HTS due to disadvantages like high costs and low hit rates (Section 1.5), and rather developed binding and functional assays characterized by high data content and moderate throughput. Combined with the virtual screening campaigns that will be introduced in later this strategy proved to be suitable for our hit-finding process. Once established, the assays allowed us to verify or falsify predictions which were based upon the results of virtual screenings (Chapter 4). More precisely, the presumed potency of “virtual hits” found by virtual screening campaigns had to be supported by data from real experiments.

Functional and binding assays for targeting mGlu1 and –5 receptors were already developed in-house. However, the existing binding assays were relatively cumbersome to handle and were associated with a low throughput of test compounds. Consequently, the first step of the practical work was to establish new binding assays for both receptor subtypes. More detailed, one goal was to convert the read out formats of mGluR1 and mGluR5 binding assays based on a 12-well millipore system to a state of the art 96-well plate format, hence facilitating the performance of binding experiments with an increased number of compounds whilst saving materials and time.

Note: For the sake of clarity most experiments that failed were not mentioned within this chapter. Only a few of them have explicitly been included in case they could give helpful hints for further assay development processes. Furthermore, it must be stressed that affinity values were given as IC_{50} -values and not as K_i -values. The K_d -value of the radioligand, which is necessary to calculate the K_i -value from the IC_{50} -value (Section 3.1.11), is specific for a particular binding assay / radioligand and was indeed determined by binding saturation experiments [McKinney, 1998] during the assay development process (Section 2.5). However, the radioligand concentration chosen for displacement experiments was low enough

to have only a modest effect on the difference between K_i and IC_{50} . Furthermore, for SAR, relative differences are more important, and these are the same for both IC_{50} and K_i .

Eventually, it should also be emphasized that all results calculated from the luminescence reader MicroBeta[®] Trilux (e.g., IC_{50} , percent of inhibition, etc.) were based on raw data given as counts per minute (CPM) and not as disintegrations per minute (DPM). We are well aware that DPMs denote the more precise values since they are bias corrected (i.e., they only consider flashlights caused by radioactive decays). However, the procedure for determining this ratio between flashlights triggered by decays or by any other influences (“quenching”) cannot be performed for the present assay conditions.

2.1 Membrane Quality - Preliminary Tests

Preliminary binding tests were necessary to evaluate several basic parameters like the choice of an appropriate membrane / protein concentration and suitable screening plates. They were performed with cortical rat membranes expressing NMDA-receptors using [³H]-(+)-MK-801 as a radioligand, since this assay is well characterized in house (using the millipore system), robust, exhibits low non-specific binding values and is easy to perform, e.g., long incubation times at room temperature.

2.1.1 Characterization of NMDA receptors within the membrane

In a pilot experiment only positive (“bound”) and negative (“non-specific”) controls were tested on various screening plates at different membrane concentrations. Positive control describes a status where the radiotracer can interact with the membrane without being displaced by any competitor. In contrast, the negative control denotes that status where the radioligand should be totally displaced from the binding site with a highly potent competitor. The competitor or “cold displacer” is generally the unlabeled compound or, where possible, a closely related, potent and specific analogue in roughly several thousand-fold higher concentrations. In general, a background negative control of less than 20% of the full signal is assumed to be adequate for screening purposes.

The reaction volumes of positive and negative controls (containing a radioligand concentration of 5nM, a membrane-suspension of 0.2/0.4/0.6 mg/ml, glycine/glutamate at a concentration of 10 μ M to facilitate channel access of the radioligand and 10 μ M (+)-MK-801 as cold displacer) were either incubated on a regular 96-well plate (transparent plastic plate

with flat-bottom wells) [Greiner Bio-One GmbH] and afterwards transferred for filtration to an opaque 96-well plate with glass fiber filters at the bottom of each well (“multiscreen plate”) [Millipore GmbH] or directly incubated on a “multiscreen plate”. Incubation was terminated after two hours by rapid vacuum filtration of the reaction volume through the filters using a vacuum manifold. The filters were rinsed four times with 150 μ l ice-cold Tris-buffer (50mM, pH 7.5). After washing scintillation cocktail Ultima-GoldTM [Perkin Elmer Life Sciences] (40 μ l / well) was added to the filter and the plates were incubated for another 16 hours. Then radioactivity was measured in a MicroBeta[®]Trilux [Perkin Elmer Life Sciences].

For the first plate (incubated on an opaque 96-well plate) a good signal-to-background ratio was only obtained at 0.60 mg/ml membrane concentration (11.4% non-specific). For the second plate (incubated on a multiscreen plate) there was no signal over background for any protein concentration, leading to the assumption that the reaction volume should preferably be incubated on a regular 96-well plate prior to transferring to a multiscreen plate.

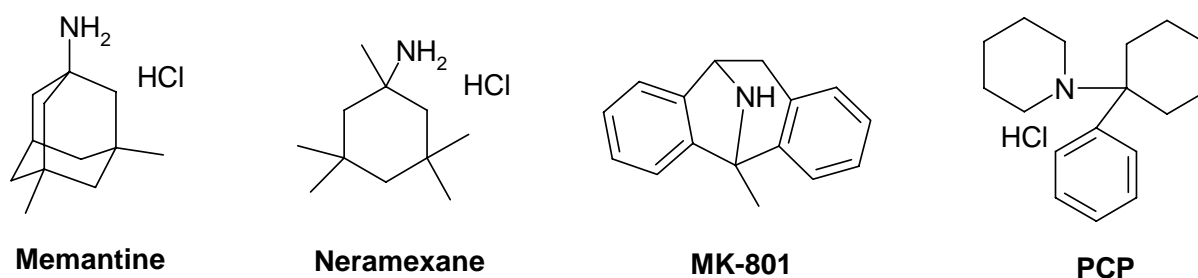


Figure 2.1.1-a. Chemical structures of known NMDA receptor antagonists.

In a subsequent experiment, the influence of varying protein concentrations on the IC_{50} -value was evaluated by means of conducting full concentration response curves (CRC) for (+)MK-801 (Figure 2.1.1-a) at two different membrane concentrations. Since membrane concentrations of 0.20 mg/ml or 0.40 mg/ml were previously found to be too low for sufficiently high signals, membrane concentrations of 0.60 mg/ml and 0.80 mg/ml were used (Figure 2.1.1-b). A good signal-to-background ratio (12-13% background) was obtained for both whereas the absolute counts were dependent on membrane concentration (1715 CPM for 0.60 mg/ml vs. 1914 CPM for 0.80 mg/ml, data not shown).

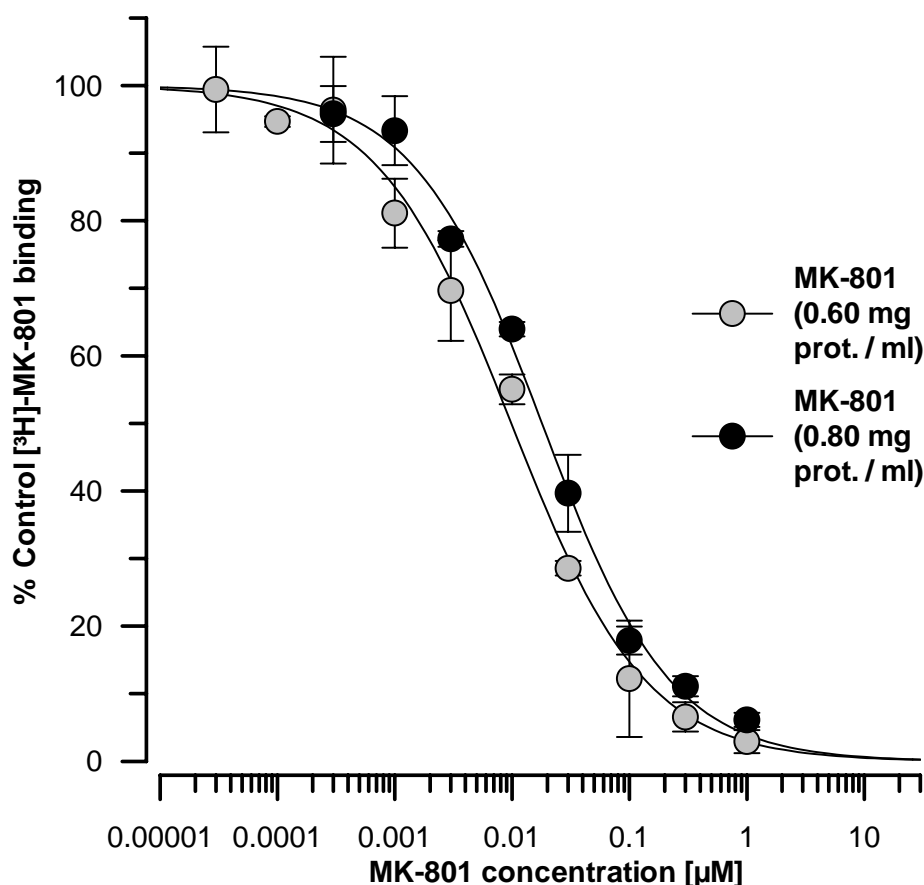


Figure 2.1.1-b. Concentration response curves for (+)MK-801 displacing [³H]-(+)-MK-801 at two different concentrations of membrane. The unlabeled ligand revealed a calculated IC_{50} -value of 9.9 nM (lower membrane concentration) and 18.0 nM (higher membrane concentration), respectively.

The affinity values of (+)MK-801 obtained for this experiment correspond well with those given in literature (K_d -value of the radioligand 16.5nM) [Foster & Wong, 1987], which demonstrated that the binding assay was successfully performed giving reliable results. Moreover, the significantly increased CPM values for the higher membrane concentration (~12%) showed that no binding saturation was reached at least for the experiment with the lower membrane concentration since DPM values and also CPM values could linearly correlate with the radioactive emission of a sample.

To confirm the robustness of the assay the experiment was repeated twice with a sufficiently high membrane concentration (0.80 mg protein per ml) by means of conducting CRCs for other NMDA antagonists namely Phencyclidine (PCP), Memantine and Neramexane (Figure 2.1.1-a, Figure 2.1.1-c). Other parameters like incubation time and temperature (2 hrs, room temperature), plate format and washing process remained unchanged.

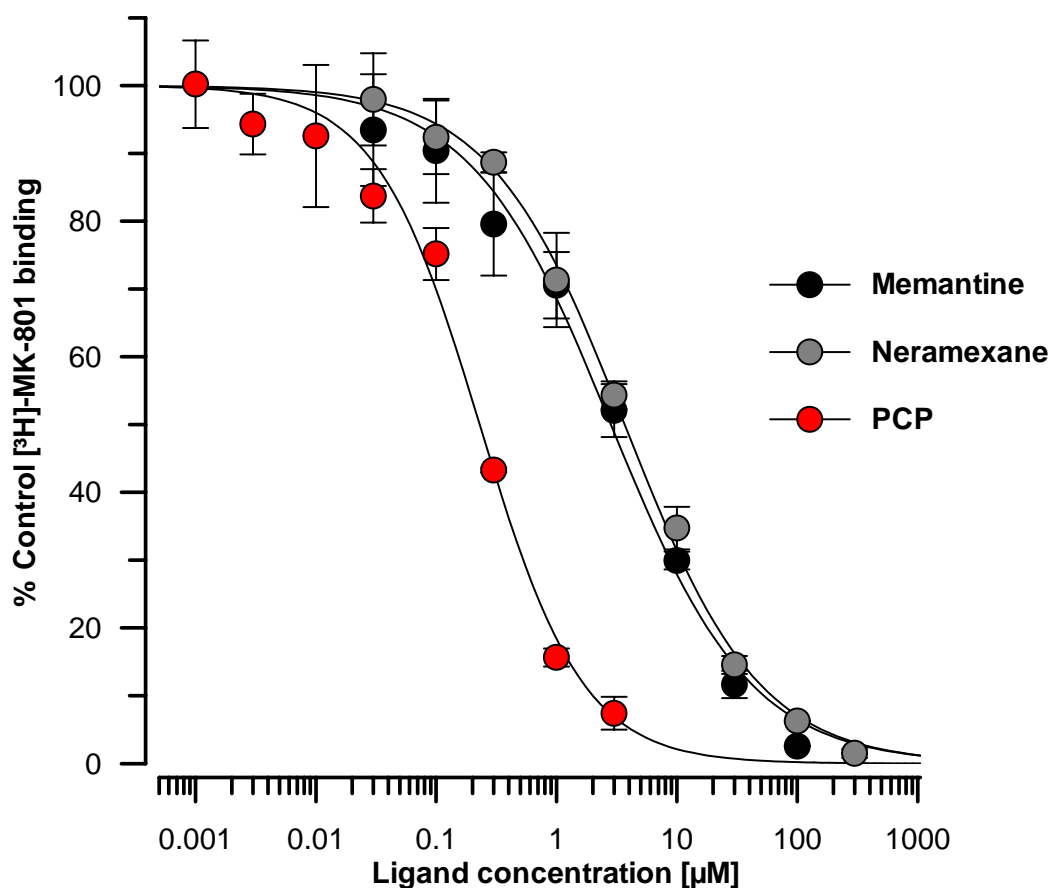


Figure 2.1.1-c. Concentration response curves for Memantine (IC_{50} -value: $2.82\mu\text{M}$; SEM: 0.33), Neramexane ($3.68\mu\text{M}$; 0.31) and PCP ($0.229\mu\text{M}$; 0.023) displacing $[^3\text{H}]$ -(+)-MK-801 from the NMDAR binding site. Results represent the mean values of two independent experiments performed in quadruplicate.

Both experiments were successfully carried out and reliable results for all reference compounds were obtained when comparing the IC_{50} -values to K_i -values published in literature (Memantine $0.69\mu\text{M}$, Neramexane $0.68\mu\text{M}$ and PCP $0.04\mu\text{M}$) [Bresink *et al.*, 1995; Parsons *et al.*, 2000]. Satisfying signal-to-background ratios were achieved for all ligands (9-12% background, data not shown).

2.1.2 Conclusions

The NMDAR binding assay is simple to perform and facilitated the transfer of general binding assay procedures to a new system. All parameters applied herein served as initial parameters for setting up binding experiments for mGluR1 and -5, respectively.

2.2 Development of a Binding Assay for mGluR1

First, a binding assay with increased throughput to detect allosteric mGluR1 modulators was developed.

2.2.1 Experiments

The same conditions as for the NMDAR binding assay were applied for an initial mGluR1 binding assay (membrane conc. 0.80 mg/ml, incubation time 2hrs at room temperature). Radio labeled (+)MK-801 was replaced with [³H]-EMQMCM, which is a high-affinity ligand at the allosteric site of the mGlu1 receptor [Mabire *et al.*, 2005] and a structural analog to the quinoline R214127 [Lavreysen *et al.*, 2003]. The concentration of radioligand was changed from 5nM to 1nM because of its potent binding affinity. R193845 (30μM), which is also an analog of R214127 served as cold displacer (Figure 2.2-a). To evaluate the validity of the assay the affinities of three already known non-competitive mGluR1 antagonists that served as reference compounds, R193845, NPS 2390 and the propenone AMMP [Mabire *et al.*, 2005; Van Wagenen *et al.*, 2000; Parsons *et al.*, 2006], were determined by full CRCs (Figure 2.2.1-a, Figure 2.2.1-b). EMQMCM served also as a reference compound in several mGluR1 experiments and was frequently used within this thesis.

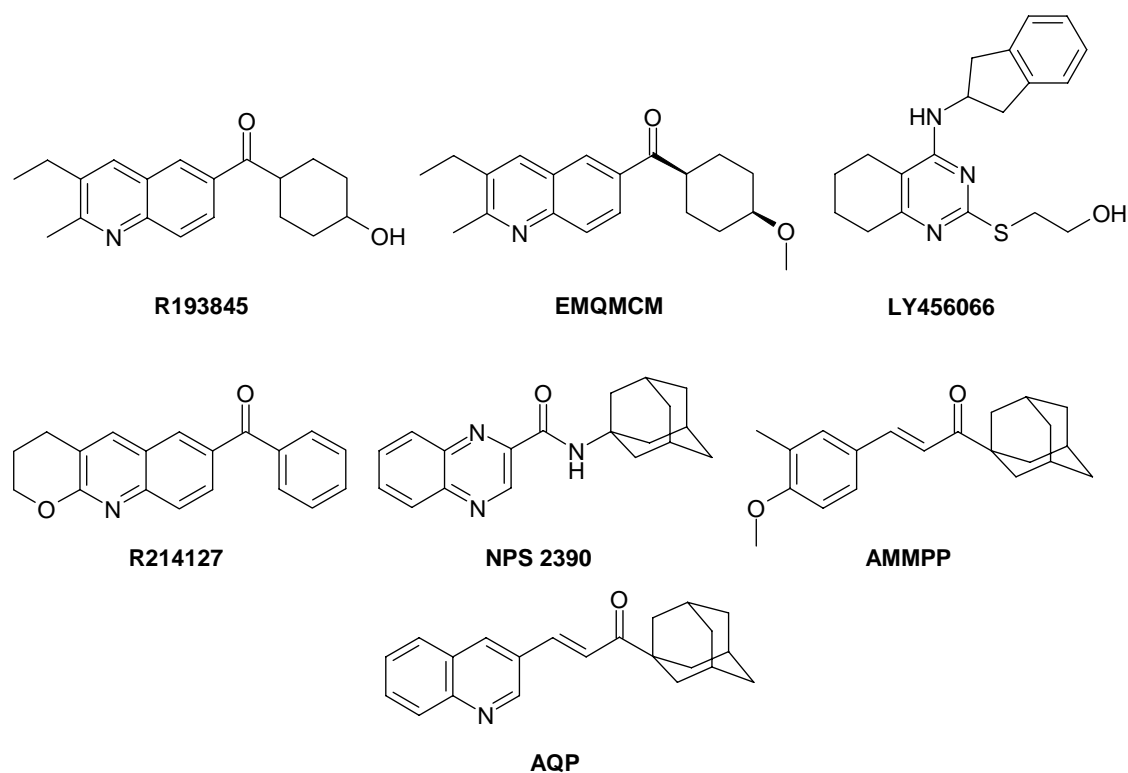


Figure 2.2.1-a. Chemical structures of known non-competitive mGluR1 antagonists that were used during assay development.

A surprisingly high signal-to-background ratio was achieved with a mean background of 5% (data not shown). In this context, relatively high absolute values of above 2500 CPM were obtained giving a hint that either the protein concentration or the incubation time could be reduced. However, the obtained IC_{50} -value of NPS 2390 was more than 100-fold weaker than reported in literature (K_d -value 1.4nM) [Lavreysen *et al.*, 2003]. Here, an IC_{50} -value of 259nM for NPS 2390 [Van Wagenen *et al.*, 2000] and 120nM for R193845 was obtained (Figure 2.2.1-b). The considerable deviation between experimentally obtained affinity for NPS 2390 and the affinity given in literature was probably caused by slight precipitation, which was observed while diluting the stock solution (compound dissolved in pure DMSO) with an excess of buffer. As demonstrated by the error bars, the raw data of AMMPP (IC_{50} -value: 497nM) also showed strong variation. This was probably also due to poor solubility.

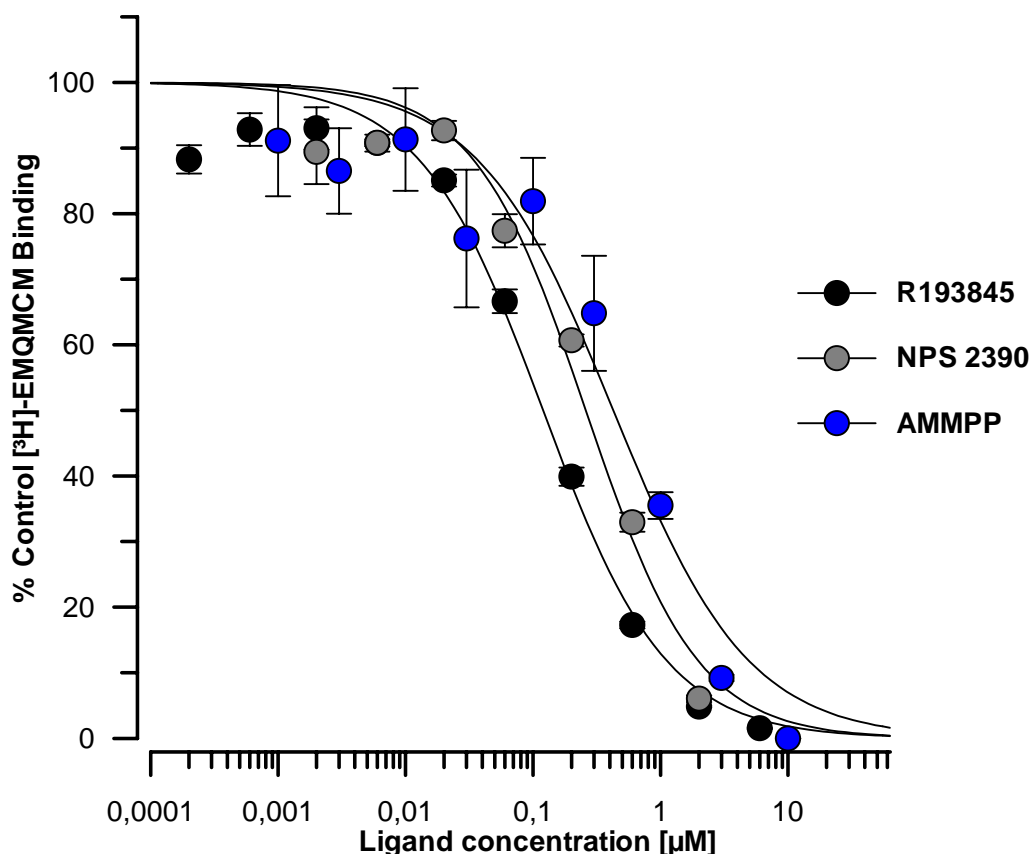


Figure 2.2.1-b. Concentration response curves for R193845 (IC_{50} -value: 0.120μM; SEM: 0.017), NPS 2390 (0.259μM; 0.038) and AMMPP (0.497μM; 0.116) displacing $[^3H]$ -EMQMCM from the rmGluR1 binding site. Experiment was performed in quadruplicate. Error bars denote SEM.

The less than optimal concentration response curves indicate that the assay was not yet suitable for screening. For the next experiment the settings were slightly changed in terms of

the incubation time, which was shortened to one hour. To avoid solubility problems connected with the compounds tested before, concentration response curves were conducted for two other allosteric mGlu1 receptor modulators namely LY456066 [Li *et al.*, 2002] and the propenone AQP [Parsons *et al.*, 2006] (Figure 2.2.1-c). However, AQP turned out to be poorly soluble when the stock solution was diluted with buffer to the desired concentrations. This is confirmed by the corresponding CRC where data points deviate considerably from the fitted curve. Moreover, LY456066 elicited more than ten-fold weaker binding compared with literature values (IC_{50} -value 142nM vs. K_d -value 9.3nM).

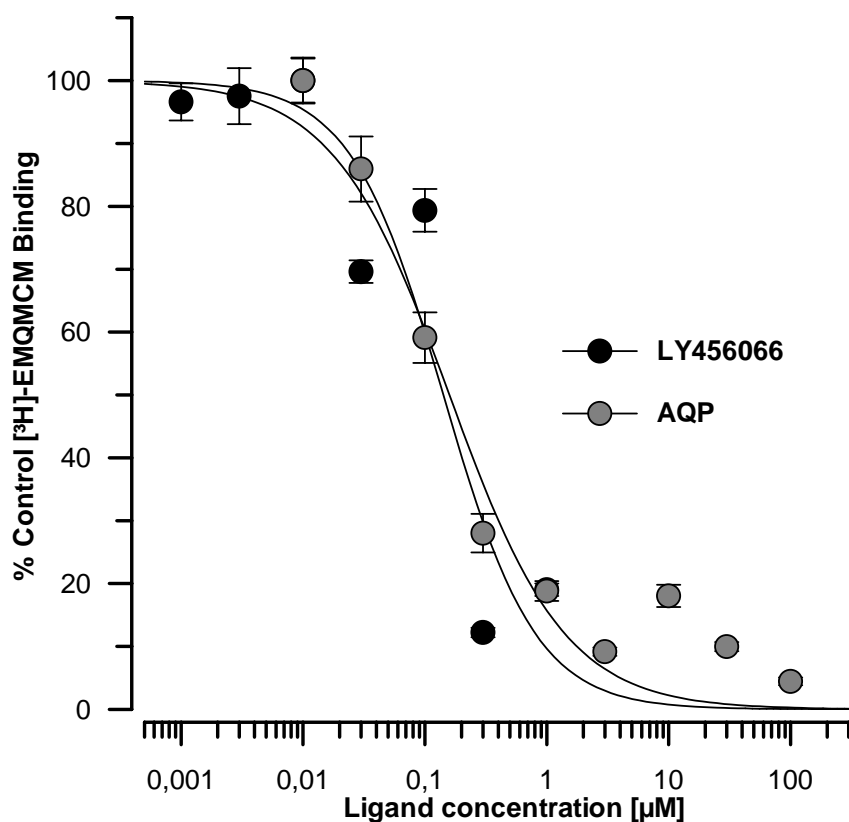


Figure 2.2.1-c. Concentration response curves for LY456066 (IC_{50} -value: 0.142 μ M; SEM: 0.041) and AQP (0.159 μ M; 0.036) displacing [3 H]-EMQMCM from the rmGluR1 binding site. Experiment was performed in quadruplicate. Error bars denote SEM.

At this stage, the binding assay was still not optimized since it lacked reliable results for well-known mGluR1 antagonists, i.e., results that were consistent with those reported in literature. As the poor solubility of some test compounds seems to be a major pitfall of the incorrect affinity values it was decided to add DMSO as solvent with a final concentration of 5%. The procedure is detailed in Section 2.4.

In this context another binding experiment was performed (Figure 2.2.1-d) determining the potency of EMQMCM, a potent allosteric mGluR1 antagonist [Mabire *et al.*, 2005]. The

previous assay parameters remained unchanged except for the addition of 5% DMSO (final concentration) to increase the solubility of the compounds to be tested. The experiment was repeated twice and the resulting affinity values were consistent with activity data published by Mabire *et al.* (binding 3.4nM vs. functional 3nM). This clearly demonstrates that reliable results can be produced allowing for screening test compounds thereafter.

The final assay procedure is given in the experimental part (Section 3.1.3).

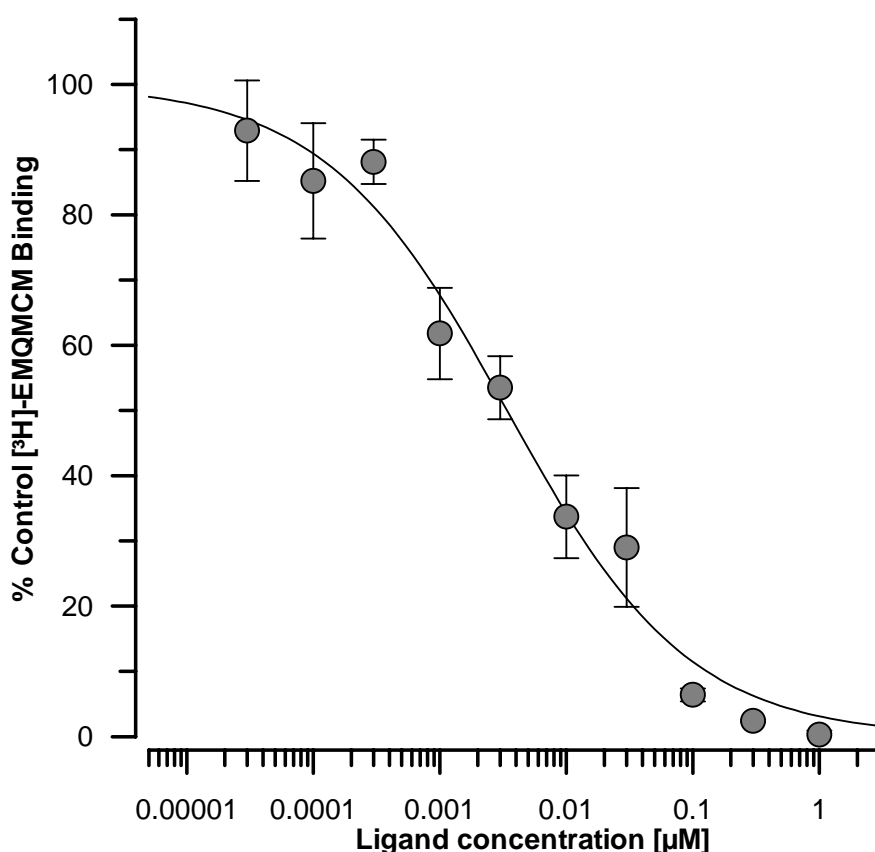


Figure 2.2.1-d. Concentration response curves for EMQMCM (IC_{50} -value: 3.4nM; SEM: 0.6) displacing [3 H]-EMQMCM from the rmGluR1-binding site. Results are mean values of three independent experiment conducted in quadruplicate. Error bars indicate SEM.

Finally, to validate the robustness of the present binding assay for future screening an experiment was performed to define the Z' -factor [Zhang *et al.*, 1999]. This simple statistical parameter can be calculated using only control data without the need for test compounds. It is normally employed to assess the overall assay quality of an HTS assay taking the data variation of the assay signal into account (i.e., the Z' -factor gives a hint whether a compound should preferably tested in singlet or duplicate, etc.). The following equation is applied:

$$Z' = 1 - \frac{(3\sigma_{c+} + 3\sigma_{c-})}{|\mu_{c+} - \mu_{c-}|}, \quad (\text{Eq. 2.2.1-a})$$

where σ_{c+} is the SD of the positive control, σ_{c-} the SD of the negative control and μ_{c+} and μ_{c-} denote the mean values of positive and negative control, respectively. A Z' -value above 0.5 is assumed to give reliable results and a value of 1 would indicate an ideal assay.

Positive (bound) and negative (non-specific) control values were measured on a 96-well plate according to the regular assay protocol (Section 3.1.3). Odd column numbers (1, 3, etc.) were used for positive control samples and even column numbers for negative control samples. The result was a Z' -factor of 0.61 for the total plate which is in accordance with a required value of ≥ 0.50 . It was decided to keep the previously defined settings (each concentration or control assayed in quadruplicate).

2.2.2 Conclusions

Several experiments were carried out one after the other and the results of the previous experiment were taken into account in order to improve the performance of the next test. This allowed iterative improvements in the assay procedure to satisfy all criteria necessary for a mGluR1 binding assay with limited throughput. It has been demonstrated that the preliminary NMDA binding assay experiments (Section 2.1) served as a useful basis for the development of mGluR binding assays. However, the assay procedure had to be modified to fulfill mGluR1 specific assay requirements. Finally, the optimized experimental procedure was successfully tested in terms of robustness of the system by means of determining the Z' -factor.

2.3 Development of a Binding Assay for mGluR5

A binding assay for mGluR1 was successfully established based upon the NMDAR binding assay. Likewise, a binding assay for allosteric mGluR5 antagonists was developed, which is described in the following section.

2.3.1 Experiments

The assay parameters for an initial mGluR5 binding assay were taken directly from the preliminary experiments of section 2.1. The first test was carried out on a regular 96-well

plate at room temperature and [^3H]-MPEP (5nM) served as the radioligand for rat cortical membrane (0.80 mg/ml). The test ligand MTEP (Figure 2.3.1-a) was applied in various concentrations to give a full concentration response curve. Membrane suspension and test ligand as well as positive and negative controls were prepared on the 96-well plate and the reaction was initialized by the addition of radioligand. After two hours the regular process was continued (transfer to multiscreen plate, wash steps, scintillation-cocktail addition and second incubation). Since no discrimination between positive (bound) and negative (non-specific) values could be made for this experiment (data not shown) it clearly failed. These results demonstrated that the experimental procedure of the NMDA binding assay could not directly be used for the mGluR5 binding assay.

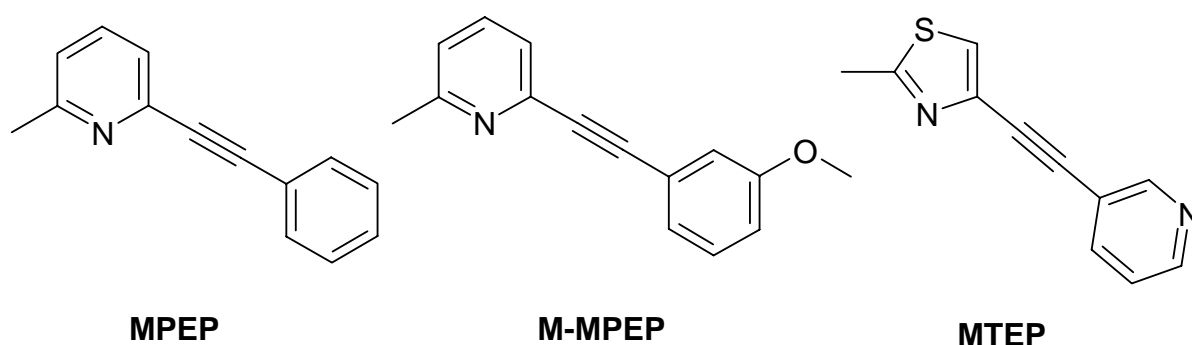


Figure 2.3.1-a. Chemical structures of known non-competitive mGluR5 antagonists that were used during the assay development.

Consequently, the experiment was repeated while slightly changing the settings. First, the reaction was started by addition of membrane and not by addition of the radiotracer, second, the incubation time was reduced to one hour and performed under cooled conditions (1°C, ice), as temperature was presumed to influence the reaction, and finally the rinse process was extended to four steps of ice cold buffer (150 μl). CRCs were conducted for the potent allosteric mGlu5 receptor antagonists MPEP and MTEP (Figure 2.3.1-a, Figure 2.3.1-b).

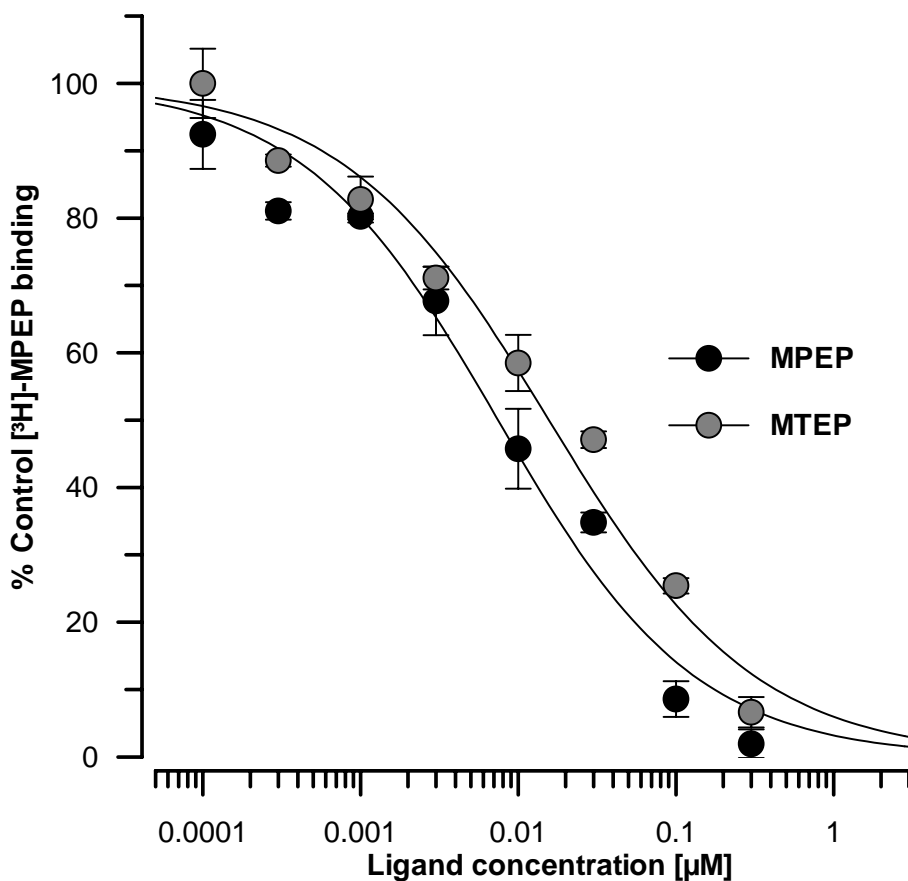


Figure 2.3.1-b. Concentration response curves for the antagonists MPEP (IC_{50} : 0.0074 μ M) and MTEP (0.0156 μ M) displacing [³H]-MPEP from the allosteric binding site of the mGlu5 receptor.

The experiment revealed somewhat too potent IC_{50} -values for both compounds [Anderson *et al.*, 2002] and the background in relation to the total signal was too high (40% and 47%, respectively). Therefore, the opaque 96-well plate was replaced by a transparent 96-well plate and the experiment was repeated for MPEP, MTEP and additionally M-MPEP (Figure 2.3.1-a, Figure 2.3.1-c).

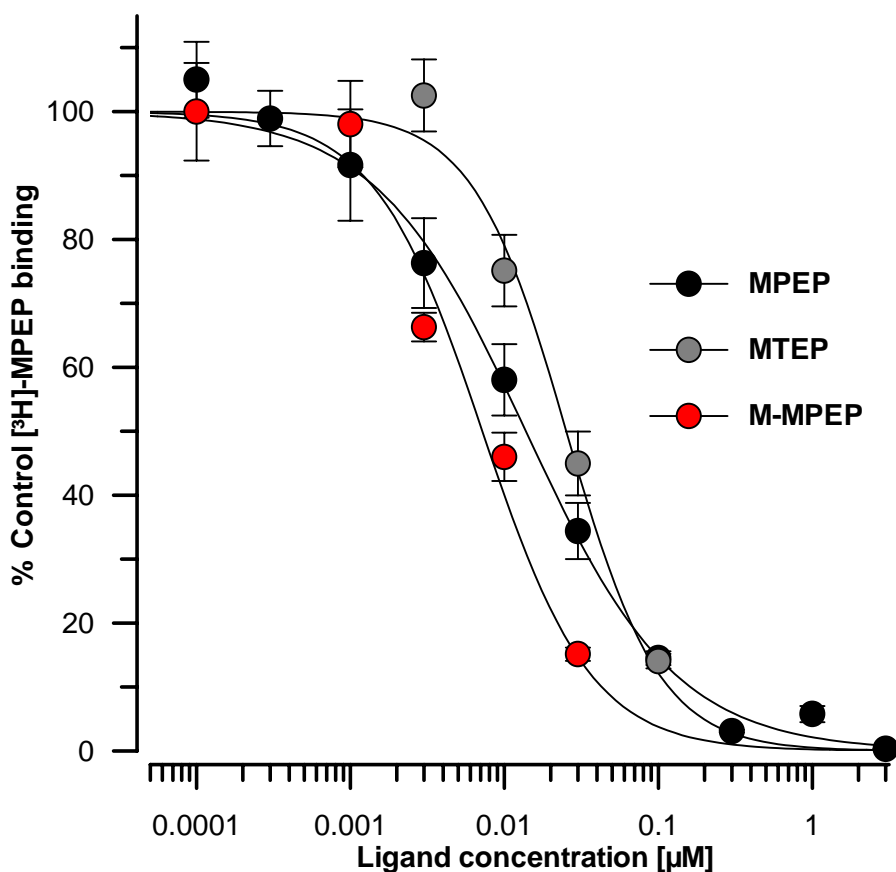


Figure 2.3.1-c. Concentration response curves for the antagonists MPEP (IC_{50} : $0.0138\mu\text{M}$), MTEP ($0.0252\mu\text{M}$) and M-MPEP ($0.0072\mu\text{M}$) displacing $[^3\text{H}]\text{-MPEP}$ from the allosteric binding site of mGluR5.

The background signal was further reduced (MPEP / MTEP / M-MPEP: 30 / 45 / 31%) and the IC_{50} -values calculated from the concentration response curves displayed much better accordance with the values given in the literature (MPEP: 15nM; MTEP: 30nM; M-MPEP: 3.6nM) [Anderson *et al.*, 2002; Gasparini *et al.*, 2001].

Apart from the background signal, which is still somewhat too high, the mGluR5 binding assay with labeled MPEP as the radiotracer produced reliable results. For screening the cooling conditions were further optimized (blue ice was replaced with dry ice maintaining a mean temperature of 1-2°C in each well). Eventually, background values of roughly 15% from total signal were obtained when test compounds were screened (data not shown).

2.3.2 Conclusions

Like in Section 2.2 the NMDAR binding assay procedure served as a starting point for setting up the present assay in order to speed up the optimization process. “Trouble-shooting” was done by iterative changing of assay parameters. The fact that incubation of compounds

with membrane had to be conducted under cooled conditions considerably hampered the developmental process. This was attributed to an assumed rapid dissociation of bound ligand from the receptor (see also Section 2.6). Apart from the cooled conditions both, mGluR1 and mGluR5 binding assays were performed in the same way.

The final assay procedure is given in the experimental part (Section 3.1.4).

2.4 The Influence of DMSO

The molecules that were retrieved from commercial compound libraries by virtual screening methods are assumed to bind to the allosteric site of group I mGluRs in particular of mGluR1. Since the allosteric binding site is embedded in the hydrophobic transmembrane region (Section 1.3.1) ligands interacting with the binding pocket elicit predominantly poor aqueous solubility.

Hence, this led to a pitfall, which became especially apparent within the hit optimization procedure: higher affinity often correlated with higher lipophilicity. The binding assays initially used were solely conducted in aqueous solutions meaning that all constituents were dissolved in pure Tris-buffer. As some reference compounds (EMQMCM, NPS 2390 and AMMPP) used for CRCs during the assay development process were poorly soluble in buffer, their testing was hampered by precipitation problems especially at high concentrations (Section 2.2.1). Likewise, when test compounds were screened substance precipitations occurred for many molecules, in particular during the preparation of dilution series for CRCs. Consequently, a considerable percentage of all test structures was not suited for testing under the conditions used. It turned out that nearly all solids showed acceptable solubility in the organic solvent dimethyl sulfoxide (DMSO). The relatively polar solvent DMSO, in turn, can be diluted with buffer in any ratio. Tris-buffer containing up to 5% DMSO was capable of solving nearly all test compounds even at relatively high concentrations.

2.4.1 Experiments

First, the influence of two DMSO concentrations was investigated for the mGluR1 binding assay. Figure 2.4.1-a clearly demonstrates the significant signal reduction caused by DMSO: While 1% DMSO displayed little influence on control values 5% DMSO led to approx. 20% signal reduction. Higher DMSO concentrations were not tested. The ratio between positive and negative control remained unchanged for both DMSO concentrations (<10%).

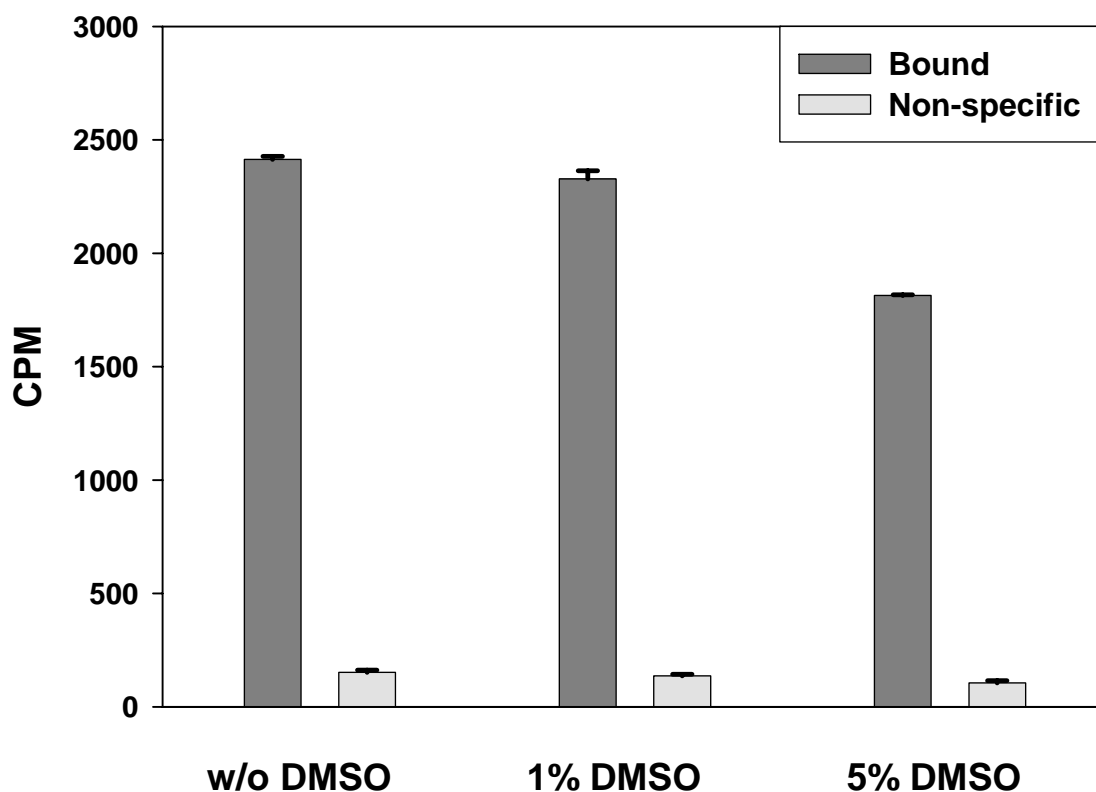


Figure 2.4.1-a. Bar chart representing the influence of DMSO as solvent in the mGluR1 binding assay on positive (bound) and negative (non-specific) control values.

To further evaluate the influence of DMSO on ligand affinity concentration response curves were performed for some standards. A selection is given in Figure 2.4.1-b demonstrating that there is little (if any) influence of DMSO on the affinity towards the allosteric binding site. The IC_{50} -value for EMQMCM, which is well soluble in both DMSO and water, was 11nM/12nM (with 1% and 5% DMSO, respectively) and 6nM without DMSO; the affinity of R193845, an analogue of EMQMCM, did not change at all (233nM/235nM vs. 218nM without DMSO). Only the affinity of NPS 2390 was significantly reduced from 210nM to 311nM at 5% DMSO (271nM without DMSO, data not shown). However, as the IC_{50} -value calculated in aqueous solution lay between the values determined in the presence of DMSO one could assume that the values calculated in this experiment showed a typical error of measurement.

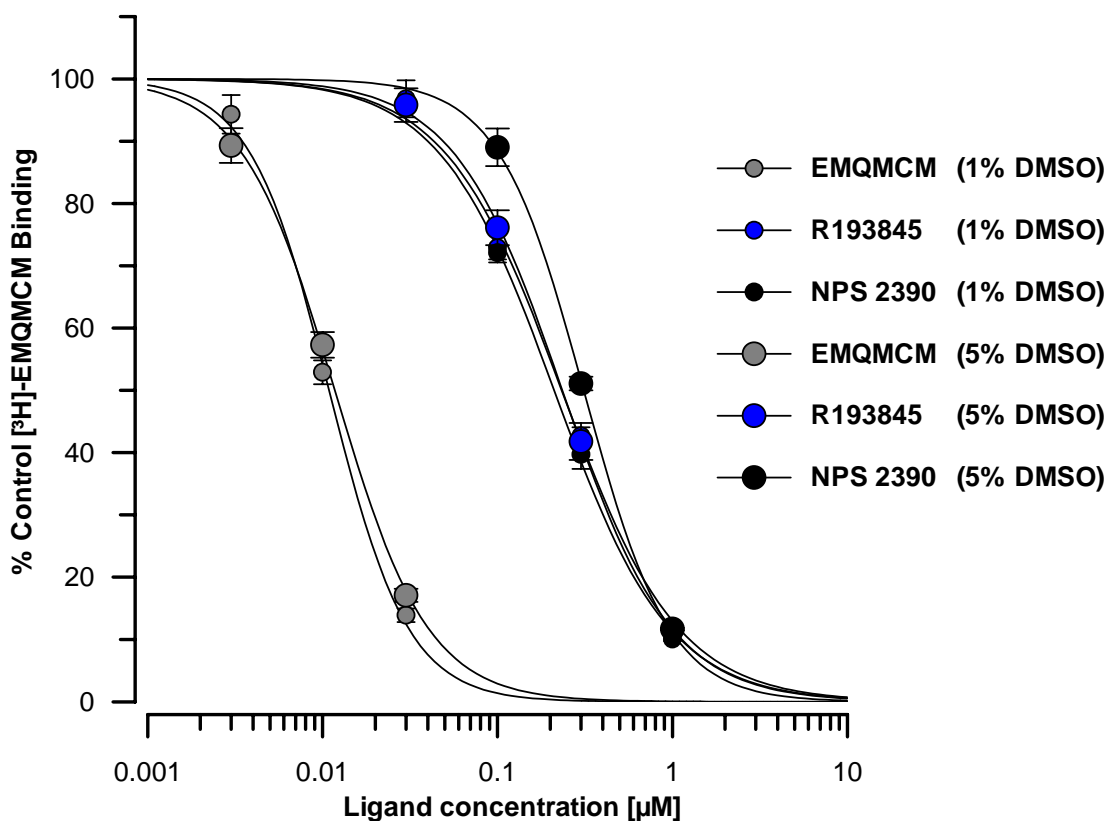


Figure 2.4.1-b. 3-concentration CRCs for three allosteric mGluR1 antagonists at two different DMSO concentrations performed in quadruplicate. Calculated IC_{50} -values in the presence of 1% and 5% DMSO: **EMQMCM** 11nM (SEM: 0.6nM) vs. 12nM (0.3nM), **R193845** 233nM (24.3nM) vs. 235nM (7.7nM), **NPS 2390** 211nM (9.1nM) vs. 311nM (6.4nM).

2.4.2 Conclusions

Summarized, DMSO up to 5% final concentration had no influence on the interaction of ligands binding to the allosteric site of mGluRs. In contrast to living cells, which are sensitive even to low DMSO concentrations (< 0.5%) membranes are relatively insensitive to DMSO at the concentrations applied.

2.5 Scatchard Analysis

Binding saturation experiments (Scatchard analyses) describe a method to directly determine the true potency of a radioligand for its binding site under the conditions used [McKinney, 1998]. Here, a radio labeled ligand is tested in various concentrations but at a fixed protein level. Only positive (total binding) and negative controls (non-specific binding) are measured. Based upon the results of Scatchard analyses the K_d -value of a given

radioligand can be determined. This value in turn is indispensable to calculate K_i -values for test compounds according to the Cheng-Prussoff Equation (Section 3.1.11). It must be emphasized that K_d -values resulting from such saturation experiments are specific for a particular assay. Consequently, changing any fundamental parameters which probably influence the binding behavior of ligands towards receptors (e.g., protein concentration and temperature) necessarily means that the K_d -value becomes invalid and has to be experimentally determined again.

Saturation experiments were performed for both types of tissue: the cerebellar and cortical rat membranes containing mGluR1 and mGluR5, respectively. Thus, the procedure of Scatchard analyses followed the assay protocols of the corresponding binding assays of mGluR1 and mGluR5 for later compound screening (Section 3.1.3 and 3.1.4).

2.5.1 Saturation Experiments on Cerebellar Membranes

For saturation experiment at the allosteric binding site of mGluR1 the binding behavior of the potent and highly selective non-competitive antagonist [³H]-EMQMCM was investigated. Experiments were carried out according to the established binding assay protocol (Table 2.5.2-a). The practical work was performed by Sabine Denk, a technical assistant at Merz.

Table 2.5.1-a. Assay protocol giving the parameters for mGluR1 binding saturation experiments.

Parameter	Setting
Radiotracer	[³ H]-EMQMCM (0.36nM – 100nM)
Cold displacer	EMQMCM (10μM)
Protein	Rat cerebellum (0.80 mg/ml)
Total volume	250μl/well
Detection volume	150μl/well
1 st Incubation	60 min. (room temperature, shaker)
2 nd Incubation	16 hours (room temperature, dark)
Buffer	Tris-HCl 50mM, pH 7.5
Detecting device	Microbeta TriLux®

Positive and negative controls were tested at twelve different concentrations of radioligand starting with 0.36nM up to a three hundred-fold higher concentration (Figure 2.5.1-a).

Specific binding was calculated by subtracting negative control from positive control at each concentration.

The signal-to-background ratio was exceptionally good over a wide range of radiotracer concentrations with the best ratio at 15nM [^3H]-EMQMCM. However, with increasing radioligand concentrations the ratio steadily degrades since the background values (non-specific) linearly increase whereas the total signal asymptotically approaches a certain threshold (i.e., the binding saturation).

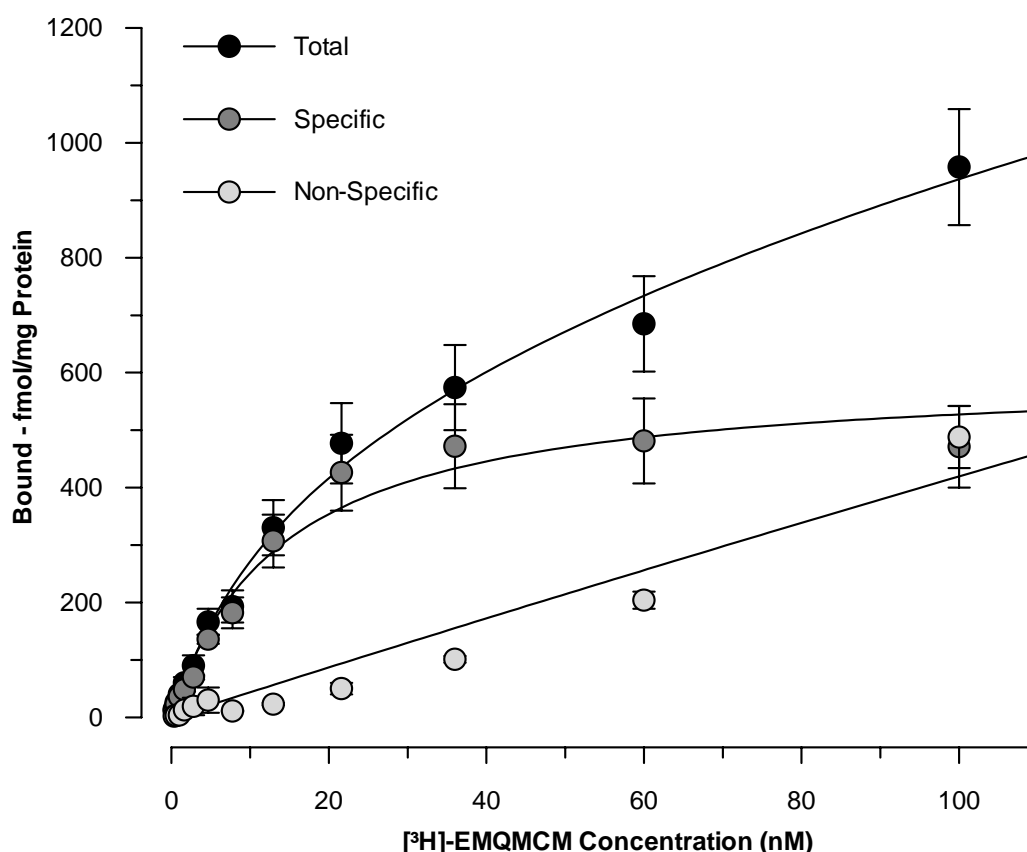


Figure 2.5.1-a. Saturation curve of [^3H]-EMQMCM binding in rat cortical membranes. Results represent mean values of three independent experiments performed in quadruplicate. Error bars indicate SEM.

Analysis of [^3H]-EMQMCM binding to rat cortical membranes revealed a single binding site that was of high affinity and saturable (Figure 2.5.1-b). The K_d -value of [^3H]-EMQMCM is equal to the slope of the regression line. B_{max} in turn is the intercept of this line of best fit with the abscissa. However, to determine the receptor capacity (B_{max}) of cerebellar membranes it was first necessary to calculate which amount of ligand is specifically bound to the membranes (i.e., ideally the receptors) per given protein concentration (abscissa in Figure

2.5.1-b) resulting in a certain signal. Therefore, the total signal of various amounts of radioligand has been measured (data not shown) to determine this amount.

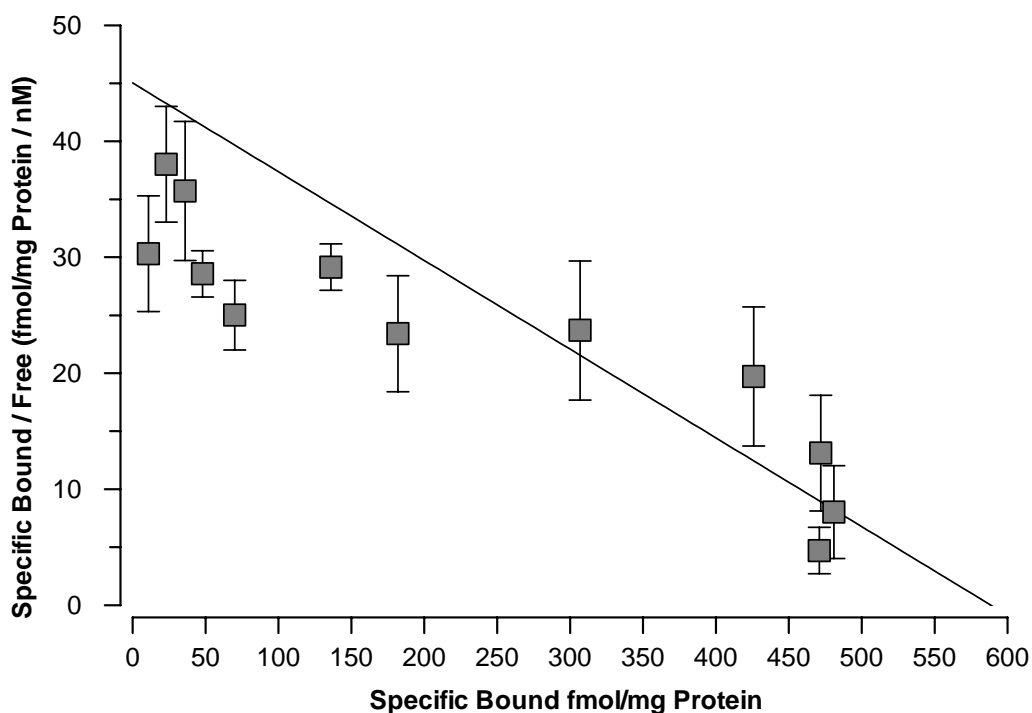


Figure 2.5.1-b. Scatchard plot of [³H]-EMQMCM binding in rat cerebellar membranes. The binding site has a capacity of 0.59 pmol/mg protein with high affinity of the ligand (K_d -value: 13.1nM). Results represent mean values (and SEM) of three independent experiments performed in quadruplicate.

The assay specific K_d -values determined in this section for [³H]-EMQMCM and in the following section for [³H]-MPEP were implemented in Equation 3.1.11-e [Cheng & Prussoff, 1973] to calculate K_i -values for further compound screening.

2.5.2 Saturation Experiments on Cortical Membranes

For saturation experiments at the allosteric binding site of mGluR5 the binding of [³H]-MPEP was investigated. Experiments were carried out according to the established binding assay protocol (Table 2.5.2-a).

Table 2.5.2-a. Assay protocol giving the parameters for mGluR5 binding saturation experiments.

Parameter	Setting
Radiotracer	[³ H]-MPEP (0.4nM – 40nM)
Cold displacer	MPEP (10μM)
Protein	Rat cortex (0.80 mg/ml)

Total volume	250µl/well
Detection volume	150µl/well
1 st Incubation	70 min. (cooled conditions, shaker)
2 nd Incubation	16 hours (room temperature, dark)
Buffer	Tris-HCl 50mM, pH 7.5
Detecting device	Microbeta TriLux®

Positive and negative controls were tested at twelve different concentrations of radioligand starting with 0.4nM up to a hundred-fold higher concentration (Figure 2.5.2-a). Likewise, specific binding was calculated by subtracting negative control from positive control at each concentration. Here, the saturation curve displays a poor signal-to-background ratio exhibiting ~30% of background only at radiotracer concentrations of up to 2nM. At higher concentrations the background increases dramatically.

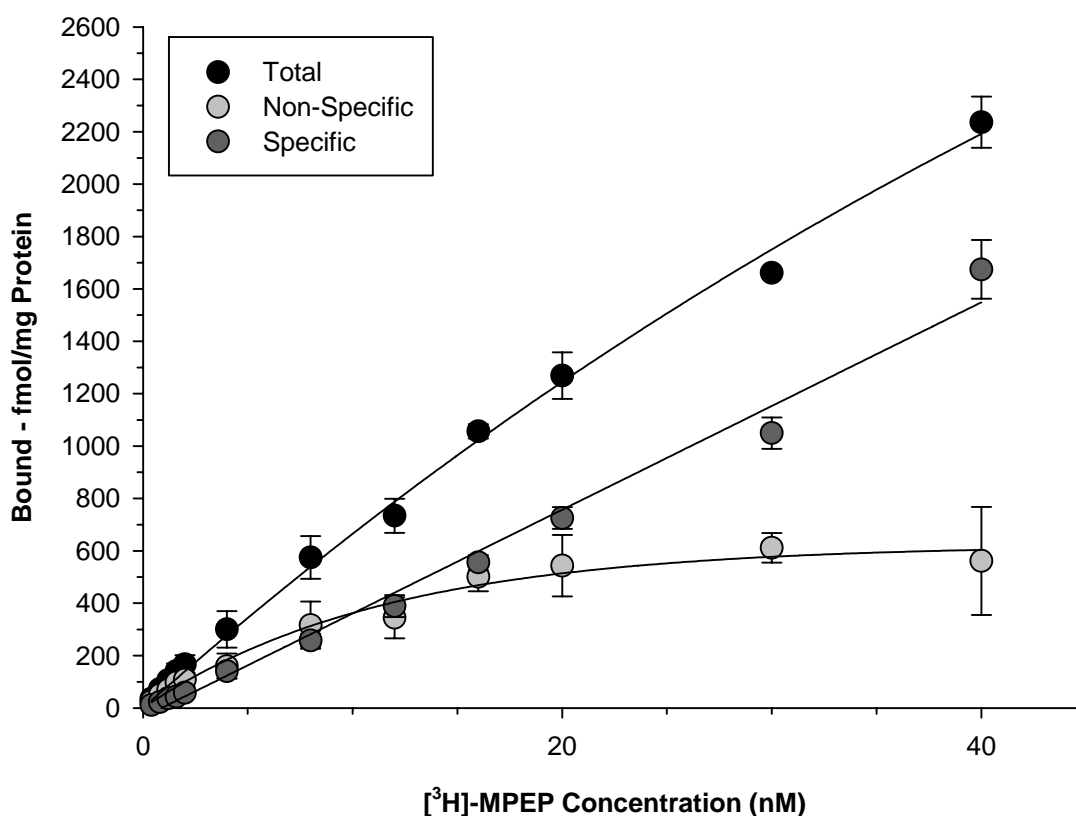


Figure 2.5.2-a. Saturation curve of [³H]-MPEP binding in rat cortical membranes. Results represent mean values of three independent experiments performed in quadruplicate. Error bars indicate SEM.

Likewise [³H]-EMQMCM binding (Figure 2.5.1-b), analysis of [³H]-MPEP binding in cortical rat brain membranes revealed a single binding site that was saturable and of high

affinity (Figure 2.5.2-b). The K_d -value of [^3H]-EMQMCM is equal to the slope of the regression line. B_{max} in turn is the intercept of this line of best fit with the abscissa. To determine the receptor capacity (B_{max}) of cerebellar membranes it was first necessary to calculate which amount of ligand is specifically bound to the membranes (i.e., ideally the receptors) per given protein concentration (abscissa in Figure 2.5.2-b) resulting in a certain signal. Therefore, the total signal of various amounts of radioligand has been measured (data not shown) to determine this amount.

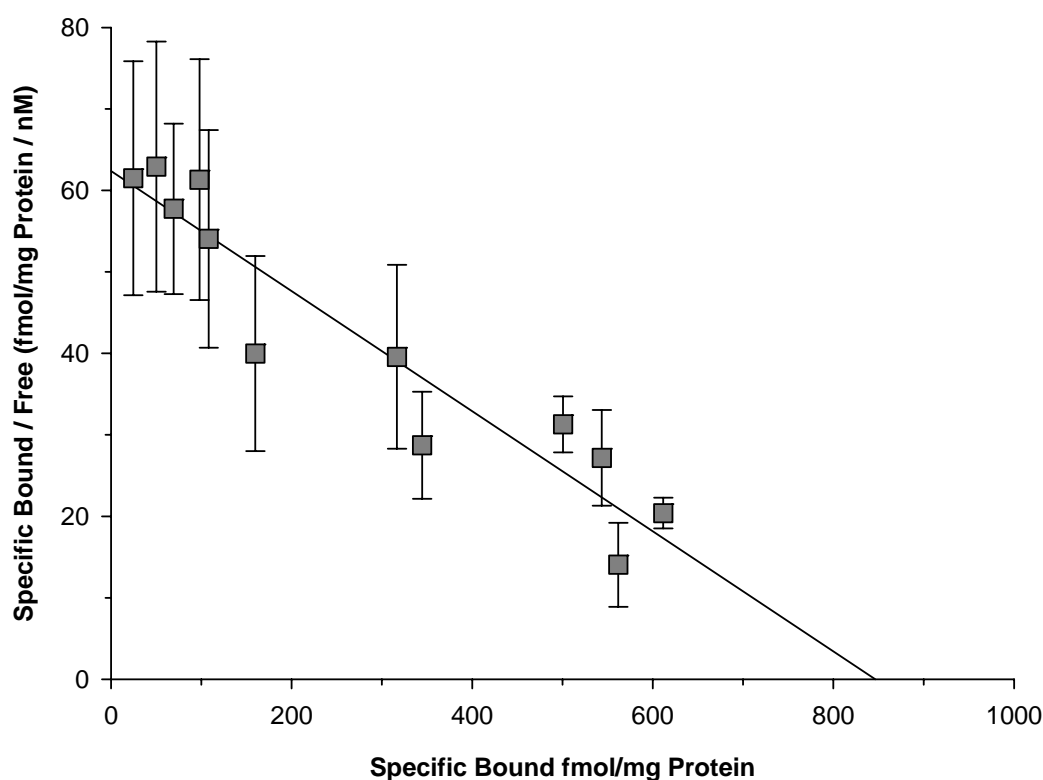


Figure 2.5.2-b. Scatchard plot of [^3H]-MPEP binding in rat cortical membranes. The binding site has a capacity of 0.82 pmol/mg protein with high affinity of the ligand (K_d -value: 12.9nM). Results represent mean values (and SEM) of three independent experiments performed in quadruplicate.

2.5.3 Conclusions

Both radioligands, [^3H]-EMQMCM and [^3H]-MPEP, showed properties that exhibit similar binding behaviors at their corresponding binding pockets. They bind with high affinity to their saturable binding sites (mGluR1 vs. mGluR5; K_d : 13.1nM vs. 12.9nM), which have similar binding capacities (B_{max} : 0.59 vs. 0.82 pmol/mg protein). Regarding the scatchard plots, there seems to be only one site in the HD of each receptor to which the radioligand binds.

The ratio between total binding and specific binding significantly differs between the mGluR1 and mGluR5 scatchard experiments (Figures 2.5.1-a and 2.5.2-a). Regarding mGluR1 we observed a relatively good ratio for all [³H]-EMQMCM concentrations (Figure 2.5.1-a) ranging between 49% and close to 100% for specific binding. Contrary to these results, the ratio between total and specific bound ligand for [³H]-MPEP concentrations was worse where specific bound ligand ranged between 25% and 70% of total binding (i.e., 30% – 75% background). The reason for poor specific binding of the radioligand to the allosteric mGluR5 receptor site is probably the fast dissociation rate of MPEP-like ligands from the mGluR5 binding pocket, which occurs even at low temperature and is shown in the following chapter.

2.6 Kinetic Experiments

The kinetics of ligand (agonistic or antagonistic) actions observed in vitro can yield valuable information about ligand-receptor interactions [Kenakin, 1987]. Kinetic experiments allow for determining the actual association and dissociation constant for a given ligand.

In contrast to the mGluR1 binding assay, the mGluR5 binding experiments revealed considerably higher background levels (~5% vs. >15% background from total bound). Several assay settings were changed until it became apparent that the assay had to be performed under optimized cooled conditions in order to minimize background bias to an acceptable level (Section 2.3). Hence, the conclusion drawn was that the unfavorable signal-to-background ratio was caused by the temperature (i.e., the fast dissociation kinetics from specific sites). Within this section the binding kinetic for [³H]-M-MPEP, an analogue of [³H]-MPEP, was investigated. It was hypothesized that association and dissociation kinetics of the radioligand were fast, even at a cold temperature close to the freezing point of water. Especially a rapid offset kinetic where the bound radioligand becomes rapidly displaced by another potent cold ligand could lead to the assumption that the radiotracer binds relatively weak to the binding site though it shows high equilibrium affinity towards the receptor. This in turn may give a hint that even the duration of the rinse step could have a large impact on the signal-to-background ratio since even the buffer could probably wash out the bound radioligand to a certain degree.

2.6.1 On-set and Off-set Studies on Cortical Membranes

Association and dissociation kinetic experiments were carried out according to the corresponding protocols given in the experimental part (Section 3.1.9 and 3.1.10). Two different concentrations of radiotracer were used in order to determine which amount of radio labeled ligand leads to sufficiently high signals.

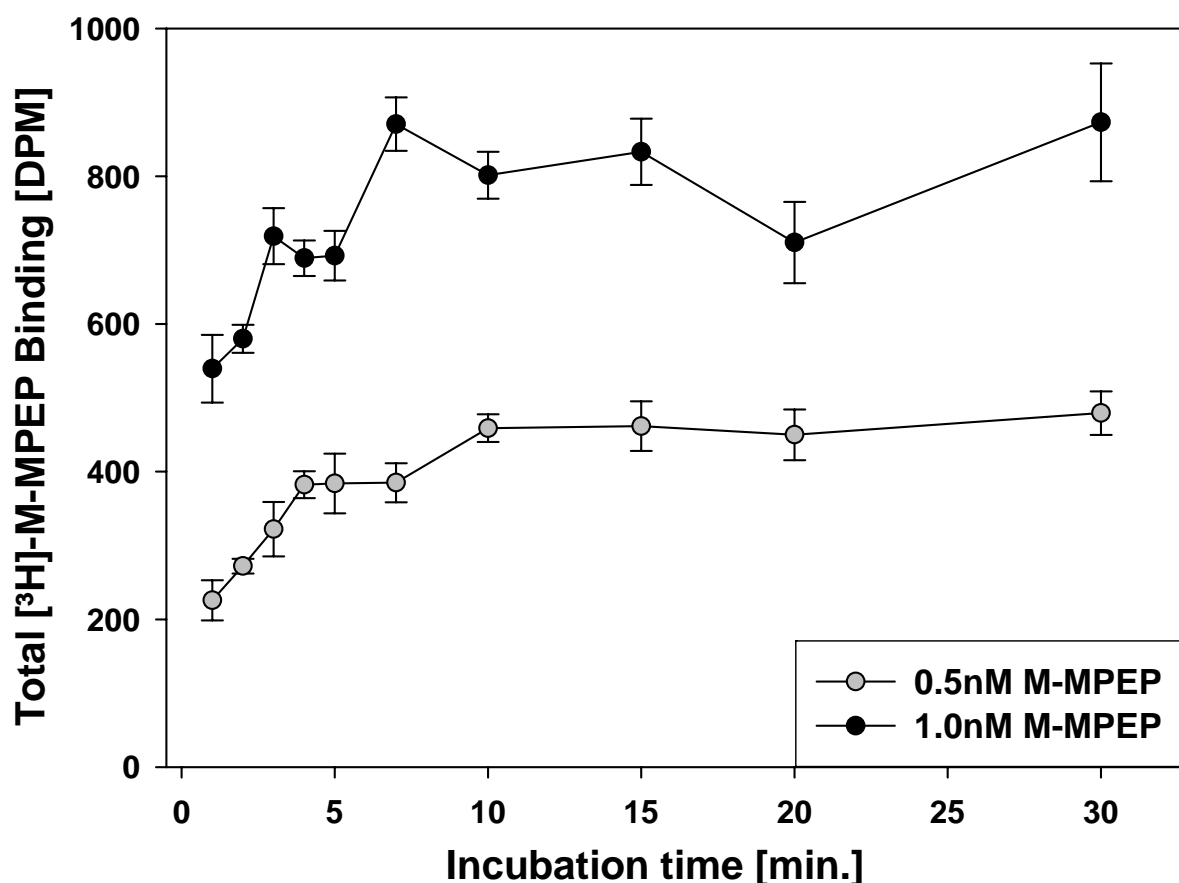


Figure 2.6.1-a. Association time course curve for $[^3\text{H}]\text{-M-MPEP}$ binding to rat cortical membranes. Association kinetics were measured at different incubation times and at room temperature. The experiment was performed in quadruplicate. Error bars represent SEM.

Although the total binding values corresponding to the higher radioligand concentration (1nM) are roughly twice as high as those of the lower concentration, they cover an absolute range which is only slightly increased in relation to the values of 0.5nM $[^3\text{H}]\text{-M-MPEP}$ (~300 CPM vs. ~200 CPM). Samples with higher radioligand concentration would considerably deviate from a fitted curve. For 1nM ligand concentration, around 70% of the maximal binding was achieved within one minute. This fast onset kinetic indicates a potent ligand.

In fact, the time course curve clearly demonstrates that association of [^3H]-M-MPEP to membranes was extremely fast since maximal binding was reached within ten minutes of incubation, irrespective of the radioligand concentration.

Also dissociation of [^3H]-M-MPEP showed fast kinetics at room temperature (Figure 2.6.1-b). The reaction seems to be finished after one minute of interaction between the proteins and the cold displacer, i.e., the radioligand that was bound to the membrane was displaced by an excessively high amount of unlabeled ligand within a few seconds.

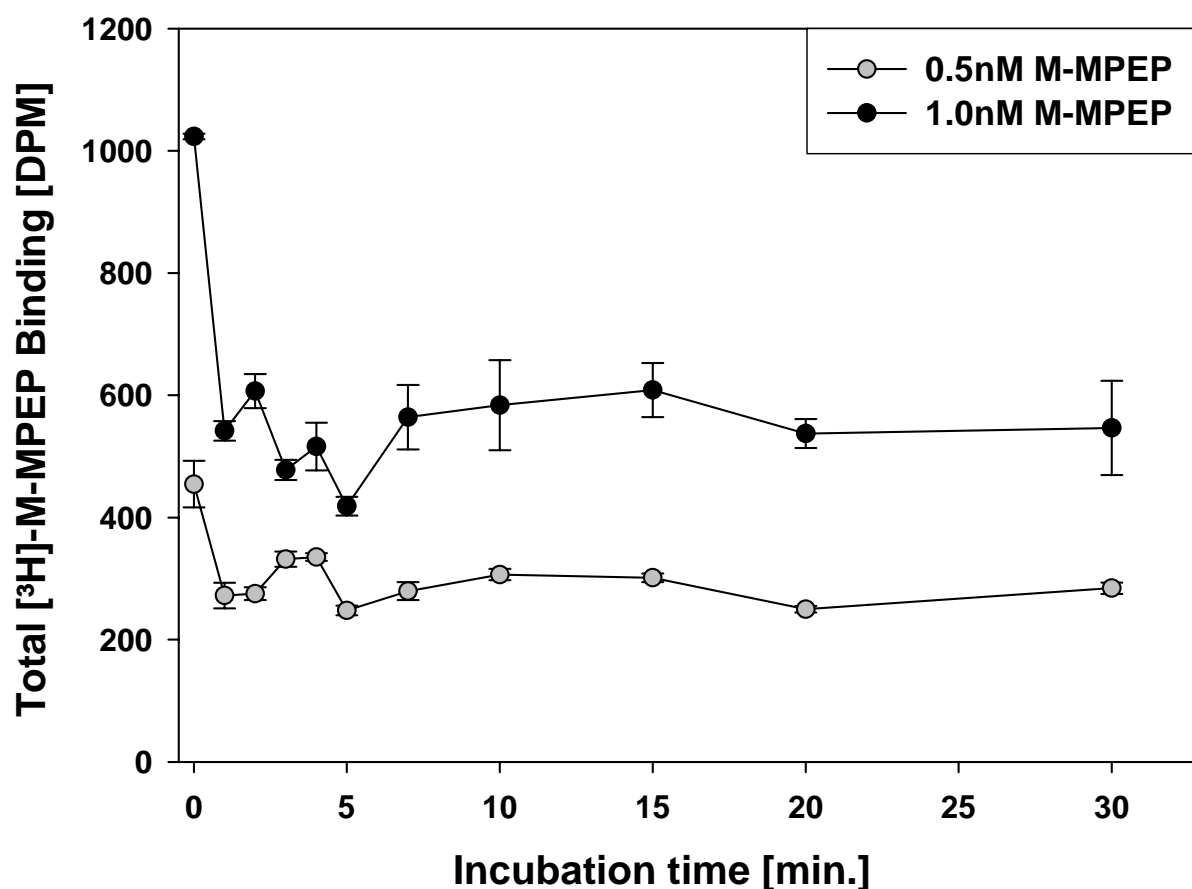


Figure 2.6.1-b. Dissociation time course curve for [^3H]-M-MPEP binding to rat cerebellar membranes. Dissociation kinetics were measured after different incubation times of cold displacer (M-MPEP, $10\mu\text{M}$) and at room temperature. Experiment was performed in quadruplicate. Error bars represent SEM.

It must be stressed that the dissociation experiment was also carried out at room temperature. The kinetics will be slower under cooled conditions. There were two reasons for performing kinetic experiments at room temperature: (i) To directly compare on-set and off-set experiments both have to be performed under the same conditions and (ii) conduction at

cooled temperatures would have led to extensive technical problems for which we could find no solution with our laboratory conditions – one would need a cool room.

2.6.2 Conclusions

The observation that the mGluR5 radiotracer [³H]-M-MPEP follows a fast association and dissociation kinetic at room temperature has considerable impact on cold displacement in mGluR5 binding assays: Assuming that MPEP and its structural analogue M-MPEP behave in the same manner at their binding site, one may conclude that the fast dissociation kinetics are the reason for the failure of attempted cold displacement experiments when conducted at room temperature. If the radioligand is indeed only loosely bound to the membrane (at least at room temperature) then it might perhaps be easy to remove it from the receptor binding site during the rinse steps. This in turn can account for the poor signal to background ratio. To overcome this problem, the mGluR5 binding assay for compound screening must be performed under cooled conditions to obtain an acceptable signal-to-background ratio (15%).

3 Methods

3.1 Experimental Details

Note: Some of the following experimental procedures and methods (indicated by an asterisk in the headline) were not performed by the author of the thesis. They have been included for completeness of the scientific results.

3.1.1 Preparation of Solutions

Each compound was delivered as powder and was dissolved in pure DMSO and shaken for two hours on a shaker “RM5 Assistant” [Karl Hecht GmbH] to give a 10 mM stock-solution. Insoluble compounds were assumed to be inactive. The final concentration of DMSO in the assay was 5% (binding) and 0.5% (functional), respectively. The influence of DMSO on the membranes and cells was evaluated previously and turned out to be negligibly low at the concentrations used. Full concentration-response curves were performed using seven different concentrations (binding) or five different concentrations (functional), respectively with a log 3 concentration progression. For these curves, serial dilutions of the stock solutions were made in pure DMSO before dilution in buffer to obtain the desired final concentration. This assured that, even for poorly soluble compounds, at least the lower concentrations tested really contained the required concentration of compound.

3.1.2 Membrane Preparation

Male Sprague Dawley Rats (approx. 200-250g) were anaesthetized and decapitated. Cerebelli (forebrains for cortex preparation) were removed and homogenized (Ultra Turrax, 8 strokes, 600 rpm) in 0.32M Sucrose. The suspension was centrifuged at 1,500g for 4 min. using a Sorvall Discovery 90 SE ultracentrifuge [Kendro Laboratory Products]. Supernatant was removed and centrifuged at 20,800g for 20 min. The resulting pellet was resuspended in ice-cold distilled water and centrifuged at 7,600g for another 20 min. Supernatant and loosely associated flocculent membrane material (buffy coat) were removed by gentle trituration of the pellet and centrifuged at 75,000g for 20 min. Supernatant was discarded and the membrane pellet was resuspended by sonication in Tris-Buffer (5mM, pH 7.4) and afterwards centrifuged at 75,000g for 20 min. The last step was repeated twice and membranes were resuspended in Tris-Buffer (50mM, pH 7.5).

The concentration of protein was determined by the Lowry protein assay with bovine serum albumin as a standard [Lowry *et al.*, 1951]. Membranes were stored frozen at -24°C , thawed on the day of the assay and washed once again at $75,000g$ for 20 min. All centrifugation steps were carried out at 4°C .

3.1.3 [^3H]-EMQMCM Binding Assay

Binding assays were performed at room temperature in quadruplicate in a 96-well format using fixed concentrations of test compound ($10\mu\text{M}$). On a MS2 mini-shaker [IKA Werke GmbH] rotating with ~ 600 rpm the assay was incubated for 1h in the presence of 1nM [^3H]-EMQMCM (23.9 Ci/mmol) and membranes (0.8 mg/ml) and non-specific binding was estimated using $30\mu\text{M}$ (3-Ethyl-2-methyl-quinolin-6-yl)-(4-hydroxy-cyclohexyl)-methanone [Asinex Ltd.]. Directly after transferring the reaction volume onto a 96-well multiscreen plate with glass fiber filter $0.22\mu\text{m}$ [Millipore GmbH] binding was terminated by rapid filtration using a multiscreen vacuum manifold [Millipore GmbH]. Afterwards, filters were washed three times with ice-cold assay-buffer and Ultima-GoldTM MV Scintillation Cocktail [Perkin Elmer Life Sciences] was added. After 14h – 16h, radioactivity was counted in a MicroBeta[®] Trilux [Perkin Elmer Life Sciences].

3.1.4 [^3H]-MPEP-Binding Assay

Binding assays were performed under cooled conditions (4°C) in quadruplicate in a 96-well format using fixed concentrations of test compound ($10\mu\text{M}$). On a MS2 mini-shaker [IKA Werke GmbH] rotating with ~ 600 rpm the assay was incubated for 1h in the presence of 5nM [^3H]-MPEP (50.2 Ci/mmol, Tocris) and membranes (0.8 mg/ml) and non-specific binding was estimated using $10\mu\text{M}$ MPEP. Directly after transferring the reaction volume onto a 96-well multiscreen plate with glass fiber filter $0.22\mu\text{m}$ [Millipore GmbH] binding was terminated by rapid filtration using a multiscreen vacuum manifold [Millipore GmbH]. Afterwards, filters were washed three times with ice-cold assay-buffer and Ultima-GoldTM MV Scintillation Cocktail [Perkin Elmer Life Sciences] was added. After 14h – 16h radioactivity was counted in a MicroBeta[®] Trilux [Perkin Elmer Life Sciences].

3.1.5 Preparation of Cerebellar Granule-cells*

Cerebellar cortici were obtained from P8 postnatal Sprague Dawley rats, mechanically disrupted into small pieces with forceps and then transferred to Ca^{2+} - and Mg^{2+} -free Hank's buffered salt solution (HBSS-CMF) on ice. After three washes in HBSS-CMF, the tissue pieces were incubated at 37°C for 8 minutes in the presence of 0.25% trypsin / 0.05% DNase. The enzymatic reaction was stopped with 0.016% DNase / 0.1% ovomucoid before centrifugation at 800 rpm for 5 minutes. The supernatant was replaced twice with NaHCO_3 /HEPES-buffered basal Eagle medium (BEM) plus 20mM KCl. Cells were mechanically dissociated in 2 ml of BEM by trituration through three Pasteur pipettes of successively decreasing tip diameter and then filtered through a 48 μm gauge filter. Cells were plated at a density of 150,000 cells in 50 μl in each well of poly-L-Lysin pre-coated 96-well plates [BD Biosciences]. The cells were nourished with BEM supplemented with 10% fetal calf serum, 2 mM glutamine [Biochrom AG], 20 mM KCl and gentamycin [Biochrom AG] and incubated at 36°C with 5% CO_2 at 95% humidity. After 24 hours cytosine- β -D-arabinofuranoside (AraC, 10 μM) was added to the medium.

3.1.6 IP_3 -Assay with [^3H]-myo-Inositol*

After 6 DIV the culture medium was replaced completely with inositol free DMEM [MP Biomedicals] containing [^3H]-myo-inositol [Perkin Elmer Life Sciences] at a final concentration of 0.5 μCi / 100 μl / well and incubated for a further 48 hours. The culture medium in each well was replaced with 100 μL Locke's buffer (plus 20 mM LiCl, pH 7.4) and incubated for 15 min at 37°C. Locke's buffer was replaced with agonists / antagonists / putative mGluR1 ligands in Locke's buffer and incubated for 45 min. These solutions were then replaced with 100 μL 0.1 M HCl in each well and incubated for a further 10 mins on ice in order to lyse the cells. The 96-well plates can be frozen at -20°C at this stage until further analysis.

Home made resin exchange columns were prepared as follows. Empty Bio-Spin Chromatography columns [Biorad Laboratories] were plugged with filter paper before filling with 1.1-1.3 ml of resin (AG1-X8 Biorad, 140-14444) suspended in 0.1M formic acid (24 g resin per 50 ml acid). The formic acid was allowed to run out before sealing the syringe tips and filling with 200-300 μL of 0.1M formic acid before storage at 4°C.

On the day of assay, columns were washed with 1 ml of 0.1M formic acid followed by 1 ml of distilled water. Then the contents of each assay well were added to one column and washed

with 1 ml distilled water followed by 1 ml of 5mM Sodium tetra borate / 60mM sodium formate. Thereafter, the retained radioactive inositol phosphates were eluted with 2 x 1ml of 1M ammonium formate / 0.1M formic acid into 24-well visiplates. Scintillation liquid (1.2 ml UltimaFlow AF [Perkin Elmer Life Sciences]) was added to each well, the plate sealed and vortexed before radioactivity was determined by conventional liquid scintillation counting (MicroBeta[®] Trilux) [Perkin Elmer Life Sciences]. Unless otherwise stated, all reagents were obtained from Sigma-Aldrich [Sigma-Aldrich Chemie GmbH].

3.1.7 Preparation of and Cultivation of Rat Cortical Astrocytes*

Astrocytes were prepared mechanically from cortices of newborn Sprague Dawley rats as described earlier [Booher & Sensenbrenner, 1972]. The tissue was disintegrated with a nylon filter (20x20 cm; pore size 80 µm) and carefully triturated. The cell suspension was seeded in a T 225 flask and cultivated in DMEM containing 10% fetal calf serum, 2mM glutamine and 50 µg/ml gentamycin at 37°C in 5% CO² and 95% humidity for 7 days with a medium change at day 2. After 7 days in culture, cells were shaken overnight [Miller *et al.*, 1993] to remove oligodendrocytes. The next day astrocytes were washed, trypsinized and seeded into 96-well plates coated with Poly-L-Lysin at a density of 40.000 cells / well. One day after trypsination, the medium was switched to serum free chemical defined DMEM (ADM) containing 1x G5-supplement, 50 µg/ml heparan sulfate, and 1.5 µg/ml fibronectin.

3.1.8 Calcium FLIPR Studies*

Cultured astrocytes expressed mGluR5 receptors as shown by immunostaining. The increase of intracellular calcium after stimulation with the mGluR5 agonist DHPG or L-quisqualate was measured using the fluorometric imaging plate reader (FLIPR) and the Ca-Kit. Prior to addition of agonist or antagonist the medium was aspirated and cells were loaded for 2 h at RT with 150 µL of loading buffer consisting of a calcium-sensitive dye reconstituted in NaCl (123mM), KCl (5.4mM), MgCl₂ (0.8 mM), CaCl₂ (1.8mM), D-glucose (15mM), and HEPES (20mM), pH 7.3. Subsequently, plates were transferred to FLIPR to detect calcium increase with the addition of DHPG (300µM) or L-quisqualate (100nM) measured as relative fluorescence units (RFU). If antagonists were tested, these compounds were pre-incubated for 10 min at room temperature before addition of the respective agonist. The fluorescence signal increase after addition of agonist reflects the increase of intracellular calcium. Inconsistencies in the amount of cells per well were normalized by using the spatial

uniformity correction of the FLIPR software. The mean of replicated temporal data (n=5) was calculated and used for graphical representation. For the evaluation of the pharmacology, the calcium changes in response to different concentrations of agonist or antagonist were determined using a maximum minus minimum (MaxMin) or an area under the curve (AUC) calculation. All responses (CPM- or RFU-values) were determined as percentage of control (= maximum response at 50 nM CBC).

3.1.9 Association Kinetic Studies

Solutions containing assay-buffer (Tris-HCl 50mM, pH 7.5), radioligand ($[^3\text{H}]$ -M-MPEP 0.5nM and 1nM) and cold displacer (M-MPEP 10 μM) for negative control values were prepared on a regular 96-well plate and transferred to a 96-well multiscreen plate with moistened glass fiber filter 0.22 μm [Millipore GmbH]. Incubation was started by the non-synchronous addition of a suspension containing rat cortical membranes (0.24 mg/ml) for incubations lasting 1, 2, 3, 4, 5, 7, 10, 15, 20 and 30 min., respectively, at room temperature. Then incubation was terminated by synchronous, rapid filtration using a multiscreen vacuum manifold [Millipore GmbH]. Afterwards, filters were washed three times with ice-cold assay-buffer and Ultima-GoldTM MV Scintillation Cocktail [Perkin Elmer Life Sciences] was added. After 14h – 16h radioactivity was counted in a MicroBeta[®]Trilux [Perkin Elmer Life Sciences].

3.1.10 Dissociation Kinetic Studies

Suspensions of rat cortical membranes were incubated on a regular 96-well plate for one hour in the presence of assay-buffer (Tris-HCl 50mM, pH 7.5) and different radioligand concentrations ($[^3\text{H}]$ -M-MPEP 0.5nM and 1nM). After addition of cold displacer (M-MPEP 10 μM) reaction volumes were incubated for 1, 2, 3, 4, 5, 7, 10, 15, 20 and 30 min., respectively. Reaction was stopped by transferring solutions to a 96-well multiscreen plate with moistened glass fiber filter 0.22 μm [Millipore GmbH] and rapidly removing the solutions using a multiscreen vacuum manifold [Millipore GmbH]. Afterwards, filters were washed three times with ice-cold assay-buffer and Ultima-GoldTM MV Scintillation Cocktail [Perkin Elmer Life Sciences] was added. After 14h – 16h radioactivity was counted in a MicroBeta[®]Trilux [Perkin Elmer Life Sciences].

3.1.11 Estimation of IC_{50} -values

To estimate the IC_{50} -value of each compound without assaying the compound solution in a full dose-response-curve the result of the assay for each compound (% of Control) had to be inserted into a two-parameter equation.

$$y = \frac{100\%}{1 + \left(\frac{x}{IC_{50}}\right)^s}, \quad (\text{Eq. 3.1.11-a})$$

where s is the slope factor ($= 1$), x is the final concentration of the compound to be tested (μM) in the assay and y denotes the result of the experiment for the compound to be tested (% of Control). This applies for both, functional and binding assays. If s is assumed to be 1 Equation 3.1.11-a can be reformulated as follows:

$$IC_{50} = \frac{x}{\left(\frac{100\%}{y} - 1\right)}. \quad (\text{Eq. 3.1.11-b})$$

Full concentration response curves (7-10 concentrations, depending on assay conditions) have been conducted for SAR studies to determine precise activity or affinity values whereas calculations based upon two-concentration CRCs ($1\mu\text{M}$ and $10\mu\text{M}$) were carried out for regular screens.

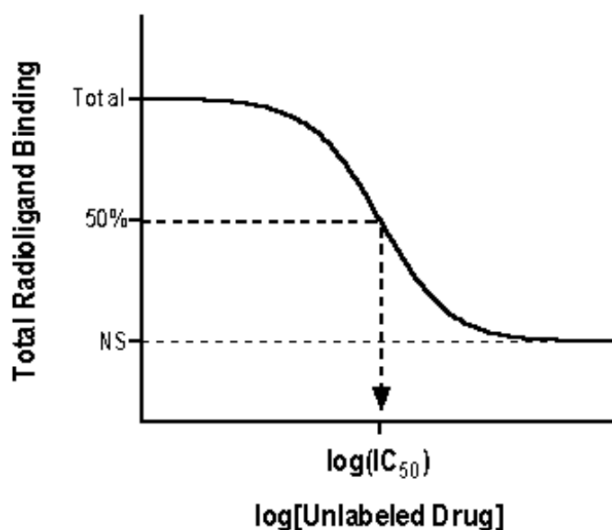


Figure 3.1.11-a. Full concentration response curve of a test ligand in a radioactive binding assay.

Results of binding experiment are normally given as K_i , a value that depends on the radioligand's properties. K_i -values were calculated from the IC_{50} -values by the Cheng-Prussoff Equation [Cheng & Prussoff, 1973]:

$$K_i = \frac{IC_{50}}{1 + \frac{L}{K_d}}, \quad (\text{Eq. 3.1.11-c})$$

where L corresponds to the radioligand concentration and K_d to its dissociation constant in a particular assay.

3.1.12 Muscarinic Acetylcholine Receptor Assay*

The increase of intracellular calcium after stimulation with carbachol was measured using the fluorometric imaging plate reader (FLIPR) and the Ca-Kit [both Molecular Devices]. Cells were seeded in black 96 well plates with clear bottom [CoStar] at a density of 60,000 cells/well and incubated in Ham's F12 medium for one night. Prior to addition of agonist or antagonist the medium was aspirated and cells were loaded for 1h at 37°C with 150 μ L of loading buffer consisting of Ca-sensitive dye [Molecular Devices] reconstituted in HBSS, MgCl₂ (0.8 mM), CaCl₂ (1.8 mM), probenecid (2.5 mM), and HEPES (20 mM), pH 7.3. Subsequently, plates were transferred to FLIPR to detect calcium increase with the addition of CBC (50 nM final concentration) measured as relative fluorescence units (RFU). If antagonists were tested, these compounds were pre-incubated for 20 min at RT before addition of CBC.

The fluorescence signal increase after addition of agonist reflects the increase of intracellular calcium. Inconsistencies in the amount of cells per well were normalised by using the spatial uniformity correction of the FLIPR software. The mean of replicated temporal data (n=5) was calculated and used for graphical representation. For the evaluation of the pharmacology, the calcium changes in response to different concentrations of agonist or antagonist were determined using a maximum minus minimum (MaxMin) or an area under the curve (AUC) calculation. All responses (CPM- or RFU-values) were determined as percentage of control (= maximum response at 50 nM CBC).

3.1.13 Dopamine D_{2short}- and D₃-Receptor Binding Assay*

Membrane preparations of CHO-cells stably expressing human D_{2short}- and D₃-receptors were used for displacement studies [Hayes *et al.*, 1992; Sokoloff *et al.*, 1992]. [³H]-Spiperone (0.2 nM) served as a radioligand and non-specific binding was determined in the presence of BP 897 (10 μM). Stock solutions (10 mM) of test compounds were prepared with pure DMSO. They were diluted to give final concentration ranges either from 1 μM to 1 mM or from 10 nM to 10 μM, depending on the test compound's affinity. The assay was incubated for 2 h at RT and terminated by rapid filtration through PerkinElmer GF/B glass fibre filters [Perkin Elmer Life Sciences] coated with 0.3% polyethylenimine [Sigma-Aldrich Chemie GmbH] using an Inotech cell harvester (Inotech AG, Dottikon, Switzerland). Radioactivity was counted using a PerkinElmer MicroBeta[®]Trilux scintillation counter [Perkin Elmer Life Sciences]. For all compounds two independent experiments were performed in triplicates. Competition binding data were analyzed by GraphPad Prism 3.02 [GraphPad Software, Inc.], using non-linear least squares fit. K_i values were calculated from the IC_{50} values according to Cheng-Prussoff (Equation 3.1.11-c).

3.1.14 Histamine H₁-Receptor Binding Assay*

Membrane preparations of CHO-cells stably expressing human H₁-receptors were used for displacement studies [Smit *et al.*, 1996]. [Pyridinyl-5-³H]-pyrilamine (1 nM) served as a radioligand and non-specific binding was determined in the presence of chlorphenamine hydrogenmaleate (10 μM). Stock solutions (10 mM) of test compounds were prepared with pure DMSO. They were diluted to give final concentration ranges from 1 μM to 1 mM. The assay was incubated for 2 h at RT and terminated by rapid filtration through PerkinElmer GF/B glass fiber filters [Perkin Elmer Life Sciences] coated with 0.3% polyethylenimine using an Inotech cell harvester. Radioactivity was counted using a PerkinElmer MicroBeta[®]Trilux scintillation counter [Perkin Elmer Life Sciences]. For all compounds two independent experiments were performed in triplicates. Competition binding data were analyzed by GraphPad Prism 3.02 [GraphPad Software, Inc.], using non-linear least squares fit. K_i values were calculated from the IC_{50} values according to Cheng-Prussoff (Equation 3.1.11-c).

3.2 Computational Methods

3.2.1 CATS 2D Similarity Search

CATS (Chemically Advanced Template Search) enables a topological pharmacophore search applicable for virtual screening procedures. The CATS descriptor denotes a topological atom-pair descriptor and has been reported earlier [Schneider *et al.*, 1999]. Since it is based on the two-dimensional structure of a molecule it circumvents problems derived from conformational flexibility. Topological information of a molecule is encoded with the CATS descriptor by the following procedure: Assigning each atom (i.e., a node of the molecular graph) to one of the following generalized atom types: hydrogen-bond donor (D), hydrogen-bond acceptor (A), positively charged (P), negatively charged (N) or lipophilic (L) (Figure 3.2.1-a). Atoms which do not belong to one of the five mentioned potential pharmacophore point groups are not taken into account. Atom pairs denote the shortest distance connecting two nodes. The frequency of all 15 possible atom pairs of CATS types (DD, DA, etc.) is determined and the resulting histogram is divided by the number of non-hydrogen atoms in the molecule to get a scaled vector [Fechner *et al.*, 2003].

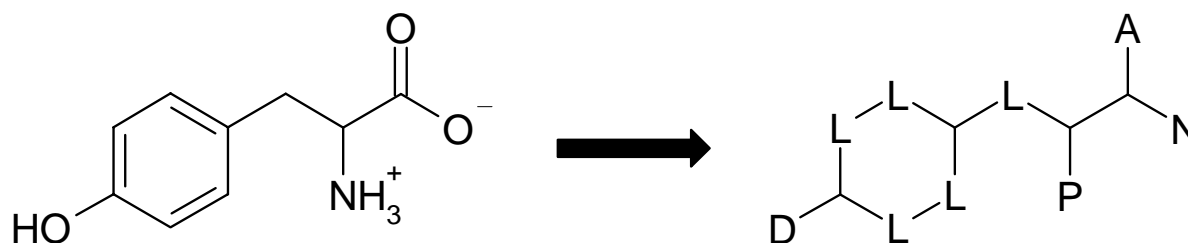


Figure 3.2.1-a. Schematic conversion of a two-dimensional molecular representation into a molecular graph with assigned generalized atom types.

The CATS-similarity is defined by the degree as to which the topological pharmacophore descriptors of two molecules A and B match and is expressed by the euclidian distance measure $D(A,B)$ (Equation 3.2.1-a):

$$D(A, B) = \sqrt{\sum_{i=1}^{150} (v_i^A - v_i^B)^2} \quad (\text{Eq. 3.2.1-a})$$

where v^A and v^B denote the correlation-vectors derived from molecules A and B.

To obtain a final ranked list the compounds were sorted by increasing order according to the CATS-dissimilarity - that is the distance given as Tanimoto coefficient - of the test compound towards the reference compound within the individual lists that resulted from the similarity searches.

3.2.2 Self-Organizing Maps

For the studies presented within this thesis two-dimensional Kohonen-maps with a toroidal topology were used and visualized as squares consisting of either 100 or 225 neurons.

The SOM training process is comparable to vector quantization, where the network weight vectors move towards the centers of data distribution [Nasrabadi & King, 1988]. During the SOM training input patterns χ (here: descriptor vectors) are compared to all neurons w of the output layer (“fan-out” units). The neuron vector displaying the highest similarity to a particular input vector gets activated (“winner neuron”) while the other neurons remain inactive. For SOM training the Kohonen-algorithm was applied:

1. Initialize a map M to contain $N=N_1*N_2$ neurons c_i with the reference vectors $w_{ci} \in R^n$ randomly chosen according to $p(\chi)$ from the input patterns. Initialize the connections to form a rectangular N_1*N_2 grid and the time parameter $t = 0$.
2. Generate randomly an input signal χ according to $p(\chi)$.
3. Determine the “winner neuron” according to the vector distance between the training patterns χ and the neurons w .
4. Adapt each neuron r to $p(\chi)$ according to

$$\Delta w_r = \varepsilon(t)h_{rs}(\chi - w_r). \quad (\text{Eq. 3.2.2-a})$$

The Gaussian neighborhood function around the winner neuron s is

$$h_{rs} = \exp\left(\frac{-d_l(r,s)^2}{2\sigma(t)^2}\right). \quad (\text{Eq. 3.2.2-b})$$

where the Hamming distance d_l defines the distance between two neurons and σ is the standard deviation. The time dependent standard deviation can be calculated by:

$$\sigma(t)_{initial} = \left(\frac{\sigma_{final}}{\sigma_{initial}} \right)^{\frac{t}{t_{max}}}, \quad (\text{Eq. 3.2.2-c})$$

and the time dependent learning rate by:

$$\varepsilon(t)_{initial} = \left(\frac{\varepsilon_{final}}{\varepsilon_{initial}} \right)^{\frac{t}{t_{max}}}. \quad (\text{Eq. 3.2.2-d})$$

5. Increase time parameter $t = t + 1$.
6. If $t < t_{max}$ continue with 2., otherwise abort.

The training of SOMs was computed with *som_create* using 10x10 (100) and 15x15 (225) neurons, $t_{max} = 60,000$, $\sigma_{initial} = 1$ and $\varepsilon_{initial} = 6$. Visualization was performed with *som-show* (software by Schneider, unpublished).

3.2.3 Principal Component Analysis

For definitions of the matrices used for *ChemSpaceShuttle* (CSS) the reader is referred to the original literature [Givehchi *et al.*, 2003]. Data projections for this particular study have been done by the NIPALS algorithm and encoder networks, implemented in CSS. The input vectors were projected to the space covered by the first three eigenvectors calculated with the NIPALS algorithm:

1. Normalize the data set (unit variance scaling and mean entering).
2. Set the array of the of the score matrix \overline{s}_i to the first column \overrightarrow{x}_1 of the input vector matrix \overline{X} (each row of this matrix denotes a different compound and each column a different matrix).
3. Calculate:

$$\frac{\overrightarrow{l}_i}{\overrightarrow{l}_i^T} = s_i^{step3^T}, \quad (\text{Eq. 3.2.3-a})$$

where T means transpose.

4. Normalize the vector \vec{l}_i to the length 1:

$$\vec{l}_i = \frac{\vec{l}_i}{\|\vec{l}_i\|}. \quad (\text{Eq. 3.2.3-b})$$

5. Calculate:

$$s_i^{\text{step5}} = \bar{X} \cdot \frac{\vec{l}_i}{\|\vec{l}_i\|^2}. \quad (\text{Eq. 3.2.3-c})$$

6. Compare s_i^{step5} from step 5 to s_i^{step3} from step 3 ; if the sum of squared residual is smaller than 10^{-10} then go to step 7, else go to step 3 and calculate \vec{l}_i again.
7. Calculate the residual \bar{R} : $\bar{R} = \bar{X} - s_i^{\text{step5}} \vec{l}_i^T$ and set $\bar{X} = \bar{R}$. If $i = p$ or $R < 10^{-10}$ then stop the calculation, else go to step 3.

After i loops the composition of the X-matrix will be obtained, i.e., $\bar{X} = s_1 l_1^T + s_2 l_2^T + \dots + s_i l_i^T$.

Data projection performed by encoder networks can be divided into two procedures. In the first step the input vectors are supplied to the input and output layer (Figure 3.2.3-a). The input data can reasonably be described by the values of the neurons forming the parameter (i.e., hidden) layer only if the network weights are optimized. Therefore, CSS applies a $(1, \lambda)$ evolution strategy representing an adaptive stochastic search method [Bäck & Schwefel, 1993; Schneider & Wrede, 1998]. Here, Kruskal's STRESS serves as a goodness-of-fit measure [Kruskal, 1964]:

$$S = \sqrt{\frac{\sum_i \sum_j (d_{ij}^t - d_{ij}^o)^2}{\sum_i \sum_j d_{ij}^{o^2}}}, \quad (\text{Eq. 3.2.3-d})$$

where d_{ij}^t denotes the Euclidean distance between the 3D-vectors i and j , and d_{ij}^o is the Euclidean distance between the original descriptor vectors i and j .

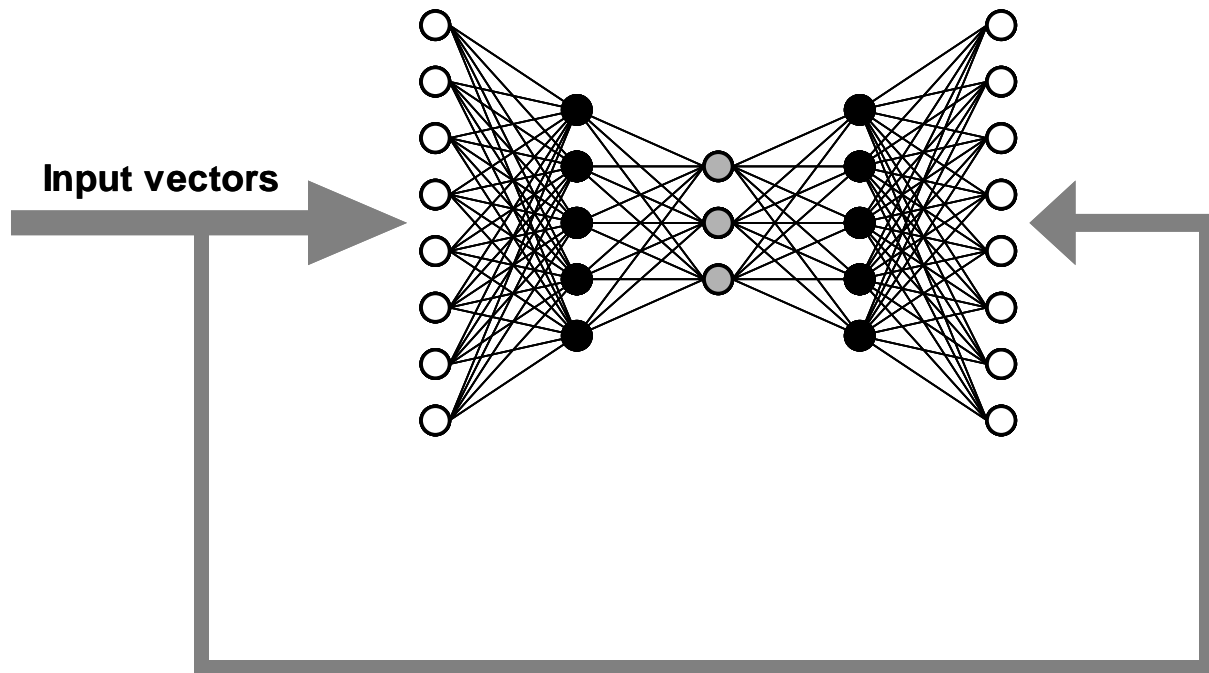


Figure 3.2.3-a. Architecture of an encoder network in the training mode implemented in CSS. Descriptor (input) vectors supply both, the input and output layers (empty circles) with original data.

Once a previously defined STRESS value is reached, the training mode is completed. Now the optimized net enables the transformation of the high-dimensional to low-dimensional data (Figure 3.2.3-b) from the input layer to the parameter layer leaving out the output layer. The three neurons of the parameter layer represent the final vectors in the 3D-plot.

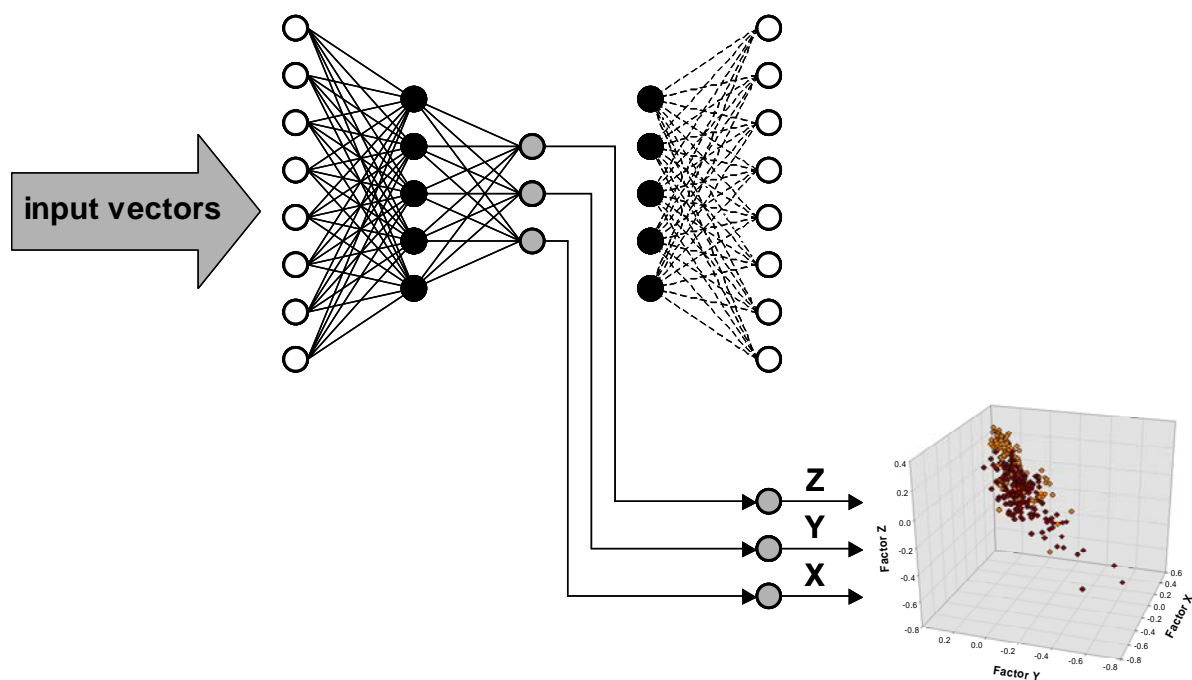


Figure 3.2.3-b. Architecture of an encoder network in the projection mode implemented in CSS. The output values of the three central neurons (grey circles) can be visualized by representing a 3D-plot.

3.2.4 Comparative Molecular Field Analysis

The CoMFA method has been detailed nearly two decades ago [Cramer *et al.*, 1988]. A set of chemically similar molecules (optimal number of structures: 20-50) has to be flexibly aligned in a proper way according to structural pharmacophore features (e.g., H-bond donor/acceptor, etc.). These molecules should bear a consistent core structure differing only in type and position of substituents. Setting up a reasonable alignment is a pivotal step since the predictive capability of a CoMFA model strongly depends on the alignment.

In the next step the aligned structures have to be embedded into a three-dimensional rectangular grid with sufficient space to encompass all molecules. Each lattice point represents a positively charged carbon atom with sp^3 properties, which measures the steric interaction energy (Lennard-Jones potential) and the electrostatic energy (Coulomb potential) for all atoms of each molecule. To minimize domination by large steric and electrostatic energies, all energies that exceed a previously defined threshold value are set to this cutoff value. These energy calculations produce an extraordinary large amount of data resulting in by far more columns than rows. To extract a stable QSAR from such an unproportioned data table the partial least-squares (PLS) method was employed [Wold, 1966; Lindberg *et al.*, 1983]. The columns are not auto scaled since the units of all columns are the same (kcal/mol). Cross-validation evaluates a model by how well it predicts data points, not used for the

calculation. Noteworthy, activities of molecules that extend into regions not covered by the training set cannot be predicted, which pertains to all QSAR methods.

CoMFA models have been established using the QSAR tool implemented in the Sybyl 7.1 software package [Tripos Inc.]:

Initially, the EMQMCM-data collection (Section 3.2.6) was loaded in Sybyl 7.1 as sd-file. Activity data have been added by means of pIC_{50} -values. 3D structures of ligands were generated using CONCORD. The structure energy minimization was performed for CoMFA using the Tripos molecular force field [Clark *et al.*, 1989] and Gasteiger-Hückel charges. Steric and electrostatic interactions were calculated with same force field using a distance dependent dielectric constant at all intersections in an evenly spaced 2.0Å grid. The cutoff was set to 30 kcal/mol. To create an initial model, the dataset was divided into a training and a test set as follows: all molecules were sorted in ascending order with respect to their internal ID. The first nine entries constituted the test set and the remaining 30 entries the training set. Regression analysis was performed using the full cross-validated PLS method (leave one out). Based on the training set the final model was calculated using the optimum number of components to that yielding the highest q^2 (cross-validated). Optimum number does not necessarily mean the number of components yielding the highest $q^2(cv)$: According to the “parsimony-principle” an increase of $q^2(cv)$ values of less than 5% for the use of an additional component was used as a stop criterion [Thibaut *et al.*, 1993]. For improved statistical significance of the results ten new models were established by randomly dividing the total dataset into two subsets of nearly equivalent size (20 molecules training set, 19 molecules test set).

Several parameters reflect the quality of a given model and indicate how well it fits existing data. PRESS and q^2 have been proposed for cross-validation to give good estimates of the real prediction of a model :

$$PRESS = \sum_{i=1}^N (y_{pred,i} - y_{obs,i})^2, \quad (\text{Eq. 3.2.4-a})$$

where N is the number of objects and y denotes the target parameter in the activity data. Based upon this equation q^2 can be calculated as follows:

$$q^2 = 1 - \frac{PRESS}{\sum_{i=1}^N (y_{obs,i} - \overline{y_{obs}})^2}. \quad (\text{Eq. 3.2.4-b})$$

To validate the derived CoMFA models, activity data of the external test sets were predicted using the models derived from the training set. The predictive abilities of the training sets were expressed by $q^2(cv)$ whereas the predictive ability of the test sets were expressed by the analogous r^2_{pred} using the formula

$$r^2_{pred} = \frac{SD - PRESS}{SD}, \quad (\text{Equation 3.2.4-c})$$

where SD denotes the sum of squared deviations between the activity of the test set compounds and the mean activity of the training set compounds, and $PRESS$ is the sum of squared deviations between the observed and the predicted activity of the test set molecules.

All-placement search (APS) and all-orientation search (AOS) describe techniques which optimize the field sampling routine in the CoMFA approach [Wang *et al.*, 1998]. They allow for assessing the statistical relevance of a given model. Since steric and electrostatic interactions are distance dependent there exists a strong influence of the relative orientation of the alignment against the probe grid [Böhm *et al.*, 1999]. Starting from an arbitrary orientation APS and AOS provide a way to stepwise translate the molecular aggregate within the lattice and to detect a specific orientation leading to the highest q^2 and consequently the most valid CoMFA model.

The corresponding spl-scripts and shell scripts obtained from the authors were implemented in Sybyl 7.1. For APS the whole grid was systematically translated in 0.1\AA -steps against the molecular aggregate. This process was performed in all three dimensions of the coordinate system and finished after 2.0\AA since in this case the grid had overlapped the original one. Therefore, $20 \times 20 \times 20 = 8000$ placements were obtained. In contrast, AOS allowed for rotating the molecular aggregate in the grid around the x-, y- and z-axis. The stepwise rotation was divided into increments of 20° resulting in $18 \times 18 \times 18 = 5832$ orientations.

3.2.5 Homology Modeling

Note: The homology model of the transmembrane region of the mGlu1 receptor presented in this thesis has not been built by the author. It was solely developed by Steffen Renner, a former postdoctoral student at Merz.

The mGluR1 receptor was modeled based on the template of bovine rhodopsin (PDB code 1I9h). An alignment of the transmembrane region of the rat mGluR1 sequence to the transmembrane region of bovine rhodopsin was adapted from previously published mutational studies on mGluR1 and other related class C GPCRs:

Based on the effect of mutations in the transmembrane region on binding of the mGluR1 negative allosteric modulator EM-TBPC an alignment for mGluR1 to bovine rhodopsin was proposed [Malherbe *et al.*, 2003a]. Alignments for transmembrane helices for which mutations affected the binding of EM-TBPC (3, 5, 6, and 7) were adopted directly. These alignments were consistent with mutational data for mGluR5 for the binding of M-MPEP [Pagano *et al.*, 2000] and MPEP [Malherbe *et al.*, 2003b]. The only reported mutation in a family 3 GPCR for transmembrane helix 2 (TM2), that was found to influence the binding of an allosteric modulator, was found in the calcium sensing receptor [Miedlich *et al.*, 2004]. Thus, the alignment of TM2 was overtaken from this study and converted into the mGluR1 sequence. The alignment of TM1 was used from Malherbe *et al.* [Malherbe *et al.*, 2003a]. For TM4 a more reasonable alignment was found for the model of the calcium sensing receptor [Miedlich *et al.*, 2004], where two neighboring prolines at the C-terminal end of TM4 were aligned with two prolines in the C-terminus of the rhodopsin TM4. Since these two prolines were conserved in mGluR1 and in other family 3 GPCRs this alignment was used. The final alignment is given in the following Figure.

TM1

```
>bopsd      38  SMLAAYMPLLIMGFPINFLTLVTVQ
>rmGluR1    590  DIESIIAIAASCLGILVTLFVTLIFVL
Consensus/80%  sbbthbhbhb.hLGb.lsbshblhVb
```

TM2

```
>bopsd      71  PLNYILLNLAVVDLDMVFGGFTITLY
>rmGluR1    625  SSSRELICYIILGIFLGYVCPFLIA
Consensus/80%  s.sbbLh.lh1AslFbsass.hThlh
```

TM3

```
>bopsd      108  TGCNLEGFATGGGEIALWSLVVLAIRYVVC
>rmGluR1    655  TSCYLQRLLVGLSSAMCYSAVTKTNRIARILA
Consensus/80%  TtC.Lp.bbssLtt.bsb.tLVsbs.cbh.l1s
```

TM4

```
>bopsd      150  ENHATMGVAFTWVMALACAAPPDVA
>rmGluR1    709  TASILISVQTEFVVTLLIIMEPPMP
Consensus/80%  bsphlbtV.bTbVhsLhhh.PPbs
```

EL2

```
>bopsd      178  YIPE      185  CSCG
>rmGluR1    736  YPSI      744  LICN
Consensus/80%  Y.sb.....h.Cs
```

TM5

```

>bopsd      205  IYMFVVHFIIPLVVIFFCYGLVFTV
>rmGluR1    750  NLGVVAPVGVNGLTIMSCTYFAKTR
Consensus/80%  .bhhVs.hhbsh11Ib.ChhbhbT.

```

TM6

```

>bopsd      249  EVTRMVIIMVIAFLICWLPYAGVAFY
>rmGluR1    782  NEAKYIAFTMTTCIIWLAFLVPIYEG
Consensus/80%  p.s+blhbhbshhIhWLSasslhFh

```

TM7

```

>bopsd      288  MTIPAFFAKTSAVYNPVIYIMN
>rmGluR1    811  KIITTCEAVLSVTVALGCMFTP
Consensus/80%  bhIsshFA.*.tVhsslhbhbhs

```

Figure 3.2.5-a: Alignment of transmembrane helices and EL2 of rat mGluR1 to the bovine rhodopsin structural template. Consensus symbols other than residue letters are: - = negative, * = ser/thr, | = aliphatic, + = positive, t = tiny, a = aromatic, c = charged, s = small, p = polar, b = big, h = hydrophobic. Identical residues are highlighted in grey. Similar amino acids are colored according to the following scheme: red = negative, cyan = S/T, grey highlighted yellow = aliphatic, dark blue = positive, light green = tiny, dark blue highlighted yellow = aromatic, pink = charged, dark green = small, light blue = polar, light blue highlighted yellow = big, black highlighted yellow = hydrophobic.

For the initial model of mGluR1 the HOMER server (version 1.3) [Tosatto, 2005] was used. HOMER was successful for the transmembrane regions, however, most of the modeled loops were not closed, i.e., they were only connected to a single helix instead of connecting two helices. Thus the torsion angles of the loop residues were refined manually to enable the connection of the helices. The loops were minimized with the Tripos force field (max. 500 steps Powell with Simplex initiation) within Sybyl 7.1 [Tripos Inc.]. The extracellular loop 2 (EL2) in direct contact with the inverse agonist in bovine rhodopsin was modeled by taking the backbone coordinates of the conserved disulfide bridge and neighboring residues (Figure 3.2.5-a). In class C GPCRs the linker from the disulfide Cys in EL2 to TM5 is much shorter compared to bovine rhodopsin. To enable a connection between TM5 and EL2, TM5 was moved towards the center of the seven helices until the residues were sufficiently near to each other to be connected. The structure was minimized, and irresolvable side chain clashes were solved by using different rotamers. Ligands were placed manually into the receptor, based on the position of 11-*cis*-retinal in bovine rhodopsin, and subsequently minimized with the Tripos force field. Residue numberings are used according to the scheme proposed by Malherbe [Malherbe *et al.*, 2003b].

3.2.6 Datasets

Four different datasets were employed for the present studies: The EMQMCM-data collection has been compiled based on a series of quinoline-derivatives [Mabire *et al.*, 2005] and was used for the QSAR studies. Initially, it contained 49 compounds bearing the same core structure including precise activity data for the rmGlu1 receptor. Ten molecules have been removed from the dataset either lacking precise bioactivity values or being structurally distinct from the other molecules (that is their residues point into spatial regions not covered by other molecules; consequently, they would falsify the QSAR models).

The Asinex Gold Collection provided by Asinex [Asinex Ltd.] was used in sd-format for virtual screening purposes. This external compound library is continuously being updated and we applied the versions of February 2003 (194,598 entries) and October 2003 (201,304 entries). Apart from the 2D-chemical structures they include predicted Lipinski rule properties [Lipinski *et al.*, 1997]. Both versions contain many compounds violating these rules, as it was exemplified for the latter version (October 2003). The database was filtered for drug-likeness according to the following cut-offs [Lipinski *et al.*, 1997]: five or less H-bond donor atoms, 10 or less H-bond acceptor atoms, MW < 500 and SlogP < 5. 156,112 structures (77.55%) fulfilled these criteria but 45,192 (22.45%) failed.

The COBRA 3.12 database was solely used for developing SOMs. This collection (5,376 molecules) was compiled from scientific literature and is a set of bioactive reference compounds affecting a large number of different targets like proteases, kinases, GPCRs and ion channels [Schneider & Schneider, 2003]. The COBRA compounds have mean values of MW and logP which are within the limits proposed by Lipinski's rule of five (MW<500 and logP<5) [Lipinski *et al.*, 1997].

The mGluR-data collection comprises 357 positive and negative allosteric modulators of mGluR1 and mGluR5 and was manually compiled from literature. It served as reference molecule dataset for all campaigns in this thesis (detailed description in Section 4.1)

4 Scaffold Identification

A goal of this thesis was to improve the understanding of function and ligand binding in the transmembrane region (HD) of group I metabotropic glutamate receptors (mGluR) and in particular of subtype 1. The identification of ligands acting as allosteric modulators and providing novel core structures (i.e., “scaffolds”) was one of the two main rationales of this thesis since these ligands may facilitate further insight into the binding mode at the allosteric binding site (e.g., knowledge about structural requirements for (i) potent and selective binding and (ii) inactivation of receptor function). The precise architecture of the HD of group I mGluRs is still unexplored; yet some hypotheses have been published [Belenikin *et al.*, 2003; Malherbe *et al.*, 2003a/b]. Therefore, a structure-based approach for the detection of novel ligands remains inherently difficult so we pursued a ligand-based approach. Several methods of virtual screening have been employed (Section 1.5). In the following chapter we describe their application and evaluate their suitability for the given research objective. The whole hit finding procedure describes a sensible alternative to simple compound screening pursued by HTS.

4.1 Data Consolidation

The elucidation of novel hits for mGlu1 receptor *via* virtual screening requires the collection of ligands affecting mGluR1. More precisely, before applying several virtual screening methods the need of compiling a data collection of reference molecules providing as much structural information as possible arose. Homology models of the transmembrane region of the mGlu1 receptor have been reported [Belenikin *et al.*, 2003; Malherbe *et al.*, 2003a] but they remain only hypotheses as long as the crystal structure is not known. Thus, we pursued the ligand-based approach. Such approaches aiming at detecting novel ligands for a given target regarding the chemical core structure need at least one known bioactive molecule as a starting point. This requirement was fulfilled for both, mGluR1 and mGluR5 (Section 1.4.2). Since success or failure of performing virtual screening procedures and setting up a valid pharmacophore hypothesis strongly depends on the reference dataset, compounds to be included in such a library have to be carefully selected concerning the subtype selectivity and the correct chemical structure.

4.1.1 Assembling a Data collection

A collection of reference molecules in the following referred to as mGluR-data collection has been compiled. This library comprises in total 357 ligands acting at the allosteric sites of the mGlu1 and mGlu5 receptor (Table 4.1.1, Table 7.1-a), which have been solely collected from scientific literature and patents published until August 2003. Though this dataset has been continuously updated by adding recently published molecules, a copy of the original compilation was saved for the purpose of retrospective analyses. Each entry is described by the chemical structure of the molecule and its activity and, if available, affinity data. However, it must be stressed that the functional assays that were performed to determine the activities differ to some extent between different research groups, mainly concerning the tissue (e.g., membranes or cell lines) and the detecting devices. Consequently, the relative potency at the same receptor could not strictly be compared for molecules from different publications or patents. During the hit finding process such differences were not crucial since no SAR studies were performed where precise activity values are generally required. Therefore, at this stage it was sufficient to discriminate mainly between “potent” (< 1 μ M cut-off) and “highly potent” (< 100 nM cut-off) compounds.

Table 4.1.1-a. Distribution of the mGluR-compounds in the mGluR-data collection regarding the receptor subtype and interaction mode.

Target	Molecules
Negative allosteric modulators of mGluR1	212
Positive allosteric modulators of mGluR1	19
Negative allosteric modulators of mGluR5	125
Positive allosteric modulators of mGluR5	1

4.2 Pharmacophore Model

To initiate a hit finding process it seemed reasonable to create a flexible overlay of known allosteric mGluR1 antagonists. Such an alignment describes the template for establishing a pharmacophore model. A pharmacophore model in turn can be interpreted as a visualized pharmacophore hypothesis. It displays a set of structural features, which preferably several ligands have in common and is related to the ligand's recognition at the target site (Section 1.5.1).

The underlying idea of starting a hit identification process in this way has several reasons: (i) Some of the ligand-based screening approaches rely on a three-dimensional pharmacophore model or at least on certain molecules used for that model. (ii) It was helpful to get a first impression of common structural features of ligands bearing different core structures and of their potentially pivotal interaction points. In general, initial knowledge of relevant pharmacophore features obtained, e.g., by collecting reference molecules as starting point for virtual screening and postulating a hypothesis is inevitable to correctly interpret screening results. In particular, visually revising a set of retrieved virtual hits in order to sort out potentially non-relevant molecules is only feasible when the medicinal chemist is provided with sufficient information about already known ligands (meaning structural requirements, that is features being crucial for binding to the receptor).

4.2.1 Molecules from the Reference Data collection

The pharmacophore hypothesis presented herein is based on a set of six reference molecules. They were selected from the mGluR-data collection as they were corresponding to the following requirements:

- Ligands known as allosteric antagonists of mGluR1
- Ligands being structural diverse to each other
- Ligands revealing high activity (< 100 nM cut-off) at mGluR1.

In total, six compounds were selected fulfilling these criteria (Figure 4.2.1-a). This number was assumed to be sufficient since a proper pharmacophore model should comprise as few molecules as necessary providing as much structural information as possible.

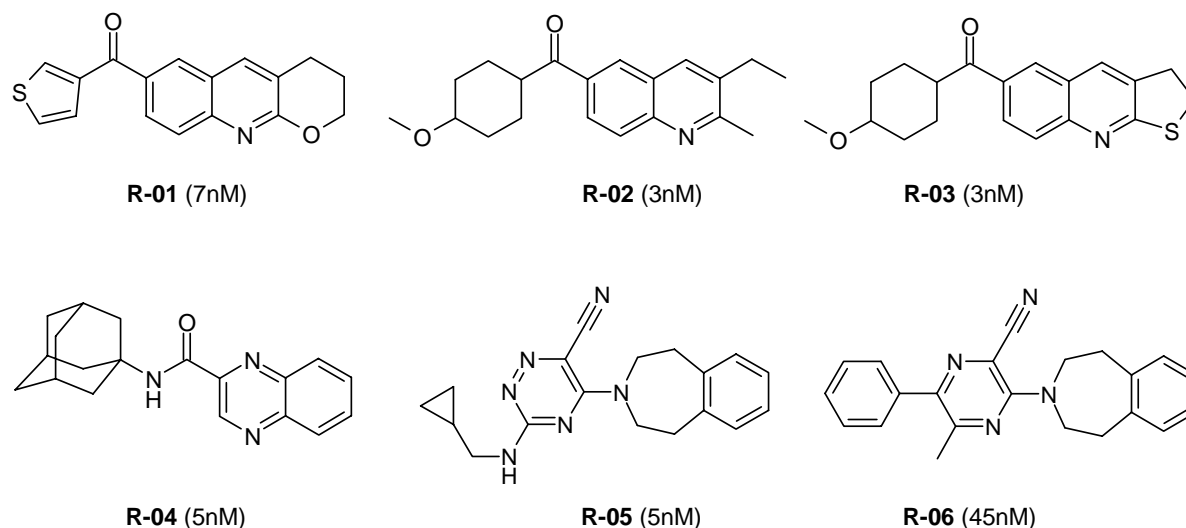


Figure 4.2.1-a. Chemical structures including functional activity at mGluR1 of reference molecules **R-01-R-06** selected from the mGluR-data collection and used for the pharmacophore model. Molecules **R-01** and **R-03** closely resemble R214127, molecules **R-05** and **R-06** are EM-TBPC analogues. **R-02** is identical to R193548 and **R-04** is identical to NPS 2390 (both Figure 2.2.1-a).

Molecules **R-01-R-03** present an almost identical scaffold, since it has proven in the past to be advantageous to use at least two molecules providing the same scaffold as starting point to perform a flexible overlay (Section 4.2.2). In this context, similarities of the reference molecules according to MACCS keys are given in Table 4.2.1-a. Molecules **R-05** and **R-06** display the highest degree of structural similarity, whereas similarity between **R-02** – **R-03** is less pronounced. Overall, the similarity index is below 0.8, which is usually considered as an indication of different chemotypes [Matter, 1997; Martin *et al.*, 2002].

Table 4.2.1-a. Similarities of the six mGluR-data collection representatives. Values denote Tanimoto coefficient of MACCS similarity.

Number	MACCS Similarity to R-01	MACCS Similarity to R-02	MACCS Similarity to R-03	MACCS Similarity to R-04	MACCS Similarity to R-05	MACCS Similarity to R-06
R-01	1	0.457	0.614	0.442	0.258	0.304
R-02	0.457	1	0.674	0.316	0.292	0.346
R-03	0.614	0.674	1	0.318	0.275	0.345
R-04	0.442	0.313	0.318	1	0.362	0.380
R-05	0.258	0.292	0.275	0.362	1	0.765
R-06	0.304	0.346	0.345	0.380	0.765	1

4.2.2 Creating the Pharmacophore Model

After generating 3D structures for all molecules using a favored force field for small compounds (MMFF94) [Halgren, 1996], molecules **R-01** and **R-02** were superimposed in a flexible manner using the *Flexible Alignment* tool included in the MOE software package Version 2003.02 [Chemical Computing Group] according to the following settings (Iteration limit: 200 attempts; Failure limit: 20 configurations in a row; Energy Cutoff: 10.0 energy value plus the minimum generated value; Configuration limit: 1000 alignment configurations; Alpha: 2.5; Gradient Test: 0.01; RMSD Tolerance: 0.5Å; Maximum steps: 500 energy minimization steps; Similarity Terms: H-bond Donor/Acceptor (1/1), Aromaticity (3), Acid/Base (1), Hydrophobe (1), Polar Hydrogens (1), Volume (3)). Several orientations have been calculated including their corresponding energy values. One orientation with a low energy value and a reasonable overlay (i.e., the most complete overlay with respect to the core structures) was manually selected and both molecules were kept in a fixed position relative to each other for further alignments. In the next step, molecule **R-03** was superimposed onto this orientation and a sensible overlay was saved and fixed for the next alignment procedure. Eventually, the remaining three structures were aligned one after the other on this orientation resulting in a final alignment for allosteric mGluR1 antagonists (Figure 4.2.2-a). Alignment settings remained unchanged throughout the whole process.

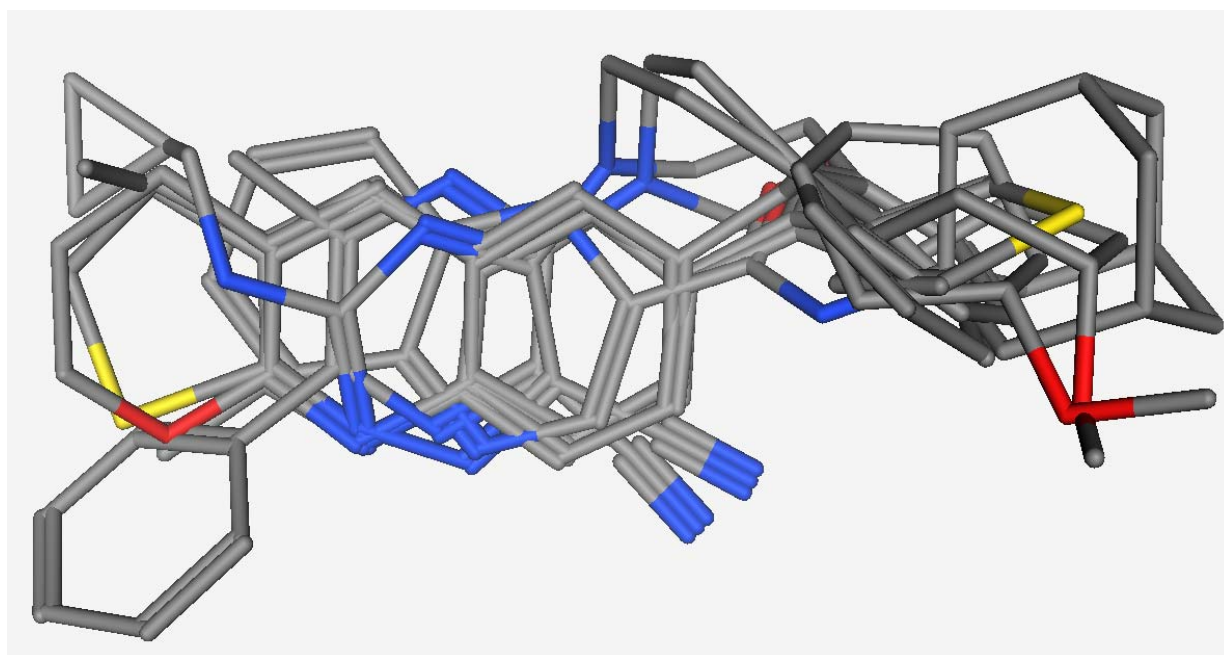


Figure 4.2.2-a. Flexible alignment of reference compounds **R-01-R-06** (hydrogen atoms not shown).

A pharmacophore hypothesis was established based upon this flexible overlay using the *Pharmacophore Query Editor* of the MOE software. This tool displays certain chemical properties (H-bond donor/acceptor, etc.) of non-hydrogen atoms of each molecule to be edited, which are here referred to as annotation points (a complete list is given in the Appendix, Table 7.2-a). A pharmacophore scheme defines how each ligand in the database to be searched is annotated. Depending on the selected pharmacophore scheme, lipophilic or aromatic properties of ring systems, for instance, can be displayed either for each carbon atom of the corresponding ring (*Planar-Polarity-Charge-Hydrophobicity*; PPCH-type) or by one annotation point for the whole ring located in its center (*Polarity-Charge-Hydrophobicity*; PCH-type). For this model the default PCH-type was employed. Here, annotation points of the same label, which occur in all reference molecules at nearly the same spatial position were presumed to be important, for instance item *F2:Acc* in the lower left part of Figure 4.2.2-b. Query features were then assigned to these important annotation points (Figure 4.2.2-b).

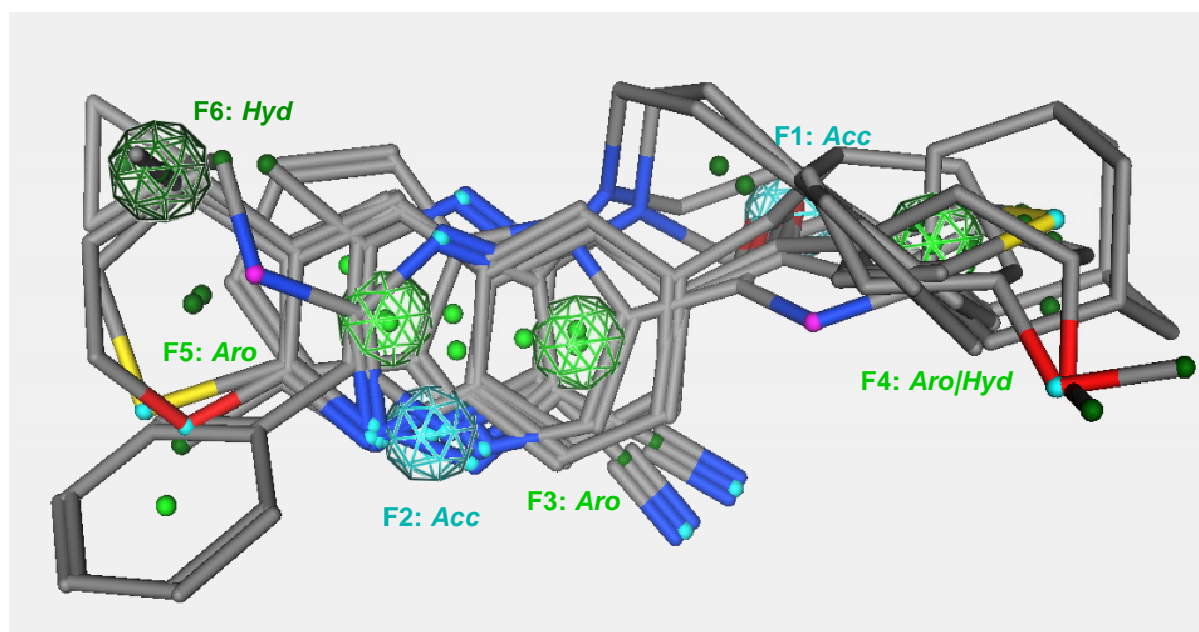


Figure 4.2.2-b. Preliminary pharmacophore hypothesis and underlying reference alignment for non-competitive antagonists of the mGlu1 receptor (H-atoms were hidden for more clarity). Small and solid balls in various colors according to their properties indicate the automatically proposed annotation points. Light blue spheres denote manually allocated query features for H-bond acceptors, light green spheres represent aromatic features and dark green spheres show hydrophobic query features. For details see text.

A query feature denotes a point in space with a radius-like tolerance on spatial proximity and an associated expression. Expression and radius of each query feature were manually edited as follows: The expression corresponds to the annotation points found here (e.g., query

feature *F4:Aro/Hyd* in Figure 4.2.2-b denotes a region where aromatic and hydrophobic labeled annotation points were found). The diameter of each tolerance radius was chosen sufficiently large to cover identical annotation points of every molecule in that region.

Constraints and partial matches (both are options within the *Pharmacophore Query Editor*) have not been applied to the initial pharmacophore model. A constraint groups query features that tie the required presence of one feature to the presence of another feature. A partial match in turn allows a certain degree of violations within a constraint (e.g., a constraint of three query features combined with a partial match of at least one query feature means that at least one of these three queries must be matched irrespective which of them).

The preliminary pharmacophore hypothesis contains six query features assumed to play an important role (Figure 4.2.2-b). Excluded volumes, which denote spheres that must not contain any non-hydrogen atom of a ligand to be aligned have not been allocated.

4.2.3 Validation

Prior to performing a pharmacophore search on an external compound library the preliminary model had to be assessed for its validity. Therefore, a set of ten 3D-conformations was calculated for each molecule of the mGluR-data collection using *MOE Conformation Input* (10 conformations, no input filters (physicochemical properties) but default Constraints; MM Settings (default): Stochastic Search Strain Limit: 7, Superpose RMSD Test: 0.15, Refinement Conformation Limit: 300, Stochastic Search Failure Limit: 30, Stochastic Search Iteration Limit: 500, Energy Minimization Iteration Limit: 200, Energy Minimization Gradient Test: 0.01).

The mGluR-data collection was then virtually screened by employing the preliminary model and the aim was to retrieve as many of the 212 non-competitive mGluR1 antagonists as possible and as few other data collection members as possible. In general, an automatic pharmacophore search can be described as follows: When a new ligand is aligned with the query set, its ligand annotation points will match the given query feature only if the points lie within the specified radius of the query feature and if its set of attached labels satisfies the expression associated with the feature.

After a first pharmacophore search of the mGluR-data collection certain settings of the query set were slightly changed in order to optimize the screening results. This was an iterative process where only one parameter was manually modified in each step. However, no crucial modifications have been done like removing or adding essential query features. Mainly, the radius-like tolerance of a query feature was enlarged or reduced.

Visual inspections of the first pharmacophore search results revealed that many mGluR1 antagonists being members of the mGluR-data collection failed to match the query set since their structures did not satisfy all query features allocated to the pharmacophore model. To circumvent this pitfall initially all query features were tied together to one constraint and a partial match was introduced. During the iterative validation process one or two query features were alternately removed from the constraint or incorporated into it and the partial match restriction was changed accordingly.

Table 4.2.3-a. Distribution of the mGluR-data collection and the mGluR1-enriched subset after the pharmacophore search.

Target	mGluR-data collection	Retrieved subset
Negative allosteric modulators of mGluR1	212	69
Positive allosteric modulators of mGluR1	19	5
Negative allosteric modulators of mGluR5	125	2
Positive allosteric modulators of mGluR5	1	-

The validation process was terminated after roughly ten steps when no further enrichment in the subset of correctly retrieved mGluR1-reference compounds was yielded (Table 4.2.3-a). The results illustrate a successful performed search, which is confirmed by an enrichment-factor ef of 1.53 (Equation 1.5.2-b). Interestingly, a fourth of all positive mGluR1 modulators has also been extracted, whereas less than 2% of all mGluR5 antagonists matched the pharmacophore model's queries. Only a third of all target compounds (69 of 212) has been correctly classified, which impairs the model to a certain extent as it does not retrieve all chemotypes of the reference molecules. This is caused by the fact that only a small selection of the many different scaffolds of mGluR1 antagonists was considered in the molecule alignment. The integration of additional scaffolds would most likely have led to an impaired molecule alignment (less overlay) and consequently to a less precise pharmacophore model.

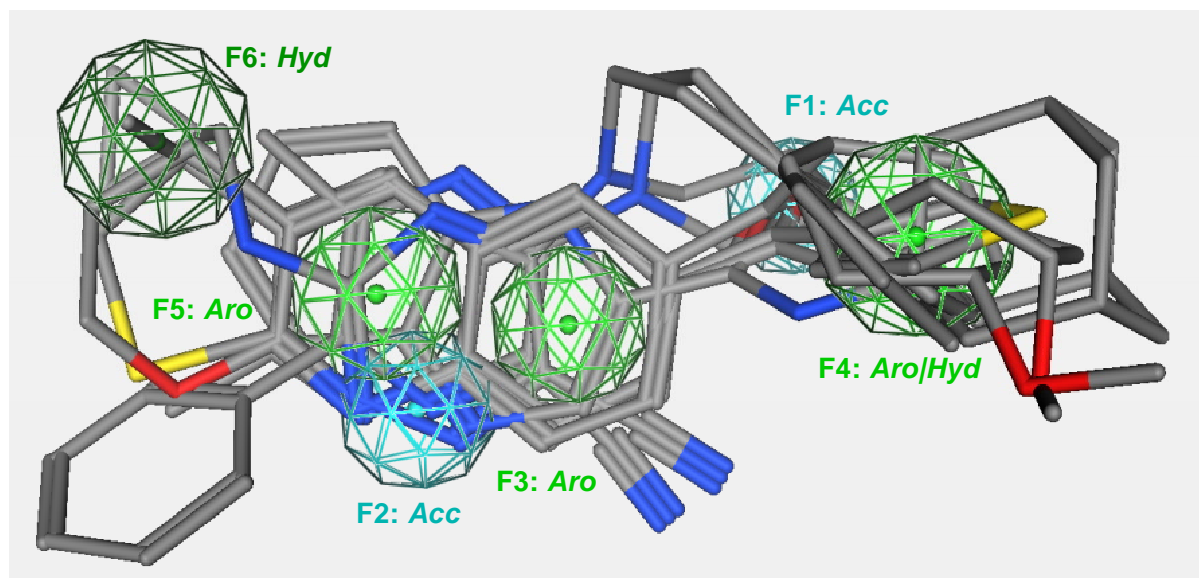


Figure 4.2.3-a. Final pharmacophore hypothesis and underlying reference alignment for non-competitive antagonists of the mGlu1 receptor (H-atoms not shown). Light blue spheres denote query features for H-bond acceptors, light green spheres represent aromatic features and dark green spheres show hydrophobic query features.

The final hypothesis still contained the initial six query features that were assumed to best describe the properties of potential allosteric mGluR1 modulators (Figure 4.2.3-a, Table 4.2.3-b). Eventually, query features F1, F2, F3 and F5 were tied together in a way that at least three of them had to be matched by a newly aligned ligand (i.e., queries F4 and F6 had to be satisfied by all means).

Table 4.2.3-b. Collection of all relevant features for the final pharmacophore hypothesis.

Code	Feature	Description	Radius [Å]
F1	Acc	H-bond acceptor	0.9
F2	Acc	H-bond acceptor	1.0
F3	Aro	aromatic system	1.0
F4	Aro Hyd	either aromatic or hydrophobic system	1.2
F5	Aro	aromatic system	1.1
F6	Hyd	hydrophobic residue	1.2
C1	Constraint	matching at least three features of F1, F2, F3, F5	-

Based upon iterative validation steps the crude, preliminary pharmacophore hypothesis was refined leading to an improved final pharmacophore model: The manually compiled mGluR-data collection served as reference dataset comprising “active” (negative mGluR1 antagonists) and “inactive” (others) members for retrospective analyses. However, we did not

perform retrospective virtual screenings on a large dataset of many thousand “inactive” members spiked with some “actives”. The reason can be found in a drawback associated with datasets containing numerous “inactive” (better: negative) compounds: We know that “inactive” members of our mGluR-data collection are definitely inactive mGluR1 antagonists, which has been experimentally proven (according to literature). In contrast, the tremendous number of “negative” members of large datasets is usually randomly selected from even larger databases but not tested on the target of interest.

4.2.4 Conclusions

The proposed final pharmacophore hypothesis for non-competitive mGluR1 antagonists (Figure 4.2.3-a) was capable of selectively retrieving allosteric mGluR1 modulators of the mGluR-data collection during a validation step of retrospective screening. This hypothesis was established to recover negative mGluR1 modulators listed in the reference collection (32.5% of them have been correctly identified), yet it also identified five of nineteen positive mGluR1 modulators (~26%) from the reference mGluR-dataset.

4.3 Virtual Screening by CATS Similarity Search

A topological pharmacophore search based upon an atom-pair descriptor and the Euclidian distance measure is provided by CATS [Schneider *et al.*, 1999]. It allows for rapidly screening even largest compound libraries with a speed nearly comparable to simple substructure searches. The notable advantage of CATS and related molecule descriptors is, however, that molecules might be retrieved or designed bearing core structures unlike the structures of the reference molecules [Schneider *et al.*, 1999; Nærum *et al.*, 2002]. Here, the rationale was to retrieve molecules from the Asinex Gold Collection February 2003 [Asinex Ltd.] that are similar - according to the CATS atom-pair descriptor - to a set of six reference compounds. In this study we employed as reference compounds the same six molecules that were used for setting up the pharmacophore model for mGluR1 antagonists (Figure 4.2.1-a).

4.3.1 Reference Compounds and Test Compounds

Test compounds as well as reference compounds were encoded with the CATS atom-pair descriptor (Section 3.2.1) as follows: 2D structures of test and reference molecules were saved as MDL MOL-file and all hydrogen atoms were removed using CLIFF software [Molecular

Networks GmbH]. Distance (Euclidean metric) calculation was restricted to 10 (0 to 9 bonds) intervening bonds resulting in a 150-dimensional correlation vector representation for each molecule (10 bonds multiplied with 15 possible atom-pairs). This vector was scaled to relative counts (S2).

Here, six separate similarity searches were carried out: Each reference compound served as query structure for one search process, and the remaining five molecules were merged with all compounds of the Asinex Gold Collection 2003 (Section 3.2.6). This database “spiking” was done to get an idea of the relevance of the obtained virtual hit lists [Schneider & Schneider, 2004]. For each run the CATS-software was prompted to create a ranked list for the 100 most similar molecules (according to the CATS descriptor) of the “spiked” database. Hence, we obtained six top 100 ranking lists (Appendix, Section 7.3). The first five test compounds of each list as well as all test compounds, which occur in at least three top 100 scoring lists simultaneously, were purchased and their pharmacological profile (mGluR1 binding assay, mGluR1 functional assay) was characterized.

4.3.2 Results of the CATS Similarity Searches and Discussion

Regarding the first five test molecules of each list four molecules appeared twice in different top five scoring lists (6 lists multiplied with 5 entries leading to 30 test molecules minus 4 doubles: 26 selected compounds). Additionally, twelve test compounds appeared in three different scoring lists among the first hundred compounds. The fact that they occurred solely in the scoring lists of reference compounds **R-01-R-03** can be explained by the degree of similarity of compounds **R-01-R-03** according to MACCS keys and CATS similarity (Table 4.2.1-a, Figure 4.3.2-a), which consequently also applies for the members of their scoring lists. In accordance to this observations, reference compounds **R-01**, **R-02** and **R-03** appeared among the top 100 scoring lists of each other (e.g., **R-02** is ranked as number one and **R-03** as number 58 among the first 100 entries for **R-01**'s similarity search; Appendix, Table 7.3-a).

In total, 38 compounds were found in the Asinex Gold Collection and ordered, but only 23 of them were delivered (Table 4.3.2-a). Compound **C-23** has accidentally been ordered and delivered although it was retrieved only by the first and second CATS run (reference molecules **R-01** and **R-02**) among the top 100 molecules. A detailed overview about all ordered and delivered compounds of this study is given in the Appendix, Section 7.3.

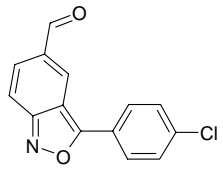
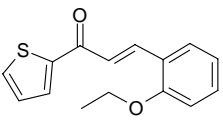
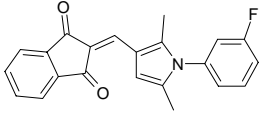
The structural similarity between the seed compounds **R-01-R-03** and the test compounds **C-05**, **C-19** and in particular **C-20** was confirmed by the similarity values (Table 4.3.2-a).

Visual inspection detected also similarity between **R-04** and test compound **C-08**: Both molecules have similar scaffolds with two H-bond acceptors (nitrogens were replaced with oxygens), the same polar linker and hydrophobic moieties of comparable size (Figure 4.2.1-a, Table 4.3.2-a). The vast majority of test compounds is, however, structurally distinct from the reference compounds.

Table 4.3.2-a. Retrieved (available) test compounds of the output of six separate CATS runs. The number of a CATS run corresponds to the reference compound's ID this search was based on (e.g., for CATS run 1: **R-01**). Similarity Score indicates the Euclidean distance between reference and test molecule. Experiments were performed in quadruplicate (binding) or sextuplicate (fct.), respectively.

CATS Run	Rank	Similarity Score	Chemical Structure	Number	Binding K_i [μM]	Functional IC_{50} [μM]
1	3	0.3986		C-01	>40	7.9 (\pm 2.5)
2	2	0.3671				
1	4	0.4144		C-02	>40	20.8 (\pm 0.8)
1	5	0.4279		C-03	>40	>40
2	5	0.4031				
1	6	0.4279		C-04	>40	18.9 (\pm 3.0)
2	6	0.4031				
3	1	0.2863		C-05	>40	>40
3	2	0.3369		C-06	25.3 (\pm 5.1)	13.5 (\pm 7.0)
3	3	0.3470		C-07	0.75 (\pm 0.05)	0.36 (\pm 0.03)
4	2	0.3401		C-08	>40	>40

4	3	0.3616		C-09	>40	>40
5	1	0.7360		C-10	>40	>40
5	3	0.8153		C-11	>40	>40
6	1	0.5254		C-12	>40	29.1 (± 3.7)
6	3	0.5640		C-13	21.6 (± 3.6)	12.9 (± 1.0)
6	4	0.5804		C-14	>40	>40
1	75	0.5670		C-15	>40	>40
2	54	0.5313				
3	91	0.4568				
1	65	0.5511		C-16	33.8	17.3 (± 0.9)
2	59	0.5364				
3	16	0.3886				
1	74	0.5666		C-17	>40	20.9 (± 1.6)
2	29	0.5014				
3	76	0.4505				
1	100	0.5847		C-18	>40	>40
2	66	0.5445				
3	40	0.4200				
1	8	0.4569		C-19	>40	23.8 (± 3.3)
2	8	0.4312				
3	38	0.4187				
1	24	0.5031		C-20	>40	17.2 (± 4.7)
2	10	0.4405				
3	46	0.4280				

1	77	0.5684		C-21	>40	13.2 (± 4.1)
2	41	0.5114				
3	72	0.4495				
1	32	0.5196		C-22	>40	11.1 (± 3.0)
2	18	0.4763				
3	95	0.4570				
1	38	0.5275		C-23	9.3	>40
2	99	0.5711				

The occurrence of test molecules representing structurally distinct chemotypes (with respect to the reference molecules) might be explained due to the fact that non-hydrogen atoms of the molecules are classified into five generalized atom types for this study, meaning that molecules with the same atom types (e.g., H-bond donor) but not necessarily with the same atom (e.g., a hydroxyl group could be replaced with a thiol) within a given bond distance are assumed to be similar. Moreover, since the distance counted between two atom types solely depends on the absolute number intervening of bonds, the spatial distance could vary to some extent depending on the bond length, the bond angle and whether or not the bond is rotatable (Figure 4.3.2-a).

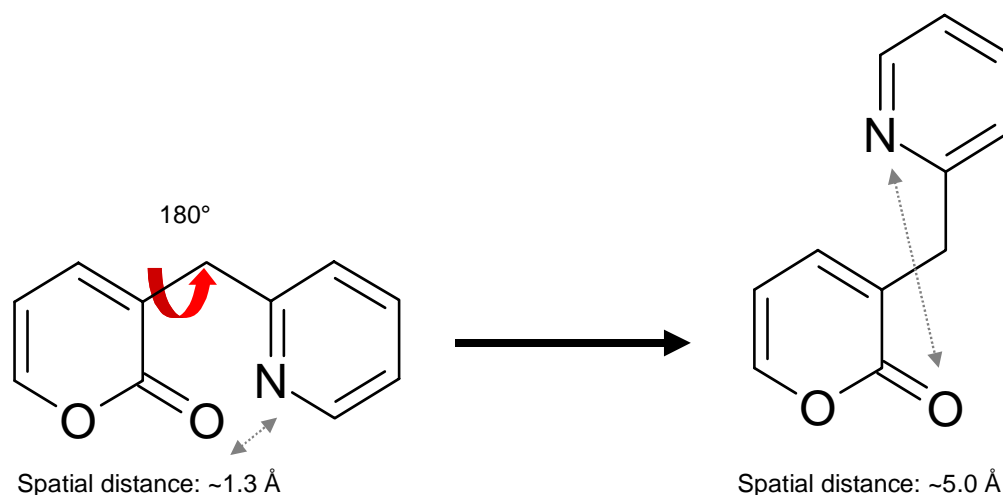


Figure 4.3.2-a. Sketch of two hypothetical 3D-arrangements of a sample molecule (here: 3-Pyridin-2-ylmethyl-pyran-2-one). In both orientations the bond distance between carbonyl-oxygen and nitrogen (both H-bond acceptors) is five (CATS atom-pair: AA5). The calculated spatial distance between both features, however, increases from the left to the right molecule arrangement.

Consequently, a given test compound could resemble a particular seed compound regarding potentially important interacting points but the possible difference in the spatial orientation of these pharmacophore features could lead to a change or even a loss of binding affinity and functional activity.

Affinity and activity of compounds **C-01-C-23** has been characterized using mGluR1 binding and functional assays. First, single concentration determinations were carried out in both assays in order to roughly classify a given compound as a high (K_i or IC_{50} : $< 1\mu\text{M}$), medium (K_i or IC_{50} : $< 15\mu\text{M}$), low active (K_i or IC_{50} : $15 - 40\mu\text{M}$) or inactive (K_i or IC_{50} : $> 40\mu\text{M}$) candidate rather than to reflect its precise activity value for structure activity relationships. The correlation between estimated IC_{50} -values via a single point measurement and determined IC_{50} -values for a certain concentration range were given in Section 3.1.11. In general, all test compounds showing baseline corrected values from $>80\%$ ($\sim 40\mu\text{M}$) were assumed to be inactive (Section 3.1.11). Full CRCs were only recorded for those compounds displaying IC_{50} -values below $10\mu\text{M}$ due to limited solubility. Table 4.3.2-a reveals the antagonistic activity of all test compounds. Results are given as mean values of two independent experiments performed in quadruplicate (binding) or sextuplicate (functional), respectively. Asterisks denote values determined by full CRCs. In total, one compound was found to be “highly active” (IC_{50} : $< 1\mu\text{M}$) and five compounds were “moderately active” with IC_{50} -values between $1-15\mu\text{M}$ in functional assay (Figure 4.3.2-b). Furthermore, eight compounds revealed a low activity (IC_{50} : $15 - 40\mu\text{M}$) and nine compounds were inactive (IC_{50} : $> 40\mu\text{M}$) leading to a total hit rate of approximately 26% (IC_{50} : $< 15\mu\text{M}$).

It must be emphasized that such a small subset of virtual hits (here: 23 compounds) hardly allows for giving reliable (i.e., precise) information in terms of hit rates for a given task. This applies for all methods where only a limited number of test compounds was retrieved, ordered and assayed.

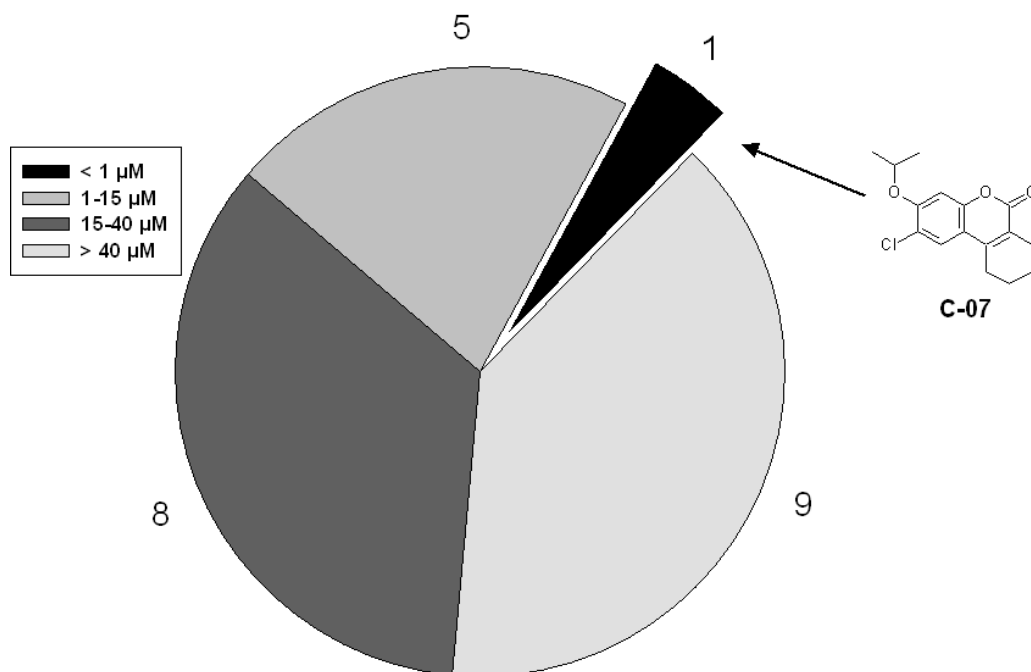


Figure 4.3.2-b. Graphical summary of the screening results (mGluR1 functional assay) of 23 hit compounds retrieved from the Asinex Gold Collection by the CATS similarity search.

The test compounds elicited predominantly low activity at the receptor except for molecule **C-07**. In contrast, the six seed compounds that were used for the similarity search in this study are of extremely high potency (Figure 4.2.1-a). However, similarity searches aim at discovering new core structures (“scaffold-hopping”), which does not necessarily mean that these ligands perfectly fit into the binding pocket. New chemotypes can be structurally optimized afterwards.

We focused on compound **C-07** that was found to bind to the allosteric site of the mGlu1 receptor with an IC_{50} -value in the nano molar range and significantly inhibits DHPG-induced receptor activation (Figure 4.3.2-c). Moreover, compound **C-07** seems to selectively interact with mGluR1 since no affinity towards mGluR5, the closest related subtype according to sequence similarity, was observed (Figure 4.3.2-d).

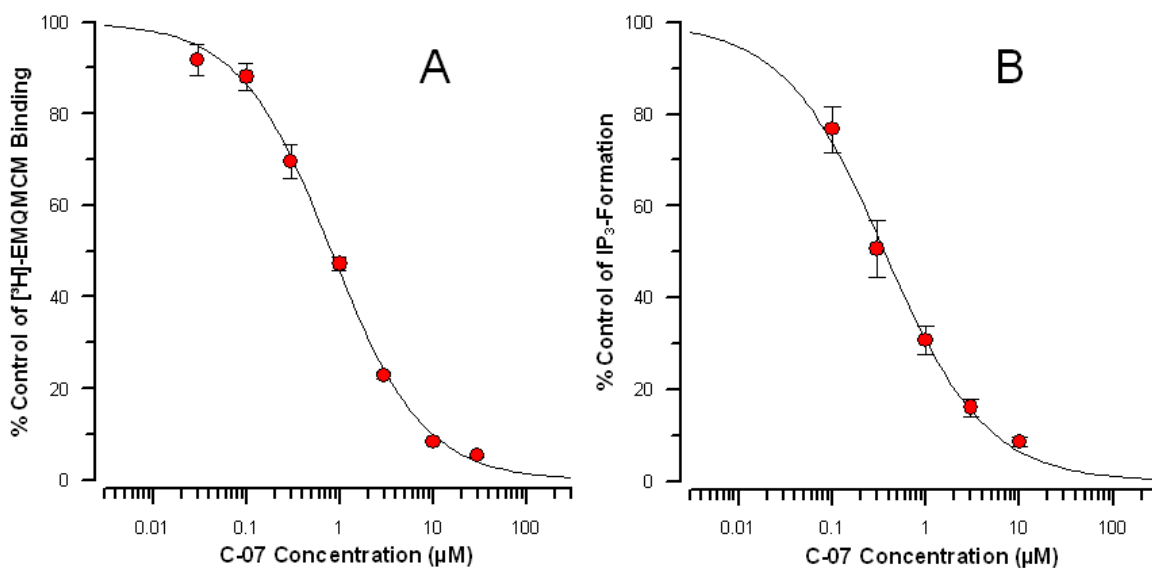


Figure 4.3.2-c. Compound **C-07** is a non-competitive antagonist of the mGlu1 receptor. It displaces [³H]-EMQMCM binding to the allosteric mGluR1 site with an K_i -value of $0.753\mu\text{M}$ (A, SEM: 0.048) and inhibits DHPG-induced intracellular IP₃-formation with an IC_{50} -value of $0.362\mu\text{M}$ (B, SEM: 0.031). Results are the mean values of two independent experiments performed in quadruplicate (binding) or sextuplicate (functional), respectively.

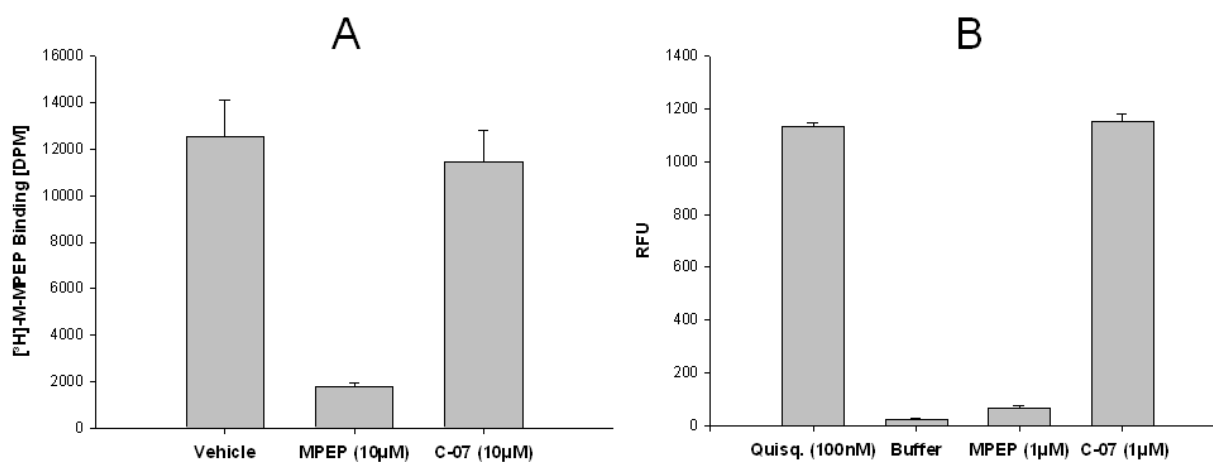


Figure 4.3.2-d. Compound **C-07** does not displace [³H]-MPEP (5 nM) binding to the allosteric site of the mGlu5 receptor (A) nor does it significantly inhibit quisqualate induced intracellular Ca²⁺ release in rat cortical astrocytes (B, for detailed experimental procedures see Section 3.1.4 and 3.1.8). Results are the mean values of two independent experiments conducted in duplicate (MPEP binding) or quintuplicate (Ca-flux). Error bars denote SEM.

Apart from the promising pharmacological data the chemical structure of molecule **C-07** is attractive since to the best of our knowledge no interaction with family 3 GPCRs has been reported for any coumarine-derivatives to date. The most prominent coumarine-derivatives phenprocoumon and warfarin are well known drugs acting as indirect anticoagulants due to interfering with the vitamin-K synthesis. They are used for the prophylaxis of thrombosis and

embolism in many disorders. The therapeutic potential of other coumarines like scoparone (reduces total cholesterol and triglycerides), osthole (causes hypotension in vivo, inhibits platelet aggregation in vivo) and cloricromene (reveals antithrombotic antiplatelet actions, causes vasodilatation) has been reviewed [Hoult & Paya, 1996]. Since some 3,4-dimethylcoumarines like esuprone inhibit either monoamine oxidase type A or B the treatment of epilepsy by representatives of this chemical class has been discussed [Loscher *et al.*, 1999]. Coumarine-derivatives were hereby introduced as potential drug candidates to the therapy of mental disorders connected with mGlu1 receptor interaction.

4.3.3 Conclusions

In this study we have performed similarity searches based on a topological pharmacophore descriptor for six reference compounds on a large and diverse database. A set of 23 test compounds showing high similarity towards the reference compounds was selected and assayed for affinity and functional activity at mGluR1. All compounds selectively interacted with mGluR1 as they did not evoke any response on the closely related subtype mGluR5. An overall hit rate of 26 % (activity < 15 μ M) demonstrated the applicability of this concept. One compound, structurally belonging to the chemical class of coumarines, exhibited binding affinity and functional activity at mGluR1 below 1 μ M.

4.4 Data mining by *ChemSpaceShuttle*

ChemSpaceShuttle (CSS) is an application that facilitates the reduction of a multi-dimensional space to a 3D-representation [Givehchi *et al.*, 2003] (Section 1.5.3, Section 3.2.3). Noteworthy, this data mining application is not a SAR tool since the network training algorithm does not implement any biological data like activity or affinity. It allows for revealing hidden relationships within a large set of molecular data and gives an overview over the occupied and unoccupied chemical space. Thus, commercial databases can be analyzed with respect to their molecular distribution which in turn facilitates the design of activity-enriched subsets. The rationale of CSS within this study was to select a few virtual hits from a potentially activity-enriched library (here referred to as “focused library”). This “cherry-picking” procedure was part of a virtual screening campaign.

4.4.1 Compilation of a focused library

The idea was to visualize not the total compound library but a single subset. Thus, a “focused library” was compiled by performing a pharmacophore search as follows: The complete Asinex Gold Collection February 2003 [Asinex Ltd.] was virtually screened with the final pharmacophore model for non-competitive mGlu1 receptor antagonists (Figure 4.2.3-a). This searching process was carried out by running the *Pharmacophore Search* tool of the MOE software package Version 2003.02 [Chemical Computing Group]. The following settings were applied: Asinex database (single conformation for each molecule) was specified as input database. It was preprocessed to make searching faster: For each database entry an annotation field (pharmacophore scheme: PCH; Section 4.2.2) was automatically calculated. The refined pharmacophore model (Section 4.2.3) was specified as query set. The search tool was prompted to create a new output database, containing the same indication fields (e.g., molecule and ID) as the input database.

The search resulted in a subset A of 3137 virtual hits, retrieved from a total number of 194104 molecules out of the Asinex database. Next, subset A as well as the mGluR-data collection were characterized by two 2D-descriptors implemented in MOE, namely *SlogP* and *Weight*. According to the Gaussian-like distribution of the reference compounds of the mGluR-data collection (Figure 4.4.1-a), a range of descriptor values restricted by defined thresholds for both descriptors was set for all entries in subset A:

Lipophilicity (*SlogP*): lower threshold = 0, upper threshold = 6

Molecular weight (*Weight*): lower threshold = 230, upper threshold = 500

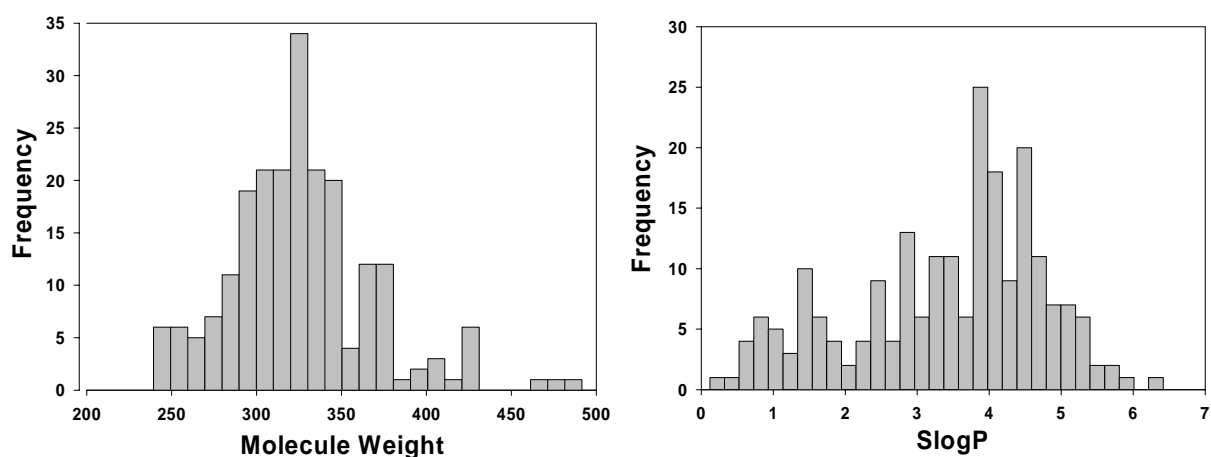


Figure 4.4.1-a. Distribution pattern for molecule weight and lipophilicity of the mGluR1-data collection (212 members). Values are binned into ranges of 10 unit size (*MW*) or 0.2 unit size (*SlogP*), respectively.

As it turned out that nearly all reference compounds exhibited values to be found within the proposed threshold ranges, subset A was narrowed down to the “focused library” by removing all test compounds eliciting values beyond the given parameter range (i.e., exceedingly high or low *MW* and poor lipophilicity) irrespective of the original distribution patterns of subset A (Figure 4.4.1-b). The bell-shaped distribution for the test compounds was shifted to the right if compared with the reference compounds. Approximately one third of all test compounds (926 of 3137 or 29.5%) did not match the defined criteria, which is also demonstrated by the distribution patterns for test molecules (Figure 4.4.1-b).

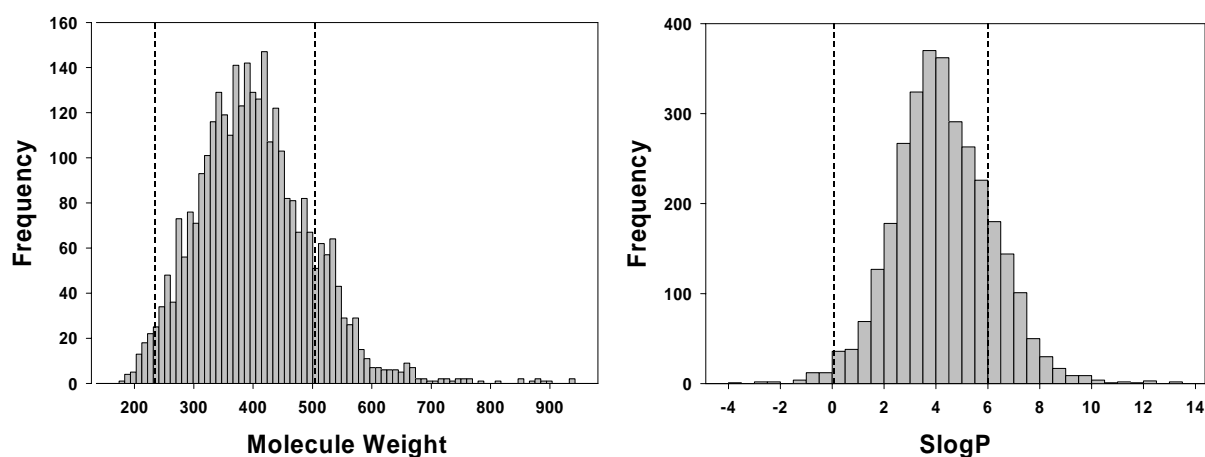


Figure 4.4.1-b. Distribution pattern for molecule weight and lipophilicity of subset A (3137 members). Dashed lines border the range for molecules of the “focused library”. Values are binned into ranges of 10 unit size (*MW*) or 0.25 unit size (*SlogP*), respectively.

4.4.2 Processing the Data

All molecules of the focused library (2211 members) as well as the “washed” mGluR-data collection (negative allosteric modulators of mGluR1 and -5; positive modulators were discarded; 337 members) were encoded with all 146 2D-descriptors provided by MOE. Non-relevant descriptors (i.e., descriptors displaying the same value for all reference compounds) were removed resulting in 130 2D-descriptors. Potentially redundant descriptors have been retained. Reference compounds were classified as “R-1” or “R-5”, respectively and test compounds as “unknown” without changing the original ID number. After transforming both datasets into tab-separated text files, the mGluR-data collection was imported in *ChemSpaceShuttle*, a weight optimization was performed in the training mode and the three principal components were calculated and visualized in the projection mode (Figure 4.4.2-a). The scatter plot demonstrates that this method allows for discriminating between “R-1” and “R-5” compounds: “R-5” compounds form a sharply defined cluster pointing to the upper

background. All members of this cluster belong to the same chemical class of modulators. In contrast, “R-1” compounds are predominantly located in the upper foreground apart from some widely distributed molecules in the lower front. However, both groups of modulators are not completely spatially separated as they partly overlap with each other. Especially the main cumulation of “R-1” compounds is spotted with several “R-5” molecules.

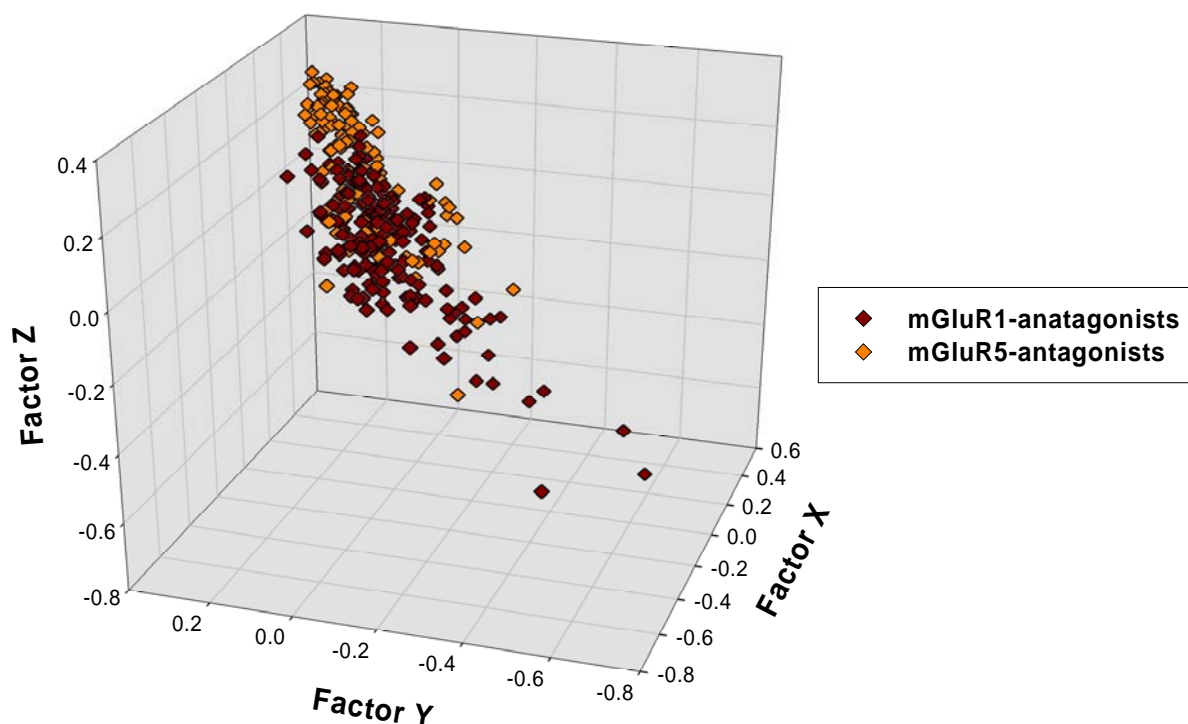


Figure 4.4.2-a. 3D-Plot displaying the distribution of reference compounds. Factors X, Y and Z represent the principal components calculated from the multidimensional space.

In the next step, reference compounds were plotted together with all test members of the focused library (Figure 4.4.2-b). Compared to the reference compounds test molecules cover a large area where they are mainly located in one prolate cluster. However, they do not extend to all regions occupied by the reference compounds, which is most likely due to the limited number of subset members. Therefore, not the total space, which is covered by the reference molecules can be exploited for analysis (i.e., the distance dependent detection of test molecules, *vide infra*).

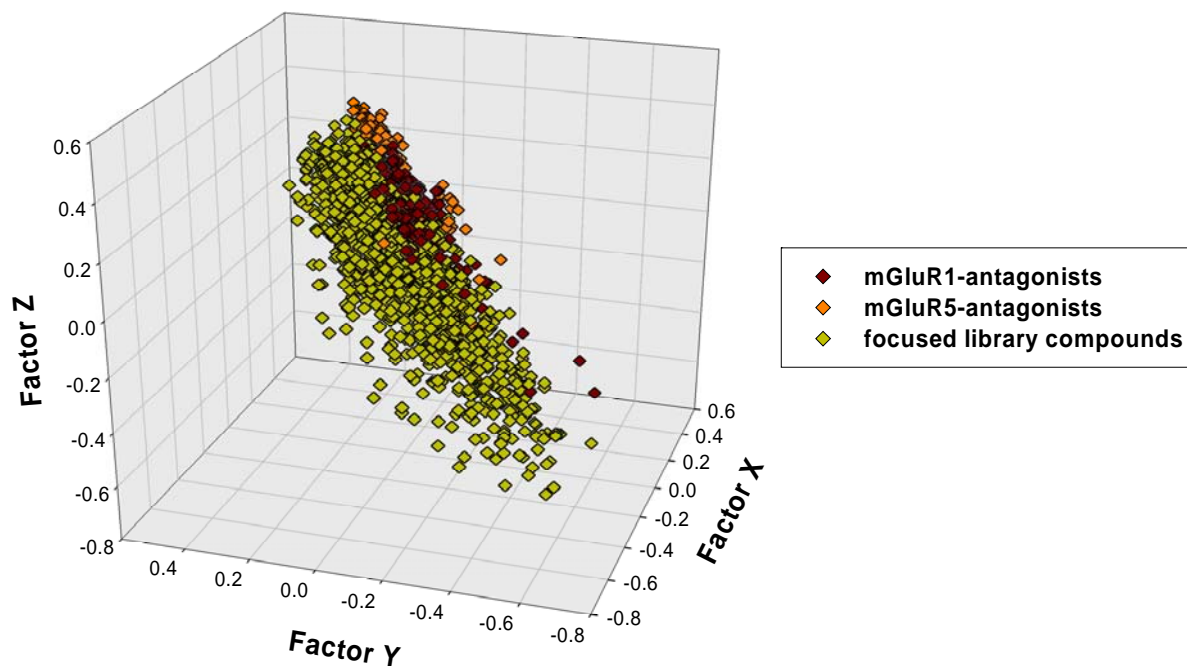


Figure 4.4.2-b. 3D-Plot displaying the distribution of reference compounds and test compounds. Factors X, Y and Z represent the principal components calculated from the multidimensional space.

Since these three-dimensional plots provide topology-preserved mappings, compounds which are close to each other on this grid are also assumed to be in close proximity in the original multidimensional space. Consequently, they are assumed to bear similar properties with respect to the descriptors they are encoded with. Therefore, a radius-like distance tolerance (marked distance) was applied for all “R-1” compounds to detect adjacent compounds within this certain range irrespective of their type (Figure 4.4.2-c). In some densely populated regions many compounds were detected by a single “R-1” compound. In contrast, some of the widespread reference molecules (in the lower right corner on Figure 4.4.2-c) were not able to find any molecules within the defined distance.

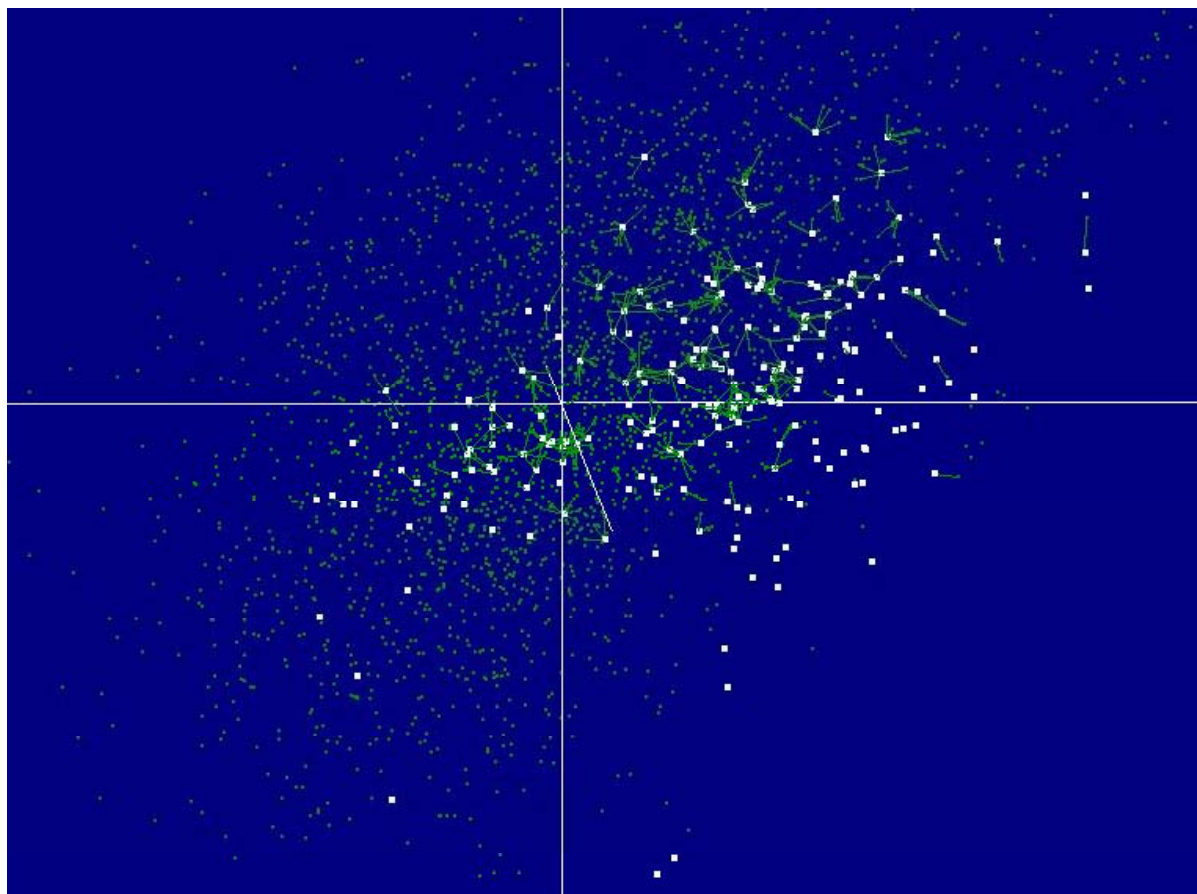


Figure 4.4.2-c. Original 3D-Plot visualized in CSS (display detail). White spots denote mGluR1 reference compounds, green spots are test compounds and other reference compounds. White lines represent the three axes spanning the coordinate system. Green lines represent the distance between the mGluR1 reference compounds and their neighbors within a marked distance in the 3D space.

All molecules located within this radius were listed in a tab-separated text file and reference compounds labeled with “R-1” and “R-5” were removed. The remaining 46 test molecules were then sorted according to their distance to the corresponding reference compound and 30 compounds displaying the lowest distance-value were selected. After visual revision, eighteen of those were ordered from the database vendor [Asinex Ltd.].

4.4.3 Results of the Neighborhood Search and Discussion

Fifteen virtual hits have been delivered as solids and tested in-house for binding affinity and functional activity on mGluR1. The chemical structures and a list of all ordered and delivered compounds can be found in the appendix (Section 7.4). Summarized, no compound was found to be “highly active” ($<1\mu\text{M}$), three compounds were “moderately active” with IC_{50} -values between 1-15 μM in functional assay (Figure 4.4.3-a). Furthermore, two compounds revealed

a low activity (15 – 40 μ M) and ten compounds were inactive (>40 μ M) leading to a total hit rate of 20 % (cut off <15 μ M).

Table 4.4.3-a. Overall result of *in vitro* pharmacological experiments for all test compounds. Results are the mean values of at least two independent experiments performed in quadruplicate (binding) or sextuplicate (functional), respectively. Asterisks denote values, which were determined by full CRCs. Compounds with IC_{50} -values higher than 40 μ M were assumed to be inactive. SEM are given in parentheses.

Number	Binding K_i [μ M]	Functional IC_{50} [μ M]
P-01	>40	>40
P-02	>40	>40
P-03	>40	>40
P-04	21.9 (\pm 4.0)	>40
P-05	>40	>40
P-06	*33.27 (\pm 5.34)	*1.11 (\pm 0.41)
P-07	>40	>40
P-08	>40	>40
P-09	>40	25.7 (\pm 1.6)
P-10	>40	>40
P-11	>40	12.9 (\pm 0.4)
P-12	>40	>40
P-13	>40	25.1 (\pm 2.5)
P-14	*13.05 (\pm 0.94)	7.4 (\pm 0.5)
P-15	>40	>40

Compound **P-06** was found to be the most potent molecule among all compounds of this subset. It structurally resembles the prominent negative allosteric modulator LY456066 (Figure 4.4.3-a, Figure 1.4.2-a). The remaining compounds display poor, if any, functional activity and binding affinity.

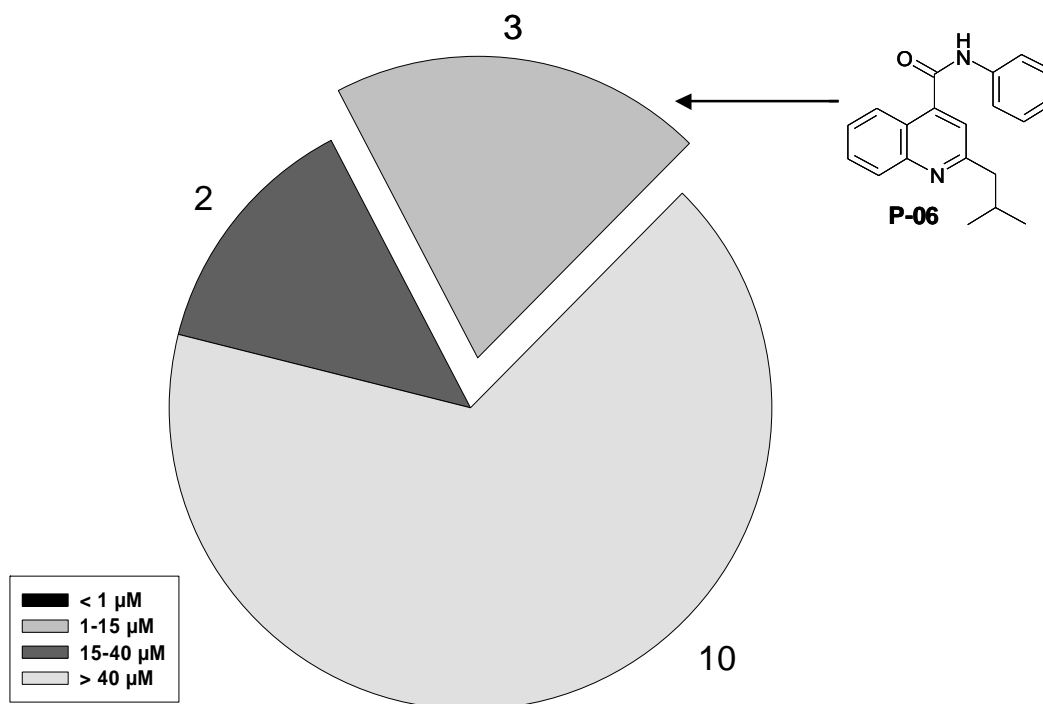


Figure 4.4.3-a. Graphical summary of the screening results (rmGluR1 functional assay) of 15 hit compounds retrieved from the Asinex Gold Collection by the 3D-pharmacophore searches combined with non-linear PCA (performed by CSS).

Regarding the scaffolds most of the structures closely resemble either LY456066 or R214147. This could probably have several reasons: The previously performed pharmacophore search retrieved a subset mainly comprising molecules structurally related to R214147 since the underlying pharmacophore alignment predominantly contains R214147 derivatives. Second, due to the fact that the majority of reference compounds belongs to either groups many test compounds have been found being located within a marked distance of those reference molecules. Based upon this, we assumed that the chosen descriptors encode molecules in a way that mainly structures bearing the same scaffold are adjacently located (in the high- and low-dimensional space) and not molecules with similar features but different scaffolds.

The low hit rates might be caused due to the following facts: (i) The high number of reference compounds revealing weak activity, (ii) test compounds were ranked, selected and ordered according to their distance to *any* reference compound, not just to the potent reference molecules and (iii) the focused library serving as test compound collection contained molecules with less structural diversity than the complete Asinex database. This loss of diversity was most likely attributed to the pharmacophore search based on a model that has proven not to match all chemotypes of mGluR1 antagonists during validation (Section 4.2.3).

One can conclude in turn that this pharmacophore model ignores several potential hits from the Asinex database.

Moreover, the total amount of compounds retrieved by the pharmacophore search and analyzed by CSS was probably too low. Initially, the pharmacophore search was employed to reduce the amount of test compounds and to apply a “focused library” to CSS. After analyzing the results of the CSS run and visualizing the plot we observed that for many reference compounds no test compounds were found within the defined distance (Figure 4.4.2-b). The application of the whole Asinex database for data mining by CSS would have solved probably the issues of (i) a too specific data subset (regarding chemical diversity) and of (ii) a too small subset not covering the whole space provided by the reference compounds. Furthermore, ranking criteria solely considering highly potent reference molecules combined with an increased marked distance for neighborhood search would have presumably enhanced the chance of detecting more promising structures.

4.4.4 Conclusions

The strategy for identifying novel scaffolds presented in this section aimed at combining the advantages of two methods: (i) The design of a potentially activity-enriched subset from a large library by pharmacophore search and (ii) the retrieval of some “virtual hits” from this subset *via* a data mining tool suitable to reduce and visualize the data distribution. Since the focused library comprised too many compounds to manually select some of them for follow-up (i.e., order and assay), it was decided to apply the “filter” presented in this section to minimize the subset. We recovered a set of 18 molecules from the focused library. This set was ordered and the delivered 15 compounds were tested on binding affinity and functional activity on mGluR1. One molecule revealed inhibitory activity of 1.1 μM (K_i -value).

4.5 Virtual Screening using Self-Organizing Maps

SOMs or Kohonen-networks -- describing a certain type of unsupervised neural networks -- are predominantly applied for molecule clustering and topology preserving projections. They allow for designing focused libraries of ligands affecting a given target [Schneider & Nettekoven, 2003]. Consequently, they are understood more as an application to assist and support a given virtual screening campaign rather than as a virtual screening tool itself.

Once again the Asinex Gold Collection February 2003 [Asinex Ltd.] was employed as source for retrieving molecules potentially interacting with the allosteric mGluR1 binding site, whereas the COBRA database [Schneider & Schneider, 2003] was used to unfold and train a SOM and the mGluR-data collection contained the necessary reference molecules. The CATS atom-pair descriptor was applied to encode all compounds for the network. The aim was to create and visualize 2D-distribution patterns for mGluR1 and mGluR5 antagonists, which should facilitate a clear discrimination between ligands of both subtypes. Based upon two-dimensional mappings of the Asinex database activity-enriched subsets should be retrieved from this database and tested afterwards for affinity and activity on the mGlu1 receptor.

4.5.1 Training the Maps

The first step of this virtual screening procedure was the conversion of all molecules of the three different datasets into a 150-dimensional vector representation using the CATS topological pharmacophore descriptor. Thereafter, a SOM was developed based on the COBRA database that means the 150-dimensional space was mapped onto a plane by applying a slightly modified version of the Kohonen algorithm [Schneider & Schneider, 2004]. Since the projection is topology-preserving, molecules, which are in close proximity on the two-dimensional projection, are also adjacently located in high-dimensional space (Section 1.5.3). Here, a SOM is composed of a grid of 100 (or 225) neurons, each of which containing molecules having certain pharmacophore features in common. The map was visualized according to the density value of each neuron meaning the number of molecules to be included in a certain neuron (Figure 4.5.1-a). As it can be seen, the molecular distribution is more or less consistent apart from some highly occupied clusters close to neurons with low density. Only 1% (2.7%) of all neurons is unoccupied demonstrating a successfully trained and unfolded SOM.

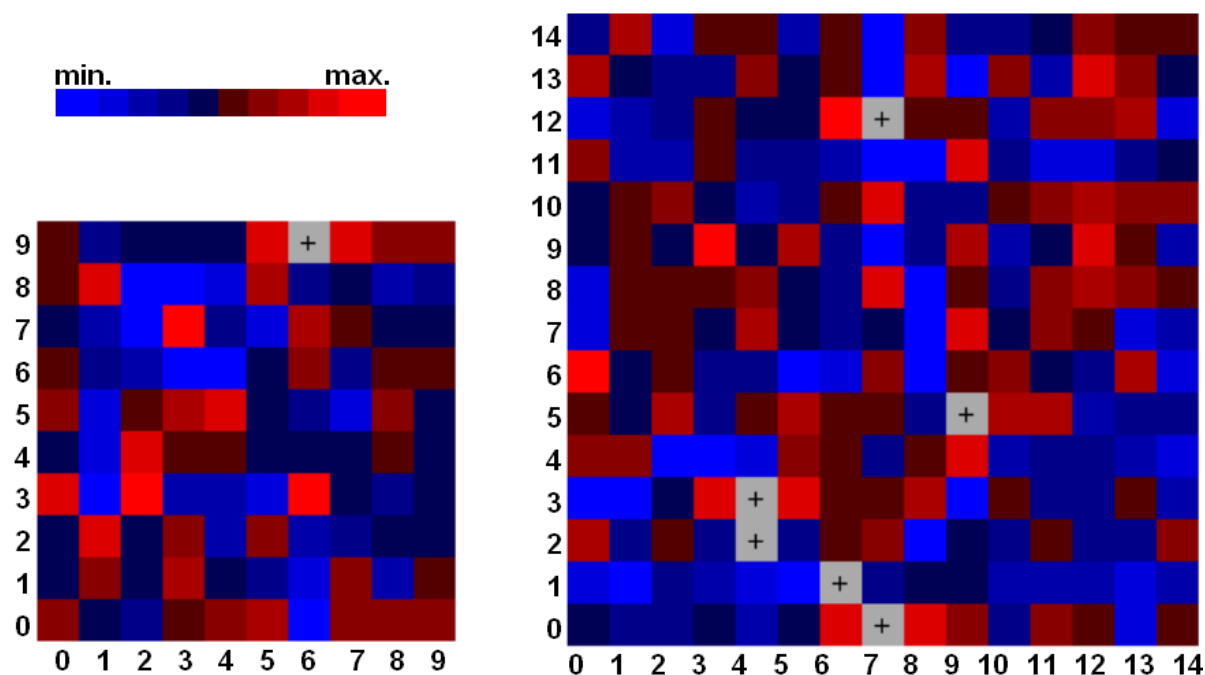


Figure 4.5.1-a. Self-organizing maps showing the distribution of the COBRA database molecules in CATS topological pharmacophore space according to the density values of the neurons.

Since this study aimed at detecting novel and selective allosteric antagonists of the mGlu1 receptor the selectivity aspect was firstly investigated, meaning the discrimination between molecules acting on mGluR1 and mGluR5. Here, the main question was whether it is possible to separate between non-competitive antagonists of mGluR1 and mGluR5. In this context, the mGluR dataset was projected onto the smaller SOM (10x10 grid) developed before. Then, the map was visualized according to the mGluR subtype selectivity of each compound (Figure 4.5.1-b). One large mGluR1 cluster in the upper right corner and two mGluR5 cluster were found, one in the upper center and the other in the lower right corner. Only six neurons (6%) contain molecules of both subtypes. However, it should be stressed that this particular visualization gives no hint about the molecular density of the neurons. Yet, the map demonstrated that one could successfully discriminate between molecules of each receptor subtype. This result substantiates earlier findings that both the CATS descriptor and the SOM procedure are suited for clustering compounds according to their pharmacological activity [Anzali *et al.*, 1996; Polanski & Walczak, 2000; Schneider & Nettekoven, 2003; Teckentrup *et al.*, 2004; Xiao *et al.*, 2005].

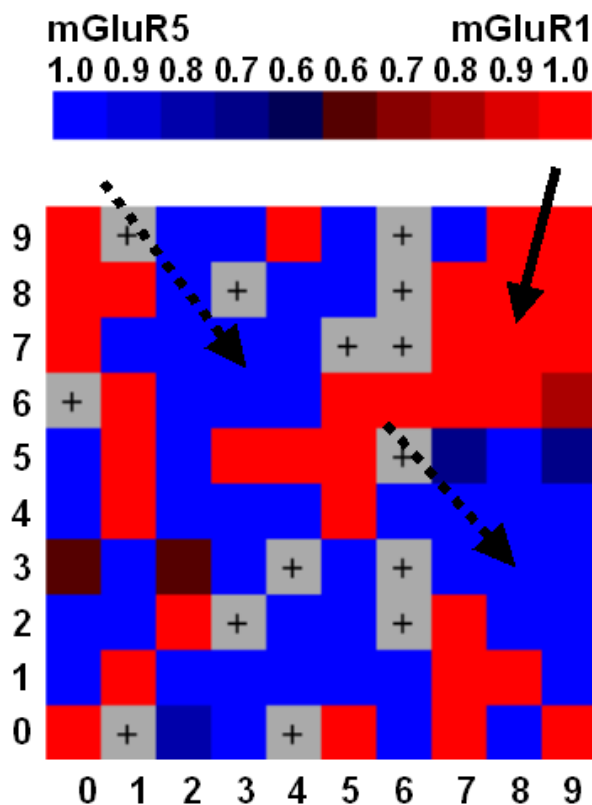


Figure 4.5.1-b. Self-organizing map showing the selectivity of the mGluR data collection molecules in the CATS topological pharmacophore space according to discrimination between subtype 1 and 5. Dashed arrows point to mGluR5 clusters and the black arrow to the mGluR1 cluster.

In the next step only the mGluR1 subset of the mGluR data collection was mapped onto the SOM that was trained by the COBRA database. The map was once again visualized according to the density value of each neuron (Figure 4.5.1-c). Considering that these SOMs have a toroidal “donut-like” shape in the three-dimensional space, both of them (10x10 and 15x15 grid) reveal one large cluster, one smaller cluster and several “activity islands” distributed over the whole map. The large cluster comprises derivatives of R214127, EM-TBPC, CPCCOEt and LY456066 (Figure 1.4.2-a). Neurons 8/7 and 6/6, respectively displayed the highest density of reference compounds. These are structurally related to some extent in the topological pharmacophore space. This mapping was necessary to detect those areas in the Asinex database where test compounds can be found with pharmacophore properties similar to those of the mGluR1 reference compounds (Section 4.5.2).

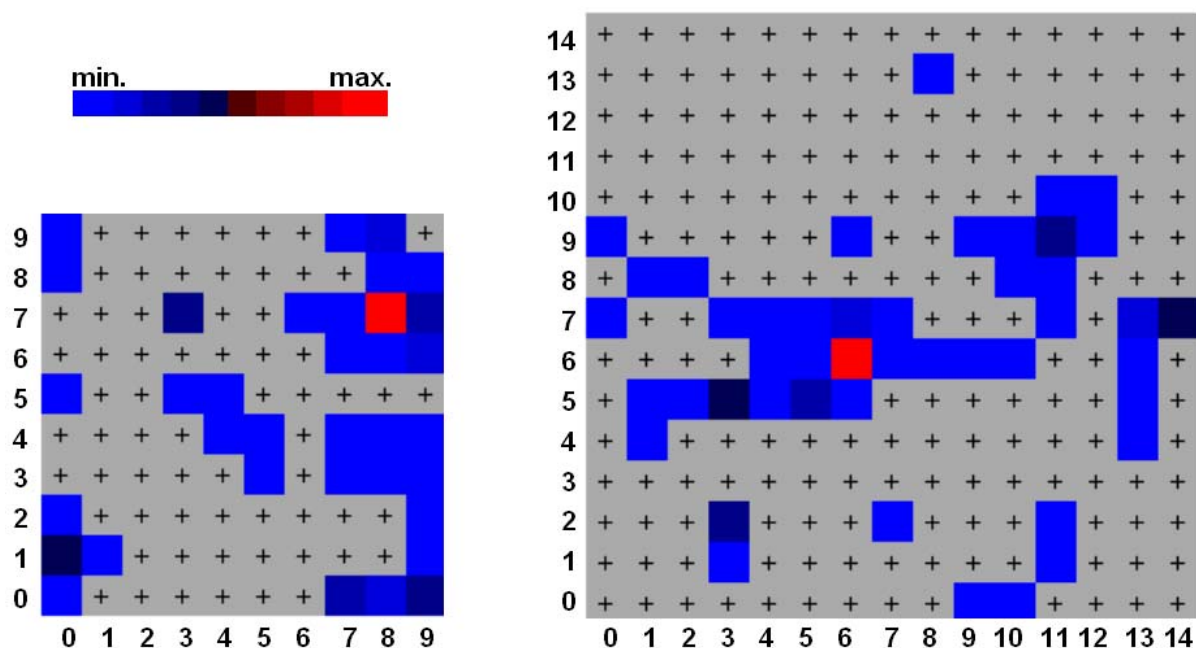


Figure 4.5.1-c. Self-organizing maps showing the distribution of the mGluR1 dataset molecules in the CATS topological pharmacophore space according to the density values of the neurons.

4.5.2 Selection of Virtual Hits

Finally, the complete Asinex Gold Collection was projected onto the SOM that was trained with the COBRA database. The map was visualized according to the density value of each neuron (Figure 4.5.2-a). Apart from one densely populated “receptive field” (neuron) the molecules of the Asinex library were consistently distributed over the whole space that was provided by the trained SOM. Only three neurons (1.3%) of the larger grid were unoccupied.

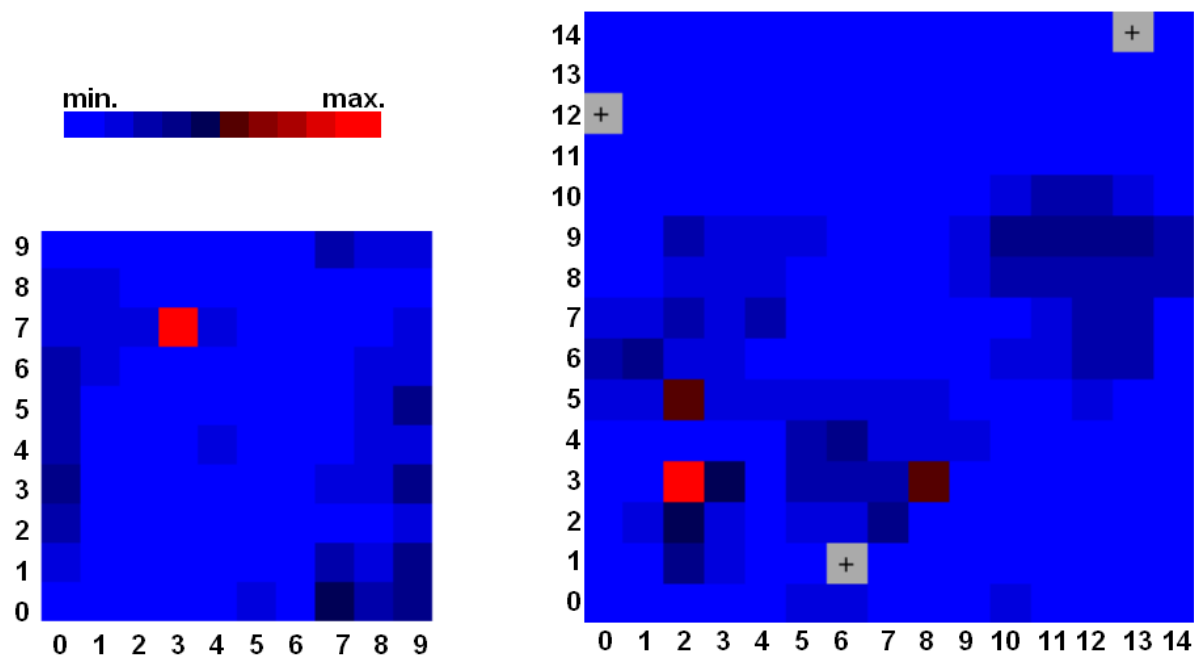


Figure 4.5.2-a. Self-organizing maps showing the selectivity of the Asinex database molecules in the CATS topological pharmacophore space according to the density values of the neurons.

Since we were interested in those Asinex test compounds that bear topological pharmacophore features similar to those of the mGluR-reference data collection we focused on neurons 8/7 and 6/6, respectively displaying the highest density of mGluR-reference compounds on the mGluR1 map (Figure 4.5.1-c). In general, molecules included in neurons 8/7 and 6/6 of the Asinex map were assumed to be similar to molecules incorporated in neurons 8/7 and 6/6 of the mGluR1 map. Neuron 8/7 (10x10 grid) comprised 1864 cluster members whereas 6/6 (15x15) contained 749 cluster members. All molecules that were represented by both maps (10x10 and 15x15) – altogether 407 – have been selected and ranked by ascending order according to their distance to the centroid of neuron 6/6 (15x15). We selected this neuron and not neuron 8/7 of the small grid (10x10) as the large map provides higher resolution. A total of 29 compounds from the first 50 compounds being in closest proximity to the centroid were ordered from Asinex (a detailed list of the 50 best ranked compounds is given in the appendix, Section 7.5). 28 of them were delivered and tested in binding and functional assays of mGluR1 (Table 4.5.2-a).

Table 4.5.2-a. Overall results of *in vitro* pharmacological experiments for all test compounds. Results are the mean values of at least two independent experiments performed in quadruplicate (mGluR1 binding assay) or sextuplicate (mGluR1 functional assay), respectively. Asterisks denote values which were determined by full CRCs. Compounds with IC_{50} -values above 40 μ M were assumed to be inactive. SEM are given in parentheses.

Number	Binding K_i [μ M]	Functional IC_{50} [μ M]
S-01	>40	>40
S-02	>40	>40
S-03	>40	23.9 (\pm 1.2)
S-04	>40	22.5 (\pm 7.3)
S-05	*9.18 (\pm 1.08)	*1,71 (\pm 0.15)
S-06	>40	*8.49 (\pm 0.62)
S-07	>40	>40
S-08	*9.93 (\pm 1.25)	*0.74 (\pm 0.29)
S-09	*17.23 (\pm 2.14)	*2.97 (\pm 0.40)
S-10	>40	14.8 (\pm 3.5)
S-11	>40	25.7 (\pm 4.9)
S-12	>40	>40
S-13	>40	>40
S-14	>40	>40
S-15	>40	>40
S-16	>40	9.0 (\pm 2.2)
S-17	>40	>40
S-18	>40	23.9 (\pm 0.9)
S-19	>40	30.0
S-20	>40	>40
S-21	>40	>40
S-22	>40	>40
S-23	>40	>40
S-24	>40	28.4 (\pm 3.9)
S-25	>40	>40
S-26	>40	>40
S-27	>40	>40
S-28	*36.16 (\pm 2.60)	*10.63 (\pm 1.80)

Full CRCs were only recorded for those compounds displaying IC_{50} -values below 10 μ M due to their limited solubility. Regarding functional activity values nearly half of molecules S-

01-S-28 reveal at least low activity. We achieved a higher hit rate than standard HTS. One compound (3.6%) was classified as “highly active” ($>1\mu\text{M}$), six compounds (21.4%) were “moderately active” (1-15 μM), six compounds revealed low activity (15-40 μM) and for fifteen compounds (53.6%) we observed “no activity” ($>40\mu\text{M}$) leading to a total hit rate of approximately 46% ($<15\mu\text{M}$). Concerning binding affinity values the majority of the compounds displays no affinity towards the allosteric site of the mGlu1 receptor. Two compounds (7.1%) were of “moderate affinity” (1-15 μM) and two compounds exhibited “low affinity” (15-40 μM), whereas the remaining 24 compounds (85.7%) showed “no affinity” ($>40\mu\text{M}$) towards the binding site.

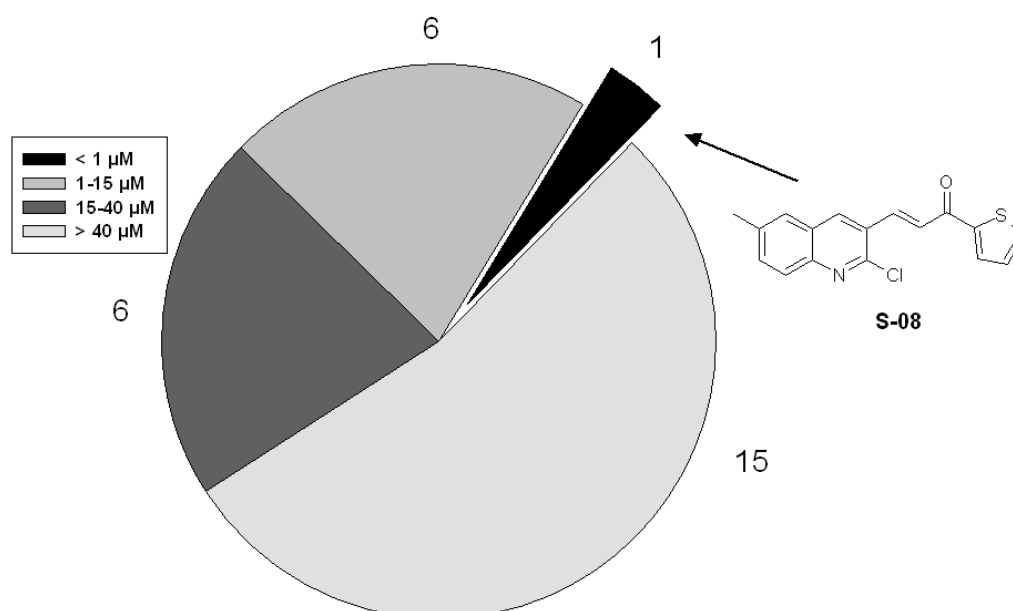


Figure 4.5.2-b. Graphical summary of the screening results (mGluR1 functional assay) of 28 hit compounds selected from the Asinex Gold Collection visualized by self-organizing maps.

A detailed pharmacological profile has been created for molecules **S-05**, **S-06**, **S-08**, **S-09** and **S-28**, the five most active compounds. Full dose-response curves have been carried out in order to precisely determine affinity and activity values. Possible interactions of these compounds with the closely related mGlu5 receptor were also in our focus in order to evaluate their selectivity: All active compounds displayed no interaction with the allosteric binding site of mGluR5 (Figure 4.5.2-c) indicating that we have found selective allosteric mGluR1 modulators. These findings correspond well with the predictions that were made before: According to Figure 4.5.1-b there is only few overlap between compounds of both mGluR subtypes and molecules **S-05**, **S-06**, **S-08**, **S-09** and **S-28** were located in areas with no mGluR5 reference compounds.

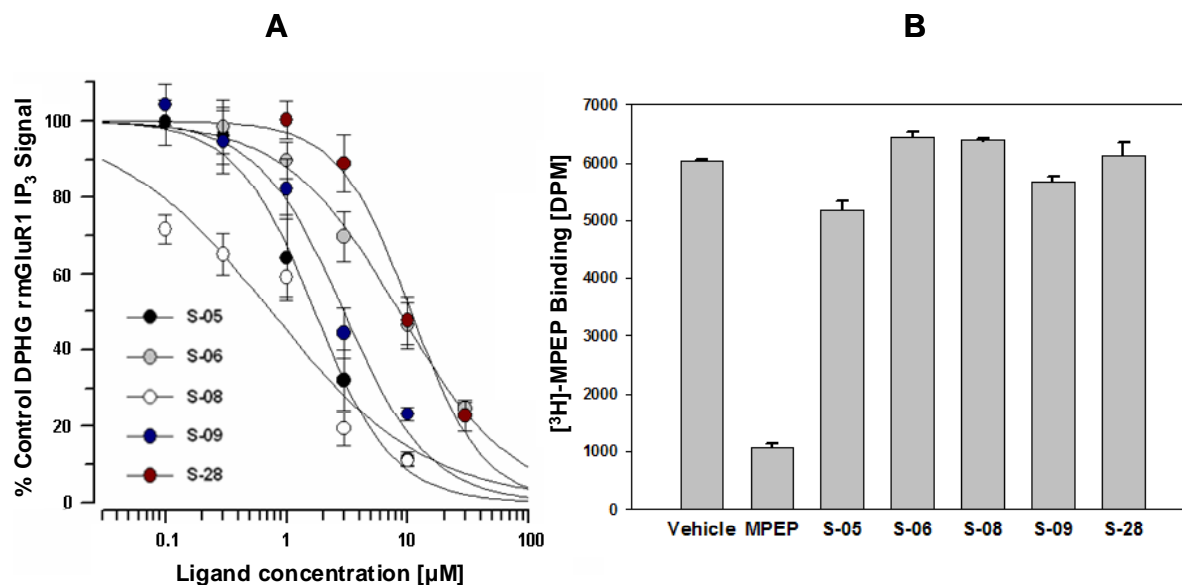
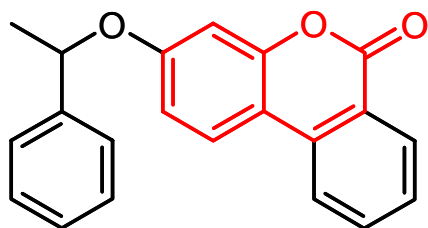


Figure 4.5.2-c. A: Compounds **S-05**, **S-06**, **S-08**, **S-09** and **S-28** are non-competitive antagonists of the mGlu1 receptor. They inhibit DHPG-induced intracellular IP₃-formation with IC₅₀-values of 1.706 μM (SEM: 0.1508 μM), 8.488 μM (0.6187 μM), 0.744 μM (0.2676 μM), 2.973 μM (0.4046 μM) and 10.633 μM (SEM 1.7972), respectively. Results are the mean values of two independent experiments performed in sextuplicate. **B:** Compounds **S-05**, **S-06**, **S-08**, **S-09** and **S-28** (10 μM) do not displace [³H]-MPEP, binding to the allosteric site of the mGlu5 receptor (MPEP: 10 μM). Results are the mean values of two independent experiments conducted in duplicate. Error bars denote SEM.

4.5.3 Discussion

Despite the fact that most of the reference compounds used for this study exhibited high potency, the corresponding test compounds were structural similar and elicited predominantly low inhibitory activity at the mGlu1 receptor. This discrepancy regarding the activity values is not surprising since virtual screening techniques mainly detect structurally new molecules with low rather than high activity. Nevertheless, the five outstanding compounds, **S-05**, **S-06**, **S-08**, **S-09** and **S-28**, interacted subtype-selectively with the mGlu1 receptor, hence confirming the applicability of this method. Apart from compounds representing various different core structures, nearly half of all retrieved molecules (11 structures of 28, ~40%) can be assigned to one of two different scaffolds. They belong either to the 2*H*-Chromen-2-one derivatives, which can also be interpreted as coumarine analogues, or the 2-Chloroquinoline derivatives (Figure 4.5.3-a).

2*H*-Chromene-2-one derivative

2-Chloroquinoline derivative

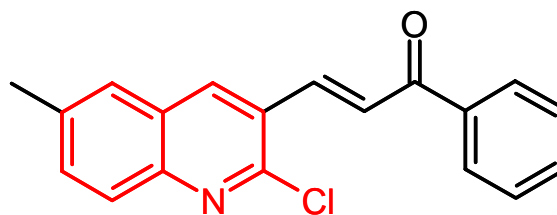


Figure 4.5.3-a. The two chemotypes found within the 28 virtual hits as exemplified by **S-07** (left) and **S-05** (right), respectively. Red bonds and atoms represent the common scaffold.

The chemical structures of all 28 molecules are given in the appendix. One promising coumarine derivative has also been found by the CATS similarity search (Section 4.3). The fact that all training and test molecules used within the CATS similarity search and for the Kohonen maps have been encoded with the same descriptor could serve as a reasonable explanation. In contrast to the 2-Chloroquinolines that closely resemble the R214127-analogues (quinolines), a strategy of further optimizing the coumarine derivatives has been pursued (Section 5.3).

4.5.4 Conclusions

The rationale of the present campaign was to reduce molecule clusters – encoded with the CATS descriptor - from a multidimensional space to a 2D-representation and, thus, to detect hidden relationships between molecules of several classes (e.g., test compounds and reference compounds). Since the selectivity aspect plays an important role for group I mGluRs it was also inevitable for further analysis to prove whether or not our method allows to discriminate between ligands affecting either receptor subtype 1 or subtype 5.

The complete Asinex database was employed for this study, which is in contrast to the previous concept based on *ChemSpaceShuttle*, where we performed data reduction and visualization on a “focused library” (Section 4.3). Here, a subset of 28 test compounds - comprising only two different chemotypes - was selected and assayed for binding affinity and functional activity on mGluR1 and nearly a half of them (13) evoked inhibitory activity below 15 μ M.

5 Scaffold Optimization

In chapter 4 the application of virtual screening concepts like similarity searching (Section 4.3) and SOM-based clustering (Section 4.5) to identify novel structures affecting the mGlu1 receptor were proposed. Chemical classes were detected so far not associated with family 3 GPCRs. In particular, coumarine derivatives introduced in Section 4.3 seemed to provide the most promising scaffold. The following chapter contains procedures that aimed at exploiting the results of the screening campaigns in terms of optimizing the detected coumarine scaffold with respect to activity and investigating a potential binding mode for quinolines (e.g., EMQMCM, R193845) by comparative molecular field analyses (CoMFA). The conclusions drawn from a reliable CoMFA model improved the understanding of the binding mode of coumarines. Furthermore, we introduced a simple yet effective method to predict potential cross-activities for a set of group I allosteric mGluR antagonists. Compound selectivities were predicted by self-organizing maps. Since selectivity plays a crucial role for potential drugs this procedure also pertains to the hit optimization process.

Based on the detection of **C-07**, a promising mGluR1 antagonist, a hit optimization project was started (Section 5.3). Structure-Activity Relationships for coumarines were investigated. Eventually, the hypothesized binding mode of two prominent chemotypes of allosteric mGluR1 antagonists – coumarines and quinolines - was discussed by means of a homology model for the transmembrane region of mGluR1 (Section 5.2.2).

5.1 QSAR Studies on Quinoline Derivatives

Conventional structure-activity relationships (SAR) will be applied based upon a large data set of coumarine analogues to emphasize the impact of this novel class of non-competitive mGlu1 receptor antagonists (Section 5.3). Quantitative structure-activity relationships for a chemical classes of negative allosteric modulators on mGluR1 will be reported within this section: Computer assisted comparative molecular field analyses (CoMFA) were employed to quantitatively describe the influence of a certain structure on bioactivity values for the prominent class of quinoline derivatives [Mabire *et al.*, 2005].

5.1.1 Statistical Evaluation of a CoMFA Model

The structure-activity relationship of the quinolines exemplified for the potent molecules EMQMCM and its derivatives is probably one of the best-evaluated SAR and it represents an ideal data set to quantitatively describe this relationship and to obtain further insights into the binding mode of this group of ligands. A detailed SAR study has been reported [Mabire *et al.*, 2005] and based upon molecular structures and functional activity values (rmGluR1) included therein, QSAR analyses were conducted. Coumarines, structurally not resembling the quinolines, were assumed to bind to the same cavity like the latter group since they were found to selectively displace EMQMCM from its binding site within the transmembrane region of mGluR1 (Section 4.3.2, Figures 4.3.2-b and 4.3.2-c). Considerations regarding the alignment of EMQMCM as quinoline and **B-04** as coumarine relative to each other will also be proposed (Section 5.4.2).

The above-mentioned study of Mabire and co-workers contains 49 quinoline derivatives with a common core structure differing only in the nature and position of the attached substituent at the core scaffold. Initially, a preselection of the structure dataset was done as follows: Five compounds were removed from the subset since they were lacking precise bioactivity data. Another five molecules were discarded as they exhibited structural inconsistency with respect to other ligands. Thus, it was difficult to calculate reliable predictions since they pointed into spatial regions that were not covered by other molecules. The remaining 39 compounds formed the EMQMCM-data collection (Section 3.2.6) and were further subdivided into a training set (thirty entries) and a test set (nine entries) according to the following procedure: All molecules were sorted alphanumerically with respect to their ID values in ascending order. The first nine molecules denoted the test set and the remaining 30 molecules the training set (Appendix, Section 7.6). We are well aware that this procedure is far from a random allocation and for statistical safety random classifications and analyses were performed as well (*vide infra*). Molecular flexible alignment and CoMFA studies were carried out as given in Section 3.2.4.

The CoMFA study yielded a model with the following statistical parameters for the training set: $q^2(cv)_{training}$ gave 0.617 for nine components with a conventional *non* cross-validated correlation coefficient r^2 of 0.991 and a *SEP* of 0.679. The estimated error *SEE* was 0.104 with a relatively high estimated *F*-test value of 246.257. In general, higher r^2 and *F*-values indicate higher accuracy and in most cases a high $q^2(cv)$ corresponds to a low *SEP*. Sterical properties contributed with 59.2% to the model and electrostatic properties with 40.8%.

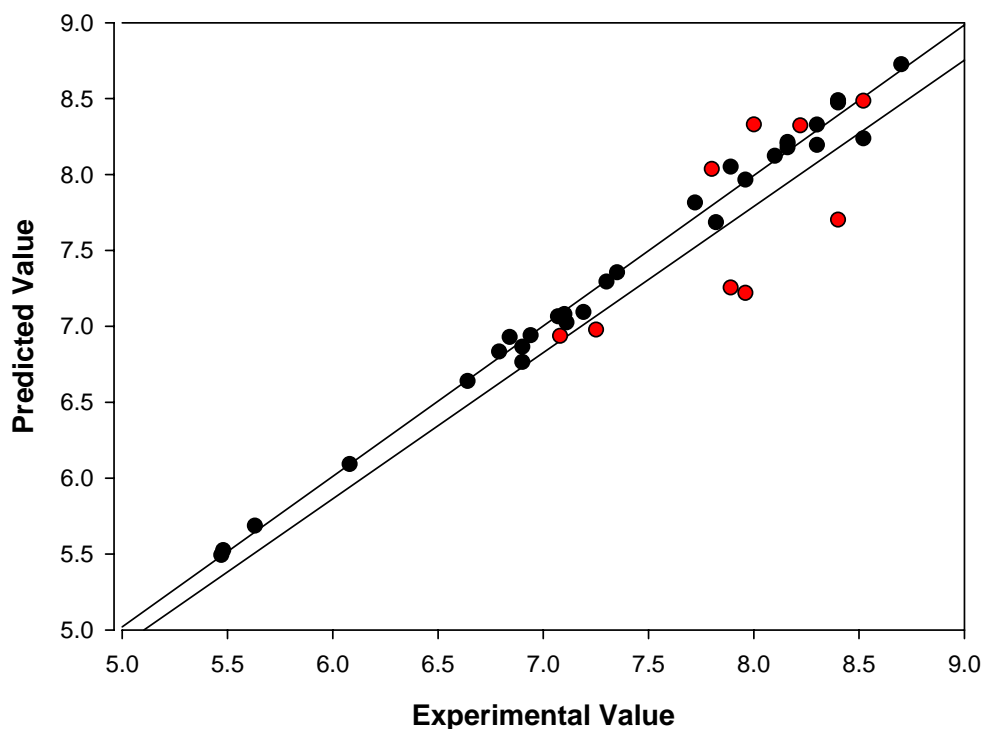


Figure 5.1.1-a. Graphic plotting the experimentally obtained bioactivity data (given as pIC_{50} -values) vs. the predicted data for the initial model where $q^2(cv)_{training}$ was 0.62 and $q^2(cv)_{test}$ was 0.60. Black circles denote the training set members and red circles the test set members. Training and test set are fitted by the black regression lines.

The relatively high $q^2(cv)_{training}$ and r^2 values confirm the predictive power and the applicability of this model. This is also supported by Figure 5.1.1-a: Only a few molecules of the training set slightly deviate from the regression line, which nearly traverses the point of origin. Three of the test compounds deviate from the regression line by nearly one logarithmic unit, which is due to the fact that they bear certain functional groups which are either flexible or do not occur within the set of training molecules. Thus, significant changes in activity are associated with a certain degree of predictive error. Consequently, the $q^2(cv)_{test}$ -value is marginally impaired when compared to $q^2(cv)_{training}$. As a rule $q^2(cv)$ values above 0.4-0.5 are assumed to result in a statistically significant analysis.

To evaluate the statistical significance of the given model new subsets have been created and models have been derived. This was done as follows: The whole data set was divided into two subsets of equal size (training set: 20 entries; test set: 19 entries). The 39 molecules were ten times randomly assigned to one of the subsets resulting in ten different training and test sets. For each data set a CoMFA model was established in the same way as it was shown for the initial model and an average model was calculated (Table 5.1.1-a). A detailed list including all CoMFA parameters for each single dataset is given in the Appendix (Section 7.6).

Table 5.1.1-a. Results of an average CoMFA model based upon ten independent datasets.

Parameters	Mean value	SEM
$q^2(\text{cv})_{\text{training}}$	0.507	0.036
SEP	0.645	0.020
Components	3.6	0.499
F	87.122	28.874
$r^2(\text{conventional})$	0.912	0.023
SEE	0.247	0.028
Electrostatic contributions	0.681	0.018
Steric contributions	0.319	0.018

The predictive power of this average model was significantly impaired when compared to the previous model. This may have two reasons. First, the more members a training set consists of (20 vs. 30) the more data are available leading to a gain of information to be exploited. Hence, the resulting model is more reliable. Second, the initial allocation of molecules to either the training or the test set led by chance to a model with considerable predictive power.

Figure 5.1.1-b visualizes the decrease of predictive power from the initial model to the average model. The actual regression line significantly deviates from the ideal (dashed) regression line representing an ideal data distribution. Although of poorer quality than the initial model, the average model still has sufficient predictive capabilities.

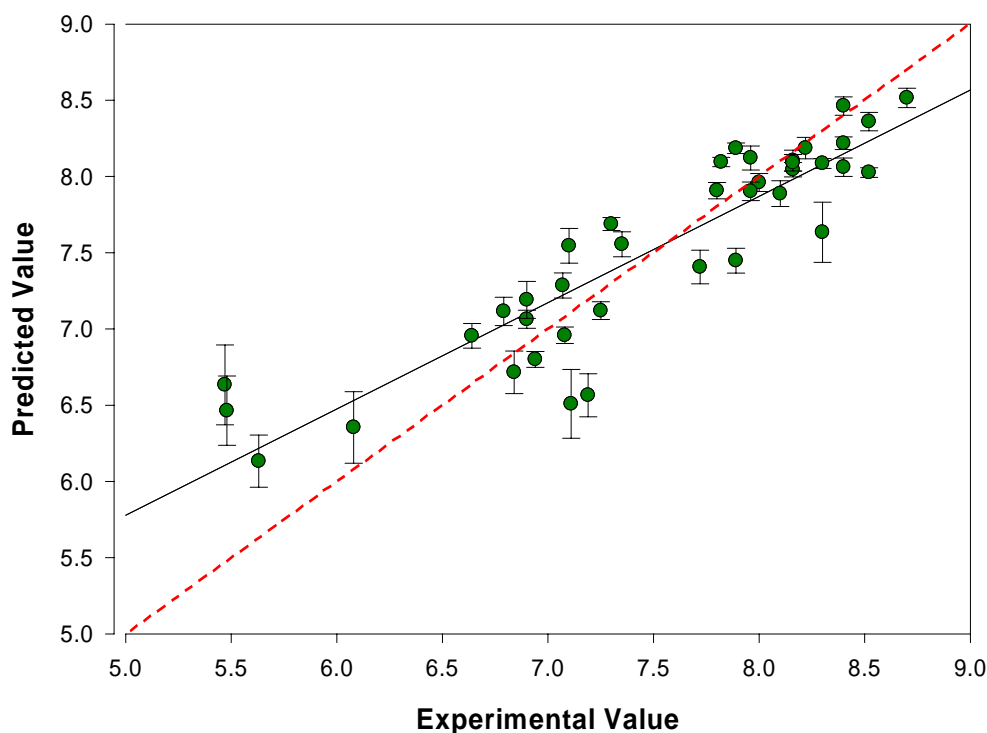


Figure 5.1.1-b. Graphic plotting the experimentally obtained bioactivity data (given as pIC_{50} -values) vs. the predicted data showing the average of ten independent models where the mean $q^2(cv)_{training}$ was 0.51. Green circles denote the molecules of the whole data set. Error bars indicate SEM. The black line is the resulting regression line whereas the dashed red line represents the ideal course of the regression line.

Since steric and electrostatic interactions of CoMFA studies are sensitive to the distance between probe atoms and molecule atoms, there exists a considerable dependence of q^2 values on the relative orientation of the molecular aggregate with respect to the probe lattice [Böhm *et al.*, 1999]. Two methods, All-Orientation Search (AOS) and All-Placement Search (APS), have been reported to evaluate this influence [Wang *et al.*, 1998] (Section 3.2.4). They have proven to be helpful in (i) searching for the optimal orientation resulting in the highest q^2 value and in (ii) detecting the q^2 value of the initial model relative to all possible models.

The result for the training set of the present CoMFA model is given in Figure 5.1.1-c. Both searches clearly demonstrate that the initial model is among the best 5% (AOS) and 10% (APS), respectively of all possible models for this particular alignment. The histogram plots nearly correspond to a normal (Gaussian) distribution. However, the relatively broad ranges of obtained q^2 values varying between 0.3 and 0.7 slightly impair the robustness of the model.

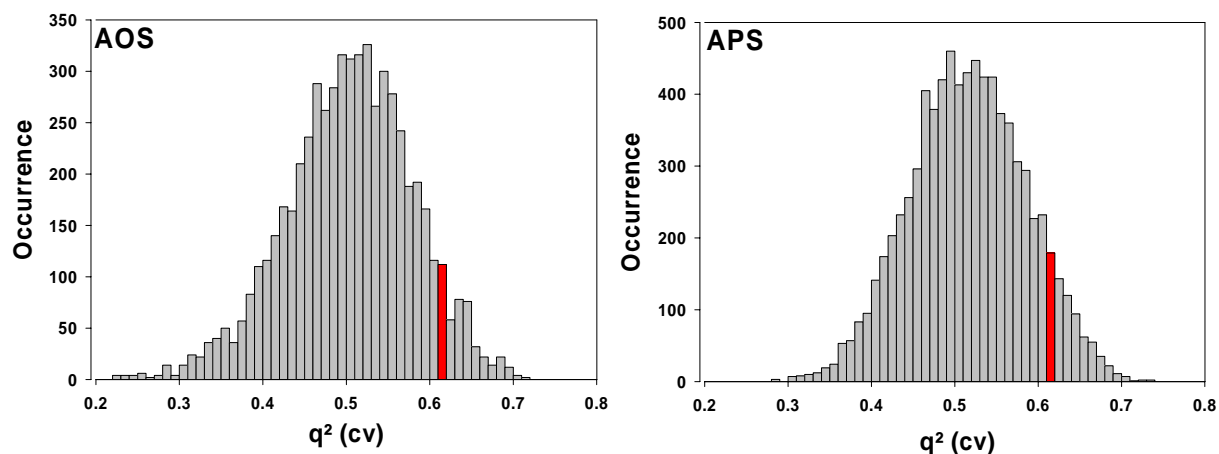


Figure 5.1.1-c. Histograms displaying the distribution of the $q^2(cv)_{training}$ values calculated as LOO cross-validation of the training set after rotation of the molecular aggregate around x-, y- and z-axis (AOS) and after systematic translation of the grid relative to the aligned molecules (APS). The $q^2(cv)$ values are binned into ranges of 0.01 units size and red bins denote the range where the $q^2(cv)$ of the initial model is located.

5.1.2 Contour Maps

Before analyzing the CoMFA studies it has to be emphasized that in addition to pharmacophore models CoMFA models remain hypotheses as long as they are not verified or falsified by experiments. The present spatial orientation of substituents (the molecular alignment) attached to the common core is the most likely arrangement i.e., the energetically most favored arrangement since the protein structure is not taken into account. However, the real orientation of the side chains of the bound ligand could differ to some extent. But it is assumed that the arrangement of substituents from different molecules relative to each other will always be similar.

Having a closer look at the electrostatic CoMFA plots (Figure 5.1.2-a) we observed that the carbonyl group, connecting the aromatic with the hydrophobic moiety (“polar linker”) is crucial for a potent ligand. This is evidenced by a large red isocontour below and a small isocontour above the carbonyl oxygen. Interestingly, this map allows for visualizing an important feature: Methoxy-groups attached to the cyclohexane of the hydrophobic moiety in *cis*-conformation are favored against the *trans*-conformation. The oxygen in *trans*-position points to a large blue isopleth indicating a region where negative charges and H-bond acceptors are disfavored. In contrast, the oxygen in *cis*-position directs to a red isopleth. Here, the weak H-bond acceptor and negatively charged oxygen is favored. Indeed, switching from *cis*-conformation to *trans*-conformation in one molecule leads to a significantly attenuated activity. The blue bulky contour at the left end of the aromatic moiety denotes a region where

H-bond donors or positively charged heteroatoms or substituents are favored. It should be stressed that, in contrast to the “polar linker”, no prediction can be made for the quinoline core structure since this molecular part is retained in all structures.

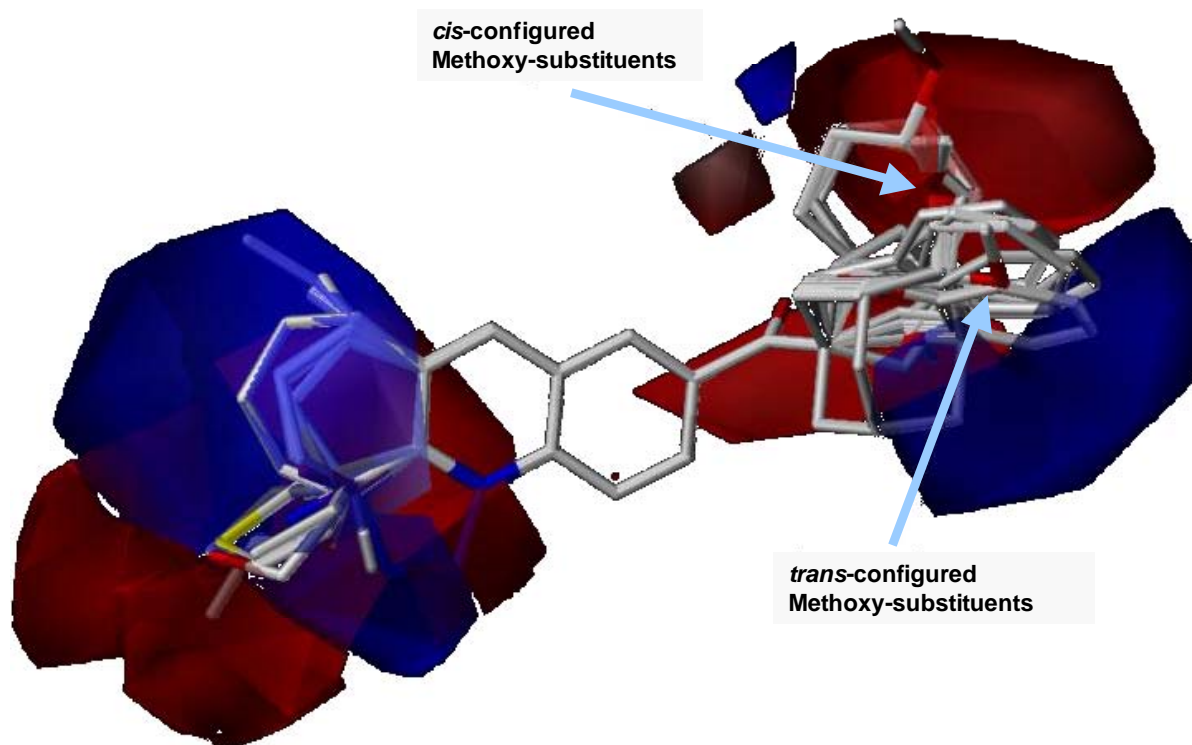


Figure 5.1.2-a. Contour map displaying electrostatic fields for the 39 molecules of the EMQMCM-data collection. Blue polyhedrons denote regions where positive charges (H-bond donors) are favored and negative charges (H-bond acceptors) are detrimental. Red polyhedrons show the opposite case.

The steric contour map visualizes bulky features inevitable for potent ligands not considering any properties related to charges or partial charges. Regarding the present model (Figure 5.1.2-b) we noticed that the hydrophobic moiety on the right may extend downwards and in particular upwards. The lack of yellow polyhedrons in this region does not necessarily mean that the hydrophobic residue may rotate freely into each direction. The model does not explore areas not covered by either type of isocontours. Thus, no conclusion could be drawn for this space.

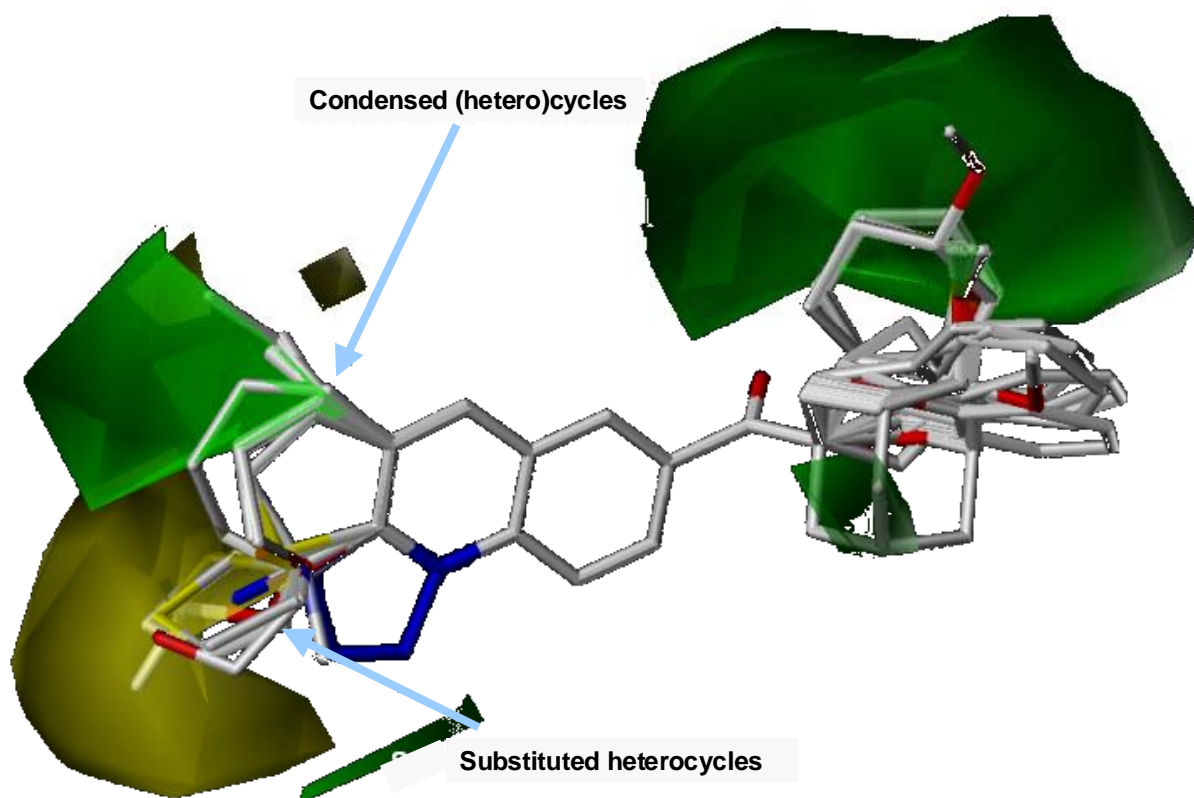


Figure 5.1.2-b. Contour map displaying steric fields for the 39 molecules of the EMQMCM-data collection. Green polyhedrons denote sterically favored regions and yellow polyhedrons show regions where steric bulk is disfavored.

The yellow polyhedrons denote sterically detrimental regions and they can also be assumed as restricted volumes. Accordingly, those substituents of the quinoline core structure pointing to the lower left corner (mainly heterocycles) considerably diminish activity. An additional (hetero)cycle condensed to the quinoline scaffold or a short aliphatic side chain retains activity of a potent ligand. This is visualized by the green polyhedron in the upper left corner.

Exploiting all information given by the contour maps lead to the following proposed results, which are summarized in Figure 5.1.2-c. Starting from the quinoline scaffold the hydrophilic carbonyl linker is crucial for high activity at mGluR1. The hydrophobic residue (R3) may contain either aromatic or alicyclic structures. A weak H-bond acceptor (methoxy group) is favored in *p*-position of the alicycle (cyclohexane) preferably in *cis*-conformation. Ali- or heterocycles (O and S as heteroatoms) condensed at the quinoline ring at position 2 (R2) and 3 (R1) retain high activity (R214127) if they replace a short (max. 3 carbon-atoms) aliphatic side chain at position 3. Heterocycles (e.g., thiophene, thiazole) substituted at R2 attenuate activity of the ligand.

R1/2: No bulky and flexible residues (e.g. substituted ringsystems); condensed (hetero)cycles preferred.

R3: Bulky (alicyclic, aromatic) substituents favoured; alicycles devoid of *trans*-configured substituents.

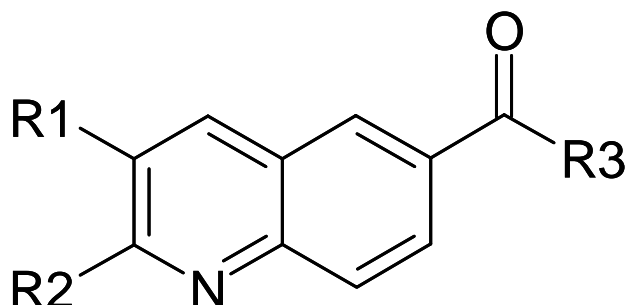


Figure 5.1.2-c. Overview about the structural requirements for potent quinoline derivatives as non-competitive mGlu1 receptor antagonists.

5.1.3 Conclusions

It has been demonstrated that the structural (relatively) consistent quinoline derivatives combined with precise functional activity data facilitated the development of a consistent and presumably reliable CoMFA model. Predictions made for a test set of molecules support this assumption (*vide supra*). However, apart from such “virtual” model evaluations no “real” verifications were done, i.e., no molecule was sketched based on the present model and afterwards synthesized or ordered to check in functional assays whether the predicted bioactivity could be experimentally confirmed or not. The rationale for performing CoMFA studies on quinolines was the visualization of steric and electrostatic properties of the molecules of interest in order to detect substituents important for exerting the desired inhibitory activity. Likewise conventional SAR studies on coumarines (Section 4.3), the quantitative SAR of quinolines presented herein served as a basis for suggesting a ligand orientation at the allosteric mGluR1 binding domain for members of this class.

5.2 Cross-Activities of Group I mGluR Antagonists

As poor selectivity of potential drug candidates is often inherently associated with undesired side effects in later drug development phases, target specificity plays a pivotal role in today’s early hit optimization processes. Therefore, the aspect of selectivity must be taken into account as soon as possible. Testing a given compound on a large panel of different

targets is ineffective and expensive to perform and attempts have been made to find concepts that circumvent this step [e.g., Schnur *et al.*, 2006; Cleves & Jain, 2006]. In the following chapter a simple yet effective way to predict potential cross-activities for known allosteric antagonists of group I metabotropic glutamate receptors will be presented.

The principle and the application of self-organizing maps (SOM) in terms of hit finding has been introduced before (Section 1.5.4, Section 4.5). We used the mapping results presented in Section 4.5 to predict potential cross-activities for group I mGluRs. Since it turned out that the CATS descriptor was able to precisely discriminate antagonists of mGluR1 and mGluR5 we tried to exploit the SOM results of the 15x15 grid for predicting potential additional binding behavior of the ligands.

5.2.1 Target Prediction and Proof of Cross-Activity

First, the mGluR-data collection was complemented by the molecules from the COBRA database [Schneider & Schneider, 2003] containing a broad set of known drugs, leads, and lead candidates affecting a large number of different drug targets. Subsequently, the molecules were converted to a vector representation giving the scaled occurrence frequencies of topological potential pharmacophore point pairs (CATS2D method). In this study, intramolecular distances from zero to nine bonds were considered, resulting in a 150-dimensional vector representation of each molecular compound.

The complete COBRA database was subjected to clustering and mapping onto a two-dimensional grid by the SOM approach (Section 4.5.1). As a result, all molecules from COBRA were distributed into 225 (15×15) clusters (“neurons” or “receptive fields”). The distribution of these compounds is also shown in Figure 5.2.1-a, panel A. It is evident that the SOM is devoid of large patches of empty clusters (< 3%) and pronounced densities, which indicates successful mapping and also reflects the diversity of the COBRA entries. After SOM training the mGluR data were projected onto this map and the resulting distribution patterns were analyzed. The two mGluR ligand classes form separate localized distributions, where the distribution of the mGluR5 antagonists (Figure 5.2.1-a, panel B) appears to be slightly more focused than the mGluR1 data (Figure 5.2.1-a, panel C). Noteworthy, only 6% of the two ligand classes were clustered together (Figure 4.5.1-b). The SOM was able to discriminate between antagonists of the two mGluR subtypes.

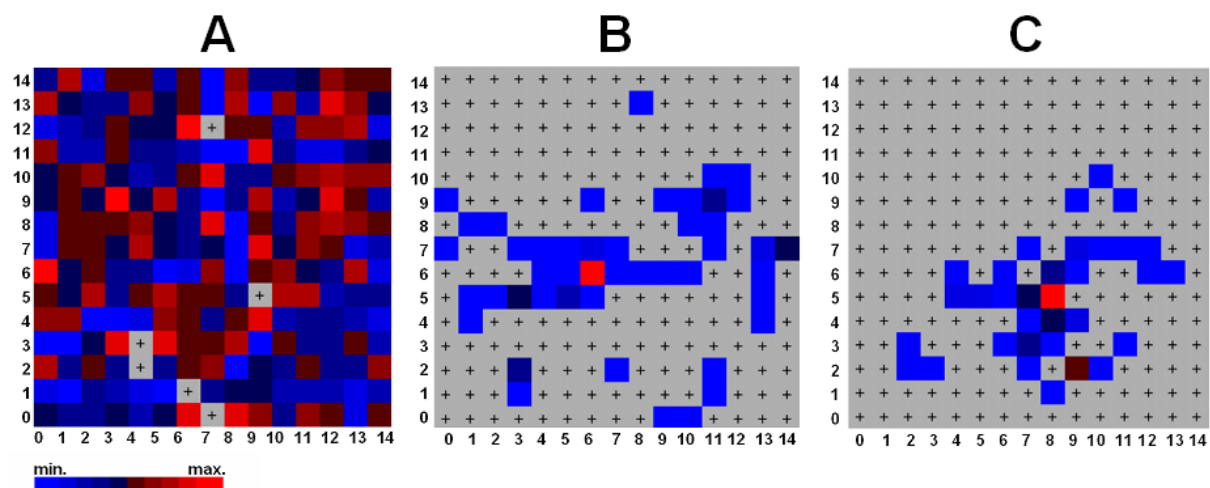


Figure 5.2.1-a. SOM projection of the complete COBRA data (A), the mGluR1 antagonists (B), and mGluR5 antagonists (C). The distribution of the compounds on the map was separately scaled for each figure. Field (6/6) was selected as the target “mGluR1 cluster”, and field (8/5) as the target “mGluR5 cluster”. Gray fields indicate empty clusters. Note that the map forms a torus. See also Section 4.5.1.

Clusters (6/6) and (8/5) revealed the highest density of mGluR1 and mGluR5 reference molecules, respectively (Figure 5.2.1-a). For prediction of potential side effects or additional binding behavior of the mGluR antagonists, the targets of those COBRA ligands that were co-located in these two clusters were listed. Based on this analysis, mGluR1 antagonists of cluster (6/6) and mGluR5 antagonists of cluster (8/5) were predicted to interact with human dopamine D₂-like receptors, histamine H₁ receptor, and muscarinic acetylcholine (mACh) receptor. For pharmacological testing, we selected representative molecules from each cluster and if not available structurally related compounds from a Merz molecule collection (Figure 5.2.1-b). Except EMQMCM, R193845, M-MPEP, MTEP and **D-06** all molecules were from a Merz library but closely resemble their pendants in the mGluR data collection.

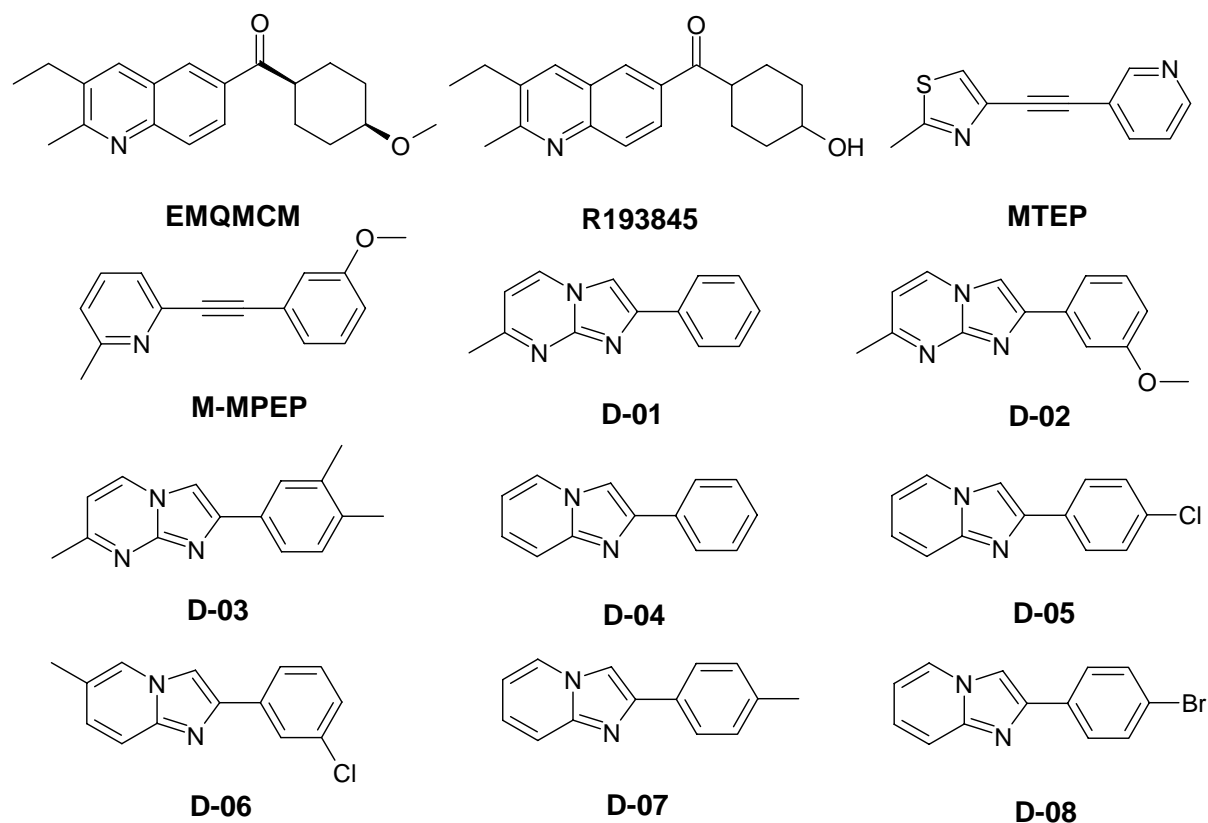


Figure 5.2.1-b. Known mGluR1 (EMQMCM, R193845) and mGluR5 antagonists, which were selected for activity testing based on the SOM results.

Representatives were defined as being closest to the cluster centroids in descriptor space. Four scaffold classes were found: Molecules EMQMCM, R193845, MTEP and M-MPEP have been described elsewhere (Section 1.4.2, Section 2.2), **D-01 - D-03** are imidazo[1,2-a]pyrazine derivatives, and **D-04 - D-08** represent imidazo[1,2-a]pyridine derivatives [Mutel *et al.*, 2002]. In addition, for each of these test compounds individual predictions of target preference were made. This prediction was based on the relative occurrence frequencies of known COBRA compounds in the clusters, for example in the mGluR5 cluster we found $4 \times H_1$, $2 \times D_2$, $1 \times \text{mACh}$ ligands. Based on this crude statistics, compounds EMQMCM and R193845 were predicted to interact with all four targets, the remaining compounds preferably with H_1 . We also found aromatase inhibitors co-located in cluster (8/5), which was not further pursued but might be worthwhile testing.

Table 5.2.1-a. IC_{50} values (mACh, mGluR1, mGluR5) and K_i values (D_2 , D_3 , H_1) of selected compounds. Underlined values indicate the predictions according to the SOM analysis.

Identifier	mACh (M_1) [μ M]	D_2 [μ M]	D_3 [μ M]	H_1 [μ M]	mGluR1 [μ M]	mGluR5 [μ M]
EMQMCM	<u>54.7</u> (± 2.8)	<u>91.6</u> (± 13.6)	<u>45.4</u> (± 27.1)	<u>22.0</u> (± 3.7)	0.008	-
R193845	<u>n.d.</u>	<u>80.7</u> (± 0.8)	<u>25.4</u> (± 9.4)	<u>20.6</u> (± 1.1)	0.080	-
MTEP	n.d.	n.d.	76.2 (± 46.9)	<u>26.3</u> (± 4.1)	-	0.005
M-MPEP	n.d.	n.d.	75.6 (± 23.5)	<u>33.6</u> (± 3.2)	-	0.010
D-01	n.d.	n.d.	n.d.	<u>22.9</u> (± 1.9)	-	> 30.0
D-02	n.d.	n.d.	90.9 (± 78.4)	<u>16.2</u> (± 7.1)	-	> 30.0
D-03	n.d.	n.d.	16.0 (± 6.5)	<u>4.6</u> (± 1.7)	-	28.8
D-04	n.d.	n.d.	n.d.	<u>36.4</u> (± 33)	-	> 30.0
D-05	n.d.	n.d.	53.4 (± 37.2)	<u>4.8</u> (± 0.8)	-	> 30.0
D-06	n.d.	n.d.	24.3 (± 4.4)	<u>6.5</u> (± 3.4)	-	8.8
D-07	n.d.	n.d.	32.9 (± 16.7)	<u>4.5</u> (± 1.1)	-	> 30.0
D-08	n.d.	n.d.	n.d.	<u>4.3</u> (± 0.6)	-	> 30.0

n.d.: no detectable activity/affinity at the concentrations tested.

The pharmacological assays results are summarized in Table 5.2.1-a. Although only weak binding constants in the low to medium micro molar range were determined, the results confirm the SOM predictions. Noteworthy, all tested compounds exhibit binding affinity in our H_1 receptor assay, indicating a potential general interaction of mGluR1/5 antagonists with the histamine receptor. It might thus be meaningful testing affinities to other histamine receptor subtypes. With the exception of **D-01**, **D-04**, and **D-08**, the compounds showed moderate binding to dopamine D_3 receptors. Only EMQMCM and R193845 also exhibited dopamine D_2 receptor binding affinity, all others were inactive at dopamine D_2 receptors, meaning that three out of the four substance classes represent D_2 -selective chemotypes. The known mGluR1 antagonists EMQMCM and R193845 were most “promiscuous”. These are the only compounds that comprise additional mACh activity and dopamine D_2 receptor binding affinity.

5.2.2 Conclusions

In summary, we successfully applied a topological pharmacophore descriptor and SOM-based clustering to predicting potential activities of known mGluR antagonists. This prediction concept, which includes molecule encoding, clustering and visualization gives no

hint about the potency of compounds at the predicted targets. Nevertheless, in this study the tested compounds exhibited weak yet detectable affinities towards the allosteric binding site of mGluR1 and mGluR5, respectively, with binding constants in the micro molar range. Whether such activity or affinity is of actual pharmacological relevance remains to be shown.

Irrespective of the outcome of such studies for the particular compounds employed here, the present virtual screening concept might provide a basis for early recognition of potential side-effects in lead discovery. Moreover, this concept could perhaps also be applied to other issues or tasks in drug discovery. Assumed that suitable descriptors and databases are available many predictions regarding, e.g., toxicity and ADME properties may be proposed.

5.3 Hit Optimization and SAR Analysis of Coumarines

Since **C-07** has proven to be a potent novel allosteric antagonist of mGluR1 a hit optimization project for the promising coumarine core structure was raised. Compounds bearing this scaffold were found by the topological pharmacophore search (Section 4.3) as well as the self-organizing maps (Section 4.5). In both studies, the molecules were encoded with the CATS atom-pair descriptor. However, the five coumarine derivatives detected within the SOM study (**S-03**, **S-07**, **S-12**, **S-18**, **S-21**; Section 4.5.2 and Appendix, Section 7.5) did not show any affinity or activity at the mGlu1 receptor.

The synthesis of all compounds described herein has been carried out at the Institute of Organic Synthesis (IOS, Riga, Latvia), which is a co-operation partner of Merz. Aigars Jirgensons, group leader in Organic Synthesis at the IOS, managed the synthesis project. Structure-activity relationship investigations have been performed at Merz. Synthesis proposals based upon bioactivity data of already assayed compounds were presented to the chemists of the IOS and discussed with them. The complete project was supervised by Tanja Weil from Merz.

5.3.1 Synthesis Strategy

The idea of this project was to systematically explore potential influences of various substituents attached to the common core at all possible positions. Newly designed molecules should have (i) higher affinity and activity than the reference compound **C-07** and (ii) they

should show the same or improved solubility compared to **C-07**. In a further step the scaffold was also partially modified.

The initial strategy comprised the following modifications of **C-07** (Figure 5.3.1-a): Attaching small hydrophobic side chains (methyl, trifluoromethyl) at several positions of the cyclohexyl ring at R1, R2 and R3; introducing new substituents at position R6, predominantly small and polar (nitro-, amino-groups and short alkylamino groups) residues; replacing the chloro-substituent (R4) with other halogens, (C₁-C₆alkyl)amino-, nitro- or heteroaryl-substituents.

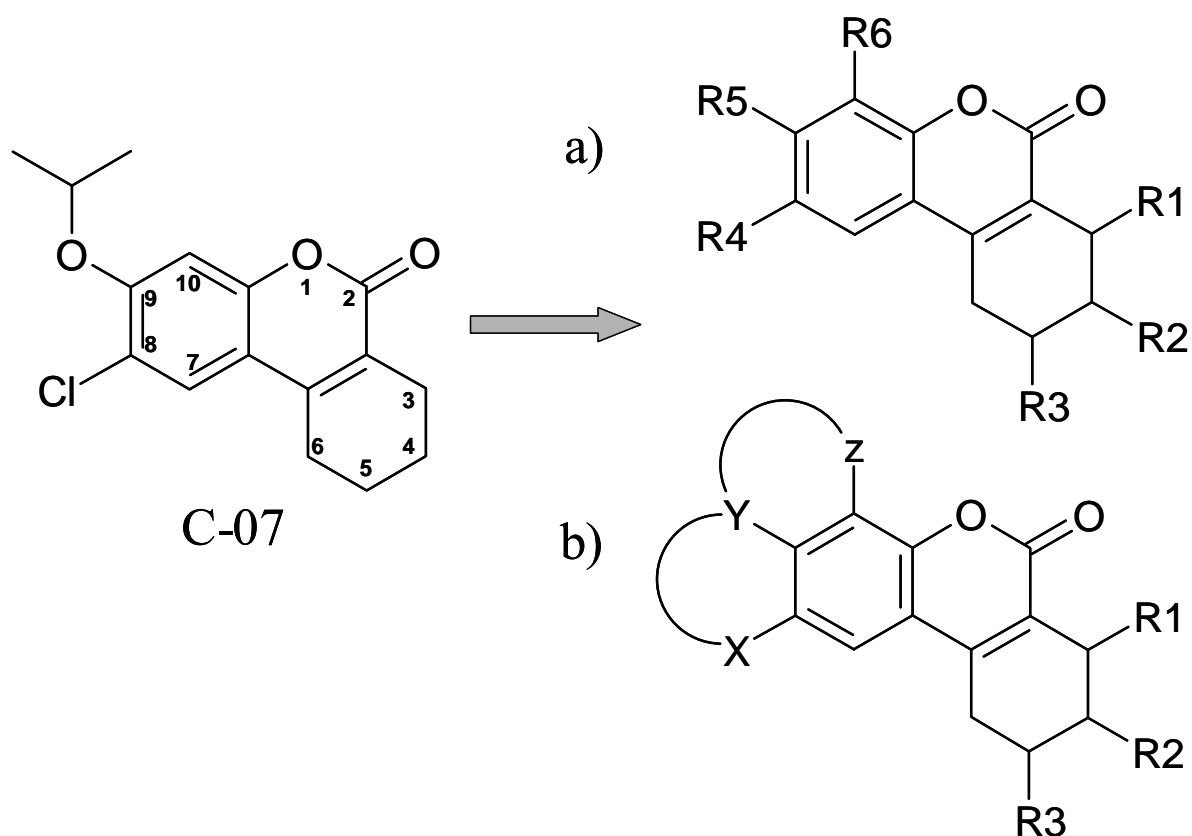
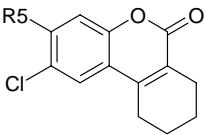
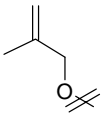
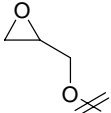
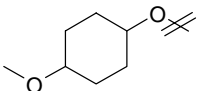


Figure 5.3.1-a. Chemical structure of **C-07** and the proposed positions for side chain modifications of the scaffold (a) and the introduction of new ring systems (b). Black digits denote potential substitution positions of the common scaffold according to the IUPAC nomenclature.

The most thorough modifications were achieved at position R5. While retaining the oxygen as linker, the *i*-propyl group was replaced, e.g., with short and flexible groups like allyl- or difluoromethyl-groups as well as with bulky cycloalkyl-substituents. A similar strategy was followed for short alkylthio- and amino-groups where the oxygen has been replaced with sulfur or nitrogen. Furthermore, some derivatives were synthesized where R5 was linked either to R4 or R6, thus adding another ring system to the coumarin scaffold (Figure 5.3.1-a, panel b). Other modifications aimed at opening the coumarin core structure by cleaving the

in the quinoline EMQMCM is also assumed to nearly retain activity (**B-04**). This synthesis allowed for comparing both scaffolds, the quinolines and coumarines and gave hints to the hypothesized binding mode of them at the receptor site (Section 5.4.2).

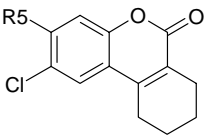
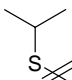
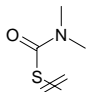
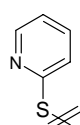
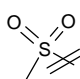
Table 5.3.2-a. Pharmacological data of diverse 9-substituted coumarines (ether linker). Values in *italic* indicate estimated data (tested at 10 μ M). SEM are given in parentheses.

				
Compound-No.	R5	rmGluR1 <i>K_i</i> (μ M)	rmGluR1 <i>IC₅₀</i> (μ M)	hmGluR1 <i>IC₅₀</i> (μ M)
C-07	i-propoxy	0.753 (\pm 0.048)	0.362 (\pm 0.031)	9.8 (\pm 0.65)
B-01	OH	>100	>100	n.t.
B-02		31.9 (\pm 1.08)	5.1 (\pm 0.70)	n.t.
B-03		31.6 (\pm 0.87)	4.8 (\pm 0.82)	>100
B-04		8.267 (\pm 1.27)	3.3 (\pm 0.28)	>100
B-05	difluoromethoxy	7.1 (\pm 0.19)	2.8 (\pm 0.24)	>100

n.t.: not tested on this target

The replacement of oxygen by a sulfur at position 9 of **C-07** yields **B-06** with slightly diminished activity. A short flexible side chain containing two H-bond acceptors considerably improves activity (**B-07**) and solubility (data not shown) whereas a methylsulfonate at that position results in loss of activity (**B-09**, Table 5.3.2-b).

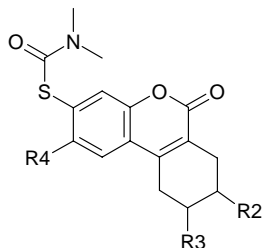
Table 5.3.2-b. Pharmacological data of diverse 9-substituted coumarines (thioether linker). Values in *italic* indicate estimated data (tested at 10 μ M). SEM are given in parentheses.

				
Compound-No.	R5	rmGluR1 <i>K_i</i> (μ M)	rmGluR1 <i>IC₅₀</i> (μ M)	hmGluR1 <i>IC₅₀</i> (μ M)
B-06		10.86 (\pm 0.09)	1.9 (\pm 0.29)	n.t.
B-07		2.728 (\pm 0.002)	0.123 (\pm 0.007)	>100
B-08		28.2 (\pm 0.50)	5.35 (\pm 0.90)	>100
B-09		>100	>100	n.t.

n.t.: not tested on this target

Since it turned out that the dimethylthiocarbonyl substituent at position 9 increases activity (**B-07**) the respective substitution pattern for this compound at R2 – R4 was investigated (Table 5.3.2-c). At least the presence of a non-hydrogen atom at position 8 (R4) seems to be crucial (**B-12**). Only an introduced methyl group at R3 could nearly retain activity (**B-11**). Other even minor modifications yielded inactive compounds or compounds with attenuated activity

Table 5.3.2-c. Pharmacological data of diverse 4,5,8-substituted coumarines. Values in *italic* indicate estimated data (tested at 10 μ M). SEM are given in parentheses.

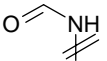
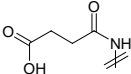
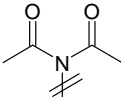
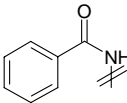
						
Compound-No.	R2	R3	R4	rmGluR1 <i>K_i</i> (μ M)	rmGluR1 <i>IC₅₀</i> (μ M)	hmGluR1 <i>IC₅₀</i> (μ M)
B-10	H	H	Cl	2.728 (\pm 0.002)	0.123 (\pm 0.007)	>100

B-11	H	methyl	Cl	5.243 (± 0.52)	0.774 (± 0.062)	n.t.
B-12	H	H	H	39.6 (± 1.26)	6.8 (± 0.92)	>100
B-13	ethyl	H	Cl	23.4 (± 0.37)	>100	n.t.
B-14	phenyl	H	Cl	>100	>100	n.t.

n.t.: not tested on this target

Starting from **C-07** an additional H-bond donor at position 10 (R6) led to a loss of activity (**B-15**) whereas a H-bond acceptor even as part of a bulky substituent only slightly decreased activity (**B-17**, **B-19**). However, in general it was found that the bulkier the moiety the weaker the observed activity is (Table 5.3.2-d).

Table 5.3.2-d. Pharmacological data of diverse 10-substituted coumarines. Values in *italic* indicate estimated data (tested at 10µM). SEM are given in parentheses.

Compound-No.	R6	rmGluR1 <i>K_i</i> (µM)	rmGluR1 <i>IC₅₀</i> (µM)	hmGluR1 <i>IC₅₀</i> (µM)
B-15	NH ₂	>100	>100	>100
B-16	NO ₂	>100	4.5 (± 0.16)	>100
B-17		16.56 (± 0.763)	1.333 (± 0.161)	n.t.
B-18		34.0 (± 0.74)	4.9 (± 0.65)	>100
B-19		17.5 (± 0.26)	3.2 (± 0.31)	n.t.
B-20		>100	6.7 (± 1.19)	>100

n.t.: not tested on this target

Changing substituents at position 8 (R4) yielded compounds with low-micro molar activity (Table 5.3.2-e). Either a H-bond acceptor or a short aliphatic side chain (**B-21**, **B-22**), which

slightly reduced activity (IC_{50} : 0.36 μ M to 2.5 μ M), have been investigated. H-bond donors are not favorable at that position (**B-24**). Here, the same applies as for position 10: a too capacious residue decreases activity (**B-23**).

Table 5.3.2-e. Pharmacological data of diverse 8-substituted coumarines. Values in *italic* indicate estimated data (tested at 10 μ M). SEM are given in parentheses.

Compound-No.	R4	rmGluR1 <i>K_i</i> (μ M)	rmGluR1 <i>IC₅₀</i> (μ M)	hmGluR1 <i>IC₅₀</i> (μ M)
C-07	Cl	0.753 (\pm 0.048)	0.362 (\pm 0.031)	9.8 (\pm 0.65)
B-21	NO ₂	7.5 (\pm 0.41)	1.6 (\pm 0.21)	n.t.
B-22	ethyl	2.625 (\pm 0.05)	2.5 (\pm 0.24)	n.t.
B-23		>100	4.0 (\pm 0.41)	>100
B-24	NH ₂	21.5 (\pm 0.27)	5.7 (\pm 0.52)	>100

n.t.: not tested on this target

Short and lipophilic side chains at positions 3, 4 and 5 (Table 5.3.2-f) were able to nearly maintain (**B-25**, **B-26**) or slightly enhance activity (**B-27**). Position 5 (R3) has even earlier proven to be a suitable place for the introduction of a methyl group (**B-11**). Unfortunately, it has not been further explored for other substituents.

Table 5.3.2-f. Pharmacological data of diverse 3,4,5-substituted coumarines. Values in *italic* indicate estimated data (tested at 10 μ M). SEM are given in parentheses.

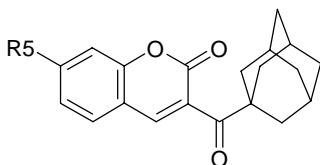
Compound-No.	R1	R2	R3	rmGluR1 <i>K_i</i> (μ M)	rmGluR1 <i>IC₅₀</i> (μ M)	hmGluR1 <i>IC₅₀</i> (μ M)
B-25	methyl	H	H	0.828 (\pm 0.131)	1.2 (\pm 0.09)	n.t.

B-26	H	trifluoromethyl	H	2.984 (± 1.05)	0.574 (± 0.052)	n.t.
B-27	H	H	methyl	0.691 (± 0.047)	0.199 (± 0.017)	<i>23.6</i> (± 1.41)

n.t.: not tested on this target

Eventually, removing the condensed cyclohexene and introducing an adamantylcarbonyl group at the new position 3 led to substantially improved activity and affinity data. Various kinds of additional residues (H-bond acceptors, lipophilic and more hydrophilic groups) at the new position 7 (R5) resulted in compounds potently binding to the allosteric site of mGluR1 and inhibiting its DHPG-induced activity (Table 5.3.2-g). The fact that this series (i) lacks the common core structure and (ii) revealed highly active inhibitors led to the assumption that these ligands bind to the receptor in a way distinct to that of the other molecules of this project. Probably the crucial role, however, plays the voluminous adamantyl substituent that forces these molecules in a slightly “shifted” orientation relative to the other coumarines, according to the hypothesis (Section 5.4.1).

Table 5.3.2-g. Pharmacological data of diverse 3-(Adamantane-1-carbonyl)-2*H*-chromen-2-one derivatives. Values in *italic* indicate estimated data (tested at 10μM). SEM are given in parentheses.



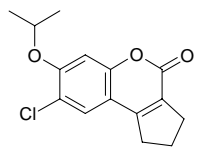
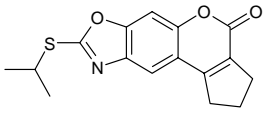
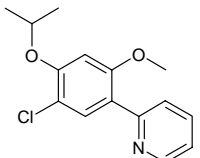
Compound-No.	R5	rmGluR1 <i>K_i</i> (μM)	rmGluR1 <i>IC₅₀</i> (μM)	hmGluR1 <i>IC₅₀</i> (μM)
B-28	methoxy	0.293 (± 0.022)	0.058 (± 0.008)	<i>30.6 (± 1.19)</i>
B-29	diethylamino	0.049 (± 0.004)	<1	>100
B-30	Br	0.431 (± 0.049)	0.197 (± 0.053)	n.t.
B-31	dimethylamino	0.088 (± 0.011)	<1	<i>17.6 (± 1.12)</i>

n.t.: not tested on this target

Several attempts to modify the core structure have been made, yet most of the resulting structures revealed no activity (data not shown). A selection of some modifications is given in Table 5.3.2-h. Replacing the cyclohexyl ring in **C-07** with a cyclopentyl ring nearly conserves inhibitory activity (**B-32**). Neither the extension of the ring system provided by **B-33** nor

cleavage of the heterocycle (**B-34**) led to molecules maintaining the activity of the structurally related compounds **B-32** and **C-07**.

Table 5.3.2-h. Pharmacological data of coumarine derivatives and related modifications. Values in *italic* indicate estimated data (tested at 10 μ M). SEM are given in parentheses.

Compound- No.	R	Others		
		rmGluR1 <i>K_i</i> (μ M)	rmGluR1 <i>IC₅₀</i> (μ M)	hmGluR1 <i>IC₅₀</i> (μ M)
B-32		3.948 (\pm 0.23)	0.494 (\pm 0.119)	>100
B-33		>100	11.8 (\pm 1.28)	n.t.
B-34		>100	>100	n.t.

n.t.: not tested on this target

5.3.3 Discussion and Summary

Summarizing the results of 189 coumarine derivatives obtained by pharmacological experiments allows for drawing some conclusions concerning a general structure activity relationship for these compounds. The coumarin structure exemplified by **C-07** is given in Figure 5.3.3-a. The potential positions for substituting are also indicated. Here, a light grey ellipse emphasizes the common core structure of the vast majority of derivatives. One important feature attached to the scaffold is the cyclohexene ring highlighted by a dark grey ellipse. Although this moiety is also assumed to be part of the scaffold, which is stressed by the red digits, it is suggested as a condensed substituent in this scheme. It could either be an aromatic or heteroaromatic ring but preferably a cyclohexene. Additional short aliphatic and hydrophobic substituents may be introduced at each position but favorably at position 5. The influence of separated side chains at position 7 has not been explored, only if connected with substituents at position 8, thus introducing an additional ring. However, they turned out to be disfavored in terms of bioactivity.

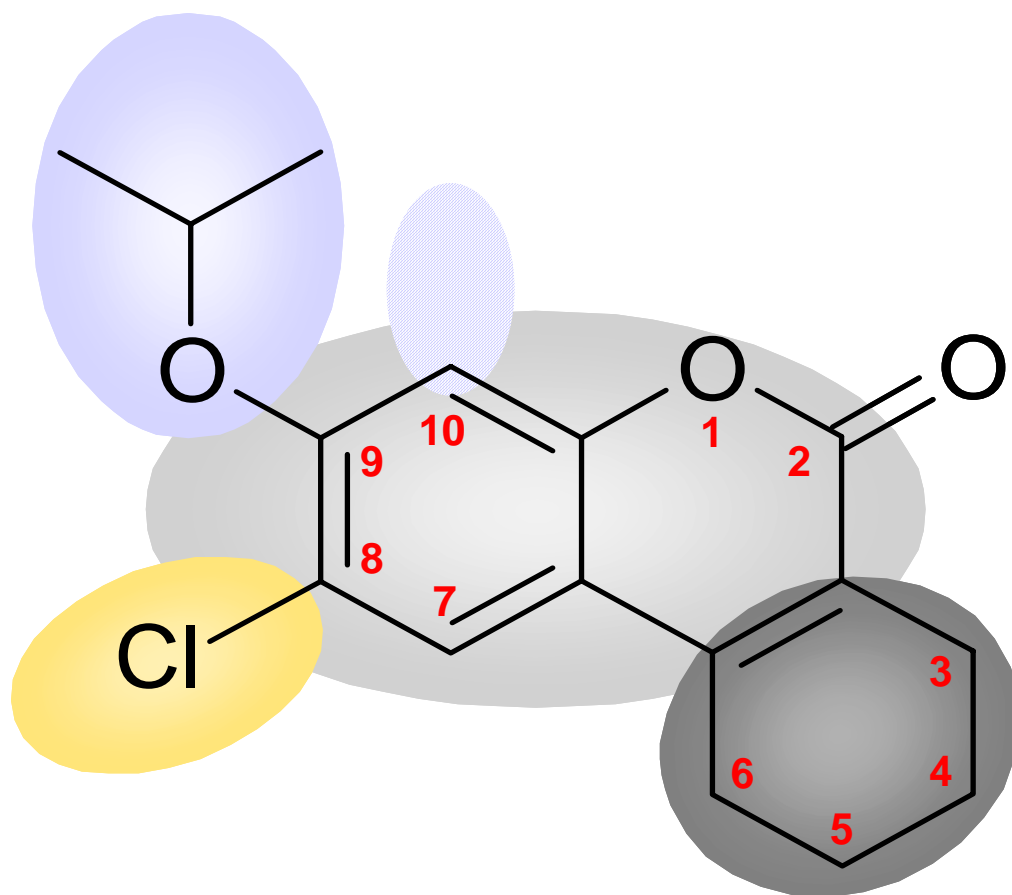


Figure 5.3.3-a. Proposed SAR scheme at a glance. The series of coumarin derivatives is exemplified by **C-07**. Red digits denote potential substitution positions of the common scaffold according to the IUPAC nomenclature. For more information see text.

A substituent at position 8 has proven to be crucial. Here, this feature is displayed as a yellow ellipse. It can either consist of a halogen, a H-bond acceptor or a short aliphatic side chain. This strongly supports the hypothesis that preferably a short yet bulky substituent should be attached at position 8 (Figure 5.3.3-a). Only H-bond donors were disfavored (Table 5.3.2-e). Another pivotal feature is the residue at position 9 highlighted by a light blue ellipse. It can comprise a ring system such as **(B-05)** although a short and relatively rigid hydrophobic side chain is preferred. It must contain at least one heteroatom (weak H-bond acceptor) directly attached to the scaffold but might also include other polar features (presumably because of increased solubility). The hypothesized influence of features at position 8 with respect to activity is detailed below (Figure 5.3.3-b). Finally, the blue-white hatched ellipse at position 10 denotes a region where bulky residues containing H-bond acceptors at least nearly retain activity whereas other features (e.g., H-bond donors) lead to a loss of activity. However, this substituent turned out to be of minor importance.

Detailed investigations have been made for the presumed interaction between substituent 8 and a H-bond donor site at the receptor. The chloro atom at position 8 in **C-07** (Figure 5.3.3-b, a) is a relatively small atom that can interact with a H-bond donor *via* weak hydrogen bonding. This residue seems to be meaningful but not essential since molecule c) exhibits a decrease but not a loss of activity (Figure 5.3.2-3, c). Furthermore, replacement with a H-bond donor attenuates activity, which is exemplified by **B-24** (Figure 5.3.2-3, d).

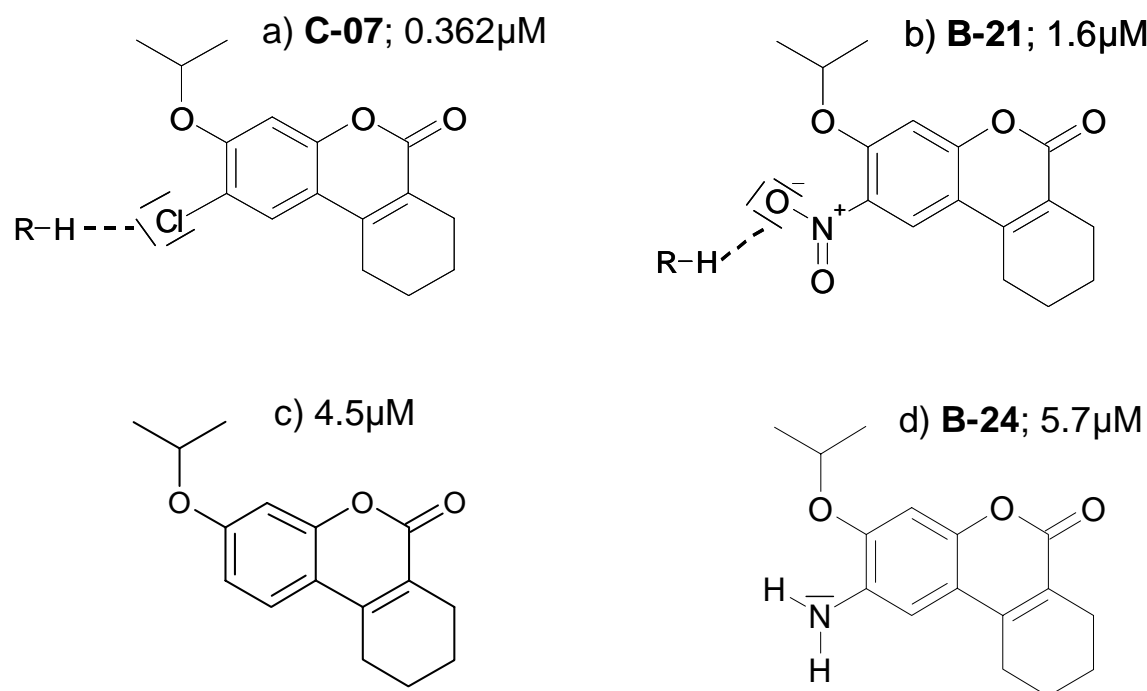


Figure 5.3.3-b. Hypothesized interactions between the substituents at positions 8 and a hydrogen provided by the receptor. Chloro atom (a) and nitro residue (b) form a weak hydrogen bond thereby presumably stabilizing a certain molecular orientation. If position 8 lacks a H-bond acceptor no interaction *via* hydrogen bonding can be established at that position. For more information see text.

Eventually, another H-bond acceptor at position 8, e.g., a nitro group can also interact with a hydrogen provided by the receptor site, which is shown for **B-21** (Figure 5.3.3-b, b). The decrease in activity from **C-07** to **B-21** might be a result of a hampered hydrogen bonding since the nitro group is more voluminous than the chloro atom. Noteworthy, a hydrogen bond $R-OH \cdots O-N-R$ is stronger than $R-OH \cdots Cl-C-R$ since the chlorine acts as a weak acceptor [Desiraju & Steiner, 1999].

Summarized, a substituent at position 8 of the coumarin scaffold should be of small size, act as a H-bond acceptor and should preferably have hydrophobic properties (**C-07** and **B-21**, Table 5.3.2-e). Within the described hit optimization project a total of 189 compounds

including the first hit **C-07** were synthesized and pharmacologically characterized. The influence of crucial features and features of less importance has been investigated for biological relevance. Even the scaffold itself was partly modified yet without success regarding the pharmacological profile. The results of all compounds have been exploited for SAR purpose leading to a proposed SAR scheme (Figure 5.3.3-a).

An overall functional activity hit rate is given in Figure 5.3.3-c. The ranges of activity classes shown here slightly differ compared to those used for hit rates of virtual screening campaigns. Fourteen compounds (7.4%) including **C-07** were classified as “highly active” ($>1\mu\text{M}$), twenty-eight compounds (14.8%) were “moderately active” (1-10 μM), nineteen compounds (10.1%) revealed moderately to low activity (10-20 μM), twenty-nine compounds had low activity (15.3%) and for ninety-nine compounds (52.4%) “no activity” was observed ($>30\mu\text{M}$) leading to a total hit rate of approximately 22% ($<10\mu\text{M}$). This is an acceptable hit rate for hit optimization projects. However, it must be stressed that only few compounds were able to allosterically antagonize the mGlu1 receptor more potently than the initial hit. Some of those molecules affecting the receptor in the low nano molar range (Table 5.3.2-g) are assumed to have an orientation in the binding pocket distinct to the others (Section 5.4.1), which will be addressed in the next chapter.

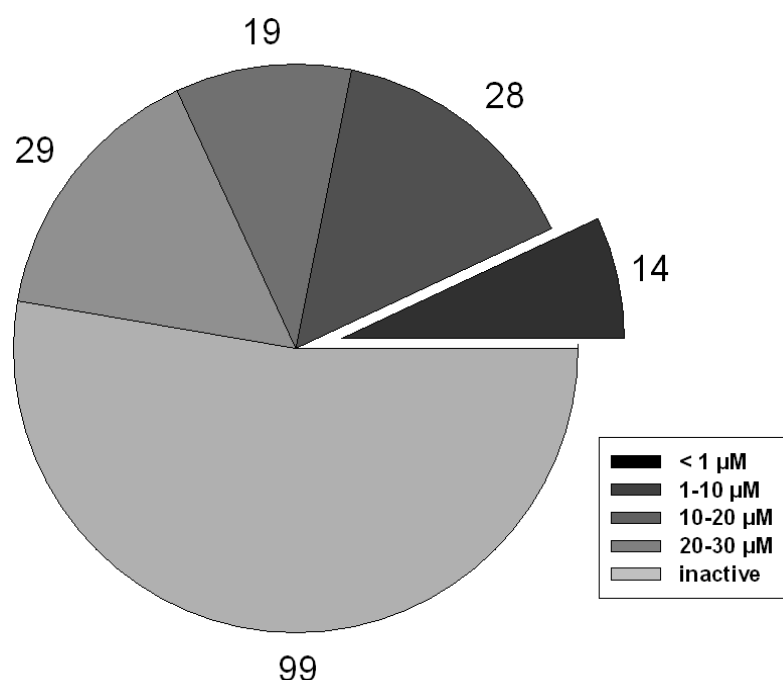


Figure 5.3.3-c. Overall hit rate for coumarine derivatives synthesized within the hit optimization project. Digits at the edge denote the absolute number of compounds of the corresponding activity subset.

5.3.4 Conclusions

Based on compound **C-07** we performed a hit optimization project for coumarines as negative allosteric modulators of mGluR1 leading to 189 coumarine related structures. Although no promising lead candidate emerged from this project the extensive exploration of the chemically feasible space of coumarine derivatives facilitated a comprehensive SAR description. Precise knowledge of the pharmacological relevance of various substituents at any scaffold position meaning their influence on ligand binding enabled or at least supported the hypothesized molecule orientation in the receptor (Section 5.4.1), which followed after analysis of the observations made in this chapter.

5.4 The Hypothesized Allosteric Binding Pocket of mGluR1

Until now, only the structures of ligands binding to group I mGluRs have been taken into account. Based on pharmacophore models (Section 4.2) as well as on SAR analyses (Section 5.3) and contour maps of a CoMFA model (Section 5.1) potential interaction points of several allosteric mGluR1 antagonists were discussed and considered as crucial features or features, which are presumably favored but not essential. Here, an attempt was done to transfer the knowledge obtained within the mentioned chapters to evaluate a possible binding behavior of those ligands at the corresponding target, the binding site in the HD of the mGlu1 receptor. Therefore, a homology model of mGluR1 was developed (Section 3.2.5) to get an idea of a potential binding mode of coumarines and quinolines.

5.4.1 Binding of Coumarines

The diverse molecules **C-07** and **B-28** (Section 5.3) were selected as coumarine representatives to investigate the binding mode of coumarines at the allosteric site of mGluR1. The ligands were placed manually into the transmembrane region in proximity to the pocket where 11-*cis*-retinal was found in bovine rhodopsin. Preliminary results with automated docking methods did not lead to reasonable results, thus we decided to place the ligands manually in a way most consistent with our SAR data and mutational results from literature [Malherbe *et al.*, 2003a] that were based on binding of EM-TBPC, a prominent mGluR1 antagonist, followed by energy minimization. It must be stressed that all presented binding modes are hypotheses fitting to our data rather than extensively evaluated and confirmed results. For some of the ligands the functional activity in human mGluR1 was also

measured (Section 5.3.2). All ligands exerted explicitly lower activity in the human receptor. This led us to the conclusion that the ligands had to be in contact with V757^{5.47} (superscript indicates TM and position [Balesteros & Weinstein, 1995]), which is replaced with an leucine in the human mGluR1, the single difference between rat and human receptor within the ligand-binding region. The hydrophobic unsaturated ring was selected as candidate for this contact.

Figure 5.4.1-a (panel a) displays the predicted binding mode of **C-07** in the binding pocket of mGluR1. The unsaturated ring is in contact with the rat selective V757^{5.47}, which is surrounded by further hydrophobic residues V753^{5.43} and P756^{5.46} that form a hydrophobic cluster (panel a).

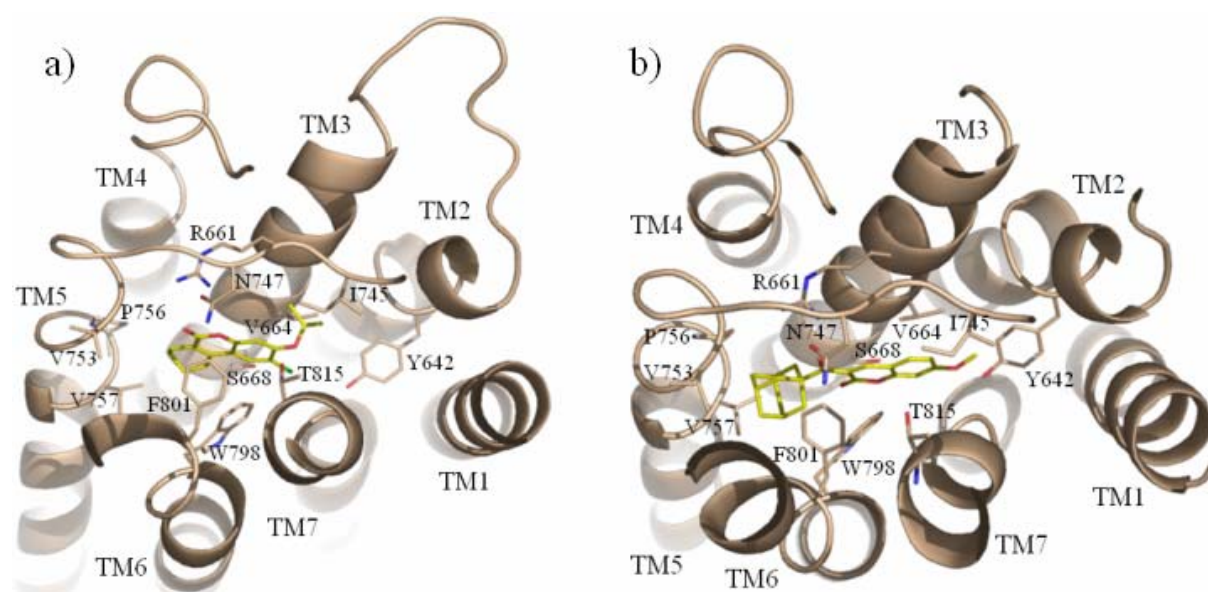


Figure 5.4.1-a. Potential binding mode of **C-07** (a) and **B-28** (b) in the allosteric binding site of mGluR1. View from the extracellular side of the membrane.

In the homology model, the two central coumarine-oxygens interact as hydrogen-bond acceptors forming a hydrogen-bonding with R661^{3.29}, N747^{45.51}. The hydrophobic *isopropoxy* substituent of **C-07** interacts with the hydrophobic residues I745^{45.49} and V664^{3.32}. The *isopropoxy* oxygen is involved in a hydrogen bond with T815^{7.39}. Replacing the *isopropoxy* group with a dimethylthiocarbamyl group resulted in increased activity (**B-10** vs. **C-07**, IC_{50} : 0.123 μ M vs. 0.362 μ M). This might be explained by the formation of a stronger hydrogen-bond to T815^{7.39}. Substituents at the chlorine site of **C-07** might interact with V664^{3.32} and T815^{7.39}.

For the ligands with an adamantyl substituent (**B-28** - **B-31**) the receptor model suggests that there is not sufficient space for the adamantyl group in the sub pocket covered by the unsaturated ring of **C-07**, given the binding mode of **C-07**. Thus, an alternative binding mode

was proposed for the adamantyl-containing ligands, illustrated by **B-28** (Figure 5.4.1-a, panel b). Here the adamantyl group fills the same part of the pocket as the unsaturated ring in **C-07**. The oxygen of the carbonyl linker of **B-28** is involved in the hydrogen bond cluster containing R661^{3,29}, and the oxygen acceptor in the ring from the coumarine core forms a hydrogen-bonding interaction with T815^{7,39}.

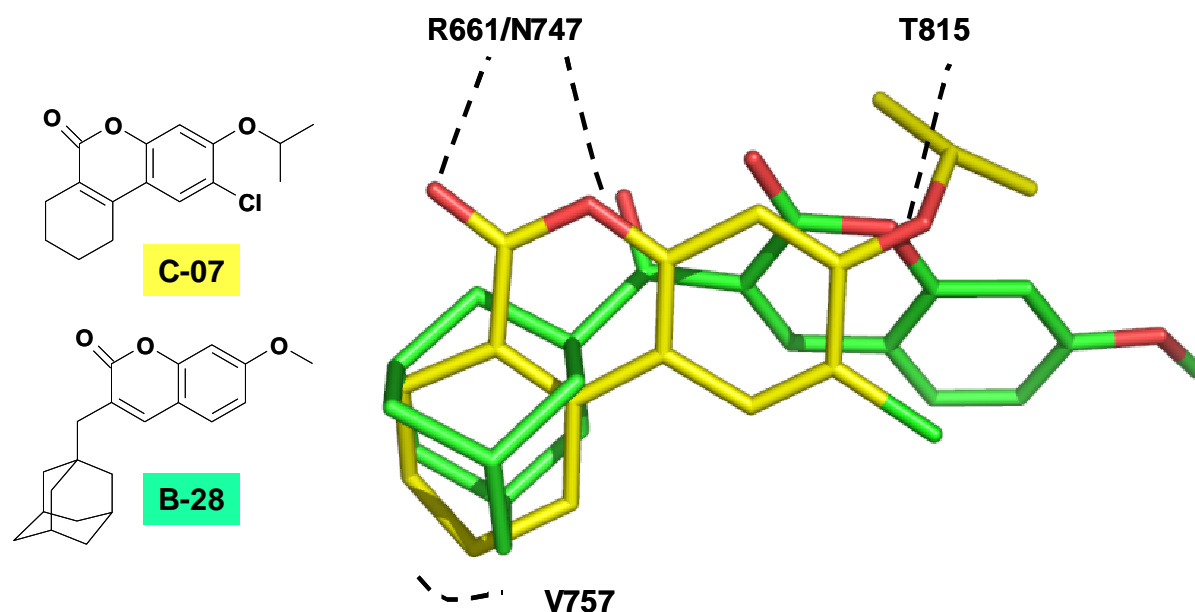


Figure 5.4.1-b. Alignment of the structurally different allosteric mGluR1 antagonists **C-07** and **B-28** and visualization of crucial interaction points within the binding pocket of the mGluR1 homology model.

The proposed binding pocket of **C-07** and **B-28** is located in a similar region compared with the negative allosteric mGluR1 modulator EM-TBPC, for which mutational data were published before [Malherbe *et al.*, 2003a]. EM-TBPC is assumed to interact with V757^{5,47}, W798^{6,48}, F801^{6,51}, Y805^{6,55}, T815^{7,39}, which are all in proximity to **C-07** and **B-28**. Mutation of N747^{45,51} and N750^{45,54} to alanine resulted in an increased effect of EM-TBPC, which might be caused by the lack of a hydrogen-bonding interaction partner of EM-TBPC. These findings are consistent with a direct interaction of N747^{45,51} with our ligands. For mGluR5 it was also shown that mutation of R647^{3,29} (R661 in mGluR1) to alanine increased the activity of the mGluR5 negative allosteric modulator MPEP [Malherbe *et al.*, 2003b]. This is confirmed by a potential direct interaction of R647^{3,29} with bound ligands.

These data support our hypothesis for the binding mode of the series of coumarines as mGluR1 negative allosteric modulators presented in Section 5.3. Furthermore, the existence of different binding modes within the pocket could serve as an explanation for the observed

differences in the functional and binding assay results as well as the failed attempt to find a quantitative SAR (data not shown).

5.4.2 Binding of Quinolines

The aim of this chapter was the comparison of quinolines and coumarines bound to the allosteric recognition site of mGluR1 with focus on their orientations relative to each other. Based on the proposed orientation it was feasible to relate the results obtained with the CoMFA studies of quinolines (Section 5.1) to the SAR of the coumarines (Section 5.3). In this context it must be stressed that our CoMFA studies were based on functional activity data for mGluR1 and not on binding affinity values.

Initially, a flexible overlay comprising one representative of each group, EMQMCM for the quinolines and **B-04** representing the coumarines, served as a starting point for the hypothesized binding mode. **B-04** was selected to simplify the automated aligning as it structurally resembles EMQMCM with respect to the cyclohexyl residue (Section 5.3.2). Both molecules were superimposed in a flexible manner using the *Flexible Alignment* tool included in the MOE software package Version 2005.06 [Chemical Computing Group] by applying the same settings as used for the flexible overlay of six reference structures in Section 4.2.2. Several orientations have been calculated including their corresponding energy values. One orientation with a low energy value and a reasonable overlay (that is the most complete overlay with respect to the molecule structures) was selected. It was then slightly modified regarding the side chains, which were adjusted to refine the overlay. The final alignment is given in Figure 5.4.2-a.

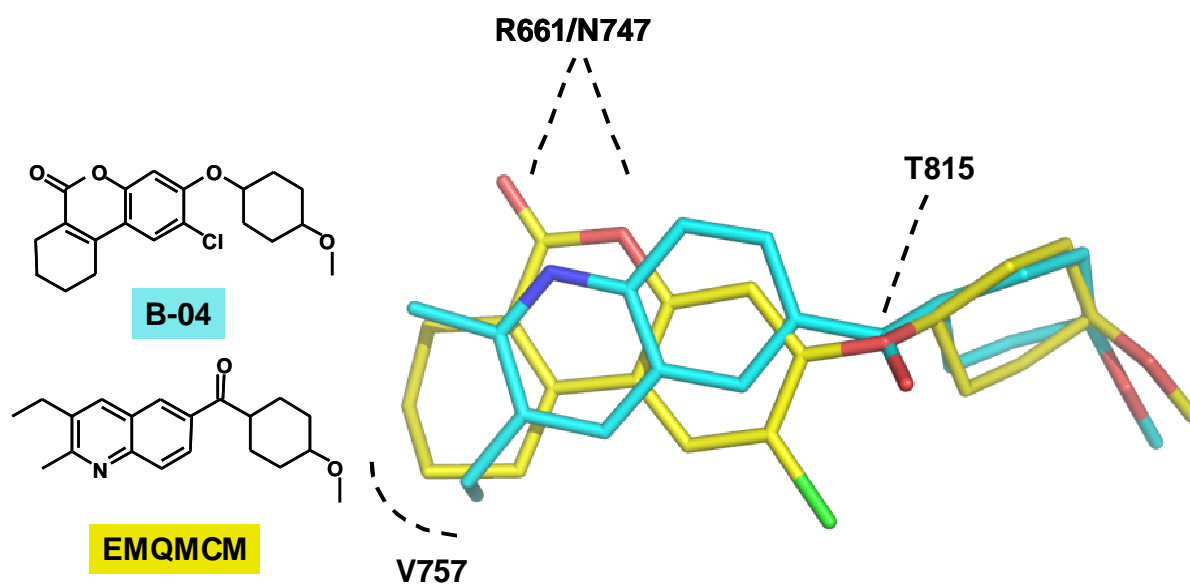


Figure 5.4.2-a. Alignment of the structurally diverse allosteric mGluR1 antagonists **B-04** (coumarin) and EMQMCM and visualization of pivotal interaction points within the binding pocket of the mGluR1 homology model.

EMQMCM representing the quinolines is assumed to interact with the same amino acids as the coumarines, thus binding in the same pocket of the receptor. The nitrogen of the the core structure potentially interacts with R661^{3,29} or N747^{45,51} *via* an H-bond bridge. 2-Methyl and 3-ethyl substituents point into a region where there is few yet sufficient space for another condensed cycle as visualized for **B-04** (Figure 5.4.2-a). It might establish a hydrophobic interaction with V757^{5,47}. This is consistent with the SAR data for quinolines postulating that an extended ring system is favored (e.g., R214127, IC_{50} : 2nM). Moreover, EMQMCM's "polar linker" connecting the aromatic quinoline moiety with the cyclohexyl moiety acts as H-bond acceptor, hence forming a bridge to T815^{7,39}. Since the *p*-methoxy substituent as weak H-bond acceptor is essential neither in **B-04** nor in EMQMCM, no interacting amino acid was proposed. However, it has influence on activity in quinolines as *cis*-conformation is preferred (Section 5.1.2).

Further amino acids potentially influencing the binding mode of quinolines and coumarines are given in Figure 4.4.2-b. V664^{3,32} or I745^{45,49} provide hydrophobic interactions with either the cyclohexyl residue or the chlorine in **B-04**, whereas W798^{6,48} is presumably responsible for π - π stacking with the coumarin or quinoline core structures, respectively. The influence of the mentioned amino acids was previously confirmed by mutation analyses [Malherbe *et al.*, 2003a] as already described (Section 5.4.1).

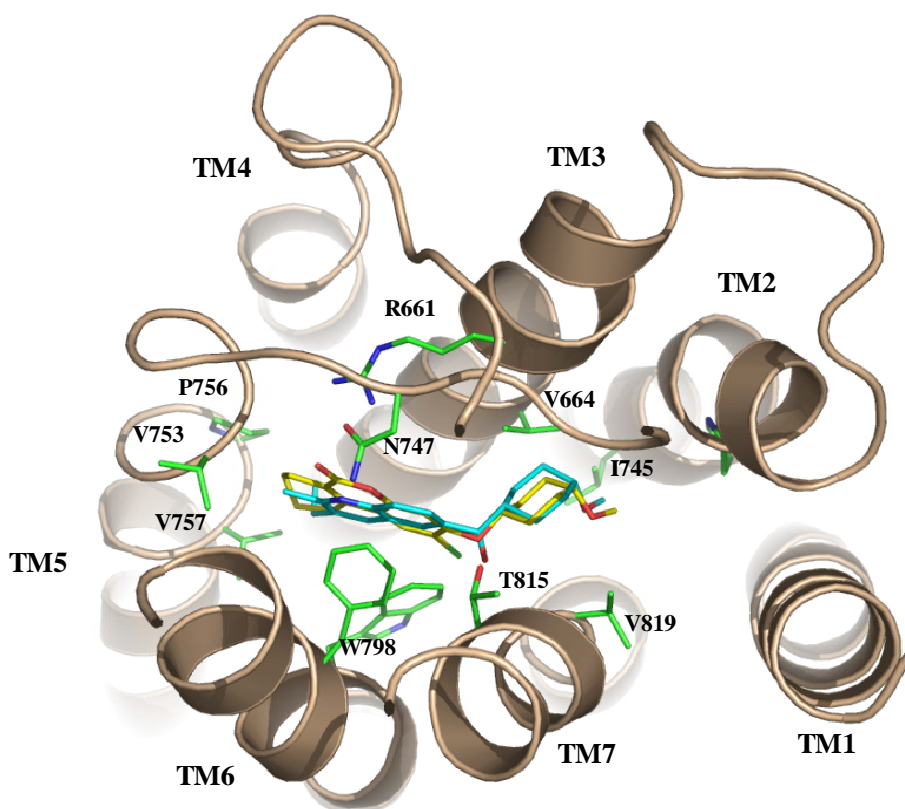


Figure 5.4.2-b. Potential binding mode of **B-04** and EMQMCM in the allosteric binding site of mGluR1. View from the extracellular side of the membrane.

Summarized, the above-proposed alignment has the advantage that several criteria for binding with amino acids of the target are fulfilled. Among these are (i) the nitrogen of the quinoline core structure providing an acceptor like the oxygen in the ring system and carbonyl oxygen in **B-04** for interaction with R661^{3,29} and/or N747^{45,51}, (ii) the planar aromatic ring system - present in both structures - to satisfy W798^{6,48} and (iii) another H-bond acceptor (carbonyl linker in EMQMCM, ether in **B-04**) forming a contact with T815^{7,39}. Moreover, the conclusions drawn from the CoMFA studies (Section 5.1.2, Figure 5.1.2-c) perfectly fit to the hypothesized alignment, which is confirmed by the following facts:

According to the QSAR analyses the quinoline core system can be extended to the left, preferably with a condensed (hetero)aromatic cycle (R1/R2 in Figure 5.1.2-c). This cycle may contain another acceptor (oxygen, sulfur), which is, however, not required. In fact, according to Figure 5.4.2-b, there is only few space left between the aligned structures and TM5. Furthermore, no amino acids can be detected potentially interacting with another H-bond acceptor in this gap. Beyond the polar linker of the quinolines there should favorably be an aliphatic or aromatic residue, which can include polar features (R3 in Figure 5.1.2-c). This is confirmed by (i) the alignment of EMQMCM and **B-04** placed into the binding pocket and

displaying sufficient space in the region where the cyclohexyl residue is located (Figure 5.4.2-b) and (ii) by the SAR scheme of the coumarines (Figure 5.3.2-a) postulating that the residue, which is attached at position 9 *via* an oxygen (or sulfur) should preferably be short and rigid but can also include a cycle and polar atoms.

5.4.3 Conclusions

Earlier studies detected a binding cavity in the HD of the mGlu1 receptor [Malherbe *et al.*, 2003a]. We exploited these receptor informations regarding crucial amino acids for ligand binding as well as our own SAR data of coumarines (ligand information) to get insights into the binding mode of coumarines in the HD of mGluR1. Binding orientations of coumarines were proposed as exemplified by two representatives of this chemotype. Furthermore, we also proposed a general binding mode for quinolines as non-competitive mGluR1 antagonists. For this purpose we exploited SAR data of quinolines [Mabire *et al.*, 2005] and the results of our own QSAR studies to detect features essential for ligand binding.

It has been proven by experiments that representatives of coumarines and quinolines bind to the same cavity in the transmembrane region of mGluR1: **C-07**, but also **B-28** and analogues are capable of almost completely displacing [³H]-EMQMCM from its binding site.

6 Summary

6.1 Conclusions and Outlook

Binding assays on cerebellar (mGluR1) and cortical membranes (mGluR5) were developed to facilitate limited throughput screening on 96-well plates. The mGluR5 binding assay, however, has the disadvantage that it has to be performed at low temperature ($< 4^{\circ}\text{C}$). Even under these conditions control values were poorer than observed in the mGluR1 binding assay. As a consequence the mGluR5 binding assay on 96-well plates was only used for studies described in this thesis and considered as not applicable for regular in-house compound screening.

In an iterative process a pharmacophore query for non-competitive mGluR1 antagonists was set up. It was revised in a validation step where the in-house mGluR-data collection was employed. The following drawbacks can be attributed to the model: (i) It is not a general model as it only considers some chemotypes of mGluR1 antagonists, (ii) retrospective screening was performed on the mGluR-data collection but not on a large dataset comprising “positive” and “negative” members and (iii) prospective screening was conducted only in combination with the data reduction tool *ChemSpaceShuttle*.

Three virtual screening campaigns were applied: CATS similarity search and data reduction with Kohonen maps and encoder networks (*ChemSpaceShuttle*). The Asinex Gold Collection February 2003 served as test database for the first two campaigns. For data clustering with Kohonen maps we applied the same topological pharmacophore descriptor as for the similarity searches. This descriptor enabled a clear discrimination of mGluR1 and mGluR5 antagonists and an acceptable hit rate was yielded, but the detected virtual hits can mainly be classified into only two chemotypes. Other descriptor sets might retrieve other scaffolds but have not been tested. A major pitfall of data clustering with *ChemSpaceShuttle* was the fact, that only a small subset (“focused library”) of the Asinex database described the test molecules: The complete database was filtered previously with the final pharmacophore query for mGluR1 antagonists. Recommendations for future screening: (i) Apply a large test database, (ii) use for neighborhood search only high potent reference compounds, (iii) select more virtual hits and (iv) test also other descriptors.

General recommendations regarding virtual screening: The application of other methods like support vector machines or random forest classification could be tested.

A CoMFA model for quinolines, a class of prominent mGluR1 antagonists, was set up to evaluate the influence of side chain modification on functional activity. It was developed to improve the understanding of ligand binding at the allosteric mGluR1 recognition site. No chemically modified quinolines have been synthesized and tested to confirm the predictive power of the CoMFA model, which might be worth proving.

We further introduced an interesting concept to predict compound selectivity for mGluR1 and mGluR5 antagonist. A successful prediction of cross-activities at several receptors was made. Some aspects have not been addressed: (i) The application of another descriptor set for the underlying SOM analysis and (ii) the exclusive use of potent ligands as reference molecules for side effect predictions.

A hit optimization project was launched for a coumarine, acting as non-competitive mGluR1 antagonist. Binding affinity and inhibitory activity were improved but no lead candidate for follow-up was yielded. A reason might be the fact that an increase in affinity/activity was associated with enhanced lipophilicity and, thus, diminished solubility. The project was finally discontinued.

For two classes of allosteric mGluR1 modulators, quinolines and coumarines, binding orientations at the known recognition site were proposed. However, they are only hypotheses as representatives of each group were manually placed into the binding pocket of a mGluR1 homology model and no automated docking was performed.

6.2 Summary

The goal of this thesis was to gain further insight into the binding behavior of ligands in the heptahelical domain (HD) of group I metabotropic glutamate receptors (mGluRs). This was realized by the establishment of strategies for the detection and optimization of molecules acting as non-competitive antagonists of group I mGluRs (mGluR1/5). These strategies should guarantee high diversity in the retrieved chemotypes of the detected compounds not resembling original reference molecules (“scaffold-hopping”). The detection of new scaffolds, in turn, was divided into two approaches: First the development of pharmacological assays to screen compounds at a certain target for bioactivity (here: affinity towards the allosteric recognition site of mGluR1 and mGluR5), and second the evaluation of computer assisted methods for the identification of virtual hits to be screened afterwards on the pharmacological assays established before. Promising molecules should be optimized with respect to

activity/affinity and selectivity, their binding mode investigated and, finally, compared to existing lead compounds.

Initially, membrane based binding assays for the HD of mGlu1 and mGlu5 receptors with enhanced throughput (shifting from 24-well plates to 96-well plates) were set up. For the mGluR1 assay the potent antagonist EMQMCM exhibited high affinity towards the binding site ($K_i \sim 3\text{nM}$), which is in accordance with published data from Mabire *et al.* (functional IC_{50} 3nM). For mGluR5 the reference antagonist MPEP binds with high affinity to the receptor (binding IC_{50} 13.8nM), which confirmed earlier findings from Anderson *et al.* (binding IC_{50} 15nM). In another series of experiments the properties of rat cerebellar (mGluR1) and cortical membranes (mGluR5) as well as of radiotracers were investigated by means of binding saturation studies and kinetic experiments. Furthermore, the influence of the solvent DMSO, necessary for compound screening of lipophilic substances, on positive and negative controls was evaluated.

As the precise architecture of the HD of mGluR1 is still not known our efforts in identifying new ligands for this receptor focused on the ligand-based approach. All computer assisted methods that were applied to virtually screen large compound collections and to retrieve potential hits (“activity-enriched subsets”) acting at the heptahelical domain of mGluR1 relied on the existence of a valid dataset of reference molecules. This was realized by an initial compilation of a mGluR reference data collection comprising in total 357 entries predominantly negative but also some positive allosteric modulators for mGluR1 and mGluR5. In the next step a pharmacophore model for non-competitive mGluR1 antagonists was constructed. It was based upon six selective, potent and structurally diverse ligands. Prospective virtual screening was performed using the CATS atom-pair descriptor. The Asinex Gold-Collection was screened for each seed compound and some of the most similar compounds (according to the CATS descriptor) were ordered and tested for binding affinity and functional activity at mGluR1. A high hit rate of approximately 26% ($IC_{50} < 15\mu\text{M}$) was yielded confirming the applicability of this method. One compound exerted functional activity below one micro molar (IC_{50} -value of **C-07**: $362\text{nM} \pm 0.03$).

Moreover, non-linear principal component analysis was employed. Again the Asinex vendor database served as test database and was filtered by the pharmacophore model for mGluR1 established before. Test molecules that were adjacently located with mGluR1 antagonist references were selected. 15 compounds were tested on mGluR1 in binding and functional assays and three of them exhibited functional activity (IC_{50}) below $15\mu\text{M}$. The most potent molecule **P-06** revealed an IC_{50} -value of $1.11\mu\text{M} (\pm 0.41)$.

The COBRA database comprising 5,376 structurally diverse bioactive molecules affecting various targets was encoded with the CATS descriptor and used for training two self-organizing maps (SOM). The encoded mGluR reference data collection was projected onto this map according to the SOM algorithm. This projection allowed to clearly distinguish between antagonists of mGluR1 and mGluR5 subtype. 28 compounds were ordered and tested on activity and affinity for mGluR1. They exhibited functional activity down to the sub-micromolar range (IC_{50} -value of **S-08**: $744\text{nM} \pm 0.29$) yielding a final hit rate of 46% ($<15\mu\text{M}$). Then, the Asinex collection was screened using the SOM approach. For a predicted target panel including the muscarinic mACh (M1) receptor, the histamine H_1 -receptor and the dopamine D_2/D_3 receptors, the tested mGluR ligands exhibited the calculated binding pattern. This virtual screening concept might provide a basis for early recognition of potential side-effects in lead discovery.

We superimposed a set of 39 quinoline derivatives as non-competitive mGluR1 antagonists that were recently published by Mabire and co-workers. A CoMFA model (QSAR) was established and the influence of several side chains on functional activity was investigated.

The coumarine derivative **C-07** was obtained as a result of similarity searching. Starting from this compound a series of chemical derivatives was synthesized. This led to the discovery of potent (**B-28**, IC_{50} : $58\text{nM} \pm 0.008$; K_i : $293\text{nM} \pm 0.022$) and selective (rmGluR5 IC_{50} : $28.6\mu\text{M}$) mGluR1 antagonists. From a homology model of mGluR1 we derived a potential binding mode for coumarines within the allosteric transmembrane region. Potential interacting patterns with amino acids were proposed considering the difference of the binding pockets between rat and human receptors. The proposed binding modes for quinolines (here: EMQMCM) and coumarines (here: **B-04**) were compared and discussed considering in particular the influence on activity of several side chains of quinolines obtained from the QSAR studies.

The present studies demonstrated the applicability of ligand-based virtual screening for non-competitive antagonists of a G-protein coupled receptor, resulting in novel, potent and selective agents.

6.3 Zusammenfassung

Ziel dieser Doktorarbeit war es weiteren Einblick in das Bindungsverhalten von Liganden in der transmembranen Region von Gruppe I metabotropen Glutamatrezeptoren (mGluRs) zu

gewinnen. Verwirklicht wurde dies durch den Entwurf von Strategien zur Auffindung und Optimierung von Molekülen die als nichtkompetitive Antagonisten an Gruppe I mGluRs (mGluR1/5) wirken. Diese Strategien sollten eine hohe Diversität der chemischen Strukturen der entdeckten Verbindungen gewährleisten und nicht den ursprünglichen Referenzmolekülen ähneln (das sogenannte „Grundgerüst-Springen“). Die Auffindung neuer Kernstrukturen wiederum wurde in zwei Herangehensweisen aufgeteilt: Zum einen die Entwicklung von pharmakologischen Tests um Substanzen auf Bioaktivität an einer bestimmten Zielstruktur zu untersuchen (hier: die Affinität zur allosterischen Bindungsstelle von mGluR1 und mGluR5), und zum anderen die Evaluierung von computergestützten Methoden für die Identifizierung von virtuellen Suchtreffern die dann in den zuvor etablierten pharmakologischen Testsystemen untersucht werden können. Basierend auf den hierin gemachten Ergebnissen sollten vielversprechende Moleküle bezüglich Aktivität, Affinität und Selektivität optimiert werden, ihr Bindungsmodus untersucht und schließlich mit dem von bereits bekannten Leitstrukturen verglichen werden.

Anfangs wurden membranbasierte Bindungstests für die transmembrane Region von mGluR1 und mGluR5 mit erhöhtem Durchsatz entworfen (Transfer vom 24-Lochplatten- auf 96-Lochplattenformat). In diesem Zusammenhang wurde das bereits vorhandene Wissen über einen zur Verfügung stehenden NMDA-Rezeptor-Bindungstest genutzt. Hierbei wurde der Einfluss verschiedener Parameter wie Proteinkonzentration, Inkubationszeit, Inkubationstemperatur, etc. erforscht. Validiert wurden die Testsysteme mit Affinitätsmessungen für Standardverbindungen: Für den mGluR1 Bindungsversuch zeigte der potente Antagonist EMQMCM hohe Affinität an der Bindungsstelle ($K_i \sim 3\text{nM}$), was in Übereinstimmung mit publizierten Daten von Mabire *et al.* steht (funktioneller IC_{50} 3nM). Für mGluR5 zeigte der Referenz-Antagonist MPEP hohe Affinität am Rezeptor (Bindungs IC_{50} 13,8nM) was durch frühere Untersuchungen von Anderson *et al.* bestätigt wird (Bindungs IC_{50} 15nM). In einer weiteren Experimentreihe wurden die Eigenschaften von Cerebellum-Membranen (mGluR1) und Cortex-Membranen (mGluR5) der Ratte untersucht sowie die Eigenschaften eines Radioliganden, und zwar in Form von Bindungs-Sättigungsversuchen und Kinetik-Experimenten. Desweiteren wurde der Einfluss des Lösungsmittels DMSO, das für das Lösen lipophiler Substanzen notwendig war, auf Positiv- und Negativkontrolle geprüft.

Da die exakte Kristallstruktur der transmembranen Region von mGluR1 noch immer unbekannt ist haben sich unsere Anstrengungen zur Identifizierung neuer Liganden für diesen Rezeptor auf den ligandenbasierten Ansatz beschränkt. Alle computergestützten Methoden

die für das virtuelle Durchforsten großer Substanzdatenbanken zur Auffindung potentieller Treffer angewandt wurden (sogenannter „aktivitätsangereicherte Untergruppen“) basieren auf der Existenz eines validen Datensatzes von Referenzmolekülen. Verwirklicht wurde dies zu Beginn durch das Zusammenstellen einer mGluR Referenzdatenbank mit 357 Einträgen, vornehmlich negative aber auch einige positive Modulatoren an mGluR1 und mGluR5. Anhand umfangreicher Suche in sachbezogener Literatur (Patente und Veröffentlichungen) wurden Angaben gesammelt. Im nächsten Schritt wurde ein Pharmakophormodell für nichtkompetitive mGluR1 Antagonisten erstellt. Es basiert auf einigen potenten, selektiven und strukturell diversen Liganden aus der mGluR Referenzdatenbank. Die Entwicklung eines aussagekräftigen Pharmakophormodells stellte einen wichtigen Schritt dar und war Grundlage für folgende Struktursuchen. Die dem Modell zu Grunde liegenden Moleküle wiederum dienten als Referenzmoleküle für eine auf einem topologischen Pharmakophordeskriptor basierende Ähnlichkeitssuche: Prospektive virtuelle Suche wurde unter Benutzung des CATS Atompaar-Deskriptors durchgeführt, einer konformationsfreien Korrelationsvektorrepräsentation. Eine große Datenbank kommerziell erhältlicher Moleküle (Asinex Gold Collection: ~ 200.000 Einträge) wurde für jede Referenzstruktur durchsucht und einige der entsprechend dem CATS Deskriptor als am ähnlichsten erachteten Verbindungen wurden bestellt und auf Aktivität und Affinität an mGluR1 untersucht. Eine Trefferrate von ungefähr 26% ($IC_{50} < 15\mu\text{M}$) die den Nutzen dieser Methode bestätigte, wurde erzielt. Darüber hinaus wies eine Verbindung submikromolare funktionelle Aktivität auf (IC_{50} -Wert von **C-07**: $362\text{nM} \pm 31$). Da dieses Cumarin auch eine vielversprechende Kernstruktur aufwies, wurde es direkt einer Leitstrukturoptimierung unterzogen.

In einer weiteren Studie wurden die Vorteile von Pharmakophorsuche und Datenreduktion anhand nichtlinearer Hauptkomponentenanalyse kombiniert. Wiederum diente die Asinex Kollektion als Testdatenbank und wurde mit dem zuvor erstellten mGluR1 Pharmakophormodell gefiltert. Die resultierende „fokussierte Datenbank“ enthielt 2211 Einträge und wurde zusammen mit der mGluR Referenzdatenbank mit einer Vielzahl von 2D-Deskriptoren kodiert und anhand von *ChemSpaceShuttle* in einen dreidimensionalen Raum projiziert. Testverbindungen die in räumlicher Nachbarschaft zu mGluR1 Referenzen zu finden waren wurden ausgewählt. Einige von ihnen wurden bestellt und auf ihre gewünschte Bioaktivität hin untersucht. Insgesamt wurden fünfzehn Verbindungen in funktionellen Tests und Bindungstest für mGluR1 gemessen wobei drei von ihnen funktionelle Aktivität unter $15\mu\text{M}$ aufwiesen. Die potenteste Verbindung **P-06** zeigte einen IC_{50} -Wert von $1,11\mu\text{M} (\pm 0,41)$.

Kohonen-Karten stellen eine Alternative zu Ähnlichkeitssuchen im Bereich der virtuellen Suche dar. Sie gruppieren Moleküle indem sie ähnliche Datenwerte zusammenstellen. In der vorliegenden Studie wurde die COBRA 3.12 Datenbank, die 5.376 strukturell unterschiedliche bioaktive Moleküle enthält die mit verschiedenen Rezeptoren und Enzymen wechselwirken, mit dem CATS Deskriptor verschlüsselt. Dann wurden zwei selbstorganisierende Karten (SOM) damit trainiert, eine mit 100 Neuronen und eine mit 225 Neuronen. Anschließend wurde die kodierte mGluR Referenzdatenbank gemäß dem SOM Algorithmus auf diese Karten projiziert. Diese Projektion erlaubte eine klare Trennung zwischen Antagonisten vom Subtyp mGluR1 und mGluR5. Ermutigt durch diese Ergebnisse wurde die Untergruppe der mGluR1 Referenzverbindungen auf die mit der COBRA Datenbank trainierten Karten projiziert und diejenigen Neurone die die höchste Dichte an Referenzverbindungen aufwiesen ausgewählt (Neuron 8/7 auf der kleinen Karte und 6/6 auf der großen Karte). In diesem Sinne wurde auch mit der Asinex Datenbank verfahren und alle Verbindungen die sich in beiden der eben erwähnten Neurone gruppiert haben wurden entsprechend ihrer räumlichen Entfernung zum Zentroid des jeweiligen Neurons sortiert. 28 der ersten 60 Molekülstrukturen wurden bestellt und auf Affinität und Aktivität an mGluR1 getestet. Sie wiesen (inhibitorische) Aktivitäten bis in den submikromolaren Bereich auf (IC_{50} -Wert von **S-08**: $744\text{nM} \pm 290$) und führten zu einer Trefferquote von 46% ($<15\mu\text{M}$).

Die Anwendung der hier beschriebenen virtuellen Suchmethoden gewährte uns eine Auswahl von selektiven mGluR1 Antagonisten mit neuen Kernstrukturen. Im folgenden wurde ihr Bindungsmodus im Verhältnis zu dem der Referenzverbindungen untersucht und eine vielversprechende Verbindung, ein Cumarin-Derivat das durch die Ähnlichkeitssuche gefunden worden ist, wurde strukturell optimiert.

Quantitative Struktur-Wirkungsbeziehung (QSAR) zielt darauf ab den Zusammenhang zwischen Ligandenstrukturen und ihren Bioaktivitätsdaten quantitativ zu beschreiben. Diesbezüglich haben wir einen Satz von 39 Chinolin-Derivaten der mGluR1 Antagonisten darstellt und kürzlich von Mabire und Mitarbeitern veröffentlicht wurde verwendet. Die Strukturen wurden flexibel in einer sinnvollen Anordnung überlagert und in einen Trainingsdatensatz (30 Moleküle) und einen Testdatensatz (9 Moleküle) aufgeteilt. Ein CoMFA-Modell das die beste Vorhersagefähigkeit besaß ($q^2(cv)$: 0,617) wurde erstellt. Zur statistischen Absicherung wurde derselbe Gesamtdatensatz zehnmal per Zufallsprinzip in Trainings- (20 Moleküle) und Testdatensatz (9 Moleküle) aufgeteilt was in einem mittleren $q^2(cv)$ von 0,507 ($\pm 0,036$) resultierte. Nachdem für das ursprüngliche Modell Konturkarten,

die sterische und elektrostatische Beiträge darstellten, berechnet worden sind wurde der Einfluss verschiedener Seitenketten auf die funktionelle Aktivität untersucht.

Für einige Gruppe I mGluR Referenzverbindungen wurden, basierend auf den Ergebnissen der virtuellen Suche mit den Kohonen-Karten, Selektivitätsbetrachtungen durchgeführt. Die Kombination eines topologischen Pharmakophor-Deskriptors (CATS) und der SOMs wurde für die Vorhersage von multiplen Rezeptorinteraktionen von bekannten Gruppe I mGluR Antagonisten verwendet. Moleküle der mGluR Referenz-Sammlung und der COBRA Datenbank, die als Testdatensatz diente, wurden mit den CATS Deskriptor kodiert und einer Klassifizierung und Projektion gemäß dem SOM Algorithmus unterzogen. Für eine vorausgesagte Auswahl an Rezeptoren, darunter der muskarinische mACh (M1) Rezeptor, der Histamin H₁-Rezeptor und die Dopamin D₂/D₃ Rezeptoren, konnten die gemessenen mGluR Liganden die berechneten Interaktionen aufweisen. Dieses Konzept des virtuellen Suchens könnte eine Basis für die frühe Erkennung von potentiellen Wechselwirkungen in der Arzneimittelforschung darstellen.

Das Cumarin-Derivat **C-07** wurde im Rahmen der Ähnlichkeitssuche mit dem CATS Deskriptor gefunden. Ausgehend von dieser Verbindung wurde in dem folgenden Aktivitäts-Optimierungsprogramm eine Reihe von chemischen Derivaten synthetisiert. Das führte zur Entdeckung von potenten (**B-28**, IC_{50} : 58nM \pm 8; K_i : 293nM \pm 22) und selektiven (rmGluR5 IC_{50} : 28,6 μ M) mGluR1 Antagonisten. Auf Grundlage unseres Homologiemodells haben wir einen potentiellen Bindungsmodus für Cumarine innerhalb der transmembranen Region ermittelt, was am Beispiel von **C-07** und **B-28** gezeigt wurde. Es wurden potentielle Interaktionsmuster mit Aminosäuren vorgeschlagen, die auch den Unterschied der Bindetaschen vom Ratten- und Humanrezeptor berücksichtigen. Desweiteren wurden die vermuteten Bindungsmodi für Chinoline (hier: EMQMCM) und Cumarine (hier: **B-04**) verglichen und diskutiert, und zwar unter besonderer Berücksichtigung des Einflusses von verschiedenen Chinolin-Seitenketten auf die Aktivität gemäß den vorausgegangenen QSAR Studien.

Die vorliegenden Untersuchungen veranschaulichen den Nutzen von ligandbasierten virtuellen Suchen für nichtkompetitive Antagonisten von G-Protein gekoppelten Rezeptoren was in der Auffindung neuer, potenter und selektiver Verbindungen mündete.

7 Appendix

7.1 Complete mGluR-Data Collection

Table 7.1-a. In-house collection of mGluR-reference compounds (release 08.03). Each molecule is depicted as SMILES string.

Molecule	Action	IC ₅₀
<chem>O1CCc2cc3cc(ccc3[nH0]c12)Cc1cccc1</chem>	mGluR1	85 nM
<chem>O=C(OC)[C@H](NC(=O)[C@](O1cccc1C(=NO)[C@H](C1)2)12)Cc1cc</chem>	mGluR1	930 nM
<chem>Clc1ccc2[nH0]c(SCCO)[nH0]c(NC3C4CCC3CC4)c2c1</chem>	mGluR1	44 nM
<chem>O(C)CCOc1[nH0][nH0]c(C#N)c([nH0]1)N1CCc2ccccc2CC1</chem>	mGluR1	3000 nM
<chem>OCCNc1[nH0][nH0]c(C#N)c([nH0]1)N1CCc2ccccc2CC1</chem>	mGluR1	31 nM
<chem>OC(C)CNc1[nH0][nH0]c(C#N)c([nH0]1)N1CCc2ccccc2CC1</chem>	mGluR1	27 nM
<chem>s1ccc2CCN(CCc12)c1[nH0]c([nH0]c(OCC)c1[N+](=O)[O-])C</chem>	mGluR1	440 nM
<chem>O=C(c1ccc2[nH0]c(C)c(cc2c1)CC)C1CCc2ccccc21</chem>	mGluR1	245 nM
<chem>O=C(c1ccc2[nH0]c(C)c(cc2c1)CC)C1COc2ccccc2C1</chem>	mGluR1	115 nM
<chem>O=C(c1ccc2[nH0]c(C)c(cc2c1)CC)C12CC3CC(CC(C3)C2)C1</chem>	mGluR1	125 nM
<chem>O=C(CC(C)C)c1ccc2[nH0]c(C)c(cc2c1)CC</chem>	mGluR1	162 nM
<chem>O=C(Cc1cccc(OC)c1)c1ccc2[nH0]c(C)c(cc2c1)CC</chem>	mGluR1	135 nM
<chem>O=C(NC1CCC(OC)CC1)c1ccc2[nH0]c(O)c(cc2c1)CC</chem>	mGluR1	10000 nM
<chem>ON=C(c1ccc2[nH0]c(O)c(cc2c1)CC)C1CCC(OC)CC1</chem>	mGluR1	10000 nM
<chem>Fc1cccc(c1)C(=O)c1ccc2[nH0]c3OCCCc3cc2c1</chem>	mGluR1	48 nM
<chem>N#Cc1[nH0][nH0]c(N)[nH0]c1N1CCc2ccccc2CC1</chem>	mGluR1	27 nM
<chem>O=C(OCCCC)c1[nH]c(C)c(c1C)C(=O)OC(C)(C)C</chem>	mGluR1	160 nM
<chem>O=C(c1cccc1)c1ccc2[nH0]c3OCCCc3cc2c1</chem>	mGluR1	5.7 nM
<chem>O=C(Cc1cccc1)c1ccc2[nH0]c3OCCCc3cc2c1</chem>	mGluR1	5.8 nM
<chem>Br1ccc2c(SC=3CC(C)(C)CCC=3C2=O)c1</chem>	mGluR1	9 nM
<chem>Clc1ccc2SC=3CC(CCC=3C(=O)c2cc1F)CC</chem>	mGluR1	97 nM
<chem>S1c2cc(ccc2C(=O)C=2CCC(C)(C)CC1=2)c1cccc(C#N)c1</chem>	mGluR1	21 nM
<chem>S1c2cc(NC(=O)CC)ccc2C(=O)C=2CCC(CC1=2)CC</chem>	mGluR1	35 nM
<chem>S1c2cc(ccc2C(=O)C=2CCC(C)(C)CC1=2)c1c[nH0]ccc1</chem>	mGluR1	31 nM
<chem>S1c2cc(ccc2C(=O)C=2CCC(CC1=2)CC)c1cccc(C#N)c1</chem>	mGluR1	23 nM
<chem>S1c2cc(N3CCCC3)ccc2C(=O)C=2CCC(CC1=2)CC</chem>	mGluR1	13 nM
<chem>S1c2cc(N3CCCC3)c(F)cc2C(=O)C=2CCC(CC1=2)CC</chem>	mGluR1	28 nM
<chem>S1c2cc(N(C)COCC)ccc2C(=O)C=2CCC(CC1=2)CC</chem>	mGluR1	22 nM
<chem>S1c2cc(ccc2C(=O)C=2CCC(CC1=2)CC)c1c[nH0]c1</chem>	mGluR1	35 nM
<chem>S1c2cc(ccc2C(=O)C=2CCC(CC1=2)CC)C1=NOC(=O)N1</chem>	mGluR1	81 nM
<chem>S1c2cc(N[S+2]([O-])([O-])C3CC3)ccc2C(=O)C=2CCC(CC1=2)CC</chem>	mGluR1	25 nM
<chem>Clc1[nH0]c([nH0]c(N2CCN(CC2)c2ccccc2)c1C#N)NCC1CC1</chem>	mGluR1	25 nM
<chem>Fc1ccc(N2CCN(CC2)C=2N=C(N(CCO)C(=O)C=2[N+](=O)[O-])C)cc1</chem>	mGluR1	42 nM
<chem>Fc1ccc(N2CCN(CC2)c2[nH0]c([nH0]c(OCCO)c2[N+](=O)[O-])C)cc1</chem>	mGluR1	58 nM
<chem>Fc1ccc(N2CCN(CC2)C=2N=C(N(CCO)C(=O)C=2[N+](=O)[O-])C)cc1</chem>	mGluR1	49 nM
<chem>N#Cc1c([nH0]c([nH0]c1N1CCN(CC1)c1ccccc1)NC1CC1)NC1CC1</chem>	mGluR1	64 nM
<chem>OCCNc1[nH0]c([nH0]c(N2CCN(CC2)c2ccccc2)c1C#N)NC1CC1</chem>	mGluR1	33 nM
<chem>OCCNc1[nH0]c([nH0]c(N2CCC(CC2)c2ccccc2)c1C#N)NCc1c[nH0]ccc</chem>	mGluR1	30 nM
<chem>O=C(OCCC)c1[nH]cc(c1)C(=O)OC(C)(C)(C)C</chem>	mGluR1	15.8 nM
<chem>Fc1ccc(N2CCN(CC2)c2[nH0]c([nH0]c(OCC)c2[N+](=O)[O-])C)cc1</chem>	mGluR1	180 nM
<chem>O=[N+](O-)]C=1C(=O)NC(=NC=1N1CCC(CC1)c1ccccc1)C</chem>	mGluR1	63 nM
<chem>Fc1ccc(N2CCN(CC2)C=2N=C(NC(=O)C=2[N+](=O)[O-])C)cc1</chem>	mGluR1	810 nM
<chem>S(C)c1ccccc1N1CCN(CC1)c1[nH0]c([nH0]c(NCCO)c1C#N)NCCO</chem>	mGluR1	350 nM
<chem>Fc1ccc(cc1)C1CCN(CC1)C=1N=C(N(CCCO)C(=O)C=1[N+](=O)[O-])C</chem>	mGluR1	280 nM
<chem>Fc1ccccc1N1CCN(CC1)c1[nH0]c([nH0]c(NCCO)c1C#N)NCCO</chem>	mGluR1	290 nM
<chem>O=[N+](O-)]c1ccccc1N1CCN(CC1)c1[nH0]c([nH0]c(NCCO)c1C#N)N</chem>	mGluR1	750 nM
<chem>Fc1ccc(cc1)C1CCN(CC1)c1[nH0]c([nH0]c(NCCO)c1C#N)NCCO</chem>	mGluR1	700 nM
<chem>Fc1ccc(cc1)C1=CCN(CC1)c1[nH0]c([nH0]c(NCCO)c1C#N)NCCO</chem>	mGluR1	390 nM
<chem>OCCNc1[nH0]c(NCCO)c(C#N)c([nH0]1)N1CCC(CC1)c1ccc(C#N)cc1</chem>	mGluR1	1800 nM
<chem>N#Cc1c([nH0]c([nH0]c1N1CCC(CC1)c1ccccc1)NCc1[nH0]ccc1)NCc</chem>	mGluR1	1500 nM
<chem>OCCNc1[nH0]c([nH0]c(N2CCN(CC2)c2ccccc2)c1C#N)NCc1c[nH0]ccc</chem>	mGluR1	150 nM
<chem>Clc1[nH0]c([nH0]c(N2CCC(CC2)c2ccc(F)cc2)c1C#N)NCCO</chem>	mGluR1	140 nM
<chem>S(C)c1[nH0]c(N)[nH0]c(N2CCN(CC2)c2ccc(F)cc2)c1C#N</chem>	mGluR1	210 nM
<chem>S(C)c1[nH0]c(N)[nH0]c(N2CCC(CC2)c2ccc(F)cc2)c1C#N</chem>	mGluR1	159 nM
<chem>N#Cc1[nH0]c(CC)c([nH0]c1N1CCN(CC1)c1ccccc1)C</chem>	mGluR1	17 nM
<chem>N#Cc1[nH0]c(C)c([nH0]c1N1CCN(CC1)c1ccccc1)CC</chem>	mGluR1	23 nM
<chem>Fc1ccc(N2CCN(CC2)c2[nH0]c(NCCO)c1[nH0]c2C#N)cc1</chem>	mGluR1	1000 nM
<chem>OCCNc1[nH0][nH0]c(C#N)c([nH0]1)N1CC=C(CC1)c1ccccc1</chem>	mGluR1	660 nM
<chem>Fc1ccc(N2CCN(CC2)c2[nH0]c(C)c([nH0+])([O-])c2C#N)CC)cc1</chem>	mGluR1	25 nM
<chem>O=C(c1ccc2[nH0]c3OCCCc3cc2c1)C1CCC(OC)CC1</chem>	mGluR1	3.2 nM
<chem>Clc1[nH0]c2ccc(cc2cc1CC)C(=O)C1CCC(OC)CC1</chem>	mGluR1	4 nM
<chem>Fc1[nH0]c2ccc(cc2cc1CC)C(=O)C1CCC(OC)CC1</chem>	mGluR1	4.2 nM

O=C(c1ccc2[nH0]c3OCCc3cc2c1)C1CCC(OC)CC1	mGluR1	4.2 nM
S1CCCC2cc3ccc(c(C)cc3[nH0]c12)C(=O)Cc1ccccc1	mGluR1	3.3 nM
O=C(c1ccc2[nH0]c3CCc3cc2c1)C1CCC(OC)CC1	mGluR1	4.4 nM
S1CCCC2cc3ccc(ccc3[nH0]c12)C(=O)C1CCC(OC)CC1	mGluR1	4.7 nM
Clc1[nH0]c2cc(C)c(cc2cc1CC)C(=O)C1CCC(OC)CC1	mGluR1	4.8 nM
O=C(c1ccc2[nH0]c(ccc2c1)CCC)C1CCC(OC)CC1	mGluR1	5.3 nM
FC1(CCC(OC)CC1)C(=O)c1ccc2[nH0]c3OCCc3cc2c1	mGluR1	5.4 nM
O=C(Cc1ccccc1)c1cc2cc3CCCOc3[nH0]c2cc1C	mGluR1	5.4 nM
Fc1ccccc1CC(=O)c1ccc2[nH0]c3OCCc3cc2c1	mGluR1	5.6 nM
S1CCCC2cc3ccc(ccc3[nH0]c12)C(=O)Cc1ccccc1	mGluR1	9.5 nM
O=C(Cc1C[C@@H](CCC1C1)1)c1ccc2[nH0]c3OCCc3cc2c1	mGluR1	9.4 nM
S1CCCC2cc3ccc(ccc3[nH0]c12)C(=O)Cc1ccccc1F	mGluR1	10 nM
slccc(c1)CC(=O)c1ccc2cc3OCCc3cc2c1	mGluR1	7.2 nM
S1CCc2cc3ccc(ccc3[nH0]c12)C(=O)C1CCC(OC)CC1	mGluR1	9 nM
O=C(Cc1ccccc1)c1ccc2[nH0]c3OC(C)Cc3cc2c1	mGluR1	8.8 nM
S1CCc2cc3ccc(ccc3[nH0]c12)C(=O)C1CCCC1	mGluR1	7.7 nM
O=C(c1ccc2[nH0]c(N)c(cc2c1)CC)C1CCC(OC)CC1	mGluR1	7.2 nM
O=C(c1ccc2[nH0]c(C)c(cc2c1)CCC)C1CCC(OC)CC1	mGluR1	7.4 nM
O=C(c1cc2cc(C)C([nH0]c2cc1C)C)C1CCC(OC)CC1	mGluR1	5.9 nM
O=C(c1ccc2[nH0]c3CCc3cc2c1)C1CCC(OC)CC1	mGluR1	7.3 nM
O(C)c1ccc2[nH0]c[nH0]c(NC3CC4CCC3C4)c2c1	mGluR1	2430 nM
O(C)c1ccc2[nH0]c[nH0]c(NC3CCCC3)c2c1	mGluR1	328 nM
Clc1[nH0]c(NC2Cc3ccccc3C2)c2cc(OC)ccc2[nH0]1	mGluR1	30 nM
Clc1ccccc1CCNc1[nH0]c[nH0]c2ccc(OC)cc12	mGluR1	300 nM
Clc1[nH0]c(Nc2ccc(OC)cc2)c2cc(OC)ccc2[nH0]1	mGluR1	40 nM
Clc1[nH0]c(NC2Cc3ccccc3C2)c2cc(Cl)ccc2[nH0]1	mGluR1	18 nM
Clc1[nH0]c(NCCc2ccccc2C1)c2cc(OC)ccc2[nH0]1	mGluR1	23 nM
Clc1ccc2[nH0]c[nH0]c(NC3CC4CCC3C4)c2c1	mGluR1	1130 nM
S(CC)c1[nH0]c(NCC(F)c2ccccc2)c2CCCCc2[nH0]1	mGluR1	10 nM
S(CC)c1[nH0]c(NOC)c2CCCCc2[nH0]1	mGluR1	32 nM
Clc1ccccc1C(OC)CNc1[nH0]c(SCC)[nH0]c2CCCCc12	mGluR1	23 nM
S(CC)c1[nH0]c(NCC(F)(F)c2ccccc2)c2CCCCc2[nH0]1	mGluR1	15 nM
Clc1ccccc1CCNc1[nH0]c(SCC)[nH0]c2CCCCc12	mGluR1	24 nM
S(CC)c1[nH0]c(Nc2ccc(F)cc2)c2CCCCc2[nH0]1	mGluR1	32 nM
S(CC)c1[nH0]c(NC2Cc3ccccc3C2)c2CCCCc2[nH0]1	mGluR1	39 nM
Clc1ccccc1C)c1CSCCNc1[nH0]c(SCC)[nH0]c2CCCCc12	mGluR1	246 nM
S(CC)c1[nH0]c(NN2Cc3ccccc3C2)c2CCCCc2[nH0]1	mGluR1	550 nM
Clc1ccccc1C(OC)CNc1[nH0]c(SCC)[nH0]c2CCCCc12	mGluR1	610 nM
Clc1ccccc1OCCNc1[nH0]c(SCC)[nH0]c2CCCCc12	mGluR1	1000 nM
S(CC)c1[nH0]c(NC2CC3CCC2C3)c2CCCCc2[nH0]1	mGluR1	320 nM
O=C(OCC)c1[nH]cc(c1C)C(=O)OC(C)(C)C	mGluR1	340 nM
O=C(OCCC)c1[nH]cc(c1C)C(=O)OC(C)(C)C	mGluR1	75 nM
O=C(OCC1[nH]c(c(C)c1C(=O)OC(C)(C)C)C(=O)OCCC)C	mGluR1	2700 nM
O=Cc1[nH]c(c(C)c1C(=O)OC(C)(C)C)C(=O)OCCC	mGluR1	2000 nM
O=C(OC)c1[nH]c(c(C)c1C(=O)OC(C)(C)C)C(=O)OCCC	mGluR1	3200 nM
O=C(OCCC)c1[nH]c(c(c1C)C(=O)OC(C)(C)C)C(=O)NCCC1CC1	mGluR1	2500 nM
O=C(OC(C)(C)C)c1[nH]cc(c1C)C(=O)OC(C)(C)C	mGluR1	100 nM
O=C(OC1occc1)c1[nH]cc(c1C)C(=O)OC(C)(C)C	mGluR1	1200 nM
O=C(OCC1CC1)c1[nH]cc(c1C)C(=O)OC(C)(C)C	mGluR1	48 nM
O=C(OCCC)c1[nH]cc(c1C)C(=O)OC(C)(C)C	mGluR1	4 nM
O=C(OC(C)(C)C)c1[nH]cc(c1C)C(=O)OC(C)(C)C	mGluR1	17 nM
Fc1c(F)c(F)c(OC(=O)c2[nH]cc(c2C)C(=O)OC(C)C(C)(C)C)c(F)c1F	mGluR1	160 nM
O=C(OC(C)CN(C)C)c1[nH]cc(c1C)C(=O)OC(C)C(C)(C)C	mGluR1	390 nM
Clc1[nH]c(c(C)c1C(=O)OC(C)C(C)(C)C)C(=O)OCCC	mGluR1	160 nM
O=C(Oc1c[nH0]ccc1)c1[nH]cc(c1C)C(=O)OC(C)C(C)C	mGluR1	720 nM
O=C(OC1CN(CCL)CC)c1[nH]cc(c1C)C(=O)OC(C)C(C)C	mGluR1	260 nM
O=C(Oc1[nH0]c[nH0]ccc1)c1[nH]cc(c1C)C(=O)OC(C)C(C)C	mGluR1	1450 nM
O=C(OCCC)c1[nH0](C)c(C)c(c1C)C(=O)OC(C)(C)C	mGluR1	1000 nM
O=C(OCCC)c1[nH0](CCCC)c(C)c(c1C)C(=O)OC(C)C(C)C	mGluR1	5800 nM
O=C(OC(C)C(C)C)c1[nH0][nH0](C)c(c1)C(=O)OCCC	mGluR1	3200 nM
O=C(OCCC)c1[nH0][nH0](C)c(c1)C(=O)OC(C)C(C)C	mGluR1	3200 nM
O=C(OC(C)C(C)C)c1[nH0][nH0](C)c(c1)C(=O)OC(C)C(C)C	mGluR1	1500 nM
O=C(OC(C)C(C)C)c1[nH0][nH0](C)c(c1)C(=O)OCCC	mGluR1	6900 nM
O=C(OCCCC)c1[nH0][nH]c(c1)C(=O)OC(C)C(C)C	mGluR1	3400 nM
O=C(OCCC)c1[nH0][nH]c(c1)C(=O)OC(C)C(C)C	mGluR1	3400 nM
slc(N)c(c(C)c1C(=O)OC)C(=O)OCC	mGluR1	8000 nM
slc(C)c(c(N)c1C(=O)OCC)C(=O)OCC	mGluR1	6000 nM
slcc(c(C)c1C(=O)OCC)C(=O)OCC	mGluR1	4000 nM
slcc(c(C)c1C(=O)OCCC)C(=O)OC(C)(C)C	mGluR1	160 nM
slcc(c(C)c1C(=O)OCCC)C(=O)OC(C)C(C)C	mGluR1	32 nM
slc(N)c(c(C)c1C(=O)OCCC)C(=O)OC(C)C(C)C	mGluR1	320 nM
O=C(OCCC)c1ccc(cc1)C(=O)OCCC	mGluR1	4000 nM
O=C(OCCC)c1ccc(cc1)C(=O)OC(C)(C)C	mGluR1	400 nM
O=C(OCCC)c1ccc(cc1)C(=O)OC(C)C(C)C	mGluR1	63 nM
O=C(OCC1CC1)c1ccc(cc1)C(=O)OC(C)C(C)C	mGluR1	26 nM
O=C(c1ccc2[nH0]c(C)c(cc2c1)CC)C1CCC(OC)CC1	mGluR1	3 nM
O=C(c1ccc2[nH0]c(OC)c(cc2c1)CC)C1CCC(OC)CC1	mGluR1	20 nM
O=C(c1ccc2[nH0]cc(cc2c1)CC)C1CCC(OC)CC1	mGluR1	3.5 nM

C1c1[nH0]c2cc(C)c(cc2cc1CC)C(=O)C1CCC(OC)CC1	mGluR1	4.8 nM
O=C(c1ccc2[nH0]c(N(C)C)c(cc2c1)CC)C1CCC(OC)CC1	mGluR1	31 nM
O=C(OCc1[nH0]c2ccc(cc2cc1CC)C(=O)C1CCC(OC)CC1)	mGluR1	91 nM
O=C(c1ccc2[nH0]c(O)c(cc2c1)CC)C1CCC(OC)CC1	mGluR1	14 nM
O=C(Cc1cccc1)c1ccc2[nH0]c(C)c(cc2c1)CC	mGluR1	9.8 nM
O=C(c1ccc2[nH0]c(C)c(cc2c1)CC)C1CC2CCC1C2	mGluR1	13 nM
O=C(Cc1CCC(OC)CC1)c1ccc2[nH0]c(C)c(cc2c1)CC	mGluR1	15 nM
O=C(c1ccc2[nH0]c(C)c(cc2c1)CC)C1CCC(C)CC1	mGluR1	15 nM
FC1(CCC(OC)CC1)C(=O)c1ccc2[nH0]c(C)c(cc2c1)CC	mGluR1	17 nM
O=C(c1ccc2[nH0]c(C)c(cc2c1)CC)C1Cc2ccccc2C1	mGluR1	56 nM
O=C(Cc1C[C@@H](CCC1C1)1)c1ccc2[nH0]c(C)c(cc2c1)CC	mGluR1	60 nM
O=C(Cc1cccc1OC)c1ccc2[nH0]c(C)c(cc2c1)CC	mGluR1	67 nM
O=C(c1ccc2[nH0]c(C)c(cc2c1)CC)C1Oc2ccccc2OC1	mGluR1	83 nM
O=C(c1ccc2[nH0]c(C#N)c(cc2c1)CC)C1CCC(OC)CC1	mGluR1	11.5 nM
O=C(c1ccc2[nH0]c(C)c(cc2c1)CC)C1CCC(O)CC1	mGluR1	19 nM
S1CCc2cc3ccc(ccc3[nH0]c12)C(=O)C1CCC(OC)CC1	mGluR1	2.6 nM
O=C(c1ccc2[nH0]c3N(C)CCc3cc2c1)C1CCC(OC)CC1	mGluR1	8.1 nM
O=C1Nc2ccc(cc2C=C1CC)C(=O)C1CCC(OC)CC1	mGluR1	8.7 nM
O=C(c1ccc2[nH0]c(C)c([nH0]c2c1)C)C1CCC(OC)CC1	mGluR1	36 nM
O=C(c1ccc2[nH0]3[nH0][nH0][nH0]c3C(=Cc2c1)CC)C1CCC(OC)CC1	mGluR1	44 nM
slccc(c1)C(=O)c1ccc2[nH0]c3OCCCC3cc2c1	mGluR1	7.2 nM
Brclccc(cc1)C(=O)c1ccc2[nH0]c3OCCCC3cc2c1	mGluR1	17 nM
Fc1ccc(cc1)C(=O)c1ccc2[nH0]c3OCCCC3cc2c1	mGluR1	20 nM
Fc1cccc(c1F)C(=O)c1ccc2[nH0]c3OCCCC3cc2c1	mGluR1	74 nM
Fc1cccc1C(=O)c1ccc2[nH0]c3OCCCC3cc2c1	mGluR1	42 nM
O=C(NC12CC3CC(C(C3)C2)C1)c1[nH0]c2ccccc2[nH0]c1	mGluR1	5 nM
O=C(OC)C12Oc3ccccc3C(=NO)C2C1	mGluR1	3400 nM
O=C(OC)[C@@](Oc1cccc1C(=NO)[C@@H](C1)2)12	mGluR1	3000 nM
O=C(OC)[C@](Oc1cccc1C(=NO)[C@H](C1)2)12	mGluR1	1500 nM
O=C(OC)[C@@H](NC(=O)[C@](Oc1cccc1C(=NO)[C@H](C1)2)12)Cc1c	mGluR1	430 nM
O=C(OC)[C@H](NC(=O)C12Oc3ccccc3C(=NO)C2C1)Cc1cccc1	mGluR1	1400 nM
O=C(OC)[C@@H](NC(=O)C12Oc3ccccc3C(=NO)C2C1)Cc1cccc1	mGluR1	1200 nM
S(CCO)c1[nH0]c(NC2Cc3ccccc3C2)c2CCCCe2[nH0]1	mGluR1	1 nM
S(CCO)c1[nH0]c(Nc2ccc(OC)cc2)c2cc(OC)ccc2[nH0]1	mGluR1	11 nM
C1c1cccc(C1)c1CSCCNc1[nH0]c([nH0]c2CCCCe12)C	mGluR1	7 nM
C1c1cccc(C1)c1CSCCNc1[nH0]c([nH0]c2cccc12)	mGluR1	46 nM
O(C)c1ccc(Nc2[nH0]c([nH0]c3ccc(OC)cc23)cc1	mGluR1	96 nM
C1c1ccc2[nH0]c([nH0]c(NC3C4CCC3CC4)c2c1	mGluR1	400 nM
C1c1cccc2c([nH0]c([nH0]c12)NC1C2CCC1CC2	mGluR1	1895 nM
N#Cc1[nH0][nH0]c(N)[nH0]c1N1CCc2ccccc2CC1	mGluR1	27 nM
N#Cc1[nH0][nH0]c([nH0]c1N1CCc2ccccc2CC1)N(C)C	mGluR1	1380 nM
N#Cc1[nH0][nH0]c([nH0]c1N1CCc2ccccc2CC1)NCC1CC1	mGluR1	5 nM
N#Cc1[nH0][nH0]c([nH0]c1N1CCc2ccccc2CC1)NN	mGluR1	370 nM
O=C(OC(C)C)NCCNc1[nH0]c([nH0]c(C#N)c([nH0]1)N1CCc2ccccc2C	mGluR1	27 nM
N#Cc1[nH0][nH0]c([nH0]c1N1CCc2ccccc2CC1)NCCc1c[nH0]ccc1	mGluR1	29 nM
N#Cc1[nH0]c(CC)c([nH0]c1N1CCc2ccccc2CC1)C	mGluR1	6 nM
N#Cc1[nH0]c(C)c([nH0]c1N1CCc2ccccc2CC1)CC	mGluR1	103 nM
N#Cc1[nH0]cc[nH0]c1N1CCc2ccccc2CC1	mGluR1	470 nM
N#Cc1[nH0]c(c([nH0]c1N1CCc2ccccc2CC1)C)c1cccc1	mGluR1	45 nM
OCCNc1[nH0]c(N2CCc3ccccc3CC2)c([nH0]c1)C#N	mGluR1	500 nM
slc2CCN(Cc2[nH0]c1C)C=1N=C(NC(=O)C=1[N+](=O)[O-])C	mGluR1	30000 nM
slc2CCN(Cc2[nH0]c1C)c1[nH0]c([nH0]c(OCC)c1[N+](=O)[O-])C	mGluR1	4200 nM
slc2CCN(Cc2[nH0]c1C)C=1N=C(N(CC)C(=O)C=1[N+](=O)[O-])C	mGluR1	2100 nM
slc2CCN(Cc2[nH0]c1N)C=1N=C(NC(=O)C=1[N+](=O)[O-])C	mGluR1	49000 nM
slc2CCN(Cc2[nH0]c1N)C=1N=C(N(CC)C(=O)C=1[N+](=O)[O-])C	mGluR1	6000 nM
slc[nH0]c2CCN(Cc12)C=1N=C(NC(=O)C=1[N+](=O)[O-])C	mGluR1	43000 nM
slccc2CCN(Cc12)C=1N=C(NC(=O)C=1[N+](=O)[O-])C	mGluR1	1900 nM
slccc2CCN(Cc12)C=1N=C(N(CC)C(=O)C=1[N+](=O)[O-])C	mGluR1	69 nM
O=C(c1ccc2[nH0]c(N3CCCC3)c(cc2c1)CC)C1CCC(OC)CC1	mGluR1	3630 nM
O=C(c1ccc2[nH0]c(c(cc2c1)CC)c1occc1)C1CCC(OC)CC1	mGluR1	257nM
O=C(Nc1ccc2[nH0]c(O)c(cc2c1)CC)C1CCC(OC)CC1	mGluR1	10000 nM
O=C(N(C)c1cccc1)C12Oc3ccccc3C(=NO)C2C1	mGluR1	2000 nM
O=C(c1cccc1)c1ccc2cc3CCCOc3[nH0]c2c1	mGluR1	8300 nM
O=C(Nc1ccc(cc1)C(=O)C1CCC(OC)CC1)C	mGluR1	7585 nM
O=C(c1ccc2[nH0]c([nH]c2c1)C)C1CCC(OC)CC1	mGluR1	575 nM
O=C(Cc1cccc1)c1ccc2[nH0]c(C)c(cc2c1)CC	mGluR1	229 nM
O=C(Cc1ccc(N(C)C)cc1)c1ccc2[nH0]c(C)c(cc2c1)CC	mGluR1	646 nM
O=C(c1ccc2[nH0]c(C)c(cc2c1)CC)C1CCNCC1	mGluR1	10000 nM
O=C(c1ccc2[nH0]c(C)c(cc2c1)CC)C1CCC(N(C)C)CC1	mGluR1	10000 nM
O=C(c1ccc(OC)c(OC)c1)c1ccc2[nH0]c(C)c(cc2c1)CC	mGluR1	10000 nM
S1c2cc(ccc2C(=O)C=2CCC(CC1=2)CC)c1[nH0][nH0][nH0][nH]1	mGluR1	9 nM
FC(F)COC1[nH0]c([nH0]c(N2CCC(CC2)c2ccccc2)c1C#N)NCCO	mGluR1	36 nM
O=C(OC)NC(=O)C(c1cccc1)c1cccc1	mGluR1 (pos.)	170 nM
O=C(OC)NC(=O)C1c2ccccc2Oc2ccccc21	mGluR1 (pos.)	9 nM
[S+2]([O-])([O-])(N1CCC[C@H]1(c1ccc(C)cc1)c1ccc(C)cc1	mGluR1 (pos.)	200 nM
O=C(Nc1[nH0]oc([nH0]1)C)C1c2ccccc2Oc2ccccc21	mGluR1 (pos.)	52 nM
O=C(Nc1[nH0]oc([nH0]1)CC)C1c2ccccc2Oc2ccccc21	mGluR1 (pos.)	6 nM
O=C(Nc1[nH0]oc([nH0]1)C(C)C)C1c2ccccc2Oc2ccccc21	mGluR1 (pos.)	22 nM

O=C(Nc1[nH0]oc([nH0]1)CCC)C1c2ccccc2Oc2ccccc21	mGluR1 (pos.)	25 nM
O=C(Nc1[nH0]oc([nH0]1)C1CC1)C1c2ccccc2Oc2ccccc21	mGluR1 (pos.)	23 nM
O=C(Nc1[nH0]oc([nH0]1)CC(C)C)C1c2ccccc2Oc2ccccc21	mGluR1 (pos.)	10 nM
O=C(Nc1[nH0][nH0][nH0]([nH0]1)C)C1c2ccccc2Oc2ccccc21	mGluR1 (pos.)	180 nM
O=C(Nc1[nH0][nH0][nH0]([nH0]1)CC)C1c2ccccc2Oc2ccccc21	mGluR1 (pos.)	65 nM
O=C(Nc1[nH0][nH0][nH0]([nH0]1)CCC)C1c2ccccc2Oc2ccccc21	mGluR1 (pos.)	29 nM
O=C(Nc1[nH0][nH0][nH0]([nH0]1)C(C)C)C1c2ccccc2Oc2ccccc21	mGluR1 (pos.)	29 nM
O=C(Nc1[nH0][nH0][nH0]([nH0]1)CC(C)C)C1c2ccccc2Oc2ccccc21	mGluR1 (pos.)	34 nM
O=C(NC1c1ccc2ccccc21)c1[nH0]cc(cc1)CCCC	mGluR1 (pos.)	135 nM
N(c1ccccc1)C1CC(C)(C)CC(C)(C)C1	mGluR1 (pos.)	158 nM
[nH0]1c1ccc1CC=C(c1ccccc1)c1ccccc1	mGluR1 (pos.)	151 nM
s1c([nH0]c1C(=O)N1CCc2cc(OC)c(OC)cc2C1)C	mGluR1 (pos.)	164 nM
O=C(N1CCCCC1)c1[nH0][nH0]2c(N=C(C=C2)c2ccccc2)c1	mGluR1 (pos.)	164 nM
O=[N+]([O-])c1ccccc1)c1[nH0]c2[nH0](C=CC=C2)c1	mGluR5	10000 nM
[nH0]1c(C)cccc1C#Cc1ccccc1	mGluR5	30 nM
[nH0]1c(C)cccc1C=Cc1ccccc1	mGluR5	3500 nM
O=C(C=Cc1ccccc1)c1[nH0]c(C)ccc1	mGluR5	10000 nM
N#Cc1ccc(C#Cc2[nH0]c(C)ccc2)cc1	mGluR5	1000 nM
[nH0]1cc(C)ccc1C#Cc1ccccc1	mGluR5	640 nM
N#Cc1ccccc1C#Cc1[nH0]c(C)ccc1	mGluR5	360 nM
N#Cc1cccc(C#Cc2[nH0]c(C)ccc2)c1	mGluR5	2 nM
Oc1ccccc1C#Cc1[nH0]c(C)ccc1	mGluR5	360 nM
[nH0]1c(C)cccc1C#Cc1ccccc1	mGluR5	48 nM
[nH0]1c(C)cccc1C#Cc1cccc(C)c1	mGluR5	33 nM
O=C(Nc1ccccc1)c1[nH0]c(C)ccc1	mGluR5	3500 nM
Oc1ccc(C#Cc2[nH0]c(C)ccc2)cc1	mGluR5	1200 nM
Oc1cccc(C#Cc2[nH0]c(C)ccc2)c1	mGluR5	2 nM
O(C)c1ccccc1C#Cc1[nH0]c(C)ccc1	mGluR5	66 nM
O(C)c1ccc(C#Cc2[nH0]c(C)ccc2)cc1	mGluR5	1700 nM
O(C)c1cccc(C#Cc2[nH0]c(C)ccc2)c1	mGluR5	10 nM
[nH0]1c(C)cccc1C#Cc1ccc(C)cc1	mGluR5	50000 nM
s1cc([nH0]c1C)C#Cc1c[nH0]ccc1	mGluR5	5 nM
s1cc([nH0]c1C)C#Cc1[nH0]cccc1	mGluR5	53 nM
s1cc([nH0]c1C)C#Cc1cc[nH0]cc1	mGluR5	120 nM
s1cc([nH0]c1C)C#Cc1ccccc1	mGluR5	14 nM
s1c[nH0]c(C#Cc2ccccc2)c1	mGluR5	97 nM
s1cc[nH0]c1C#Cc1ccccc1	mGluR5	80 nM
O(C)c1ccc(cc1OC)c1[nH0]c2[nH0](C=CC=C2)c1	mGluR5	6800 nM
O(C)C1C=C[nH0]2cc([nH0]c2C=1)c1ccc(OC)c(OC)c1	mGluR5	3300 nM
O(C)c1cc(ccc1OCc1ccccc1)c1[nH0]c2[nH0](C=CC=C2)c1	mGluR5	830 nM
Br1ccccc1)c1[nH0]c2[nH0](C=CC=C2)c1	mGluR5	950 nM
Ic1ccccc1)c1[nH0]c2[nH0](C=CC=C2)c1	mGluR5	970 nM
Clc1ccccc1)c1[nH0]c2[nH0](C=CC=C2)c1	mGluR5	1230 nM
[nH0]1c2[nH0](C=CC=C2)cc1c1cccc(C)c1	mGluR5	1550 nM
FC(F)(F)c1ccccc1)c1[nH0]c2[nH0](C=CC=C2)c1	mGluR5	2790 nM
Fc1ccccc1)c1[nH0]c2[nH0](C=CC=C2)c1	mGluR5	3410 nM
[nH0]1c2[nH0](C=CC(=C2)CC)cc1c1ccc(C)(C)c1	mGluR5	3640 nM
s1c(C)ccc1c1[nH0]c2[nH0](C=CC=C2)c1	mGluR5	6130 nM
[nH0]1c2[nH0](C=CC(C)=C2)cc1c1ccccc1	mGluR5	7500 nM
[nH0]1c2[nH0](C=CC=C2)cc1c1ccc(C)cc1	mGluR5	8770 nM
O(C)c1ccccc1)c1[nH0]c2[nH0](C=CC=C2)c1	mGluR5	1650 nM
O(C)c1ccc(cc1OC)c1[nH0]c2[nH0](C=C(C)C=C2)c1	mGluR5	8300 nM
O1C=C(OC2C=CC=CC12)c1[nH0]c2[nH0](C=CC=C2)c1	mGluR5	990 nM
[nH0]1c2[nH0](C=C(C)C=C2)cc1c1ccc(C)cc1	mGluR5	10000 nM
[nH0]1c2[nH0](C=CC=C2)cc1c1ccc2CCCc2c1	mGluR5	930 nM
o1c2ccccc2cc1c1[nH0]c2[nH0](C=CC=C2)c1	mGluR5	1660 nM
s1cc(c2ccccc12)c1[nH0]c2[nH0](C=CC=C2)c1	mGluR5	2760 nM
O1CCc2cc(ccc12)c1[nH0]c2[nH0](C=CC=C2)c1	mGluR5	2860 nM
s1cc([nH0]c1C#Cc1ccccc1)C	mGluR5	13 nM
S(CC(=O)OCC)c1[nH0]cc(Cc2[nH0](C)ccc2)c(N)[nH0]1	mGluR5	380 nM
Clc1ccc(c(Cl)c1)c1c[nH0]c(SCC(=O)OCC)[nH0]c1N	mGluR5	3850 nM
S(CC(=O)COCC)c1[nH0]cc(c(N)[nH0]1)C(=O)OCC	mGluR5	270 nM
s1ccccc1Cc1c[nH0]c(SCC(=O)OCC)[nH0]c1NCC	mGluR5	600 nM
s1ccccc1Cc1c[nH0]c(SC(C)C)[nH0]c1N	mGluR5	1390 nM
S(CC(=O)OCC1CC1C)c1[nH0]cc(Cc2ccccc2)c(N)[nH0]1	mGluR5	630 nM
S(CC(=O)OCC1CCC1)c1[nH0]cc(Cc2ccccc2)c(N)[nH0]1	mGluR5	1460 nM
S(CC(=O)OCC1CC1)c1[nH0]cc(Cc2ccccc2)c(N)[nH0]1	mGluR5	200 nM
S(Cc1o[nH0]c([nH0]1)C1CC1)c1[nH0]cc(Cc2ccccc2)c(N)[nH0]1	mGluR5	450 nM
s1ccccc1Cc1c[nH0]c(SCC=C)[nH0]c1N	mGluR5	2790 nM
s1ccccc1Cc1c[nH0]c(SCc2[nH0]oc[nH0]2)[nH0]c1N	mGluR5	400 nM
O=C(OCC)c1[nH0](C)c([nH0]c1C)C#Cc1ccccc1	mGluR5	250 nM
O=C(OCC)c1[nH]c([nH0]c1C)C#Cc1ccccc1	mGluR5	2400 nM
O(C)c1ccccc1C#Cc2[nH0]c(C)c1[nH0]2C)c1	mGluR5	350 nM
[nH0]1cc[nH0](C)c1C#Cc1ccccc1	mGluR5	720 nM
[nH0]1cc[nH]c1C#Cc1ccccc1	mGluR5	200 nM
O=[N+]([O-])c1[nH0](CCO)c([nH0]c1)C#Cc1ccccc1	mGluR5	2110 nM
Clc1ccccc1)c1C#Cc1[nH0]c(C)c([nH0]1C)C(=O)OCC	mGluR5	1000 nM
O=C(OCC)c1[nH0]c([nH0]c2ccccc2)c1C)C#Cc1ccccc1	mGluR5	not available

O=C(OCC)c1[nH0](C)c([nH0]c1C)C#Cc1cccc(C)c1	mGluR5	130 nM
O=C(Nc1cccc(C#Cc2[nH0]c(C)c([nH0]2C)C(=O)OCC)c1)C	mGluR5	2120 nM
O=C(OCC)c1[nH0](C)c([nH0]c1C)C#Cc1cccc(N2CC=CC2)c1	mGluR5	180 nM
o1[nH0]c([nH0]c1c1[nH0](C)c([nH0]c1C)C#Cc1cccc1)C	mGluR5	11 nM
Clc1ccc(C#Cc2[nH0]c(C)c([nH0]2C)C(=O)OCC)cc1	mGluR5	not available
Fc1ccc(C#Cc2[nH0]c(C)c([nH0]2C)C(=O)OCC)cc1	mGluR5	250 nM
O=C(OCC)c1[nH0](C)c([nH0]c1C)C#Cc1ccc(cc1)c1cccc1	mGluR5	210 nM
Fc1cccc1C#Cc1[nH0]c(C)c([nH0]1C)C(=O)OCC	mGluR5	90 nM
Fc1cccc1C#Cc1[nH0]cc[nH0]1C	mGluR5	70 nM
O=C(OCC)c1[nH0](C)c([nH0]c1C)C#Cc1ccc(N)cc1	mGluR5	1530 nM
Clc1cccc1C#Cc1[nH0]cc[nH0]1C	mGluR5	1100 nM
Clc1[nH0]c([nH0](CC(=O)OCC)c1C1)C#Cc1cccc1	mGluR5	520 nM
[nH0]1c[nH0](C)c(C#Cc2cccc2)c1	mGluR5	220 nM
O=C(NCCc1c2cc(OC)ccc2[nH]c1C#Cc1cccc1)C	mGluR5	580 nM
S1Cc2[nH0](c[nH0]c2C#Cc2cccc2)c2ccc[nH0]c12	mGluR5	150 nM
O1Cc2[nH0](c[nH0]c2C#Cc2cccc2)c2cccc12	mGluR5	70 nM
ClCC(O)C[nH0]1c([nH0]c(C#Cc2cccc2)c1[N+](=O)[O-])C	mGluR5	230 nM
O=Cc1[nH0](C)c[nH0]c1C#Cc1cccc1	mGluR5	1790 nM
[nH0]1c[nH]cc1C#Cc1cccc1	mGluR5	3360 nM
[nH0]1c[nH0](C)cc1C#Cc1cccc1	mGluR5	500 nM
O=[N+](O-)c1[nH0](C)c([nH0]c1C#Cc1cccc1)C	mGluR5	20 nM
[nH0]1[nH0](C)c(C#Cc2cccc2)cc1C	mGluR5	5000-10000 nM
[nH0]1c([nH0](C)c(c1C(C)C)C(C)C)C=Cc1cccc1	mGluR5	1820 nM
Fc1ccc(cc1)C=Cc1[nH0]c(c([nH0]1C)C(C)C)C(C)C	mGluR5	5000-10000 nM
Clc1ccc(cc1)C=Cc1[nH0]c(c([nH0]1C)C(C)C)C(C)C	mGluR5	5000-10000 nM
O(CCCC)c1ccc(cc1)C=Cc1[nH0]c(c([nH0]1C)C(C)C)C(C)C	mGluR5	5000-10000 nM
O(C)c1cc(C)c(C=Cc2[nH0]c(c([nH0]2C)C(C)C)C(C)C)C(C)c1C	mGluR5	5000-10000 nM
O(C)c1ccc(cc1)C=Cc1[nH0]c(c([nH0]1C)C(C)C)C(C)C	mGluR5	5000-10000 nM
Clc1ccc(cc1F)C=Cc1[nH0]c(c([nH0]1C)C(C)C)C(C)C	mGluR5	10000 nM
O(CC)c1ccc(cc1)C=Cc1[nH0]c(c([nH0]1C)C(C)C)C(C)C	mGluR5	10000 nM
O(C)c1ccc(C=Cc2[nH0]c(c([nH0]2C)C(C)C)C(C)C)C(OC)c1OC	mGluR5	10000 nM
Clc1ccc(C=Cc2[nH0]c(c([nH0]2C)C(C)C)C(C)C)C(C)c1	mGluR5	10000 nM
[nH0]1c([nH0](C)c(c1C(C)C)C(C)C)C=Cc1ccc(C)cc1	mGluR5	3250 nM
Brcl[nH0]c[nH0](C)c1C=Cc1cccc1	mGluR5	3060 nM
[nH0]1c[nH0](C)c(c1)C=Cc1cccc1	mGluR5	8000 nM
O=C(OC)N1CC[C@H]([C@H]1(CCC[C@@](O)(C#Cc1cccc(C)c1)1))1	mGluR5	20 nM
O(C)c1cc(OC)cc(c1)C=Cc1[nH0]c(C)ccc1	mGluR5	30 nM
Clc1cc(ccc1CC#N)c1oc2cccc2[nH0]1	mGluR5	6 nM
olc2cccc2[nH0]c1c1ccc(CC#N)c(OC)c1	mGluR5	3 nM
olc2cccc2[nH0]c1c1ccc(c(OC)c1)c1[nH0]cccc1	mGluR5	41 nM
olc2cccc2[nH0]c1c1ccc(c(OC)c1)c1c[nH0]cccc1	mGluR5	416 nM
O(C)c1cc(ccc1c1c[nH0]ccc1)c1[nH0]c2[nH0](C=CC=C2)c1	mGluR5	22 nM
S1C=C[nH0]2cc([nH0]c12)c1ccc(c(OC)c1)c1c[nH0]ccc1	mGluR5	23 nM
S1CC[nH0]2cc([nH0]c12)c1ccc(c(OC)c1)c1c[nH0]ccc1	mGluR5	325 nM
ol[nH0]c([nH0]c1c1cccc(C#N)c1)c1[nH0]cccc1	mGluR5	42 nM
olcc([nH0]c1c1cccc(C#N)c1)c1[nH0]cccc1	mGluR5	45 nM
S(CC(=O)OCC)c1[nH0]cc(Cc2cccc2)c(N)[nH0]1	mGluR5	140 nM
Brclccc(ecl)Cclc[nH0]c(SCC(=O)OCC)[nH0]c1N	mGluR5	180 nM
slccc(c1)Cclc[nH0]c(SCC(=O)OCC)[nH0]c1N	mGluR5	180 nM
S(CC(=O)OCC)c1[nH0]cc(Cc2cccc2)c(N)[nH0]1	mGluR5	160 nM
S(CC(=O)OCC=C)c1[nH0]cc(Cc2cccc2)c(N)[nH0]1	mGluR5	120 nM
slcccc1Cc1c[nH0]c(SCC(=O)OCC)[nH0]c1NCC(C)C	mGluR5	160 nM
ClC=1C=C[nH0]2cc([nH0]c2C=1)c1ccc(C)c(C)c1	mGluR5	100 nM
O(C)C=1C=C[nH0]2cc([nH0]c2C=1)c1ccc(C)c(C)c1	mGluR5	140 nM
[nH0]1c2[nH0](C=CC=C2)cc1c1ccc(C)c(C)c1	mGluR5	37 nM
[nH0]1c2[nH0](C=CC(C)=C2)cc1c1ccc(C)c(C)c1	mGluR5	280 nM
Brclcc(ccc1F)c1[nH0]c2[nH0](C=CC=C2)c1	mGluR5	690 nM
slc(C)cc(c1C)c1[nH0]c2[nH0](C=CC=C2)c1	mGluR5	580 nM
Oc1ccc([nH0]c1N=Nc1cccc1)C	mGluR5	3700 nM
O(C)c1ccc(cc1OC)c1[nH0]c2[nH0](C=CC(C)=C2)c1	mGluR5	1880 nM
Fc1cccc(c1)C=NN=Cc1cccc(F)c1	mGluR5 (pos.)	2000 nM

7.2 Register of Pharmacophore Features

Table 7.2-a. Annotation points defined by the PCH pharmacophore scheme in MOE Version 2003.02 (Section 4.2.2)

Type	Definition
H-bond donor (<i>Don</i>)	Hydrogen bond donors, not including tautomeric donors (e.g.: primary and secondary amines, hydroxy-groups).
H-bond acceptor (<i>Acc</i>)	Hydrogen bond acceptors, not including tautomeric acceptors (e.g.: carbonyl-groups, unsaturated nitrogens).
Cation (<i>Cat</i>)	Cations, including resonance cations (e.g.: protonated amines)
Anion (<i>Ani</i>)	Anions, including resonance anions (e.g.: carboxylate-anions).
Aromatic centers (<i>Aro</i>)	Centers of aromatic homocycles or heterocycles (e.g.: benzenes, pyridines, quinolines).
Hydrophobic areas (<i>Hyd</i>)	Areas of hydrophobic properties (e.g.: aliphatic chains, cycloalkanes)

7.3 Similarity Lists obtained in Section 4.3

Table 7.3-a. List containing the top 100 test compounds of the CATS run for reference molecule **R-01**. Molecules with blue ID were ordered, molecules with bold ID were ordered and delivered.

Rank	ID	Similarity Score	Rank	ID	Similarity Score
1	R-02	0.1461	51	BAS_2276958	0.5408
2	BAS_0391501	0.3368	52	BAS_1027129	0.5417
3	BAS_0399020	0.3986	53	BAS_0719950	0.5419
4	BAS_2276984	0.4144	54	BAS_0316110	0.5428
5	BAS_0399026	0.4279	55	BAS_0466184	0.5432
6	BAS_0398973	0.4279	56	BAS_0733586	0.5448
7	BAS_1280297	0.4477	57	BAS_0733331	0.5448
8	BAS_1293648	0.4569	58	R-03	0.5450
9	BAS_3200195	0.4643	59	BAS_0721849	0.5480
10	BAS_3200194	0.4643	60	BAS_0316106	0.5487
11	BAS_0726193	0.4644	61	BAS_0549667	0.5502
12	BAS_1293659	0.4690	62	BAS_0872503	0.5504
13	BAS_3569630	0.4770	63	BAS_0116912	0.5507
14	BAS_3840865	0.4841	64	BAS_0119421	0.5510
15	BAS_0726155	0.4848	65	BAS_0491076	0.5511
16	BAS_2276957	0.4855	66	BAS_0829447	0.5528
17	BAS_0434242	0.4885	67	BAS_0115283	0.5540
18	BAS_0484981	0.4888	68	BAS_1293655	0.5541
19	BAS_1280306	0.4937	69	BAS_0997506	0.5546
20	BAS_0032180	0.4969	70	BAS_0369581	0.5583
21	BAS_0457554	0.5008	71	BAS_0450775	0.5590
22	BAS_0369588	0.5017	72	BAS_1044756	0.5645
23	BAS_0637934	0.5022	73	BAS_0619947	0.5658
24	BAS_1293653	0.5031	74	BAS_0600286	0.5666
25	BAS_3147583	0.5048	75	BAS_0069082	0.5670
26	BAS_1123649	0.5069	76	BAS_0672186	0.5681
27	BAS_1293647	0.5103	77	BAS_1585664	0.5684
28	BAS_5307694	0.5111	78	BAS_0232984	0.5686
29	BAS_0457561	0.5134	79	BAS_0481364	0.5694
30	BAS_1053334	0.5170	80	BAS_0308659	0.5696
31	BAS_0726256	0.5175	81	BAS_0396059	0.5703
32	BAS_2303581	0.5196	82	BAS_1077633	0.5707
33	BAS_0899874	0.5198	83	BAS_2236264	0.5710
34	BAS_1293657	0.5209	84	BAS_2236261	0.5710
35	BAS_1280314	0.5215	85	BAS_0745008	0.5715
36	BAS_0530782	0.5228	86	BAS_0671951	0.5722
37	BAS_0369580	0.5267	87	BAS_0247237	0.5743
38	BAS_2603597	0.5275	88	BAS_0069084	0.5744
39	BAS_1365856	0.5287	89	BAS_0834407	0.5770
40	BAS_1077624	0.5306	90	BAS_0784504	0.5781
41	BAS_0139098	0.5306	91	BAS_1044763	0.5784
42	BAS_0099446	0.5307	92	BAS_1018141	0.5810
43	BAS_0069083	0.5326	93	BAS_0733420	0.5818
44	BAS_0129908	0.5345	94	BAS_1123751	0.5822
45	BAS_0529716	0.5361	95	BAS_1123652	0.5822
46	BAS_0459058	0.5372	96	BAS_0329602	0.5824
47	BAS_0672162	0.5385	97	BAS_0834813	0.5829
48	BAS_1123749	0.5393	98	BAS_0066965	0.5835
49	BAS_1123654	0.5393	99	BAS_5621609	0.5840
50	BAS_1293630	0.5401	100	BAS_1280290	0.5847

Table 7.3-b. List containing the top 100 test compounds of the CATS run for reference molecule **R-02**. Molecules with blue ID were ordered, molecules with bold ID were ordered and delivered.

Rank	ID	Similarity Score	Rank	ID	Similarity Score
1	R-01	0.1461	51	BAS_1123654	0.5246
2	BAS_0399020	0.3671	52	BAS_0719950	0.5253
3	BAS_1280297	0.3956	53	BAS_0454887	0.5263
4	BAS_0391501	0.3958	54	BAS_0069082	0.5313
5	BAS_0399026	0.4031	55	BAS_1053334	0.5336
6	BAS_0398973	0.4031	56	BAS_0530782	0.5339
7	BAS_2276984	0.4083	57	BAS_0997506	0.5343
8	BAS_1293648	0.4312	58	BAS_0726256	0.5350
9	BAS_0726193	0.4389	59	BAS_0491076	0.5364
10	BAS_1293653	0.4405	60	BAS_0329364	0.5398
11	BAS_1293659	0.4427	61	BAS_0829447	0.5398
12	BAS_1365856	0.4604	62	BAS_1123747	0.5401
13	BAS_3840865	0.4636	63	BAS_0637766	0.5416
14	BAS_1293647	0.4700	64	BAS_0659984	0.5437
15	BAS_0899874	0.4732	65	BAS_0066155	0.5437
16	BAS_0032180	0.4733	66	BAS_1280290	0.5445
17	BAS_3569630	0.4733	67	BAS_2236264	0.5450
18	BAS_2303581	0.4763	68	BAS_2236261	0.5450
19	BAS_1280314	0.4763	69	BAS_0119421	0.5481
20	BAS_1280306	0.4772	70	BAS_1118531	0.5508
21	BAS_3147583	0.4874	71	BAS_0733447	0.5525
22	BAS_0726155	0.4883	72	BAS_1365860	0.5540
23	BAS_1293630	0.4886	73	BAS_0726125	0.5555
24	BAS_0529716	0.4920	74	BAS_0872503	0.5560
25	BAS_1293657	0.4923	75	BAS_0672162	0.5571
26	BAS_0129908	0.4938	76	BAS_5621609	0.5574
27	BAS_1293655	0.4949	77	BAS_0327258	0.5575
28	BAS_0484981	0.4962	78	BAS_2236262	0.5576
29	BAS_0600286	0.5014	79	BAS_0834813	0.5592
30	BAS_0450775	0.5031	80	BAS_0726207	0.5595
31	R-03	0.5042	81	BAS_0725815	0.5595
32	BAS_1123649	0.5043	82	BAS_0457561	0.5622
33	BAS_0834407	0.5053	83	BAS_0705143	0.5624
34	BAS_0733586	0.5065	84	BAS_1077633	0.5629
35	BAS_0733331	0.5065	85	BAS_0667696	0.5631
36	BAS_0637934	0.5074	86	BAS_5432992	0.5637
37	BAS_0459058	0.5087	87	BAS_0329602	0.5652
38	BAS_0069083	0.5095	88	BAS_4912490	0.5657
39	BAS_5307694	0.5103	89	BAS_1256720	0.5657
40	BAS_0745008	0.5112	90	BAS_0069084	0.5664
41	BAS_1585664	0.5114	91	BAS_1209494	0.5671
42	BAS_0369588	0.5149	92	BAS_0119417	0.5675
43	BAS_2276957	0.5185	93	BAS_1293627	0.5677
44	BAS_1077624	0.5193	94	BAS_1293625	0.5677
45	BAS_0139098	0.5193	95	BAS_0099446	0.5678
46	BAS_0434242	0.5201	96	BAS_0872247	0.5695
47	BAS_3200195	0.5203	97	BAS_0066965	0.5698
48	BAS_3200194	0.5203	98	BAS_1018141	0.5704
49	BAS_0457554	0.5226	99	BAS_2603597	0.5711
50	BAS_1123749	0.5246	100	BAS_1317855	0.5715

Table 7.3-c. List containing the top 100 test compounds of the CATS run for reference molecule **R-03**. Molecules with blue ID were ordered, molecules with bold ID were ordered and delivered.

Rank	ID	Similarity Score	Rank	ID	Similarity Score
1	BAS_1293657	0.2863	51	BAS_0187775	0.4318
2	BAS_0154462	0.3369	52	BAS_0398896	0.4325
3	BAS_2236262	0.3470	53	BAS_0329591	0.4330
4	BAS_2236264	0.3475	54	BAS_0015466	0.4353
5	BAS_2236261	0.3475	55	BAS_0015465	0.4353
6	BAS_0997507	0.3558	56	BAS_2171303	0.4357
7	BAS_3603162	0.3596	57	BAS_1026950	0.4366
8	BAS_0872246	0.3625	58	BAS_0872536	0.4386
9	BAS_0872247	0.3644	59	BAS_0872357	0.4386
10	BAS_0872298	0.3650	60	BAS_2556540	0.4399
11	BAS_1152576	0.3712	61	BAS_0435696	0.4433
12	BAS_1152575	0.3712	62	BAS_1293655	0.4436
13	BAS_0872537	0.3712	63	BAS_0363772	0.4443
14	BAS_0872358	0.3712	64	BAS_3077368	0.4450
15	BAS_0231929	0.3876	65	BAS_0849059	0.4454
16	BAS_0491076	0.3886	66	BAS_0637766	0.4463
17	BAS_0883093	0.3936	67	BAS_0573103	0.4468
18	BAS_1969380	0.3949	68	BAS_0631939	0.4468
19	BAS_0872244	0.3954	69	BAS_2988684	0.4480
20	BAS_0872538	0.3961	70	BAS_1839775	0.4480
21	BAS_0872359	0.3961	71	BAS_0848995	0.4489
22	BAS_0454671	0.3975	72	BAS_1585664	0.4495
23	BAS_0872483	0.3983	73	BAS_1808748	0.4496
24	BAS_0872486	0.4014	74	BAS_4085088	0.4498
25	BAS_1121722	0.4014	75	BAS_0129908	0.4498
26	BAS_0872485	0.4019	76	BAS_0600286	0.4505
27	BAS_2236263	0.4098	77	BAS_0190164	0.4516
28	BAS_0872613	0.4118	78	BAS_0363869	0.4521
29	BAS_1053338	0.4125	79	BAS_0024127	0.4525
30	BAS_0669878	0.4125	80	BAS_0991456	0.4526
31	BAS_1355775	0.4132	81	BAS_0726125	0.4536
32	BAS_0218058	0.4159	82	BAS_2785758	0.4540
33	BAS_0653659	0.4160	83	BAS_0872534	0.4544
34	BAS_0653662	0.4168	84	BAS_0872355	0.4544
35	BAS_0203131	0.4168	85	BAS_0818838	0.4546
36	BAS_4912490	0.4182	86	BAS_0917444	0.4552
37	BAS_2556549	0.4185	87	BAS_0069083	0.4552
38	BAS_1293648	0.4187	88	BAS_1312687	0.4563
39	BAS_0534732	0.4188	89	BAS_0757453	0.4565
40	BAS_1280290	0.4200	90	BAS_0584664	0.4565
41	BAS_0869325	0.4211	91	BAS_0069082	0.4568
42	BAS_0899656	0.4213	92	BAS_1123747	0.4568
43	BAS_0129155	0.4249	93	BAS_0015469	0.4569
44	BAS_0472011	0.4253	94	BAS_0872503	0.4569
45	BAS_0345519	0.4260	95	BAS_2303581	0.4570
46	BAS_1293653	0.4280	96	BAS_0997477	0.4590
47	BAS_0717216	0.4282	97	BAS_0640325	0.4607
48	BAS_5497245	0.4287	98	BAS_0399408	0.4610
49	BAS_0119464	0.4302	99	BAS_0484084	0.4614
50	BAS_0872277	0.4312	100	BAS_0389731	0.4616

Table 7.3-d. List containing the top 100 test compounds of the CATS run for reference molecule **R-04**. Molecules with blue ID were ordered, molecules with bold ID were ordered and delivered.

Rank	ID	Similarity Score	Rank	ID	Similarity Score
1	BAS_0712884	0.2897	51	BAS_0369027	0.5719
2	BAS_2167520	0.3401	52	BAS_1939695	0.5720
3	BAS_1939555	0.3616	53	BAS_0579882	0.5737
4	BAS_1939648	0.3795	54	BAS_0407475	0.5737
5	BAS_1939535	0.4046	55	BAS_0712780	0.5739
6	BAS_1939546	0.4143	56	BAS_1316926	0.5742
7	BAS_1939573	0.4280	57	BAS_1269260	0.5742
8	BAS_1939536	0.4466	58	BAS_0579549	0.5742
9	BAS_1939639	0.4507	59	BAS_1403566	0.5745
10	BAS_0924173	0.4510	60	BAS_0369030	0.5755
11	BAS_1939665	0.4714	61	BAS_0579885	0.5774
12	BAS_1939551	0.4896	62	BAS_0369028	0.5779
13	BAS_1939628	0.4931	63	BAS_0800382	0.5779
14	BAS_1939563	0.5015	64	BAS_1939644	0.5788
15	BAS_1939603	0.5047	65	BAS_0406838	0.5797
16	BAS_1939570	0.5068	66	BAS_0578146	0.5803
17	BAS_0368608	0.5132	67	BAS_0408214	0.5806
18	BAS_1939531	0.5167	68	BAS_0542433	0.5806
19	BAS_1939533	0.5204	69	BAS_1120137	0.5812
20	BAS_1939629	0.5220	70	BAS_0579515	0.5812
21	BAS_0798537	0.5377	71	BAS_0542784	0.5817
22	BAS_1939534	0.5389	72	BAS_0579393	0.5821
23	BAS_0798536	0.5404	73	BAS_0712763	0.5832
24	BAS_1939567	0.5407	74	BAS_0579878	0.5844
25	BAS_1939565	0.5407	75	BAS_0407476	0.5851
26	BAS_0579385	0.5411	76	BAS_0838067	0.5859
27	BAS_0406832	0.5427	77	BAS_0441450	0.5862
28	BAS_0476182	0.5438	78	BAS_0579884	0.5876
29	BAS_0579396	0.5450	79	BAS_0407062	0.5898
30	BAS_1939654	0.5466	80	BAS_2778871	0.5900
31	BAS_0369029	0.5475	81	BAS_0408213	0.5945
32	BAS_1058381	0.5485	82	BAS_0579493	0.5963
33	BAS_1939537	0.5495	83	BAS_0579482	0.5963
34	BAS_1939562	0.5499	84	BAS_0369091	0.5964
35	BAS_1939554	0.5499	85	BAS_0753957	0.5965
36	BAS_1939548	0.5499	86	BAS_0408217	0.5966
37	BAS_1939547	0.5499	87	BAS_1269241	0.5971
38	BAS_0579407	0.5507	88	BAS_0758992	0.5979
39	BAS_0369033	0.5601	89	BAS_0579428	0.5985
40	BAS_0542311	0.5611	90	BAS_0579418	0.5985
41	BAS_0368609	0.5626	91	BAS_0712754	0.5985
42	BAS_0712762	0.5641	92	BAS_0579538	0.5990
43	BAS_2975101	0.5659	93	BAS_0441433	0.5991
44	BAS_0754427	0.5664	94	BAS_1939630	0.5992
45	BAS_1939661	0.5667	95	BAS_0543754	0.5993
46	BAS_0579879	0.5675	96	BAS_0712795	0.6007
47	BAS_0084847	0.5712	97	BAS_0407482	0.6008
48	BAS_0407336	0.5712	98	BAS_3374461	0.6008
49	BAS_0661907	0.5713	99	BAS_0579890	0.6010
50	BAS_0712798	0.5718	100	BAS_1939624	0.6016

Table 7.3-e. List containing the top 100 test compounds of the CATS run for reference molecule **R-05**. Molecules with blue ID were ordered, molecules with bold ID were ordered and delivered.

Rank	ID	Similarity Score	Rank	ID	Similarity Score
1	BAS_0253277	0.7360	51	BAS_3058581	0.9345
2	BAS_6264800	0.7521	52	BAS_0620124	0.9367
3	BAS_0355555	0.8153	53	BAS_0774663	0.9369
4	R-06	0.8470	54	BAS_0618998	0.9378
5	BAS_6264802	0.8664	55	BAS_0341130	0.9379
6	BAS_0253275	0.8716	56	BAS_0844616	0.9405
7	BAS_4363443	0.8821	57	BAS_0844538	0.9405
8	BAS_2720963	0.8916	58	BAS_0222891	0.9415
9	BAS_6264827	0.8917	59	BAS_0732880	0.9416
10	BAS_1377675	0.8939	60	BAS_1122474	0.9430
11	BAS_4363433	0.8944	61	BAS_1004862	0.9435
12	BAS_0022054	0.8946	62	BAS_0844509	0.9441
13	BAS_0844542	0.8947	63	BAS_3387264	0.9455
14	BAS_3387057	0.8981	64	BAS_0732884	0.9457
15	BAS_0732895	0.8991	65	BAS_3387139	0.9461
16	BAS_0964142	0.8993	66	BAS_0620125	0.9463
17	BAS_3387347	0.9006	67	BAS_0222899	0.9468
18	BAS_2725225	0.9035	68	BAS_1122473	0.9469
19	BAS_3387060	0.9039	69	BAS_0844557	0.9491
20	BAS_1122488	0.9087	70	BAS_0844502	0.9516
21	BAS_5990601	0.9137	71	BAS_1122490	0.9532
22	BAS_3635578	0.9140	72	BAS_2987851	0.9543
23	BAS_0844556	0.9152	73	BAS_5022080	0.9547
24	BAS_5990712	0.9156	74	BAS_0964143	0.9553
25	BAS_0222915	0.9161	75	BAS_0732894	0.9557
26	BAS_0222918	0.9165	76	BAS_2725212	0.9559
27	BAS_4363483	0.9165	77	BAS_5829411	0.9563
28	BAS_0222916	0.9176	78	BAS_0341126	0.9563
29	BAS_0341128	0.9180	79	BAS_1228891	0.9564
30	BAS_3387180	0.9201	80	BAS_0414917	0.9569
31	BAS_1122472	0.9211	81	BAS_3387138	0.9569
32	BAS_0021983	0.9237	82	BAS_5291804	0.9570
33	BAS_0844559	0.9238	83	BAS_0222892	0.9579
34	BAS_0896617	0.9241	84	BAS_0491907	0.9583
35	BAS_0964141	0.9242	85	BAS_3301920	0.9587
36	BAS_2600118	0.9246	86	BAS_0844541	0.9589
37	BAS_0236268	0.9250	87	BAS_0253265	0.9592
38	BAS_0732891	0.9251	88	BAS_2549735	0.9598
39	BAS_6264821	0.9256	89	BAS_0253264	0.9601
40	BAS_1322638	0.9256	90	BAS_3819173	0.9605
41	BAS_3635676	0.9257	91	BAS_0620074	0.9622
42	BAS_3301924	0.9264	92	BAS_5829394	0.9622
43	BAS_6481840	0.9270	93	BAS_0844558	0.9642
44	BAS_1322652	0.9277	94	BAS_0844523	0.9644
45	BAS_0491826	0.9277	95	BAS_0844498	0.9644
46	BAS_0222910	0.9280	96	BAS_1059074	0.9652
47	BAS_0340791	0.9285	97	BAS_3386113	0.9657
48	BAS_4914705	0.9294	98	BAS_0620113	0.9659
49	BAS_0340790	0.9302	99	BAS_0620060	0.9661
50	BAS_1002446	0.9302	100	BAS_1118258	0.9661

Table 7.3-f. List containing the top 100 test compounds of the CATS run for reference molecule **R-06**. Molecules with blue ID were ordered, molecules with bold ID were ordered and delivered.

Rank	ID	Similarity Score	Rank	ID	Similarity Score
1	BAS_4299532	0.5254	51	BAS_5291883	0.6818
2	BAS_3387180	0.5467	52	BAS_0606759	0.6849
3	BAS_0393306	0.5640	53	BAS_3635673	0.6853
4	BAS_1004866	0.5804	54	BAS_1403566	0.6862
5	BAS_3387347	0.5807	55	BAS_0705188	0.6885
6	BAS_3635578	0.5883	56	BAS_3386040	0.6889
7	BAS_3387264	0.5934	57	BAS_1416427	0.6906
8	BAS_4328488	0.5940	58	BAS_6264800	0.6907
9	BAS_3387139	0.5947	59	BAS_0253264	0.6923
10	BAS_0406650	0.5953	60	BAS_1322643	0.6938
11	BAS_0702290	0.6069	61	BAS_0705221	0.6950
12	BAS_0606878	0.6106	62	BAS_1259647	0.6962
13	BAS_0161075	0.6137	63	BAS_5932036	0.6964
14	BAS_3387138	0.6189	64	BAS_0705220	0.6964
15	BAS_3635676	0.6226	65	BAS_0523555	0.6964
16	BAS_3387057	0.6263	66	BAS_1002424	0.6979
17	BAS_1268028	0.6272	67	BAS_5291802	0.7013
18	BAS_1002446	0.6317	68	BAS_3387311	0.7055
19	BAS_1004861	0.6347	69	BAS_3245128	0.7055
20	BAS_3245127	0.6384	70	BAS_3386029	0.7056
21	BAS_0406649	0.6389	71	BAS_0606854	0.7066
22	BAS_3386064	0.6436	72	BAS_0253265	0.7066
23	BAS_0686464	0.6450	73	BAS_1002513	0.7080
24	BAS_1002477	0.6482	74	BAS_0630784	0.7089
25	BAS_0774662	0.6509	75	BAS_0630770	0.7089
26	BAS_5932079	0.6514	76	BAS_5932057	0.7095
27	BAS_2987877	0.6543	77	BAS_0774663	0.7112
28	BAS_0406651	0.6550	78	BAS_1426717	0.7114
29	BAS_1416455	0.6556	79	BAS_0630769	0.7114
30	BAS_1002428	0.6560	80	BAS_1095379	0.7115
31	BAS_2987861	0.6567	81	BAS_0236242	0.7117
32	BAS_1403567	0.6573	82	BAS_3387344	0.7138
33	BAS_3387060	0.6575	83	BAS_0599010	0.7152
34	BAS_1403569	0.6577	84	BAS_0443481	0.7168
35	BAS_1268033	0.6589	85	BAS_1322631	0.7170
36	BAS_5291892	0.6590	86	BAS_2987851	0.7179
37	BAS_1004862	0.6592	87	BAS_1322652	0.7190
38	BAS_1403573	0.6592	88	BAS_1677419	0.7190
39	BAS_5931987	0.6593	89	BAS_3387473	0.7206
40	BAS_0630794	0.6600	90	BAS_3387474	0.7236
41	BAS_5291804	0.6601	91	BAS_2987946	0.7267
42	BAS_1004869	0.6628	92	BAS_2937446	0.7274
43	BAS_1004840	0.6647	93	BAS_0606853	0.7288
44	BAS_1074213	0.6650	94	BAS_0443480	0.7291
45	BAS_1003171	0.6652	95	BAS_1002476	0.7297
46	BAS_0851285	0.6677	96	BAS_0687521	0.7302
47	BAS_1322638	0.6694	97	BAS_0253261	0.7304
48	BAS_0606868	0.6735	98	BAS_2937456	0.7310
49	BAS_0606855	0.6735	99	BAS_0606749	0.7314
50	BAS_3387305	0.6775	100	BAS_0606736	0.7314

7.4 Collection of Virtual Hits obtained in Section 4.4

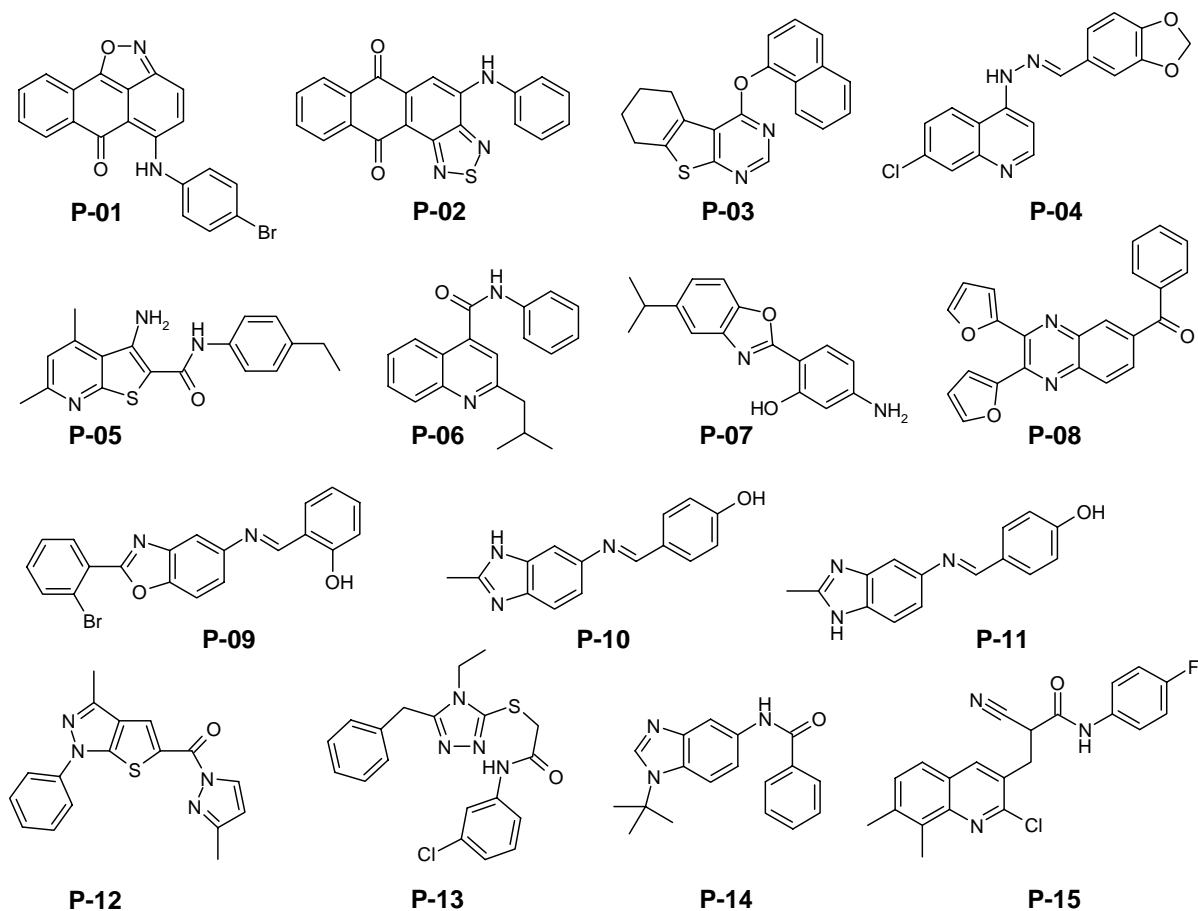


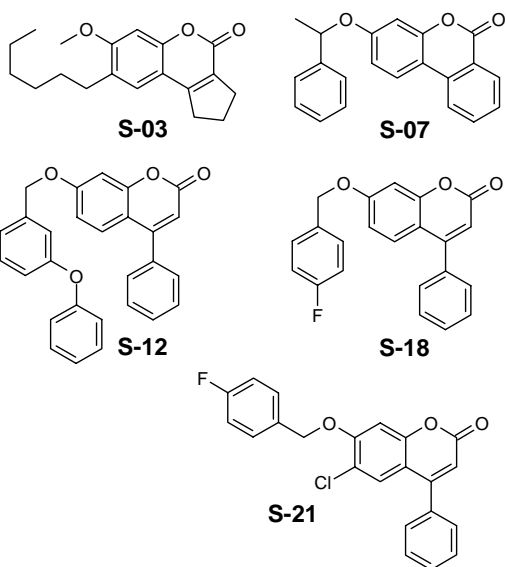
Figure 7.4-a. Set of compounds that were retrieved from the Asinex Gold Collection 2003 using the pharmacophore search and *ChemSpaceShuttle* (Section 4.4.3).

Table 7.4-a. List containing all 18 compounds that were selected by neighborhoodsearch in *ChemSpaceShuttle* and ordered (Section 4.4.3). Entries with no internal number were ordered but not delivered.

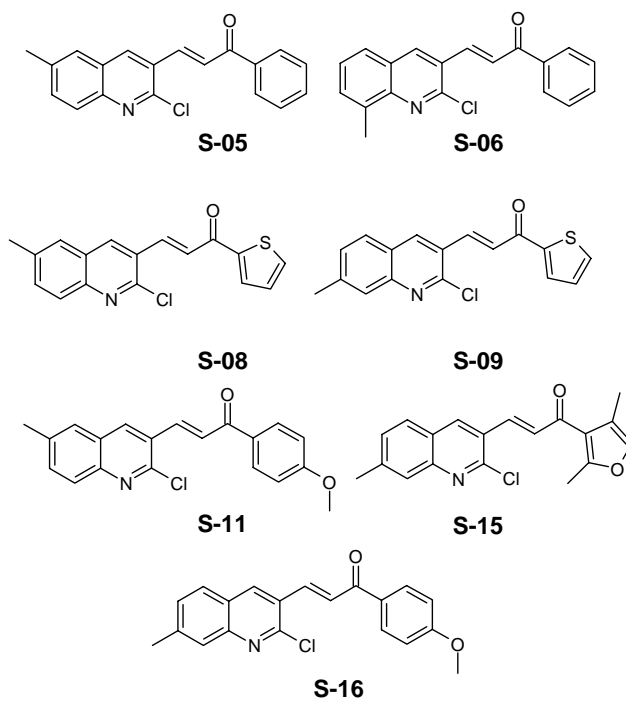
Vendor ID	Number	Vendor ID	Number
BAS_0165203	P-02	BAS_0918495	P-04
BAS_0192172	-	BAS_1121507	P-01
BAS_0272674	-	BAS_1356608	P-12
BAS_0311677	P-10	BAS_1365657	P-06
BAS_0318830	P-11	BAS_2054004	P-05
BAS_0332029	P-09	BAS_2104611	P-13
BAS_0565291	P-03	BAS_2255568	P-14
BAS_0866717	-	BAS_3108856	P-15
BAS_0914660	P-08	BAS_3847150	P-07

7.5 Collection of Virtual Hits obtained in Section 4.5

2*H*-Chromen-2-one derivatives



2-Chloroquinoline derivatives



Others

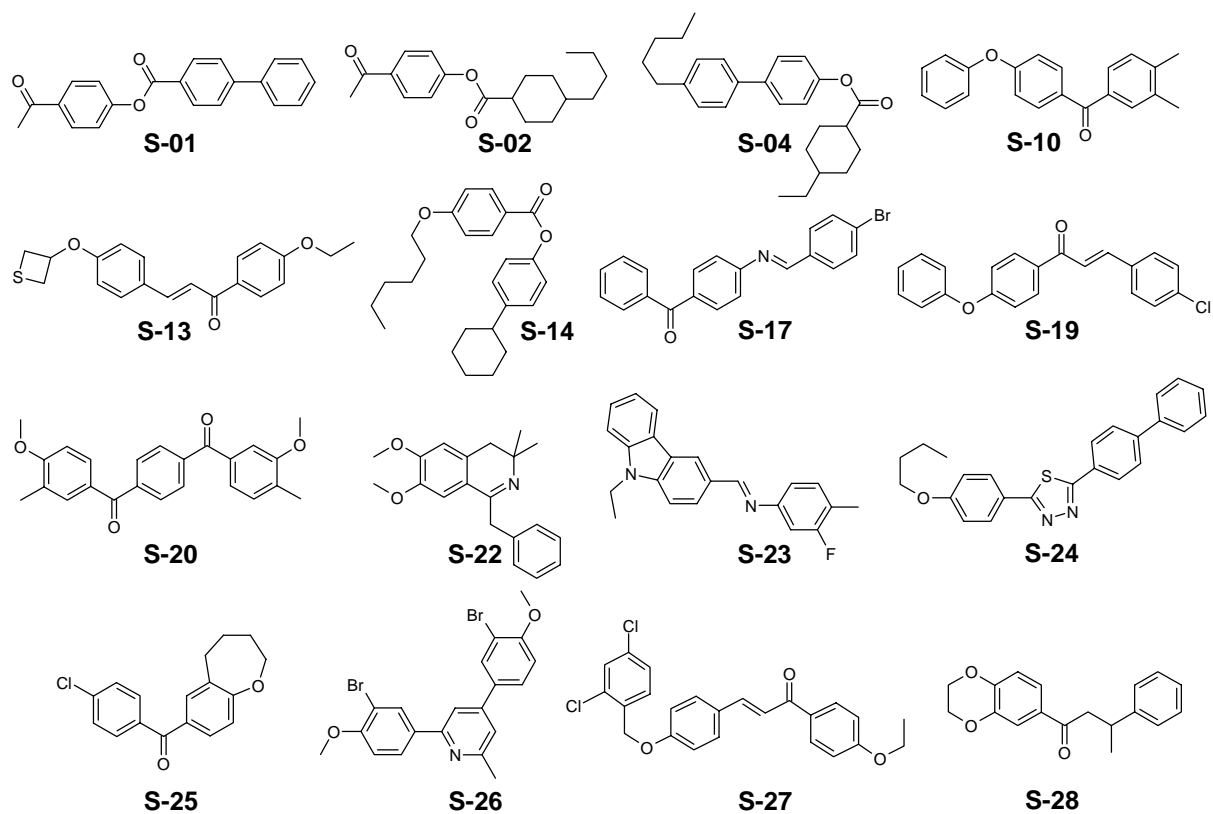


Figure 7.5-a. Set of compounds that were retrieved from the Asinex Gold Collection 2003 using the SOM approach (Section 4.5.2). Molecules were assigned to subsets according to their core structure.

Table 7.5-a. List displaying the 50 best ranked compounds retrieved from the Asinex database by the SOM approach (Section 4.5.2). Entries are sorted by ascending order with respect to their distance to the centroid of neuron 6/6 (15x15 map). Molecules with blue ID were ordered, molecules with bold ID were ordered and delivered.

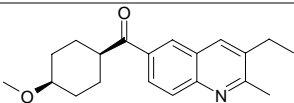
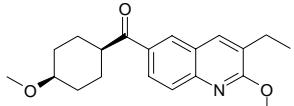
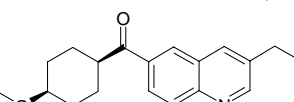
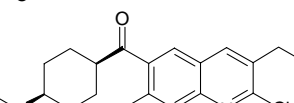
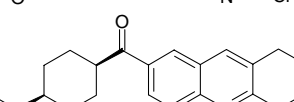
Vendor ID	Number	Distance (10x10)	Distance (15x15)
BAS_0395916	-	0.329	0.275
BAS_0395917	S-02	0.329	0.275
BAS_0511006	S-01	0.328	0.285
BAS_1123567	-	0.318	0.287
BAS_1018007	-	0.315	0.289
BAS_1018066	-	0.315	0.289
BAS_0872503	S-03	0.336	0.293
BAS_0395926	-	0.339	0.299
BAS_1123565	S-04	0.346	0.306
BAS_2276953	S-05	0.342	0.308
BAS_0084923	-	0.345	0.310
BAS_0726371	-	0.338	0.314
BAS_2276957	S-06	0.355	0.316
BAS_0872364	S-07	0.377	0.318
BAS_2276986	S-08	0.356	0.324
BAS_0297500	-	0.381	0.326
BAS_2276985	S-09	0.370	0.327
BAS_0084926	S-10	0.358	0.328
BAS_2276955	S-11	0.392	0.328
BAS_0872424	S-12	0.348	0.332
BAS_0794556	S-13	0.363	0.334
BAS_1123720	-	0.318	0.334
BAS_0434242	-	0.382	0.336
BAS_1293648	-	0.374	0.336
BAS_0203181	S-14	0.399	0.338
BAS_1416611	S-15	0.391	0.338
BAS_0308659	S-16	0.410	0.340
BAS_0594844	S-17	0.383	0.342
BAS_0872398	S-18	0.378	0.347
BAS_1018019	S-19	0.376	0.348
BAS_1018064	-	0.375	0.348
BAS_2276958	-	0.382	0.348
BAS_0316110	S-20	0.370	0.351
BAS_0872419	S-21	0.371	0.352
BAS_0329602	S-22	0.358	0.354
BAS_0099446	-	0.397	0.355
BAS_0530782	S-23	0.399	0.356
BAS_0129956	-	0.423	0.357
BAS_0260628	S-24	0.372	0.359
BAS_1293659	S-25	0.396	0.359
BAS_0369559	-	0.405	0.361
BAS_0395869	-	0.385	0.361
BAS_0119417	S-26	0.371	0.362
BAS_0872214	-	0.420	0.362
BAS_2276984	-	0.399	0.364
BAS_0530807	-	0.392	0.365
BAS_0162450	-	0.415	0.369
BAS_0393988	S-27	0.397	0.369
BAS_0669563	S-28	0.371	0.370
BAS_0203174	-	0.415	0.372

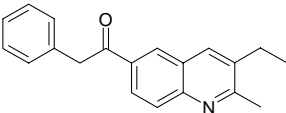
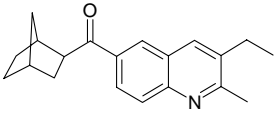
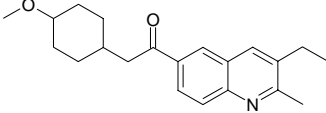
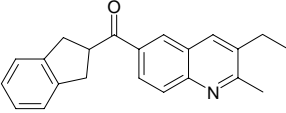
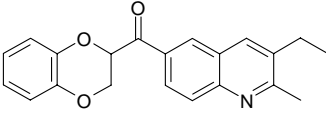
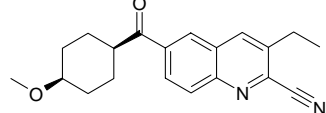
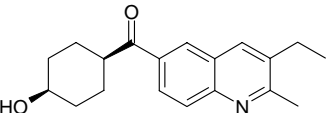
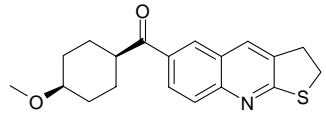
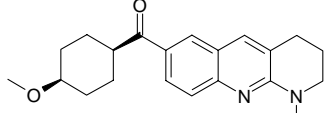
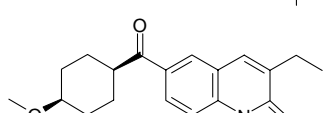
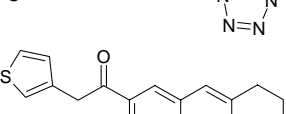
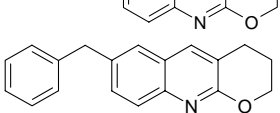
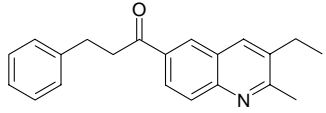
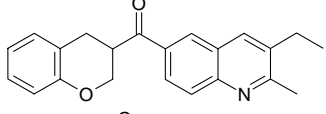
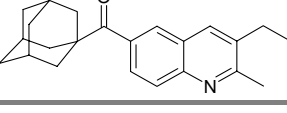
7.6 Statistical Indices and Compounds from Section 5.1.1

Table 7.6-a. Statistical indices for ten independent CoMFA models. All 39 molecules were randomly assigned either to the training or the test set, both of which having nearly equivalent size (training set: 20; test set: 19). For each model the same molecular alignment in the same spatial orientation was used.

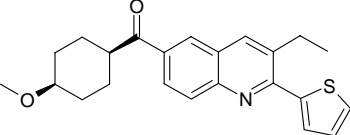
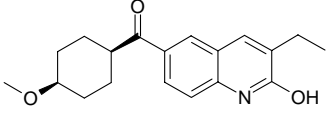
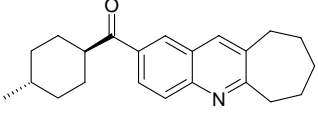
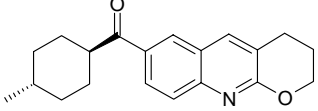
Model	q ² (cv)	SEP	Components	F	r ²	SEE	% steric	% electr.
1	0.576	0.625	4	107.576	0.966	0.176	70.2	29.8
2	0.503	0.721	3	55.115	0.912	0.304	65.9	34.1
3	0.294	0.679	2	34.856	0.804	0.358	78.0	22.0
4	0.598	0.661	4	59.741	0.941	0.253	68.8	31.2
5	0.616	0.645	3	62.371	0.921	0.292	70.1	29.9
6	0.553	0.519	1	56.260	0.758	0.382	56.2	43.8
7	0.389	0.675	4	70.535	0.950	0.194	69.8	30.2
8	0.523	0.667	4	77.466	0.951	0.214	70.0	30.0
9	0.389	0.557	4	43.546	0.921	0.208	62.1	37.9
10	0.626	0.700	7	303.750	0.994	0.086	70.0	30.0
Mean	0.507	0.645	3.6	87.122	0.912	0.247	68.1	31.9
SEM	0.036	0.020	0.5	24.874	0.023	0.028	1.8	1.8

Table 7.6-b. Series of 39 quinoline derivatives used for the present CoMFA study. Entries are sorted with respect to their internal ID number.

Molecule-ID	Structure	pIC ₅₀ -value	Dataset
2		8.52	training
3		7.72	training
4		8.40	training
5		8.30	training
8		7.82	training

10		8.00	test
11		7.89	test
12		7.80	test
15		7.25	test
18		7.08	test
19		7.96	test
20		7.30	training
21		8.70	training
22		8.10	training
25		7.35	training
26		8.16	training
30		7.07	training
458		6.64	training
464		6.94	training
465		6.90	training

466		6.79	training
1726		8.22	test
1907		8.52	test
1909		8.40	test
1912		8.40	training
1915		8.30	training
1926		8.16	training
1927		8.16	training
2155		5.63	training
2156		6.84	training
2157		7.19	training
2158		7.89	training
2159		5.47	training
2160		7.11	training
2161		6.08	training

2162		5.48	training
2164		7.10	training
2165		7.96	training
2166		6.90	training

8 References

D.M. Van Aalten, R. Bywater, J.B. Findlay, M. Hendlich, R.W. Hooft, G. Vriend, PRODRG, a program for generating molecular topologies and unique molecular descriptors from coordinates of small molecules. *J. Comput. Aided Mol. Des.* **1996**, *10*, 255-262.

F.C. Acher, H.O. Bertrand, Amino acid recognition by Venus flytrap domains is encoded in an 8-residue motif. *Biopolymers* **2005**, *80*, 357-366.

D.K. Agrafiotis, V.S. Lobanov, Nonlinear mapping methods. *J. Chem. Inf. Comput. Sci.* **2000**, *40*, 1356-1362.

D.K. Agrafiotis, V.S. Lobanov, F.R. Salemme, Combinatorial informatics in the post-genomics ERA. *Nat. Rev. Drug Discov.* **2002**, *1*, 337-346.

H. Alonso, A.A. Bliznyuk, J.E. Gready, Combining docking and molecular dynamic simulations in drug design. *Med. Res. Rev.* **2006**, *26*, 531-568.

J.J. Anderson, S.P. Rao, B. Rowe, D.R. Giracello, G. Holtz, D.F. Chapman, L. Tehrani, M.J. Bradbury, N.D.P. Cosford, M.A. Varney, [³H]Methoxymethyl-3-[(2-methyl-1,3-thiazol-4-yl)ethynyl]pyridine Binding to Metabotropic Glutamate Receptor Subtype 5 in Rodent Brain: In Vitro and in Vivo Characterization. *J. Pharmacol. Exp. Ther.* **2002**, *303*, 1044-1051.

S. Anzali, G. Barnickel, M. Krug, J. Sadowski, M. Wagener, J. Gasteiger, J. Polanski, The comparison of geometric and electronic properties of molecular surfaces by neural networks: application to the analysis of corticosteroid-binding globulin activity of steroids. *J. Comput. Aided Mol. Des.* **1996**, *10*, 521-534.

Asinex Ltd., Moscow, Russia; <http://www.asinex.com/prod/gold.html>

H. Awad, G.W. Hubert, Y. Smith, A.I. Levey, P.J. Conn, Activation of metabotropic glutamate receptor 5 has direct excitatory effects and potentiates NMDA receptor currents in neurons of the subthalamic nucleus. *J. Neurosci.* **2001**, *20*, 7871-7879.

T. Bäck, H.-P. Schwefel, An overview of evolutionary algorithms for parameter optimization. *Evol. Comput.* **1993**, *1*, 1-23.

J. Bajorath, Integration of virtual and high-throughput screening. *Nat. Rev. Drug Discov.* **2002**, *1*, 882-894.

J.M. Baldwin, The probable arrangement of the helices in G protein-coupled receptors. *EMBO J.* **1993**, *12*, 1693-1703.

J.A. Ballesteros, H. Weinstein, Integrated methods for the construction of three dimensional models and computational probing of structure-function relations in G-protein coupled receptors, in *Methods in Neuroscience*. Academic Press, San Diego, CA, USA, pp. 366-428, 1999.

C. Bargmann, Olfactory receptors, vomeronasal receptors, and the organization of olfactory information. *Cell* **1997**, *90*, 585-587.

J.M. Barnard, Substructure Searching Methods: Old and New. *J. Chem. Inf. Comput. Sci.* **1993**, *33*, 532-538.

A. Bender, H.Y. Mussa, R.C. Glen, Screening for dihydrofolate reductase inhibitors using MOLPRINT 2D, a fast fragment-based method employing the naive Bayesian classifier: limitations of the descriptor and the importance of balanced chemistry in training and test sets. *J. Biomol. Screen.* **2005**, *10*, 658-666.

BD Biosciences, Heidelberg, Germany; <http://www.bdeurope.com>

O.M. Becker, S. Shacham, Y. Marantz, S. Noiman, Modeling the 3D structure of GPCRs: advances and application to drug discovery. *Curr. Opinion in Drug Discovery & Dev.* **2003**, *6*, 353-361.

M.S. Belenikin, G. Costantino, V.A. Palyulin, R. Pellicciari, N.S. Zefirov, Molecular modeling of the mGluR1 metabotropic glutamate receptor transmembrane domain and construction of the model of its dimer. *Dokl. Biochem. Biophys.* **2003**, *393*, 341-345.

A. Bender, H.Y. Mussa, R.C. Glen, S. Reiling, Similarity searching of chemical databases using atom environment descriptors (MOLPRINT 2D): evaluation of performance. *J. Chem. Inf. Comput. Sci.* **2004**, *44*, 1708-1718.

P. Bernard, D. Guedin, M. Hibert, Molecular modeling of the GABA/GABA(B) receptor complex. *J. Med. Chem.* **2001**, *44*, 27-35.

Biochrom AG, Berlin, Germany; <http://www.biochrom.de>

Biorad Laboratories GmbH, München, Germany; <http://www.bio-rad.com>

- L. Birch, C.W. Murray, M.J. Hartshorn, I.J. Tickle, M.L. Verdonk, Sensitivity of molecular docking to induced fit effects in influenza virus neuraminidase. *J. Comput. Aided Mol. Des.* **2002**, *16*, 855-869.
- C. Bissantz, Conformational changes of G protein-coupled receptors during their activation by agonist binding. *J. Recept. Signal. Transduct. Res.* **2003**, *23*, 123-153.
- C. Bissantz, P. Bernard, M. Hibert, D. Rognan, Protein-based virtual screening of chemical databases. II. Are homology models of G-Protein Coupled Receptors suitable targets? *Proteins* **2003**, *50*, 5-25.
- C. Bissantz, C. Schalon, W. Guba, M. Stahl, Focused library design in GPCR projects on the example of 5-HT(2c) agonists: comparison of structure-based virtual screening with ligand-based search methods. *Proteins* **2005**, *61*, 938-951.
- J. Bockaert, J.P. Pin, Molecular tinkering of G protein-coupled receptors: an evolutionary process. *EMBO J.* **1999**, *18*, 1723-1729.
- A. Böcker, G. Schneider, A. Teckentrup, Status of HTS Data Mining Approaches. *QSAR & Comb. Sci.* **2004**, *23*, 207-213.
- H.-J. Böhm, G. Schneider, *Virtual Screening for Bioactive Molecules*. Wiley-VCH, Weinheim, Germany, 2000.
- M. Böhm, J. Stürzebecher, G. Klebe, Three-dimensional quantitative structure-activity relationship analyses using comparative molecular field analysis and comparative molecular similarity indices analysis to elucidate selectivity differences of inhibitors binding to trypsin, thrombin, and factor Xa. *J. Med. Chem.* **1999**, *42*, 458-477.
- C. Bonnefous, J.M. Vernier, J.H. Hutchinson, J. Chung, G. Reyes-Manalo, T. Kamenecka, Dipyrindyl amides: potent metabotropic glutamate subtype 5 (mGlu5) receptor antagonists. *Bioorg. Med. Chem. Lett.* **2005**, *15*, 1197-1200.
- J. Booher, M. Sensenbrenner, Growth and cultivation of dissociated neurons and glial cells from embryonic chick, rat and human brain in flask cultures. *Neurobiology* **1972**, *2*, 97-105.
- B.E. Boser, I.M. Guyon, V.N. Vapnik, *A training algorithm for optimal margin classifiers*. In D. Haussler (Ed.), 5th Annual ACM Workshop on COLT. ACM Press, Pittsburgh, PA, USA, pp. 144-152, 1992.
- L. Breiman, J. Friedman, R.A. Olshen, C.J. Stone, *Classification and Regression Trees*. CRC Press LLC, Boca Raton, Florida, USA, 1984.

I. Bresink, W. Danysz, C.G. Parsons, E. Mutschler, Different binding affinities of NMDA receptor channel blockers in various brain regions - indication of NMDA receptor heterogeneity. *Neuropharmacology* **1995**, *34*, 533-540.

E.M. Brown, G. Gamba, D. Riccardi, M. Lombardi, R. Butters, O. Kifor, A. Sun, M.A. Hediger, J. Lytton, S.C. Hebert, Cloning and characterization of an extracellular Ca(2+)-sensing receptor from bovine parathyroid. *Nature* **1993**, *366*, 575-580.

V. Bruno, G. Battaglia, A. Copani, R.G. Giffard, G. Raciti, R. Raffaele, H. Shinozaki, F. Nicoletti, Activation of class II or III metabotropic glutamate receptors protects cultured cortical neurons against excitotoxic degeneration. *Eur. J. Neurosci.* **1995**, *7*, 1906-1913

V. Bruno, I. Ksiazek, G. Battaglia, S. Lukic, T. Leonhardt, D. Sauer, F. Gasparini, R. Kuhn, F. Nicoletti, P.J. Flor, Selective blockade of metabotropic glutamate receptor subtype 5 is neuroprotective. *Neuropharmacology* **2000**, *39*, 2223-2230.

S. K. Burley, J. B. Bonanno, Structuring the universe of proteins. *Annu. Rev. Genomics Hum. Genet.* **2002**, *3*, 243-262.

E. Byvatov, U. Fechner, J. Sadowski, G. Schneider, Comparison of Support Vector Machine and Artificial Neural Network Systems for Drug/Nondrug Classification. *J. Chem. Inf. Comput. Sci.* **2003**, *43*, 1882-1889.

E. Byvatov, B.C. Sasse, H. Stark, G. Schneider, From Virtual to Real Screening for D₃ Dopamine Receptor Ligands. *ChemBioChem* **2005**, *6*, 997-999.

L. Camon, P. Vives, N. de Vera, E. Martinez, Seizures and neuronal damage induced in the rat by activation of group I metabotropic glutamate receptors with their selective agonist 3,5-dihydroxyphenylglycine. *J. Neurosci. Res.* **1998**, *51*, 339-348.

R.E. Carhart, D.H. Smith, R. Venkataraghavan, Atom pairs as molecular features in structure-activity studies: definition and applications. *J. Chem. Inf. Comput. Sci.* **1985**, *25*, 64-73.

F.Y. Carroll, A. Stolle, P.M. Beart, A. Voerste, I. Brabet, F. Mauler, C. Joly, H. Antonicek, J. Bockaert, T. Muller, J.P. Pin, L. Prezeau, BAY36-7620: a potent non-competitive mGlu1 receptor antagonist with inverse agonist activity. *Mol. Pharmacol.* **2001**, *59*, 965-973.

C.N. Cavasotto, A.J.W. Orry, R.A. Abagyan, Structure-based identification of binding sites, native ligands and potential inhibitors for G-protein coupled receptors. *Proteins* **2003**, *51*, 423-433.

M.Y. Cha, I.Y. Lee, J.H. Cha, K.I. Choi, Y.S. Cho, H.Y. Koh, A.N. Pae, QSAR studies on piperazinylalkylisoxazole analogues selectively acting on dopamine D3 receptor by HQSAR and CoMFA. *Bioorg. Med. Chem.* **2003**, *11*, 1293-1298.

A.G. Chapman, P.K. Yip, J.S. Yap, L.P. Quinn, E. Tang, J.R. Harris, B.S. Meldrum, Anticonvulsant actions of LY367385 ((+)-2-methyl-4-carboxyphenylglycine) and AIDA ((RS)-1-aminoindan-1,5-dicarboxylic acid). *Eur. J. Pharmacol.* **1999**, *368*, 17-24.

A.G. Chapman, K. Nanan, M. Williams, B.S. Meldrum, Anticonvulsant activity of two metabotropic glutamate group I antagonists selective for the mGlu5 receptor: 2-methyl-6-(phenylethynyl)-pyridine (MPEP), and (E)-6-methyl-2-styryl-pyridine (SIB 1893). *Neuropharmacology* **2000**, *39*, 1567-1574.

Chemical Computing Group, Montreal, Canada; <http://www.chemcomp.com>

C. Cheng, W.H. Prusoff, Relationship between the inhibition constant (K_i) and the concentration of inhibitor which causes 50 percent inhibition (IC_{50}) of an enzymatic reaction. *Biochem. Pharmacol.* **1973**, *22*, 3099-3108.

M. Clark, R.D. Cramer, N. van Opdenbosch, Validation of the general purpose tripos 5.2 force field. *J. Comput. Chem.* **1989**, *10*, 982-1012.

A.E. Cleves, A.N. Jain, Robust ligand-based modeling of the biological targets of known drugs. *J. Med. Chem.* **2006**, *49*, 2921-2938.

A.D. Conigrave, S.J. Quinn, E.M. Brown, L-amino acid sensing by the extracellular Ca^{2+} -sensing receptor. *Proc. Natl. Acad. Sci. USA* **2000**, *97*, 4814-4819.

P.J. Conn, J.P. Pin, Pharmacology and functions of metabotropic glutamate receptors. *Annu. Rev. Pharmacol. Toxicol.* **1997**, *37*, 205-237.

N.D.P. Cosford, L. Tehrani, J. Roppe, E. Schweiger, N.D. Smith, J. Anderson, L. Bristow, J. Brodtkin, X. Jiang, I. McDonald, S. Rao, M. Washburn, M.A. Varney, 3-[(2-Methyl-1,3-thiazol-4-yl)ethynyl]-pyridine: a potent and highly selective metabotropic glutamate subtype 5 receptor antagonist with anxiolytic activity. *J. Med. Chem.* **2003**, *46*, 204-206.

N.D.P. Cosford, J. Roppe, L. Tehrani, E.J. Schweiger, T.J. Seiders, A. Chaudary, S.P. Rao, M.A. Varney, [3H]-methoxymethyl-MTEP and [3H]-methoxy-PEPy: potent and selective radioligands for the metabotropic glutamate subtype 5 (mGlu5) receptor. *Bioorg. Med. Chem. Lett.* **2003**, *13*, 351-354.

CoStar Group, Inc., Bethesda, MD, USA; <http://www.costar.com>

R.D. Cramer, D.E. Patterson, J.D. Bunce, Comparative Molecular field Analysis (CoMFA). 1. Effect of Shape on Binding of Steroids to Carrier Proteins. *J. Am. Chem. Soc.* **1988**, *110*, 5959-5967.

R.D. Cramer, J.D. Bunce, D.E. Patterson, I.E., Frank, Cross-validation, Bootstrapping and Partial Least Squares Compared with Multiple Regression in Conventional QSAR Studies. *Quant. Struct.-Act. Relat.* **1988**, *7*, 18-25.

Daylight Chemical Information Systems, Inc., Mission Viejo, CA, USA;
<http://www.daylight.com>

G.R. Desiraju, T. Steiner (Ed.), *The Weak Hydrogen Bond*. Oxford University Press, New York, USA, pp. 14-16, 1999.

D.J. Devillers, Display of multivariate data using non-linear mapping. In H. van de Waterbeemd (Ed.), *Chemometric Methods in Molecular Design*. Wiley-VCH, Weinheim, pp. 255-263, 1995.

P. Diaconis, B. Efron, Computer-intensive methods in statistics. *Sci. Amer.* **1983**, 116-130.

G.M. Downs, P. Willett, Similarity Searching in Databases of Chemical Structures. *Rev. Comput. Chem.* **1995**, *7*, 1-66.

DRUQUEST International, Inc., Preclinical Development Consulting Services;
<http://www.druquest.com>

B. Eastman, C. Chen, N.D. Smith, S. Poon, J. Chung, G. Reyes-Manalo, N.D. Cosford, B. Munoz, Expedited SAR study of an mGluR5 antagonists: generation of a focused library using a solution-phase Suzuki coupling methodology. *Bioorg. Med. Chem. Lett.* **2004**, *14*, 5485-5488.

H. Eckert, J. Bajorath, Design and Evaluation of a Novel Class-Directed 2D Fingerprint to Search for Structurally Diverse Active Compounds. *J. Chem. Inf. Model.* **2006**, *46*, 2515-2526.

P. Ehrlich, Über den jetzigen Stand der Chemotherapie. *Dtsch. Chem. Ges.* **1909**, *42*, 17.

A. Evers, G. Hessler, H. Matter, T. Klabunde, Virtual screening of biogenic amine-binding G-protein coupled receptors: comparative evaluation of protein- and ligand-based virtual screening protocols. *J. Med. Chem.* **2005**, *48*, 5448-5465.

- U. Fechner, L. Franke, S. Renner, P. Schneider, G. Schneider, Comparison of correlation vector methods for ligand-based similarity searching. *J. Comput. Aided Mol. Des.* **2003**, *17*, 687-698.
- M. Fernandez, J. Caballero, A. Tundidor-Camba, Linear and nonlinear QSAR study of N-hydroxy-2-[(phenylsulfonyl)amino]acetamide derivatives as matrix metalloproteinase inhibitors. *Bioorg. Med. Chem.* **2006**, *14*, 4137-4150.
- K. Fisher, T.J. Coderre, Hyperalgesia and allodynia induced by intrathecal (RS)-dihydroxyphenylglycine in rats. *Neuroreport* **1998**, *9*, 1169-1172.
- S.M. Fitzjohn, A.J. Irving, M.J. Palmer, J. Harvey, D. Lodge, G.L. Collingridge, Activation of group I mGluRs potentiates NMDA responses in rat hippocampal slices. *Neurosci. Lett.* **1996**, *203*, 211-213.
- A.C. Foster, E.H.F. Wong, The novel anticonvulsant MK-801 binds to the activated state of the N-methyl-D-aspartate receptor in rat brain. *Br. J. Pharmac.* **1987**, *91*, 403-409.
- S.M. Free, J.A. Wilson, A mathematical contribution to structure-activity studies. *J. Med. Chem.* **1964**, *7*, 395-399.
- T. Galvez, M.L. Parmentier, C. Joly, B. Malitschek, K. Kaupmann, R. Kuhn, H. Bittiger, W. Froestl, B. Bettler, J.P. Pin, Mutagenesis and modeling of the GABAB receptor extracellular domain support a venus flytrap mechanism for ligand binding. *J. Biol. Chem.* **1999**, *274*, 13362-13369.
- T. Galvez, S. Urwyler, L. Prezeau, J. Mosbacher, C. Joly, B. Malitschek, J. Heid, I. Brabet, W. Froestl, B. Bettler, K. Kaupmann, J. P. Pin, Ca(2+) requirement for high-affinity gamma-aminobutyric acid (GABA) binding at GABA(B) receptors: involvement of serine 269 of the GABA(B)R1 subunit. *Mol. Pharmacol.* **2000**, *57*, 419-426.
- T. Galvez, B. Duthey, J. Kniazeff, J. Blahos, G. Rovelli, B. Bettler, L. Prezeau, J.P. Pin, Allosteric interactions between GB1 and GB2 subunits are required for optimal GABA(B) receptor function. *EMBO J.* **2001**, *20*, 2152-2159.
- F. Gasparini, K. Lingenhohl, N. Stoehr, P.J. Flor, M. Heinrich, I. Vranesic, M. Biollaz, H. Allgeier, R. Heckendorn, S. Urwyler, M.A. Varney, E.C. Johnson, S.D. Hess, S.P. Rao, A.I. Saccaan, E.M. Santori, G. Velicelebi, R. Kuhn, 2-Methyl-6-(phenylethynyl)-pyridine (MPEP), a potent, selective and systemically active mGlu5 receptor antagonist. *Neuropharmacology* **1999**, *38*, 1493-1503.

F. Gasparini, H. Andres, P.J. Flor, M. Heinrich, W. Inderbitzin, K. Lingenhöhl, H. Müller, V.C. Munk, K. Omilusik, C. Stierlin, N. Stoehr, I. Vranesic, R. Kuhn, [3H]-M-MPEP, a Potent, Subtype-Selective Radioligand for the Metabotropic Glutamate Receptor Subtype 5. *Bioorg. Med. Chem. Lett.* **2001**, *12*, 407-409.

F. Gasparini, R. Kuhn, J.P. Pin, Allosteric modulators of group I metabotropic glutamate receptors: novel subtype-selective ligands and therapeutic perspectives. *Curr. Op. Pharmacol.* **2002**, *2*, 43-49.

U. Gether, B.K. Kobilka, G protein-coupled receptors. II. Mechanism of agonist activation. *J. Biol. Chem.* **1998**, *273*, 17979-17982.

V.J. Gillet, P. Willett, J. Bradshaw, Identification of biological activity profiles using substructural analysis and genetic algorithms. *J. Chem. Inf. Comput. Sci.* **1998**, *38*, 165-179.

A. Givehchi, A. Dietrich, P. Wrede, G. Schneider, ChemSpaceShuttle: A tool for data mining in drug discovery by classification, projection and 3D visualization. *QSAR and Comb. Sci.* **2003**, *22*, 549-559.

R.C. Glen, G.R. Martin, A.P. Hill, R.M. Hyde, P.M. Woollard, J.A. Salmon, J. Buckingham, A.D. Robertson, Computer-aided design and synthesis of 5-substituted tryptamines and their pharmacology at the 5-HT_{1D} receptor: discovery of compounds with potential anti-migraine properties. *J. Med. Chem.* **1995**, *38*, 3566-3580.

R.C. Glen, S.E. Adams, Similarity Metrics and Descriptor Spaces – Which Combinations to Choose? *QSAR & Comb. Sci.* **2006**, *25*, 1133-1142.

A.C. Good, I.D. Kuntz, Investigating the extension of pairwise distance pharmacophore measures to triplet-base descriptors. *J. Comput. Aided Mol. Des.* **1995**, *9*, 373-379.

C. Goudet, F. Gaven, J. Kniazeff, C. Vol, J. Liu, M. Cohen-Gonsaud, Acher, L. Prezeau, J.P. Pin, Heptahelical domain of metabotropic glutamate receptor 5 behaves like rhodopsin-like receptors. *Proc. Natl. Acad. Sci. USA* **2004**, *101*, 378-383.

Grafit Erithacus Software Ltd., Surrey, UK; <http://www.erithacus.com>

GraphPad Software, Inc., San Diego, CA, USA; <http://www.graphpad.com>

S.M. Grauer, K.L. Marquis, Intracerebral administration of metabotropic glutamate receptor agonists disrupts prepulse inhibition of acoustic startle in Sprague–Dawley rats. *Psychopharmacology Berl.* **1999**, *141*, 405–412.

Greiner Bio-One GmbH, Frickenhausen, Germany; <http://www.gbo.com>

G.-A. Guérin, J. Pratuangdejkul, M. Alemany, J.-M. Launay, P. Manivet, Rational and efficient geometric definition of pharmacophores is essential for the patent process. *Drug Discov. Today* **2006**, *11*, 991-998.

T.A. Halgren, Merck molecular force field. II. MMFF94 van der Waals and electrostatic parameters for intermolecular interactions. *J. Comp. Chem.* **1996**, *17*, 520-552.

L.G. Hammerland, K.J. Krapcho, J.E. Garret, N. Alasti, B.C. Hung, R.T. Simin, C. Levinthal, E.F. Nemeth, F.H. Fuller, Domains determining ligand specificity for Ca²⁺ receptors. *Mol. Pharmacol.* **1999**, *55*, 642-648.

C. Hansch, T. Fujita, ρ - σ - π Analysis. A Method for the Correlation of Biological Activity and Chemical Structure. *J. Am. Chem. Soc.* **1964**, *86*, 1616-1626.

P.J. O'Hara, P.O. Sheppard, H. Thogersen, D. Venezia, B.A. Haldeman, V. McGrane, K.M. Houamed, C. Thomsen, T.L. Gilbert, E.R. Mulvihill, The ligand-binding domain in metabotropic glutamate receptors is related to bacterial periplasmic binding proteins. *Neuron* **1993**, *11*, 41-52.

E. Hawrot, Y. Xiao, Q.L. Shi, D. Norman, M. Kirkitadze, P.N. Barlow, Demonstration of a tandem pair of complement protein modules in GABA(B) receptor 1a. *FEBS Lett.* **1998**, *432*, 103-108.

G. Hayes, T.J. Biden, L.A. Selbie, J. Shine, Structural subtypes of the dopamine D2 receptor are functionally distinct: expression of the cloned D2A and D2B subtypes in a heterologous cell line. *Mol. Endocrinol.* **1992**, *6*, 920-926.

E. Hermans, S.R. Nahorski, R.A. Challiss, Reversible and non-competitive antagonist profile of CPCOEt at the human type 1alpha metabotropic glutamate receptor. *Neuropharmacology* **1998**, *37*, 1645-1647.

A. Hillisch, L.F. Pineda, R. Hilgenfeld, Utility of homology models in the drug discovery process. *Drug Discov. Today* **2004**, *9*, 659-669.

T.K. Ho, *Random Decision Forests*. Proc. of the 3rd Int. Conf. on Document Analysis and Recognition. Montreal, Canada, Aug. 14-18, pp. 278-282, 1995.

M. Hollmann, S. Heinemann, Cloned glutamate receptors. *Annu. Rev. Neurosci.* **1994**, *17*, 31-108.

M.A. Hoon, E. Adler, J. Lindemeier, J.F. Battey, N.J. Ryba, C.S. Zuker, Putative mammalian taste receptors: a class of taste-specific GPCRs with distinct topographic selectivity. *Cell* **1999**, *96*, 541-551.

J.R. Hoult, M. Paya, Pharmacological and biochemical actions of simple coumarins: natural products with therapeutic potential. *Gen. Pharmacol.* **1996**, *27*, 713-722.

IKA-Werke GmbH & Co. KG, Staufen, Germany; <http://www.ika.de>

P. Jaccard, Etude comparative de la distribution florale d'une portion des Alpes et du Jura. *Bull. Soc. Vaud. Sci. Nat.* **1901**, *37*, 547-579.

M. Johnson, G.M. Maggiora, *Concepts and Applications of Molecular Similarity*. John Wiley & Sons, Inc., New York, NY, USA, 1990.

K.A. Jones, B. Borowsky, J.A. Tamm, D.A. Craig, M.M. Durkin, M. Dai, W.J. Yao, M. Johnson, C. Grunwaldsen, L.Y. Huang, C. Tang, Q. Shen, J.A. Salon, K. Morse, T. Laz, K.E. Smith, D. Nagarathnam, S.A. Noble, T.A. Branchek, C. Gerald, GABA(B) receptors function as a heteromeric assembly of the subunits GABA(B)R1 and GABA(B)R2. *Nature* **1998**, *396*, 674-679.

Karl Hecht GmbH & Co. KG, Sondheim, Germany; <http://www.hecht-assistant.de>

W.T. Katz, J.W. Snell, M.B. Merickel, Artificial Neural Networks. *Methods Enzymol.* **1992**, *210*, 610-636.

K. Kaupmann, B. Malitschek, V. Schuler, J. Heid, W. Froestl, P. Beck, J. Mosbacher, S. Bischoff, A. Kulik, R. Shigemoto, A. Karschin, B. Bettler, GABA(B)-receptor subtypes assemble into functional heteromeric complexes. *Nature* **1998**, *396*, 683-687.

T.P. Kenakin, *Pharmacologic Analysis of Drug-Receptor Interaction*. Raven Press, New York, USA, pp. 286-299, 1987.

L.B. Kier, *Molecular Orbital Theory in Drug Research*. Academic, New York, USA, 1971

G.G. Kinney, J.A. O'Brien, W. Lemaire, M. Burno, D.J. Bickel, M.K. Clements, T.B. Chen, D.D. Wisnoski, C.W. Lindsley, P.R. Tiller, S. Smith, M.A. Jacobson, C. Sur, M.E. Duggan, D.J. Pettibone, P.J. Conn, D.L. Williams Jr., A novel selective positive allosteric modulator of

metabotropic glutamate receptor subtype 5 has in vivo activity and antipsychotic-like effects in rat behavioral models. *J. Pharmacol. Exp. Ther.* **2005**, *313*, 199-206.

Kendro Laboratory Products, Langenselbold, Germany; <http://www.kendro.com>

T. Klabunde, G. Hessler, Drug Design Strategies for Targeting G-Protein-Coupled Receptors. *ChemBioChem* **2002**, *3*, 928-944.

G. Klebe, U. Abraham, T. Mietzner, Molecular similarity indices in comparative analysis (CoMSIA) of drug molecules to correlate and predict their biological activity. *J. Med. Chem.* **1994**, *37*, 4130-4146.

A.E. Klon, J.F. Lowrie, D.J. Diller, Improved Naive Bayesian Modeling of Numerical Data for Absorption, Distribution, Metabolism and Excretion (ADME) Property Prediction. *J. Chem. Inf. Model.* **2006**, *46*, 1945-1956.

F. Knoflach, V. Mutel, S. Jolidon, J.N. Kew, P. Malherbe, E. Vieira, J. Wichmann, J.A. Kemp, Positive allosteric modulators of metabotropic glutamate 1 receptor: characterization, mechanism of action, and binding site. *Proc. Natl. Acad. Sci. USA* **2001**, *98*, 13402-13407.

B. Kobilka, Allosteric activation of the CaR by L-amino acids. *Proc. Natl. Acad. Sci. USA* **2000**, *97*, 4419

A. Kohara, T. Toya, S. Tamura, T. Watabiki, Y. Nagakura, Y. Shitaka, S. Hayashibe, S. Kawabata, M. Okada, Radioligand binding properties and pharmacological characterization of 6-amino-N-cyclohexyl-N,3-dimethylthiazolo[3,2-a]benzimidazole-2-carboxamide (YM-298198), a high-affinity, selective, and noncompetitive antagonist of metabotropic glutamate receptor type 1. *J. Pharmacol. Exp. Ther.* **2005**, *315*, 163-169.

T. Kohonen, Self organizing formation of topologically correct feature maps. *Biol. Cybern.* **1982**, *43*, 59-69.

J.B. Kruskal, Nonmetric multidimensional scaling: A numerical method. *Psychometrika* **1964**, *29*, 115-129.

H. Kubinyi, QSAR: Hansch Analysis and Related Approaches (Methods and Principles in Medicinal Chemistry). Wiley-VCH, Weinheim, Germany, 1993.

N. Kunishima, Y. Shimada, Y. Tsuji, T. Sato, M. Yamamoto, T. Kumasaka, S. Nakanishi, H. Jingami, K. Morikawa, Structural basis of glutamate recognition by a dimeric metabotropic glutamate receptor. *Nature* **2000**, *407*, 971-977.

H. Lavreysen, C. Janssen, F. Bischoff, X. Langlois, J.E. Leysen, A.S. Lesage, [³H]R214127: a novel high-affinity radioligand for the mGlu1 receptor reveals a common binding site shared by multiple allosteric antagonists. *Mol. Pharmacol.* **2003**, *63*, 1082-1093.

A.S.J. Lesage, F. Bischoff, L. van Beijsterveldt, T. Meert, T. Steckler, D. Ashton, Novel, centrally active mGlu1 antagonists: in vitro and in vivo pharmacology. *Neuropharmacology* **2002**, *43*, 295.

A.S.J. Lesage, Role of Group I Metabotropic Glutamate Receptors mGlu1 and mGlu5 in Nociceptive Signalling. *Current Neuropharmacology* **2004**, *2*, 363-393.

L. Li, R. Tomlinson, Y. Wang, H.C. Tsui, M. Chamberlain, M. Johnson, M.P. Baez, M. VanNieuwenhze, M. Zia-Ebrahimi, E.J. Hong, A novel series of potent and selective non-competitive antagonists of metabotropic glutamate receptor 1. *Neuropharmacology* **2002**, *43*, 295.

T.H. Lin, Y.S. Yu, H.J. Chen, Classification of some active compounds and their inactive analogues using two three-dimensional molecular descriptors derived from computation of three-dimensional convex hulls for structures theoretically generated for them. *J. Chem. Inf. Comput. Sci.* **2000**, *40*, 1210-1221.

W. Lindberg, J.-A. Persson, S. Wold, Partial least-squares method for spectrofluorimetric analysis of mixtures of humic acid and lignin sulfonate. *Anal. Chem.* **1983**, *55*, 643-648.

C.A. Lipinski, F. Lombardo, B.W. Dominy, P.J. Feeney, Experimental and computational approaches to estimate solubility and permeability in drug discovery and development settings. *Adv. Drug Del. Rev.* **1997**, *23*, 3-25.

S. Litschig, F. Gasparini, D. Ruegg, N. Stoehr, P.J. Flor, I. Vranesic, L. Prezeau, J.P. Pin, C. Thomsen, R. Kuhn., CPCCOEt, a noncompetitive metabotropic glutamate receptor 1 antagonist, inhibits receptor signaling without affecting glutamate binding. *Mol. Pharmacol.* **1999**, *55*, 453-461.

Y. Liu, A Comparative Study on Feature Selection Methods for Drug Discovery. *J. Chem. Inf. Comput. Sci.* **2004**, *44*, 1823-1828.

D.J. Livingstone, Multivariate data display using neural networks. In J. Devillers (Ed.), *Neural Networks in QSAR and Drug Design*. Academic Press, London, UK, pp. 157-176, 1996.

D.G. Lloyd, C.L. Buenemann, N.P. Todorov, D.T. Manallack, P.M. Dean, Scaffold Hopping in De Novo Design. Ligand Generation in the Absence of Receptor Information. *J. Med. Chem.* **2004**, *47*, 493-496.

W. Loscher, H. Lehmann, H.J. Teschendorf, M. Traut, G. Gross, Inhibition of monoamine oxidase type A, but not type B, is an effective means of inducing anticonvulsant activity in the kindling model of epilepsy. *J. Pharmacol. Exp. Ther.* **1999**, *288*, 984-992.

O.H. Lowry, N.J. Rosebrough, A.L. Farr, R.J. Randall, Protein measurement with the Folin phenol reagent. *J. Biol. Chem.* **1951**, *193*, 265-275.

K. Lugger, D. Flotzinger, A. Schlogl, M. Pregoner, G. Pfurtscheller, Feature extraction for on-line EEG classification using principal components and linear discriminants. *Med. Biol. Eng. Comput.* **1998**, *36*, 309-314.

D. Mabire, S. Coupa, C. Adelinet, A. Poncelet, Y. Simonnet, M. Venet, R. Wouters, A.S.J. Lesage, L. van Beijsterveldt, F. Bischoff, Synthesis, Structure-Activity Relationship, and Receptor Pharmacology of a New Series of Quinoline Derivatives Acting as Selective, Noncompetitive mGlu1 Antagonists. *J. Med. Chem.* **2005**, *48*, 2134-2153.

M. Maj, V. Bruno, Z. Dragic, R. Yamamoto, G. Battaglia, W. Inderbitzin, N. Stoehr, T. Stein, F. Gasparini, I. Vranesic, R. Kuhn, F. Nicoletti, P.J. Flor, (-)-PHCCC, a positive allosteric modulator of mGluR4: characterization, mechanism of action, and neuroprotection. *Neuropharmacology* **2003**, *34*, 895-906.

P. Malherbe, N. Kratochwil, F. Knoflach, M.T. Zenner, J.N. Kew, C. Kratzeisen, H.P. Maerki, G. Adam, V. Mutel, Mutational analysis and molecular modeling of the allosteric binding site of a novel, selective, noncompetitive antagonist of the metabotropic glutamate 1 receptor. *J. Biol. Chem.* **2003**, *278*, 8340-8347.

P. Malherbe, N. Kratochwil, M.T. Zenner, J. Piussi, C. Diener, C. Kratzeisen, C. Fischer, R. H. Porter, Mutational analysis and molecular modeling of the binding pocket of the metabotropic glutamate 5 receptor negative modulator 2-methyl-6-(phenylethynyl)-pyridine. *Mol. Pharmacol.* **2003**, *64*, 823-832.

D. Manahan-Vaughan, I. Herrero, K.G. Reymann, J.S.O. Sanchez-Prieto, Presynaptic group I metabotropic glutamate receptors may contribute to the expression of long-term potentiation in the hippocampal CA1 region. *Neuroscience* **1999**, *94*, 71-82.

D. Manahan-Vaughan, K. Schuetz, Differential participation of metabotropic glutamate receptor mGlu1 and mGlu5 in spatial learning and hippocampal long-term potentiation in vivo. *Neuropharmacology* **2002**, *43*, 297.

M.J. Marino, D.L. Williams Jr., J.A. O'Brien, O. Valenti, T.P. McDonald, M.K. Clements, R. Wang, A.G. DiLella, J.F. Hess, G.G. Kinney, P.J. Conn, Allosteric modulation of group III metabotropic glutamate receptor 4: a potential approach to Parkinson's disease treatment. *Proc. Natl. Acad. Sci. USA* **2003**, *100*, 13668-13673.

Y.C. Martin, 3D database searching in drug design. *J. Med. Chem.* **1992**, *35*, 2145-2154.

Y.C. Martin, J.L. Kofron, L.M. Traphagen, Do Structurally Similar Molecules Have Similar Biological Activities? *J. Med. Chem.* **2002**, *45*, 4350-4358.

J.M. Mateos, R. Benitez, I. Elezgarai, J.J. Azkue, E. Lazaro, A. Osorio, A. Bilbao, F. Donate, R. Sarria, F. Conquet, F. Ferraguti, R. Kuhn, T. Knopfel, P. Grandes, Immunolocalization of the mGluR1b splice variant of the metabotropic glutamate receptor 1 at parallel fiber-Purkinje cell synapses in the rat cerebellar cortex. *J. Neurochem.* **2000**, *74*, 1301-1309.

J.M. Mathiesen, N. Svendsen, H. Brauner-Osborne, C. Thomsen, M.T. Ramirez, Positive allosteric modulation of the human metabotropic glutamate receptor 4 (hmGluR4) by SIB-1893 and MPEP. *Br. J. Pharmacol.* **2003**, *138*, 1026-1030.

H. Matter, Selecting optimally diverse compounds from structure databases: a validation study of two-dimensional and three-dimensional molecular descriptors. *J. Med. Chem.* **1997**, *40*, 1219-1229.

M. McKinney, Practical Aspects of Radioligand Binding. In S.J. Enna, M. Williams, J.W. Ferkany, T. Kenakin, R.D. Porsolt, J.P. Sullivan (Eds.), *Current Protocols in Pharmacology*. John Wiley & Sons, Inc., Hoboken, NJ, USA, pp. 1.3.1-1.3.33, 1998.

MDL Information Systems Inc., San Leandro, CA, USA; <http://www.mdl.com>

Med. Ad News Staff, World's best-selling medicines. *Med. Ad News* **2004**, *23*, 60-64.

B.S. Meldrum, A.G. Chapman, Excitatory amino acid receptors and antiepileptic drug development. *Adv. Neurol.* **1999**, *79*, 965-978.

S.U. Miedlich, L. Gama, K. Seuwen, R.M. Wolf, G. Breitwieser, Homology Modeling of the Transmembrane Domain of the Human Calcium Sensing Receptor and Localization of an Allosteric Binding Site. *J. Biol. Chem.* **2004**, *279*, 7254-7263.

S. Miller, R.J. Bridges, C.W. Cotman, Stimulation of phosphoinositide hydrolysis by trans-(+/-)-ACPD is greatly enhanced when astrocytes are cultured in a serum-free defined medium. *Brain Res.* **1993**, *618*, 175-178.

Millipore GmbH, Eschborn, Germany; <http://www.millipore.com>

K. Mitsukawa, R. Yamamoto, S. Ofner, J. Nozulak, O. Pescott, S. Lukic, N. Stoehr, C. Mombereau, R. Kuhn, K.H. McAllister, H. van der Putten, J.F. Cryan, P.J. Flor, A selective metabotropic glutamate receptor 7 agonist: activation of receptor signaling via an allosteric site modulates stress parameters in vivo. *Proc. Natl. Acad. Sci. USA* **2005**, *102*, 18712-18717.

Molecular Devices Corporation, Sunnyvale, CA, USA; <http://www.moleculardevices.com>

Molecular Networks GmbH, Erlangen, Germany; <http://www.mol-net.de>

MP Biomedicals, Eschwege, Germany; <http://www.mpbio.com>

I. Muegge, S.L. Heald, D. Brittelli, Simple selection criteria for drug-like chemical matter. *J. Med. Chem.* **2001**, *44*, 1841-1846.

V. Mutel, J.-W. Peters, J. Wichmann, Imidazo[1,2]pyridine derivatives as mGluR5-Antagonists. *PCT Int. Appl.* **2002**, WO02092086.

L. Nærum, L. Nørskov-Lauritsen, P.H. Olesen, Scaffold Hopping and Optimization towards Libraries of Glycogen Synthase Kinase-3 Inhibitors. *Bioorg. & Med. Chem. Letters* **2002**, *12*, 1525-1528.

K. Nakamura, T. Nukada, T. Haga, H. Sugiyama, G protein-mediated inhibition of phosphoinositide metabolism evoked by metabotropic glutamate receptors in frog oocytes. *J. Physiol.* **1994**, *474*, 35-41.

N.M. Nasrabadi, R.A. King, *Vector quantization of images based upon the Kohonen self-organizing feature maps*. IEEE International Conference on Neural Networks 1 (San Diego, 1988). IEEE Press, New York, pp. 101-108, 1988.

S. Nakanishi, M. Masu, Molecular diversity and functions of glutamate receptors. *Annu. Rev. Biophys. Biomol. Struct.* **1994**, *23*, 319-348.

S. Nakanishi, Y. Nakajima, M. Masu, Y. Ueda, K. Nakahara, D. Watanabe, S. Yamaguchi, S. Kawabata, M. Okada, Glutamate receptors: brain function and signal transduction. *Brain Res. Brain Res. Rev.* **1998**, *26*, 230-235.

R. Ng, *Drugs – From Discovery to Approval*. John Wiley & Sons, Inc., Hoboken, NJ, USA, pp. 2-5, 2004.

R.M. Nitsch, A. Deng, R.J. Wurtman, J.H. Growdon, Metabotropic glutamate receptor subtype mGluR1alpha stimulates the secretion of the amyloid beta-protein precursor ectodomain. *J. Neurochem.* **1997**, *69*, 704-712.

T. Noeske, A. Gutcaits, C.G. Parsons, T. Weil, Allosteric modulation of family 3 GPCRs. *QSAR & Comb. Sci.* **2006**, *25*, 134-146.

J. A. O'Brien, W. Lemaire, T.-B. Chen, R. S. L. Chang, M. A. Jacobson, S. N. Ha, C. W. Lindsley, H. J. Schaffhauser, C. Sur, D. J. Pettibone, P. J. Conn, D. L. Williams, Jr., A Family of Highly Selective Allosteric Modulators of the Metabotropic Glutamate Receptor Subtype 5. *Mol. Pharmacol.* **2003**, *64*, 731-740.

T. Okada, I. Le Trong, B.A. Fox, C.A. Behnke, R.E. Stenkamp, K. Palczewski, X-Ray diffraction analysis of three-dimensional crystals of bovine rhodopsin obtained from mixed micelles. *J. Struct. Biol.* **2000**, *130*, 73-80.

M. Otto, *Chemometrics – Statistics and Computer Application in Analytical Chemistry*. Wiley-VCH, Weinheim, New York, 1999.

A. Pagano, D. Rüegg, S. Litschig, N. Stoehr, C. Stierlin, M. Heinrich, P. Floersheim, L. Prezeau, F. Carroll, J.P. Pin, A. Cambria, I. Vranesic, P.J. Flor, F. Gasparini, R. Kuhn, The Non-competitive Antagonists 2-Methyl-6-(phenylethynyl)pyridine and 7-Hydroxyiminocyclopropan[b]chromen-1a-carboxylic Acid Ethyl Ester Interact with Overlapping Binding Pockets in the Transmembrane Region of Group I Metabotropic Glutamate Receptors. *J. Biol. Chem.* **2000**, *275*, 33750-33758.

K. Palczewski, T. Kumasaka, T. Hori, C.A. Behnke, H. Motoshima, B.A. Fox, I. Le Trong, D. C. Teller, T.C. Okada, R.E. Stenkamp, M. Yamamoto, M. Miyano, Crystal structure of rhodopsin: A G protein-coupled receptor. *Science* **2000**, *289*, 739-745.

C.G. Parsons, W. Danysz, G. Quack, Memantine and the amino-alkyl-cyclohexane MRZ 2/579 are moderate affinity uncompetitive NMDA receptor antagonists--in vitro characterisation. *Amino Acids* **2000**, *19*, 157-166.

C.G. Parsons, I. Kalvinsh, V. Kauss, D. Trifanova, R. Zemribo, W. Danysz, M. Henrich, T. Weil, Novel cyclic and acyclic propenones for treating CNS disorders. *PCT Int. Appl.* **2006**, WO2006037996.

E. Pebay-Peyroula, G. Rummel, J.P. Rosenbusch, E.M. Landau, X-ray structure of bacteriorhodopsin at 2.5 angstroms from microcrystals grown in lipidic cubic phases. *Science* **1997**, *277*, 1676-1681.

Perkin Elmer Life Sciences GmbH, Rodgau-Jügesheim, Germany;
<http://www.perkinelmer.com>

C. Petrel, A. Kessler, F. Maslah, P. Dauban, R.H. Dodd, D. Rognan, M. Ruat, Modeling and Mutagenesis of the Binding Site of Calhex 231, a Novel Negative Allosteric Modulator of the Extracellular Ca²⁺-sensing Receptor. *J. Biol. Chem.* **2003**, *278*, 49487-49494.

M. Pietraszek, A. Gravius, D. Schäfer, T. Weil, D. Trifanova, W. Danysz, mGluR5, but not mGluR1, antagonist modifies MK-801-induced locomotor activity and deficit of prepulse inhibition. *Neuropharmacology* **2005**, *49*, 73-85.

J.P. Pin, C. DeColle, A.S. Bessis, F. Acher, New perspectives for the development of selective metabotropic glutamate receptor ligands. *Eur. J. Pharmacol.* **1999**, *375*, 277-294.

J. P. Pin, T. Galvez, L. Prezeau, Evolution, structure, and activation mechanism of family 3/C G-protein-coupled receptors. *Pharmacol. Ther.* **2003**, *98*, 325-354.

D. Plewczynski, S.A.H. Spieser, U. Koch, Assessing Different Classification Methods for Virtual Screening. *J. Chem. Inf. Model.* **2005**, *46*, 1098-1106.

J. Polanski, P. Walczak, The comparative molecular surface analysis (COMSA): a novel tool for molecular design. *Comput. Chem.* **2000**, *24*, 615-625.

S.F. Poon, B.W. Eastman, D.F. Chapman, J. Chung, M. Cramer, G. Holtz, N.D. Cosford, N.D. Smith, 3-[3-Fluoro-5-(5-pyridin-2-yl-2H-tetrazol-2-yl)phenyl]-4-methylpyridine: a highly potent and orally bioavailable metabotropic glutamate subtype 5 (mGlu5) receptor antagonist. *Bioorg. Med. Chem. Lett.* **2004**, *14*, 5477-5480.

L. Prézeau, J. Carrette, B. Helpap, K. Curry, J.P. Pin, J. Bockaert, Pharmacological characterization of metabotropic glutamate receptors in several types of brain cells in primary cultures. *Mol. Pharmacol.* **1994**, *45*, 570-577.

M. Rarey, J.S. Dixon, Feature trees: a new molecular similarity measure based on tree matching. *J. Comput. Aided Mol. Des.* **1998**, *12*, 471-490.

A. Rattner, H. Sun, J. Nathans, Molecular genetics of human retinal disease. *Annu. Rev. Genet.* **1999**, *33*, 89-131.

G. Riedel, Function of metabotropic glutamate receptors in learning and memory. *Trends Neurol. Sci.* **1996**, *19*, 219–224.

S.T. Rouse, M.J. Marino, S.R. Bradley, H. Awad, M. Wittmann, P.J. Conn, Distribution and roles of metabotropic glutamate receptors in the basal ganglia motor circuit: implications for treatment of Parkinson's disease and related disorders. *Pharmacol. Ther.* **2000**, *88*, 427–435.

H. Schaffhauser, B.A. Rowe, S. Morales, L.E. Chavez-Noriega, R. Yin, C. Jachec, S.P. Rao, G. Bain, A.B. Pinkerton, J.M. Vernier, L.J. Bristow, M.A. Varney, L.P. Daggett, Pharmacological characterization and identification of amino acids involved in the positive modulation of metabotropic glutamate receptor subtype 2. *Mol. Pharmacol.* **2003**, *64*, 798–810.

Schleicher & Schuell GmbH, Dassel, Germany; <http://www.schleicher-schuell.com>

G. Schneider, P. Wrede, Artificial neural networks for computer-based molecular design. *Progress in Biophysics & Molecular Biology* **1998**, *70*, 175–222.

G. Schneider, W. Neidhart, T. Giller, G. Schmid, “Scaffold-Hopping” by Topological Pharmacophore Search: A Contribution to Virtual Screening. *Angew. Chem. Int. Ed. Engl.* **1999**, *38*, 2894–2896.

G. Schneider, M. Nettekoven, Ligand-based combinatorial design of selective purinergic receptor (A2A) antagonists using self-organizing maps. *J. Comb. Chem.* **2003**, *5*, 233–237.

G. Schneider, S.-S. So, *Adaptive Systems in Drug Design*. Eureka.com / Landes Bioscience, Georgetown, USA, 2003.

G. Schneider, P. Schneider, Navigation in chemical space: ligand-based design of focused compound libraries. In H. Kubinyi, G. Müller (Eds.), *Chemogenomics in Drug Discovery*. Wiley-VCH, Weinheim, Germany, pp. 341–376, 2004.

P. Schneider, G. Schneider, Collection of Bioactive Reference Compounds for Focused Library Design. *QSAR & Comb. Sci.* **2003**, *22*, 713–718.

D.M. Schnur, M.A. Hermsmeier, A.J. Tebben, Are target-family-privileged substructures truly privileged? *J. Med. Chem.* **2006**, *49*, 2000–2009.

T. Schoneberg, A. Schulz, T. Gudermann, The structural basis of G-protein-coupled receptor function and dysfunction in human diseases. *Rev. Physiol. Biochem. Pharmacol.* **2002**, *144*, 143-227.

R.P. Sheridan, A. Rusinko III., R. Nilakantan, R. Venkataraghavan, Searching for pharmacophores in large coordinate data bases and its use in drug design. *Proc. Natl. Acad. Sci. USA* **1989**, *86*, 8165-8169.

Sigma-Aldrich Chemie GmbH, Taufkirchen, Germany; <http://www.sigmaaldrich.com>

S. Sirois, C.M. Tsoukas, K.C. Chou, D. Wei, C. Boucher, G.E. Hatzakis, Selection of molecular descriptors with artificial intelligence for the understanding of HIV-1 protease peptidomimetic inhibitors-activity. *Med. Chem.* **2005**, *2*, 173-184.

M.J. Smit, H. Timmerman, J.C. Heijzelendoorn, H. Fukui, R. Leurs, Regulation of the human histamine H1 receptor stably expressed in Chinese hamster ovary cells. *Br. J. Pharmacol.* **1996**, *117*, 1071-1080.

P. Sokoloff, M. Andrieux, R. Besancon, C. Pilon, M.P. Martres, B. Giros, J.C. Schwarz, Pharmacology of human dopamine D3 receptor expressed in a mammalian cell line: comparison with D2 receptor. *Eur. J. Pharmacol.* **1992**, *225*, 331-337.

W.P.J.M. Spooren, A. Vassout, H.C. Neijt, R. Kuhn, F. Gasparini, S. Roux, R.D. Porsolt, C. Gentsch, Anxiolytic-like effects of the prototypical metabotropic glutamate receptor 5 antagonist 2-methyl-6-(phenylethynyl)pyridine in rodents. *J. Pharmacol. Exp. Ther.* **2000**, *295*, 1267-1275.

W.P.J.M. Spooren, F. Gasparini, T.E. Salt, R. Kuhn, Novel allosteric antagonists shed light on mglu₅ receptors and CNS disorders. *TRENDS Pharm. Sci.* **2001**, *22*, 331-337.

W.P.J.M. Spooren, T. Ballard, F. Gasparini, M. Amalric, V. Mutel, R. Schreiber, Insight into function of Group I and Group II metabotropic glutamate (mGlu) receptors: behavioral characterization and implications for the treatment of CNS disorders. *Behav. Pharmacol.* **2003**, *14*, 257-277.

F.L. Stahura, J. Bajorath, Virtual screening methods that complement HTS. *Comb. Chem. High Throughput Screen.* **2004**, *7*, 259-269.

T. Steckler, A.F.M. Oliveira, C. Van Dyck, H. Van Craenendonck, A.M.A. Mateus, X. Langlois, A.S.J. Lesage, J. Prickaerts, Metabotropic glutamate receptor 1 blockade impairs acquisition and retention in a spatial Water maze task. *Behav. Brain Res.* **2005**, *164*, 52-60.

R.E. Stenkamp, S. Filipek, C.A. Driessen, D.C. Teller, K. Palczewski, Crystal structure of rhodopsin: a template for cone visual pigments and other G protein-coupled receptors. *Biochim. Biophys. Acta* **2002**, *1565*, 168-182.

V. Svetnik, A. Liaw, C. Tong, J.C. Culberson, R.P. Sheridan, B.P. Feuston, Random Forest: A Classification and Regression Tool for Compound Classification and QSAR Modeling. *J. Chem. Inf. Comput. Sci.* **2003**, *43*, 1947-1958.

A. Teckentrup, H. Briem, J. Gasteiger, Mining high-throughput screening data of combinatorial libraries: development of a filter to distinguish hits from nonhits. *J. Chem. Inf. Comput. Sci.* **2004**, *44*, 626-634.

U. Thibaut, G. Folkers, G. Klebe, H. Kubinyi, A. Merz, D. Rognan, Recommendations to CoMFA studies and 3D QSAR Publications. In H. Kubinyi (Ed.), *3D QSAR in Drug Design. Volume 1: Theory, Methods and Applications*. ESCOM, Leiden, The Netherlands, pp. 711-716, 1993.

J.P. Tizzano, K.I. Griffey, J.A. Johnson, A.S. Fix, D.R. Helton, D.D. Schoepp, Intracerebral 1S,3R-1-aminocyclopentane-1,3-dicarboxylic acid (1S,3R-ACPD) produces limbic seizures that are not blocked by ionotropic glutamate receptor antagonists. *Neurosci. Lett.* **1993**, *162*, 12-16.

J.G. Topliss, R.P. Edwards, Chance factors in studies of quantitative structure-activity relationships. *J. Med. Chem.* **1979**, *22*, 1238-1244.

S.C. Tosatto, The victor/FRST function for model quality estimation. *J. Comput. Biol.* **2005**, *12*, 1316-1327.

Tripos Inc., St. Louis, MO, USA; <http://www.tripos.com>

V. Tschinke, N.C. Cohen, The NEWLEAD program: a new method for the design of candidate structures from pharmacophoric hypotheses. *J. Med. Chem.* **1993**, *36*, 3863-3870.

V.N. Vapnik, *Statistical Learning Theory*. John Wiley & Sons, Inc., New York, NY, USA, 1998.

M.A. Varney, N.D. Cosford, C. Jachec, S.P. Rao, A. Sacaan, F.F. Lin, L. Bleicher, E.M. Santori, P.J. Flor, H. Allgeier, F. Gasparini, R. Kuhn, S.D. Hess, G. Velicelebi, E.C. Johnson, SIB-1757 and SIB-1893: selective, noncompetitive antagonists of metabotropic glutamate receptor type 5. *J. Pharmacol. Exp. Ther.* **1999**, *290*, 170-181.

- J. De Vry, E. Horvath, R. Schreiber, Neuroprotective and behavioral effects of the selective metabotropic glutamate mGlu1 receptor antagonist BAY36-7620. *Eur. J. Pharmacol.* **2001**, *428*, 203–214.
- J. De Vry, Behavioral pharmacology of metabotropic glutamate 1 receptors antagonists. *Neuropharmacology* **2002**, *43*, 284.
- B.C. Van Wagenen, S.T. Moe, D.L. Smith, S.M. Sheehan, I. Shcherbakova, R. Travato, R. Walton, R. Barmore, E.G., Delmar, T.M. Stormann, Preparation of metabotropic glutamate receptor antagonists and their use for treating central nervous system diseases. *PCT Int. Appl.* **2000**, WO 0073283.
- B. Wang, J.M. Vernier, S.P. Rao, J. Chung, J.J. Anderson, J.D. Brodtkin, X. Jiang, M.F. Gardner, X. Yang, B. Munoz, Discovery of novel modulators of metabotropic glutamate receptor subtype-5. *Bioorg. Med. Chem.* **2004**, *12*, 17-21.
- R. Wang, Y. Gao, L. Liu, L. Lai, All-orientation Search and All-placement Search in Comparative Molecular Field Analysis. *J. Mol. Model.* **1998**, *4*, 276-283.
- G.L. Warren, C.W. Andrews, A.-M. Capelli, B. Clarke, J. LaLonde, M.H. Lambert, M. Lindvall, N. Nevins, S.F. Semus, S. Senger, G. Tedesco, I.D. Wall, J.M. Woolven, C.E. Peishoff, M.S. Head, A Critical Assessment of Docking Programs and Scoring Functions. *J. Med. Chem.* **2005**, *49*, 5912–5931.
- B. Waszkowycz, D.E. Clark, D. Frenkel, J. Li, C.W. Murray, B. Robson, D.R. Westhead, PRO_LIGAND: an approach to de novo molecular design. 2. Design of novel molecules from molecular field analysis (MFA) models and pharmacophores. *J. Med. Chem.* **1994**, *37*, 3994-4002.
- C.G. Wermuth, C.R. Ganellin, P. Lindberg, L.A. Mitscher, Glossary of Terms used in Medicinal Chemistry. *Pure & Appl. Chem.* **1998**, *70*, 1129-1143.
- J. Wess, Mutational analysis of muscarinic acetylcholine receptors: structural basis of ligand/receptor/G protein interactions. *Life Sci.* **1993**, *53*, 1447-1463.
- J. Wess, Molecular basis of receptor/G-protein-coupling selectivity. *Pharmacol. Ther.* **1998**, *80*, 231-264.
- M. Whittle, V.J. Gillet, P. Willett, A. Alex, J. Loesel, Enhancing the effectiveness of virtual screening by fusing nearest neighbor lists: a comparison of similarity coefficients. *J. Chem. Inf. Comput. Sci.* **2004**, *44*, 1840-1848.

P. Willet, J.M. Barnard, G.M. Downs, Chemical Similarity Searching. *J. Chem. Inf. Comput. Sci.* **1998**, 38, 983-996.

H. Wold, Estimation of principal components and related models by iterative least squares. In P.R. Krishnaiah (Ed.), *Multivariate Analysis*. Academic Press, New York, USA, pp. 391-420, 1966.

Y.D. Xiao, A. Clauset, R. Harris, E. Bayram, P. Santago 2nd, J.D. Schmitt, Supervised self-organizing maps in drug discovery. 1. Robust behavior with overdetermined data sets. *J. Chem. Inf. Model.* **2005**, 45, 1749-1758.

H. Xu, D.K. Agrafiotis, Retrospect and Prospect of Virtual Screening in Drug Discovery. *Curr. Top. Med. Chem.* **2002**, 2, 1305-1320.

J.-H. Zhang, T.D.Y. Chung, K.R. Oldenburg, A Simple Statistical Parameter in Evaluation and Validation of High Throughput Screening Assays. *J. Biomol. Screen.* **1999**, 4, 67-73.

G.Z. Zheng, P. Bhatia, J. Daanen, T. Kolasa, M. Patel, S. Latshaw, O.F. El Kouhen, R. Chang, M.E. Uchic, L. Miller, M. Nakane, S.G. Lehto, M.P. Honore, R.B. Moreland, J.D. Brioni, A.O. Stewart, Structure-Activity Relationship of Triazafluorenone Derivatives as Potent and Selective mGluR1 Antagonists. *J. Med. Chem.* **2005**, 48, 7374-7388.

W. Zhu, G. Chen, L. Hu, X. Luo, C. Gui, C. Luo, C.M. Pua, K. Chen, H. Jiang, QSAR analyses on ginkgolides and their analogues using CoMFA, CoMSIA, and HQSAR. *Bioorg. Med. Chem.* **2005**, 13, 313-322.

J. Zupan, J. Gasteiger, *Neural Networks in Chemistry and Drug Design (Second Edition)*. Wiley-VCH, Weinheim, Germany, pp. 81-86, 1999.

9 Curriculum Vitae

Zur Person

Alexander Tobias Noeske, geboren am 11.01.1977
in Frankfurt am Main,
Staatsangehörigkeit: Deutsch,
ledig.

Schulische Ausbildung

1983 – 1987 August Gräser-Grundschule, Frankfurt-Schwanheim
1987 – 1993 Helene Lange-Schule, Frankfurt-Höchst
1993 – 1996 Friedrich Dessauer-Gymnasium, Frankfurt-Höchst
06/96 Erwerb der Allgemeinen Hochschulreife (Abitur)

Hochschulbildung

10/1997 **Studium der Pharmazie** an der Johann Wolfgang Goethe-Universität,
Frankfurt am Main.
08/1999 Erster Abschnitt zum Staatsexamen in den Bereichen Chemie,
Pharmazeutische Analytik, Biologie und Physik.
10/2001 Zweiter Abschnitt zum Staatsexamen in den Bereichen Pharmakologie,
Pharmazeutische Chemie, Pharmazeutische Biologie und Pharmazeutische
Technologie.
11/2002 Dritter Abschnitt zum Staatsexamen in den Bereichen Pharmazeutische Praxis
und Rechtsgrundlagen für Apotheker.
04/03 – 06/06 **Doktorarbeit** bei Merz Pharmaceuticals GmbH unter der Leitung von Prof.
Dr. Gisbert Schneider, Johann Wolfgang Goethe-Universität in Frankfurt am
Main:
*„Allosterische Modulatoren von metabotropen Glutamatrezeptoren: Von
virtuellem Screening zu experimenteller Validierung.“*
04/03 – 06/06 Stipendiat von Merz Pharmaceuticals GmbH in Frankfurt am Main.
seit 07/2006 **Wissenschaftlicher Mitarbeiter** bei Merz Pharmaceuticals GmbH in
Frankfurt am Main.